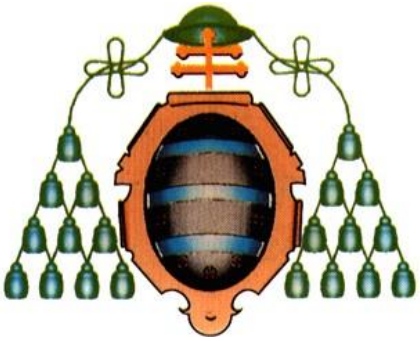

UNIVERSIDAD DE OVIEDO

Programa de Doctorado de Ciencia y Tecnología de Materiales

MATERIALES DE CARBONO MESOPOROSOS DOPADOS OBTENIDOS MEDIANTE TÉCNICAS DE NANOMOLDEO

TESIS DOCTORAL

ÁNGELA SÁNCHEZ SÁNCHEZ

NOVIEMBRE 2014

UNIVERSIDAD DE OVIEDO

Programa de Doctorado de Ciencia y Tecnología de Materiales

MATERIALES DE CARBONO MESOPOROSOS DOPADOS OBTENIDOS MEDIANTE TÉCNICAS DE NANOMOLDEO

TESIS DOCTORAL

FABIÁN SUÁREZ GARCÍA
JUAN MANUEL DIEZ TASCÓN
AMELIA MARTÍNEZ ALONSO

RESUMEN DEL CONTENIDO DE TESIS DOCTORAL

1.- Título de la Tesis	
Español: Materiales de Carbono Mesoporosos Dopados Obtenidos Mediante Técnicas de Nanomoldeo.	Inglés: Doped Mesoporous Carbon Materials Obtained Through Nanocasting Techniques

2.- Autor	
Nombre: Angela Sánchez Sánchez	DNI:
Programa de Doctorado: Ciencia y Tecnología de Materiales (Interdepartamental)	
Órgano responsable: Departamento de Ciencia de los Materiales e Ingeniería Metalúrgica	

RESUMEN (en español)

El presente trabajo tiene como objetivo principal desarrollar métodos de síntesis basados en técnicas de nanomoldeo que permitan la obtención de materiales de carbono mesoporosos dopados con heteroátomos. Para ello, se han seguido dos estrategias que difieren en el método utilizado para infiltrar la plantilla: i) depósito químico en fase vapor (CVD) y ii) infiltración en fase líquida. En ambos métodos se han estudiado sistemáticamente las variables de preparación y se han relacionado éstas con la porosidad, estructura y química superficial de los carbones obtenidos.

A través de la primera estrategia, se han preparado carbones mesoporosos ordenados (CMOs) dopados con O (hasta el 9% en peso) mediante oxidación con HNO_3 o H_2O_2 de CMOs no dopados preparados por CVD. Se ha demostrado que es posible introducir distintos grupos funcionales oxigenados modificando el tipo de agente oxidante, su concentración o el tiempo de tratamiento, sin alterar ni la textura porosa ni la estructura del CMO de partida. Mediante CVD con acetonitrilo se han preparado CMOs dopados con N (hasta el 9.4% en peso). Las características del carbón resultante dependen fundamentalmente del grado de infiltración de la plantilla.

En la segunda estrategia se han utilizado, por primera vez, poliamidas aromáticas como precursores para la obtención de CMOs dopados con N, O y/o P mediante nanomoldeo. Estos precursores han demostrado ser muy versátiles en la preparación de CMOs con diferentes características, ya que el tipo de CMO obtenido, su grado de orden estructural, textura porosa y química superficial (cantidad y naturaleza de grupos funcionales) varían en función de las variables de preparación (tipo de precursor, método de polimerización, condiciones de carbonización). Se han preparado carbones altamente porosos (áreas superficiales y volúmenes de poro hasta 1883 m^2/g y 3.01 cm^3/g, respectivamente) y contenidos en N, O y P de hasta el 9.6, 10.2 y 5.4% en peso, respectivamente.

Finalmente, se ha demostrado el efecto de la química superficial en diferentes aplicaciones de interés como la captura de CO_2, la adsorción de colorantes en disolución o la liberación controlada de medicamentos.

RESUMEN (en Inglés)

The main objective of this work is to develop methods of synthesis based on nanotemplating techniques that allow the preparation of mesoporous carbon materials doped with heteroatoms. For this purpose, two approaches have been followed, which differ in the method used to infiltrate the template: i) chemical vapor deposition (CVD) and ii) liquid-phase infiltration. In both cases, the variables of preparation have been systematically studied and they have been related to porosity, structure and surface chemistry of the resulting carbons.

Using the first strategy, we have prepared ordered mesoporous carbons (CMOs) doped with O (up to 9 wt.%) by oxidation with HNO_3 or H_2O_2 of undoped CMOs prepared by CVD. It has been proved that it is possible to introduce different oxygen-containing groups by modifying the type of oxidizing agent, its concentration or the treatment time, without altering the porous texture or the structure of the starting CMO. N-doped CMOs have been prepared by CVD with acetonitrile (up to 9.4 wt.% N). The characteristics of the resulting carbon mainly depend on the infiltration degree of the template.

In the second approach, aromatic polyamides were used, for the first time, as precursors for the preparation of CMOs doped with N, O and/or P by nanotemplating. Such precursors have been proved to be very versatile in the synthesis of CMOs with different characteristics, since the type of the resulting CMO, the structural order degree, porous texture and surface chemistry (amount and nature of functional groups) vary depending on the preparation variables (type of precursor, polymerization method, carbonization conditions). Highly porous carbons have been prepared (surface areas and pore volumes up to 1883 m^2/g and 3.01 cm^3/g, respectively) and N, O and P contents up to 9.6, 10.2 and 5.4 wt.%, respectively.

Finally, we have demonstrated the effect of surface chemistry on various interesting applications including CO_2 capture, adsorption of dyes in solution or controlled release of drugs.

SR. DIRECTOR DE DEPARTAMENTO DE CIENCIA DE LOS MATERIALES E INGENIERIA METALURGICA

INDICE GENERAL

AGRADECIMIENTOS

A lo largo de cuatro de años de trabajo es inevitable acumular montones de muestras, datos, experimentos fallidos y otros muchos que recompensan tu constancia. Nunca un día es igual al anterior y nunca sabes qué te va a sorprender o qué decisiones vas a tener que tomar para salir airoso de las dificultades. En esa montaña rusa de acontecimientos impredecibles, es necesario sentir el apoyo de las personas que aprecias y compartir con ellos tanto tus alegrías como tus momentos de desánimo. En mi caso, he tenido la gran suerte de contar con compañeros de viaje realmente increíbles.

En primer lugar, siempre he contado con el apoyo excepcional de unos padres maravillosos. Son las únicas personas que realmente conocen los orígenes de mi vocación, que comparten mis logros como si fueran suyos propios y para los que esta tesis es mucho más que un mero título. Aunque trate de encontrar palabras para explicar lo que significan en mi vida, simplemente es imposible. Sólo aspiro a demostrarles mi admiración y respeto a través de mis actos y siendo fiel a los principios que me han inculcado. Tanto ellos como el resto de mi familia sufrieron mi 'abandono' temporal de la investigación y celebraron con gran entusiasmo mi regreso a ella, siendo conscientes de que sólo así conseguiría ser feliz. Sé lo que significa para todos ellos que siga en este camino. Como castellanos que somos, nos cuesta demostrar los sentimientos abiertamente. Por ello, sé que me entenderán si les doy las gracias a toda una vida de apoyo diciéndoles que mantengo la promesa de seguir trabajando y siendo feliz con lo que más me gusta.

Aún recuerdo el primer día que recorrí los pasillos del Incar para llegar a la secretaría. Conforme iba avanzando podía ver los aparatos de los laboratorios y a la gente, con bata y mascarilla, moviéndose entre ellos. Recuerdo aquel olor tan penetrante que ya no soy capaz de distinguir y, sobre todo, el hormigueo que sentía en el pecho. En aquel momento no sabía lo importante que sería este sitio para mí ni muchas de las personas que había en él o que llegaron después. Puedo decir con orgullo que encontré grandes compañeros y amigos aquí. Tanto ellos como la gente

que he conocido fuera del Incar han contribuido a que Asturias se convierta en mi hogar.

Entre estas personas, debo mencionar expresamente a tres, mis tres directores de tesis. Me resulta imposible no emocionarme en este punto. Sin ellos, nada de esto habría sido posible. Ni siquiera creo que sean conscientes de haber cambiado la vida de una persona. Debo agradecerles no sólo su apoyo a nivel profesional, sino además su cercanía en el trato, su ayuda con las correcciones y en la dura etapa final previa a la presentación de la tesis, sus consejos, sus ánimos. Quiero agradecer especialmente a mi director Fabián haber depositado su confianza en mí hace cuatro años y durante todo este periodo, haberme dejado hacer casi cualquier cosa que le haya propuesto y estar siempre disponible con su ayuda. Los tres han valorado mi esfuerzo y los resultados que han surgido de él, y me lo han recompensado con creces, entre otras cosas financiando mi tesis por completo. Si una frase resume lo que han significado en este periodo de mi vida, no encuentro mejor manera de expresarla que, si diera marcha atrás en el tiempo, no dudaría en volver a hacer la tesis con ellos.

'Algo he aprendido en mi larga vida:
que toda nuestra ciencia,
contrastada con la realidad,
es primitiva y pueril; y, sin embargo,
es lo más valioso que tenemos'.

Albert Einstein

RESUMEN

El presente trabajo tiene como objetivo principal desarrollar métodos de síntesis basados en técnicas de nanomoldeo que permitan la obtención de materiales de carbono mesoporosos dopados con heteroátomos. Para ello, se han seguido dos estrategias que difieren en el método utilizado para infiltrar la plantilla: i) depósito químico en fase vapor (CVD) y ii) infiltración en fase líquida. En ambos métodos se han estudiado sistemáticamente las variables de preparación y se han relacionado éstas con la porosidad, estructura y química superficial de los carbones obtenidos.

A través de la primera estrategia, se han preparado carbones mesoporosos ordenados (CMOs) dopados con O (hasta el 9% en peso) mediante oxidación con HNO_3 o H_2O_2 de CMOs no dopados preparados por CVD. Se ha demostrado que es posible introducir distintos grupos funcionales oxigenados modificando el tipo de agente oxidante, su concentración o el tiempo de tratamiento, sin alterar ni la textura porosa ni la estructura del CMO de partida. Mediante CVD con acetonitrilo se han preparado CMOs dopados con N (hasta el 9.4 % en peso). Las características del carbón resultante dependen fundamentalmente del grado de infiltración de la plantilla.

En la segunda estrategia se han utilizado, por primera vez, poliamidas aromáticas como precursores para la obtención de CMOs dopados con N, O y/o P mediante nanomoldeo. Estos precursores han demostrado ser muy versátiles en la preparación de CMOs con diferentes características, ya que el tipo de CMO obtenido, su grado de orden estructural, textura porosa y química superficial (cantidad y naturaleza de grupos funcionales) varían en función de las variables de preparación (tipo de precursor, método de polimerización, condiciones de carbonización). Se han preparado carbones altamente porosos (áreas superficiales y volúmenes de poro hasta 1883 m^2/g y 3.01 cm^3/g, respectivamente) y contenidos en N, O y P de hasta el 9.6, 10.2 y 5.4% en peso, respectivamente.

Finalmente, se ha demostrado el efecto de la química superficial en diferentes aplicaciones de interés como la captura de CO_2, la adsorción de colorantes en disolución o la liberación controlada de medicamentos.

ABSTRACT

The main objective of this work is to develop methods of synthesis based on nanotemplating techniques that allow the preparation of mesoporous carbon materials doped with heteroatoms. For this purpose, two approaches have been followed, which differ in the method used to infiltrate the template: i) chemical vapor deposition (CVD) and ii) liquid-phase infiltration. In both cases, the variables of preparation have been systematically studied and they have been related to porosity, structure and surface chemistry of the resulting carbons.

Using the first strategy, we have prepared ordered mesoporous carbons (CMOs) doped with O (up to 9 wt.%) by oxidation with HNO_3 or H_2O_2 of undoped CMOs prepared by CVD. It has been proved that it is possible to introduce different oxygen-containing groups by modifying the type of oxidizing agent, its concentration or the treatment time, without altering the porous texture or the structure of the starting CMC. N-doped CMOs have been prepared by CVD with acetonitrile (up to 9.4 wt.% N). The characteristics of the resulting carbon mainly depend on the infiltration degree of the template.

In the second approach, aromatic polyamides were used, for the first time, as precursors for the preparation of CMOs doped with N, O and/or P by nanotemplating. Such precursors have been proved to be very versatile in the synthesis of CMOs with different characteristics, since the type of the resulting CMO, the structural order degree, porous texture and surface chemistry (amount and nature of functional groups) vary depending on the preparation variables (type of precursor, polymerization method, carbonization conditions). Highly porous carbons have been prepared (surface areas and pore volumes up to 1883 m^2/g and 3.01 cm^3/g, respectively) and N, O and P contents up to 9.6, 10.2 and 5.4 wt.%, respectively.

Finally, we have demonstrated the effect of surface chemistry on various interesting applications including CO_2 capture, adsorption of dyes in solution or controlled release of drugs.

Capítulo 1:

Introducción

1.1 MATERIALES NANOPOROSOS

Los materiales porosos se caracterizan fundamentalmente por poseer estructuras internas de poros, más o menos desarrolladas. Constituyen una gran familia dentro de la que se encuentran materiales de naturaleza muy diversa, como: zeolitas, sílices, carbones, polímeros orgánicos, estructuras orgánicas-metálicas, etc. Cuando las dimensiones de sus poros son del rango de los nanómetros hablamos de materiales nanoporosos.

Podemos distinguir entre dos tipos de porosidad: porosidad cerrada y porosidad abierta. La porosidad cerrada, tal como indica su nombre, está formada por poros distribuidos en el seno del material y sin contacto directo con el exterior. Este tipo de porosidad es adecuada en materiales destinados a funciones de aislamiento térmico o sonoro, y en materiales ligeros con funciones estructurales. Por el contrario, en la porosidad abierta los poros están conectados con el exterior. Por poros abiertos entendemos aquéllos cuya profundidad dentro del seno del material es superior a su diámetro. No deben confundirse con la rugosidad de la superficie, más difusa y extensa en la porción externa del material y con escasa penetración hacia su interior.

Las geometrías de los sistemas de poros pueden ser muy variadas. En la **Figura 1.1** se muestran algunos ejemplos, incluyendo diferentes tipos de poros en función de su accesibilidad. El coeficiente entre el volumen de poros y el volumen total del material, o bien la forma de los poros no constituyen en sí un criterio para efectuar una clasificación sistemática. La gran variedad de estructuras y características fisicoquímicas de los materiales porosos nos obligan a realizar diferentes clasificaciones en función características específicas.

Figura 1.1

Tipos de poros en función de su accesibilidad y forma

Accesibilidad
a: porosidad cerrada
b, c, d, e, f: porosidad abierta
b, f: poros ciegos
e: poro pasante
Forma
b: poro con forma de cuello de botella
c: poro con forma de rendija
d: poro con forma de embudo
f: poro cilíndrico ciego
g: rugosidad superficial

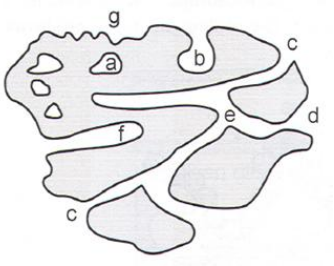

La clasificación más utilizada es la que toma como criterio el tamaño de los poros debido a la estrecha relación que existe entre este parámetro y muchas de las propiedades de los materiales porosos.

La IUPAC [1] ha propuesto una clasificación de los poros en tres grupos en función de su diámetro:

- *Microporos:* poseen diámetros inferiores a 2 nm.
- *Mesoporos:* Diámetros entre 2 y 50 nm.
- *Macroporos:* Diámetros superiores a 50 n.

Los tres tipos de poros mencionados se encuentran representados esquemáticamente en el esquema de la **Figura 1.2**, donde se muestra el corte transversal de un sólido poroso.

Cuando estudiamos sólidos porosos reales, no siempre se obtiene un único tamaño de poro sino que suelen ser sistemas complejos en los que pueden coexistir poros con distintos tamaños. Por ello hablamos de materiales 'esencialmente' microporosos, mesoporosos o macroporosos, e incluso de materiales bimodales (por ejemplo micro-mesoporosos) en función del rango predominante de tamaños de poro que presenten. En este caso y de forma generalizada, se suele determinar el diámetro promedio o especificar los intervalos concretos de tamaños de poro. Para ello se recurre a diferentes métodos, directos e indirectos, para su determinación. Algunos de los cuales se explican con detalle en el **Capítulo 3** de esta tesis.

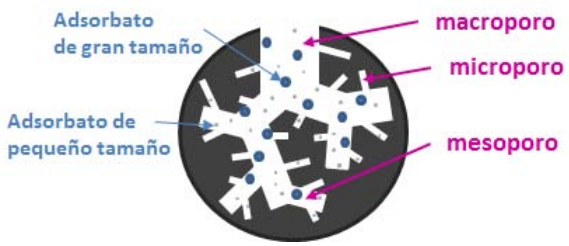

Figura 1.2

Esquema del corte transversal de un material poroso.

Los materiales pueden presentar estructura porosas bien desarrolladas, con áreas superficiales específicas que pueden alcanzar varios miles de metros cuadrados por gramo, dependiendo del material del que se trate [2]. Por ello se han utilizado

tradicionalmente en aplicaciones que requieren elevadas áreas de contacto. Pero la posibilidad de modular su porosidad, estructura y química superficial hace que estos materiales sean muy atractivos, no sólo en aplicaciones relacionadas con procesos de adsorción, sino también en procesos catalíticos, de separación, electroquímicos, etc.

Para satisfacer los requisitos en aplicaciones específicas, se han desarrollado diferentes métodos para la síntesis de materiales porosos con características ajustadas a una aplicación particular [3-5]. Así, en los últimos veinte años se han realizado grandes esfuerzos para controlar la estructura de los materiales porosos. El descubrimiento de las sílices mesoporosas ordenadas pertenecientes a la familia M41S en 1992 por la compañía *Mobil Research and Development Corporation*, obtenidas gracias al uso de surfactantes como plantillas, abrió el camino hacia asombrosos avances en el control de la estructura, morfología y composición de los materiales porosos [5, 6]. A partir de entonces, el diseño de materiales no silíceos controlando estrechamente su ordenamiento estructural y composición ha adquirido una gran importancia, desde el punto de vista tanto de la investigación fundamental como de su aplicación industrial.

Entre dichos materiales no silíceos, los materiales de carbono destacan por sus excelentes propiedades físico-químicas, que los hacen idóneos en multitud de campos de aplicación. En los últimos años, el desarrollo tecnológico ha impulsado la aparición de nuevas aplicaciones que requieren la adaptación precisa de los materiales y la mejora de otras ya existentes. Esto ha llevado a buscar materiales de carbono con estructuras de poros uniformes o que permitan establecer interacciones específicas a través de determinados grupos funcionales en su superficie. Aunque se han realizado muchos avances al respecto, es necesario profundizar aún más en el control estructural y de la química superficial para llevar a cabo una adaptación específica. Por ello, el objeto de esta tesis se centra en la obtención de materiales de carbono mesoporosos con estructuras ordenadas y dopados con heteroátomos.

En los párrafos posteriores se hará una breve descripción de los métodos utilizados para obtener materiales de carbono porosos. Se incidirá en los métodos que

permiten obtener carbones mesoporosos con estructuras de poros ordenadas (CMOs), especialmente aquéllos en los que se ejerce un control más preciso sobre la estructura, comúnmente denominados técnicas de nanomoldeo. Finalmente, se tratarán las estrategias de funcionalización de dichos CMOs.

1.2 MATERIALES DE CARBONO NANOPOROSOS

Los materiales de carbono nanoporosos poseen excelentes propiedades físico-químicas como altas áreas superficiales, baja densidad, alta estabilidad química en condiciones no oxidantes, alta conductividad térmica y eléctrica, elevada resistencia mecánica y buena biocompatibilidad [2, 6-8]. Debido a estas características son usados en un amplio rango de aplicaciones como soportes de catalizadores, adsorbentes, filtros, electrodos en supercondensadores y baterías, soportes de biomoléculas, portadores de medicamentos, etc [9-12].

1.2.1 CONTROL DE LA POROSIDAD

En este apartado se comentarán brevemente algunos de los métodos más utilizados para desarrollar y controlar la porosidad de carbones que podríamos denominar 'clásicos', aunque siguen en completa vigencia. En el apartado siguiente se comentarán en mayor extensión las técnicas basadas en el nanomoldeo, que es la herramienta utilizada en esta tesis para la preparación de los materiales objeto de estudio.

Control de la microporosidad:

a. Activación: Este término engloba todos aquellos métodos que permiten el desarrollo de la porosidad de precursores carbonosos para lograr materiales porosos, en particular carbones activados. En general podemos diferenciar dos métodos generales, denominados activación física (también conocido como activación térmica) y activación química.

La activación física o térmica suele constar de dos etapas. En la primera etapa se lleva a cabo la pirolisis o carbonización en atmósfera inerte del precursor orgánico hasta temperaturas comprendidas, generalmente, entre 800 y 950 °C. La segunda es la etapa propiamente dicha de activación y consiste en una gasificación parcial

controlada del material carbonizado, empleando gases oxidantes (vapor de agua, dióxido de carbono, aire o una mezcla de ellos) y se suele realizar a temperaturas entre 750 y 850 °C [13, 14]. La propia naturaleza del carbonizado y las variables de operación van a determinar el desarrollo de la porosidad.

La activación química, en general, consta de una única etapa de tratamiento térmico en atmósfera inerte de una mezcla del precursor con el agente activante. Se suele realizar a temperaturas inferiores a las de la activación física y pueden variar entre 400 y 900 °C, dependiendo del precursor y del agente activante. Los agentes químicos más utilizados son el ácido fosfórico [15], el cloruro de zinc [16] y los hidróxidos de metales alcalinos [17]. Tras la etapa térmica se debe de realizar un lavado para eliminar el agente activante y/o subproductos de reacción y así liberar la porosidad.

En la bibliografía existe abundante información sobre la activación química y física de una gran variedad de precursores y materiales carbonosos. Estos trabajos muestran que, controlando las diferentes variables de operación, se puede ejercer un cierto control sobre la microporosidad desarrollada, pero no de un modo completo.

b. Tamices moleculares de carbón: Los tamices moleculares de carbón se caracterizan por poseer microporos uniformes de unos pocos angstroms de diámetro y que suelen presentar elevada selectividad a las moléculas de adsorbato en función de su tamaño. Otras propiedades, como su alta resistencia mecánica y a la corrosión y su hidrofobicidad hacen que su uso sea preferible al de otros tamices moleculares inorgánicos, como las zeolitas.

Estos carbones se pueden preparar mediante dos métodos generales. El primero consiste en la carbonización de precursores o mezclas adecuadas. Así, una posibilidad es la pirólisis de mezclas de carbón o precursor carbonoso y aditivos (brea, fenol y formaldehído) [18], de modo que cambiando la proporción entre carbón/aditivos se modifica el tamaño de los poros. Otra posibilidad se basa en el uso de resinas de intercambio iónico [19] a las que se intercambia con cationes y posteriormente se carbonizan. El tamaño de los poros se modifica cambiando el tipo de catión.

El otro método para la preparación de tamices moleculares de carbón es la modificación la porosidad de un material con textura adecuada por depósito de carbón pirolítico en las entradas de los poros [20, 21]. Este método implica un control estricto de las condiciones de operación para que el depósito de carbón se produzca en la bocas de los poros, reduciendo su diámetro y no en las paredes de los mismos que haría que se redujera su volumen y se perdiera capacidad de adsorción [21].

Control de la mesoporosidad:

a. Activación catalítica: Ésta consiste en la activación física en presencia de metales alcalinotérreos, de transición (Fe, Ni) [22] o complejos organometálicos [23]. El tamaño y el volumen de los mesoporos generados va a depender de las condiciones experimentales, como temperatura de gasificación, tiempo y cantidad y tipo de catalizador.

b. Por carbonización de mezclas de polímeros: En este método se mezclan dos o más tipos de polímeros que sean inmiscibles de los que al menos uno es térmicamente inestable [24]. Los polímeros inmiscibles presentan fases separadas, que forman micro-dominios con diferentes formas (esféricos, liminares…) y cuyos tamaños pueden ir desde los nanómetros hasta los milímetros en función de la proporción de la mezcla y la compatibilidad entre los polímeros. Al pirolizar la mezcla, el polímero inestable térmicamente se descompone generando la porosidad, mientras que el polímero estable térmicamente se carbonizará y dará lugar al carbón.

c. Carbonización de geles orgánicos obtenidos por reacción sol-gel: Se basa en el uso de geles obtenidos a partir de disoluciones básicas de resorcinol y formaldehido en agua y en presencia de un catalizador [25]. La síntesis de geles de carbono se divide en tres etapas [26] que son: (i) la preparación de la mezcla de sol, su gelación y curado; (ii) el secado del gel y (iii) la carbonización del gel seco. Las características del gel de carbón resultante van a depender en gran medida de las variables de operación. Un paso clave en la síntesis de estos materiales es la etapa de secado del gel. Existen tres métodos generales de secado: subcrítico, supercrítico y por congelación, dando lugar a xerogeles, aerogeles y criogeles respectivamente.

1.2.1.1 Técnicas de nanomoldeo

Podemos definir el nanomoldeo o *nanotemplating* como un proceso en el que se usa un molde (plantilla) con una estructura definida a nivel nanoscópico para obtener otro material cuya estructura es la réplica negativa del primero. Las técnicas de nanomoldeo aportan una flexibilidad excepcional en la síntesis de materiales de carbono con estructuras ordenadas. Permiten obtener materiales con diferentes estructuras compuestas por micro, meso, macroporos o mezcla de ellos en función de la plantilla seleccionada.

En función del tipo de plantilla utilizada podemos clasificar las técnicas de nanomoldeo en: *soft-templating* y *hard-templating*.

Soft-templating

Se basa en el uso de plantillas 'blandas' (*soft*), entendiéndose como tales determinadas moléculas orgánicas. Suelen utilizarse polímeros, principalmente surfactantes, con capacidad para auto-organizarse y formar cristales líquidos. En la **Figura 1.3** se muestra una clasificación de moléculas orgánicas usadas como plantillas blandas en función de su funcionalidad y carga. Como puede observarse en dicha figura, existe una relativa variedad de moléculas orgánicas que pueden ser usadas como moldes, desde moléculas individuales, como las sales de tetrapropilamonio, hasta grandes copolímeros bloque, como el pluronic P123 o F127.

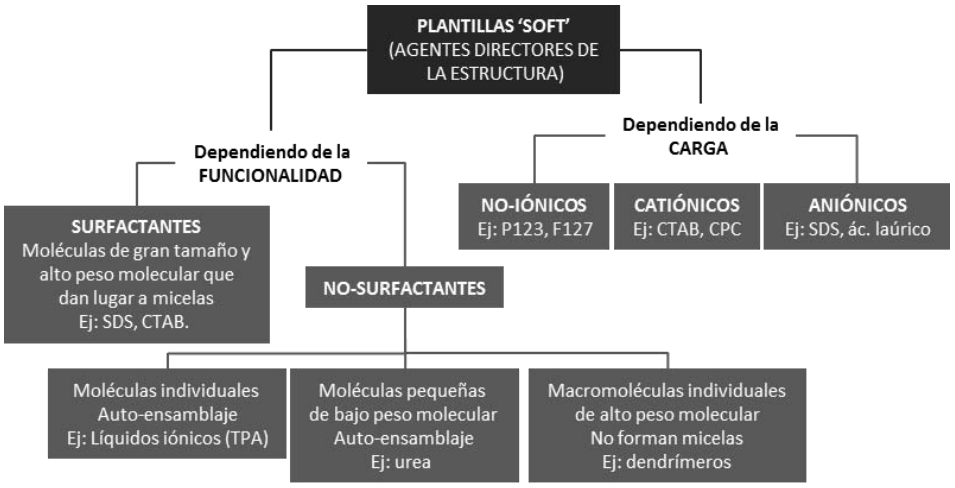

Figura 1.3

Clasificación de plantillas orgánicas utilizadas para la síntesis de materiales mesoporosos por *soft-templating*.

Debemos tener en cuenta que no todas las síntesis asistidas por surfactantes son procesos de nanomoldeo. Para que exista un proceso de nanomoldeo debe replicarse una estructura de surfactante previamente formada, y en muchos casos lo que ocurre es un ensamblaje cooperativo entre el surfactante y el componente inorgánico [2].

En la síntesis de una sílice mesoporosa asistida [2] por un surfactante determinado, se puede variar la concentración de éste en un amplio intervalo: desde valores por debajo de la concentración micelar crítica hasta altas concentraciones, para las que se forma totalmente la fase de cristal líquido. El mecanismo de síntesis varía con la concentración, siendo un mecanismo cooperativo a bajas concentraciones y un verdadero mecanismo de nanomoldeo en fase de cristal líquido (TLCT, de las siglas en inglés) a altas concentraciones. Incluso en un proceso TLCT pueden existir etapas en que la fase orgánica (plantilla) es destruida temporalmente por el alcohol que se produce en la hidrólisis del silicato [27].

La síntesis de materiales mesoporosos por *soft-templating* consta de tres etapas fundamentales, tal y como se muestra en la **Figura 1.4:**

1) Auto-organización de las moléculas que constituyen la plantilla orgánica.

2) Condensación de las moléculas de precursor (silíceo, carbonoso, etc) alrededor de la plantilla.

3) Eliminación de la plantilla mediante calcinación en atmósfera de aire o por extracción con disolventes (apropiado para materiales térmicamente inestables o sensibles a la calcinación en aire).

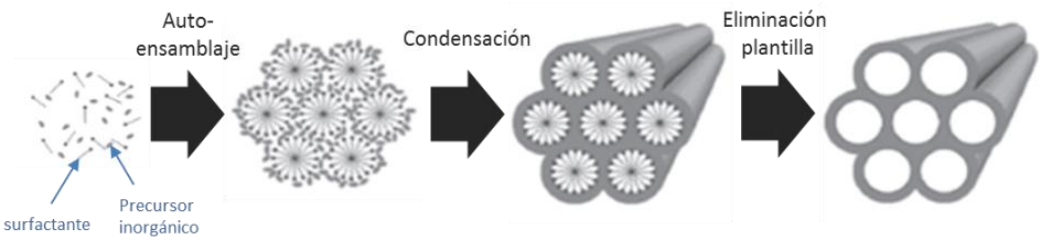

Figura 1.4

Método de *soft-tem-plating* asistido por surfactantes.

Aunque el método de *soft-templating* se ha aplicado fundamentalmente y con gran éxito a la obtención de sílices mesoporosas, también se ha utilizado para preparar otro tipo de materiales, como óxidos de metales de transición y no-transición,

sulfuros metálicos, fosfatos metálicos, etc. El número de trabajos que han conseguido obtener CMOs por esta vía es mucho más reducido debido a la compleja evolución de las estructuras de carbono y la alta energía de formación de los enlaces C-C. Para que sea llevada a cabo con éxito, los precursores de carbono deben cumplir unos requisitos básicos [28]:

- En primer lugar, deben ser capaces de auto-ensamblarse y generar estructuras a escala nanométrica.
- En segundo lugar, deben transformarse en materiales poliméricos altamente entrecruzados que mantengan la nanoestructura al eliminar la plantilla.

Estos requisitos son cumplidos por un escaso número de precursores, entre ellos los polímeros rígidos de resorcinol-formaldehído. En cuanto a las plantillas, éstas deben ser lo suficientemente estables a la temperatura de curado del precursor carbonoso, pero deben descomponerse adecuadamente a la temperatura de carbonización de éste. A estas limitaciones se une el hecho de que las condiciones experimentales de síntesis, tales como las proporciones de los reactivos, los disolventes utilizados, el pH del medio y las temperaturas usadas en el proceso influyen decisivamente sobre la correcta formación de la plantilla orgánica y sobre la estructura porosa final del material de carbono.

Hard-templating

Esta técnica utiliza sólidos (*hard*) con estructuras de poros definidas como nanomoldes y permite obtener réplicas negativas de éstos con estructuras igualmente ordenadas [2]. Entre las plantillas más utilizadas se encuentran materiales inorgánicos como las zeolitas, sílices mesoporosas, microesferas de sílice, óxidos, partículas coloidales, etc. En la **Fig. 1.5** se observa cómo se produce la replicación del material de carbono a partir de una zeolita, esto es, la red de poros de la plantilla se traduce en el esqueleto del material de carbono. Además de replicarse la estructura de poros de la plantilla, en el proceso de *hard-templating* también se replica la morfología de sus partículas.

La síntesis de carbones porosos a partir de plantillas sólidas fue realizada por primera vez en 1986 por el grupo de Knox et al. [29]. Utilizaron como plantilla partículas esféricas de sílica gel y las infiltraron con una mezcla de precursores

poliméricos (fenol y hexamina). Tras carbonizar los composites resultantes y eliminar la plantilla de sílice, obtuvieron un material de carbono formado por partículas cuya forma y tamaño eran semejantes a los del sólido poroso de partida. Posteriormente, con el descubrimiento de una nueva familia de sílices mesoporosas ordenadas preparadas mediante *soft-templating* (familias de sílices MCM, SBA, KIT [30-32]) se propulsó la síntesis de carbones mesoporosos con un control estricto sobre sus estructuras de poros. Dos grupos pioneros, Ryoo et al. [33] y Lee et al. [34], sintetizaron independientemente el uno del otro réplicas de carbono con estructuras de poros ordenadas a escala nanoscópica. Siguiendo este procedimiento, se han preparado un gran número de materiales de carbono con estructura ordenada.

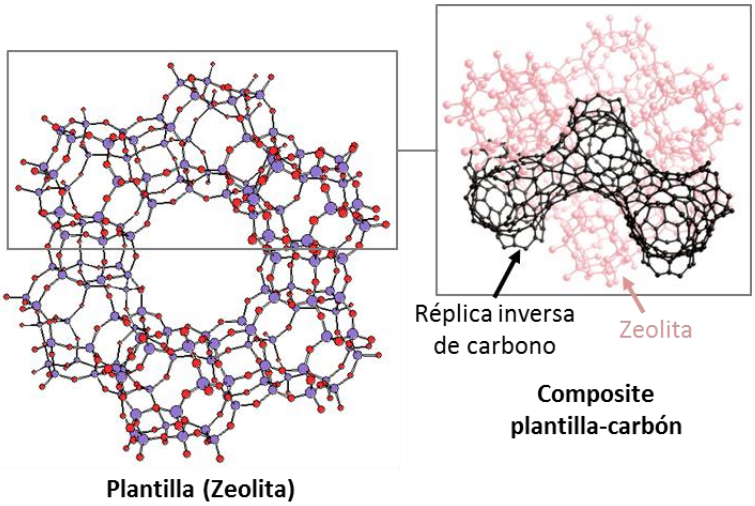

Figura 1.5

Formación de la réplica negativa de carbono a partir de una plantilla inorgánica (zeolita).

Típicamente, el procedimiento experimental para la preparación de carbones mediante *hard-templating* se compone de cuatro pasos principales [2], esquematizados en la **Figura 1.6**:

1) Obtención de la plantilla sólida, con una estructura de poros definida.

2) Infiltración de la plantilla con un precursor de carbono, monomérico o polimérico.

3) Polimerización y carbonización del precursor carbonoso que se encuentra ocupando la porosidad de la plantilla.

4) Eliminación de la plantilla.

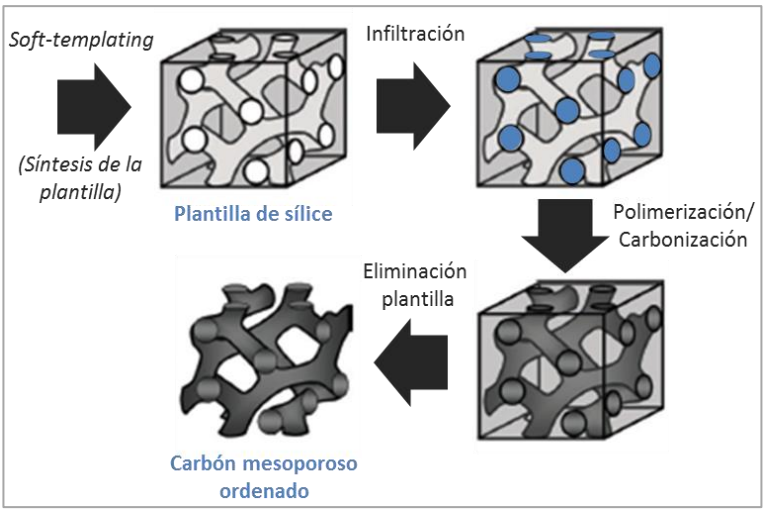

Figura 1.6

Método de *hard-templating* a partir de una plantilla de sílice MCM-48 obtenida a su vez por *soft-templating*.

Para conseguir una correcta replicación de la estructura porosa de la plantilla se deben tener en cuenta una serie de factores:

- ***La estructura porosa de la plantilla***: No todas las plantillas son adecuadas para obtener materiales de carbono ordenados. Como se observa en la **Figura 1.7**, plantillas con sistemas de poros interconectados dan lugar a materiales de carbono con estructura ordenada. Un ejemplo típico son las plantillas de sílice mesoporosa SBA-15. En cambio, cuando se parte de una plantilla con un sistema de poros desconectados entre sí pueden obtenerse materiales de carbono desordenados, por ejemplo cuando se utiliza como plantilla la sílice MCM-41, que da lugar a nanofibras de carbono.

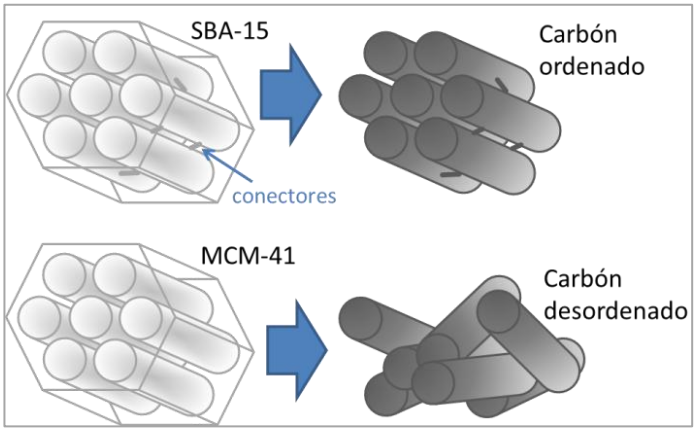

Figura 1.7

Influencia de la conectividad de la plantilla sobre el ordenamiento de la réplica.

- ***Las interacciones que se establecen entre la superficie de la plantilla y las moléculas de precursor:*** Dependen de la naturaleza química del precursor y de la plantilla. Pueden ser fuerzas de van der Waals, interacciones electrostáticas, enlaces de hidrógeno, etc. La existencia de interacciones desfavorables entre las

paredes de los poros y las moléculas de precursor pueden dificultar la difusión de éstas y, por tanto, producir una replicación pobre de la plantilla.

- ***El tipo de precursor de carbono:*** En principio, podría usarse cualquier molécula orgánica como precursor de carbono, pero, en la práctica, no todas pueden ser transformadas en un material de carbono de forma fácil, ni todas pueden ser fácilmente introducidas en los poros de la plantilla. La elección del precursor constituye por tanto otra forma de control sobre el material de carbono final.

- ***La cantidad de precursor carbonoso incorporado en la porosidad de la plantilla o porcentaje de infiltración:*** La cantidad de precursor introducida debe ser suficiente como para mantener la estructura del sistema de poros cuando la plantilla es eliminada. Además debe producirse una infiltración homogénea para evitar la formación de espacios vacíos que constituirán huecos no deseados en el material final. Para conseguir ambos objetivos, en ocasiones es necesario realizar varias etapas de infiltración (por ejemplo, cuando se usan precursores con bajo rendimiento de carbonización, como la sacarosa, o el alcohol furfurílico) o aplicar periodos largos de polimerización y estabilización (como en el caso del alcohol furfurílico o el acrilonitrilo). Por otro lado, la cantidad de precursor incorporado no debe exceder la capacidad de llenado de los poros para evitar la acumulación de carbono amorfo en la superficie externa de las partículas. Por ejemplo, en los procesos de infiltración mediante depósito químico en fase vapor (CVD) esto se consigue controlando estrechamente las variables experimentales como la concentración de precursor, el tiempo y la temperatura de depósito.

Controlando el grado de infiltración de la plantilla se pueden rellenar totalmente los poros de ésta o realizar un recubrimiento de determinado espesor sobre sus paredes. Esto da lugar a un sistema de poros (entre las barras de carbón) o a dos sistemas (entre los tubos de carbón y dentro de ellos), tal como se muestra en la **Figura 1.8**. En el caso de la plantilla de sílice mesoporosa SBA-15 (utilizada en esta tesis), el grado de infiltración puede hacer que la réplica de carbón esté compuesta por cilindros macizos (CMO tipo CMK-3) o tubos huecos (CMO tipo CMK-5) [35-37].

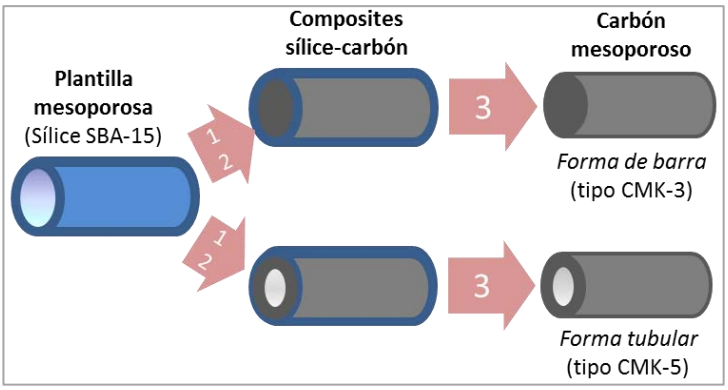

Figura 1.8

Influencia del grado de infiltración sobre la estructura de poros del carbón final.
Leyenda:
1 Infiltración
2 Carbonización
3 Eliminación plantilla

- ***La técnica utilizada para introducir el precursor***: El método de infiltración de la porosidad de la plantilla va a venir determinado en gran medida por las características del precursor (si es líquido, sólido o gas). De entre las técnicas utilizadas para infiltrar el compuesto precursor en la porosidad de la plantilla destacan las siguientes:

  - ***Impregnación en fase líquida:*** Los poros de la plantilla se llenan con el precursor en estado líquido o bien disuelto en un disolvente adecuado, que debe ser eliminado posteriormente. Entre los precursores comúnmente utilizados se encuentran los glúcidos (glucosa, sacarosa), el pirrol, el poliacrilonitrilo, el alcohol furfurílico, las resinas fenol-formaldehído, etc. La carbonización puede ser llevada a cabo en presencia de un catalizador, con el fin de promover la polimerización y entrecruzamiento del precursor.

  - ***Infiltración por depósito químico en fase vapor (CVD, Chemical Vapor Deposition):*** Un precursor carbonoso en fase gas (acetileno, propileno) o una corriente de gas inerte saturado en un precursor líquido (acetonitrilo) es descompuesto térmicamente aplicando altas temperaturas y depositado en los poros de la plantilla. La temperatura y el tiempo de depósito, la concentración y flujo de la mezcla de gases, son variables a optimizar para que el depósito tenga lugar en los poros y no en el exterior de las partículas de la plantilla y asegurar así la replicación correcta.

1.2.2 FUNCIONALIZACIÓN DE LOS MATERIALES DE CARBONO

Los materiales de carbono obtenidos mediante técnicas de nanomoldeo presentan generalmente superficies poco funcionalizadas e hidrófobas debido a que las altas

temperaturas de carbonización eliminan gran cantidad de los grupos funcionales y enlaces débiles C-X. Esto dificulta su uso en aplicaciones donde se requieren interacciones específicas así como aquellas en las que se utilizan disolventes polares. Para adaptar los materiales de carbono a los requerimientos de la aplicación en la que se van a utilizar se pueden someten a procedimientos de dopaje o funcionalización. Éstos permiten modificar la composición química de los carbones introduciendo grupos funcionales o heteroátomos en su esqueleto [38].

Numerosos trabajos han estudiado el efecto del dopaje sobre los materiales de carbono. Algunos ejemplos los podemos encontrar en libros especializados [39-45]. En general, se produce una variación de las propiedades eléctricas, mecánicas, semiconductoras y de emisión de campo. En particular, se ha comprobado que los grupos funcionales oxigenados aumentan el carácter hidrófilo de la superficie, favorecen la dispersión de los compuestos metálicos y mejoran la capacidad electroquímica de los materiales de carbono. Dichos grupos también actúan como centros activos en reacciones catalíticas o en la adsorción selectiva de especies catiónicas y aportan sitios específicos para anclar otras funcionalidades. La introducción de grupos funcionales de nitrógeno ha sido relacionada con un aumento del carácter básico de la superficie, con la mejora de las propiedades de intercambio aniónico y el incremento de la actividad catalítica. También participan en reacciones redox, de gran interés en aplicaciones electroquímicas destinadas al almacenamiento de energía, y sirven como sitios de anclaje para otras moléculas. Los grupos superficiales de fósforo aumentan la resistencia de los carbones a la oxidación y el carácter ácido de su superficie. Esto se ha asociado con una mejora de las propiedades de intercambio iónico de los materiales y con el aumento de la densidad de energía en supercondensadores. La presencia de grupos funcionales de azufre aumenta notablemente la afinidad de los materiales de carbono por el mercurio, incluso en condiciones extremas de pH (intervalo de pH entre 1.0 y 12.8) en las que los materiales silíceos son inestables. Los grupos sulfónicos son importantes desde un punto de vista catalítico, puesto que pueden ser utilizados varias veces para catalizar reacciones y evitan el uso de ácidos líquidos. Las funcionalidades de boro mejoran la resistencia de los carbones a la oxidación,

favorecen su grafitización, modifican las propiedades de quimisorción de oxígeno y dan lugar a reacciones redox, muy interesantes desde un punto de vista electroquímico.

A día de hoy, el control de la cantidad y el tipo de heteroátomos incorporados en el esqueleto carbonoso no es un cometido fácil y constituye un gran desafío. La funcionalización se puede llevar a cabo en la etapa de síntesis de los materiales (funcionalización por síntesis directa) o mediante tratamientos posteriores a dicha etapa sintética (funcionalización post-síntesis).

1.2.2.1 Funcionalización por síntesis directa

El dopaje de los materiales de carbono tiene lugar en el propio procedimiento de obtención mediante la utilización de precursores adecuados (que contengan el heteroátomo que queremos introducir). En principio, la disponibilidad de precursores orgánicos que contienen heteroátomos es muy amplia; pero sólo un número reducido de los mismos cumplen los requisitos para ser utilizados en métodos de nanomoldeo. Algunos ejemplos se comentan a continuación.

El primer CMO dopado con nitrógeno fue obtenido usando acrilonitrilo como precursor, SBA-15 como plantilla sólida y un catalizador para iniciar la polimerización radicalaria [46]. Los contenidos de nitrógeno variaban entre el 4 y 15 % mol en función de la temperatura de estabilización y se podían obtener distribuciones de poros unimodales o bimodales. También se han utilizado resinas de formaldehído-melamina como precursores y esferas de sílice fumante como plantillas, siendo el contenido final de nitrógeno del 6 % en peso [47]. Mediante CVD y usando acetonitrilo como precursor es posible infiltrar zeolitas o sílice mesoporosa [48]. El contenido de nitrógeno de los carbones resultantes (en torno al 8 % en peso) prácticamente no varía cuando se utilizan temperaturas de depósito entre 850 y 1000 °C, pero sí aumenta su carácter grafítico al aumentar la temperatura. Otro precursor apropiado para obtener CMOs por CVD es el pirrol [49], permitiendo obtener contenidos de nitrógeno en torno al 5.5 % mol. La obtención de CMOs dopados con azufre por *hard-templating* ha sido llevada a cabo mediante polimerización lineal de 2-tiofenemetanol [50]. Además de presentar

contenidos en azufre entre el 4 y 7 % en peso, los CMOs resultantes poseían volúmenes de poros superiores a 2 cm^3/g.

1.2.2.2 Funcionalización post-síntesis

En este tipo de funcionalización, los heteroátomos no se incorporan en la etapa de síntesis del material sino una vez obtenido. Entre los métodos post-síntesis más utilizados destacan los tratamientos de oxidación, aminación y aminoxidación, sulfonación, halogenación y *grafting*.

Oxidación: Los tratamientos de oxidación son los métodos más utilizados y conocidos para obtener materiales de carbono funcionalizados con oxígeno. Éstos pueden ser de varios tipos, incluyendo la oxidación seca, húmeda, electroquímica o por plasma. El comportamiento de los agentes oxidantes utilizados difiere respecto a la cantidad y tipo de grupos funcionales que son introducidos, siendo uno de los tratamientos más efectivos la oxidación húmeda con ácido nítrico [51, 52].

Aminación y amonoxidación: La aminación consiste en someter un material de carbono a un tratamiento térmico en presencia de un flujo de NH_3, mientras que la amonoxidación se basa en la reacción del material de carbono con una mezcla gaseosa NH_3/oxígeno. Se ha comprobado que aplicando ambos procesos al dopaje de carbones activados es posible incorporar en torno a un 3-4% en peso de nitrógeno, siendo mayor la eficiencia de incorporación de nitrógeno por el procedimiento de amonoxidación [50].

Sulfonación: Mediante los tratamientos post-síntesis de sulfonación se introducen grupos sulfónicos en la superficie de los materiales de carbono. Los métodos de dopaje incluyen tratamientos con ácido sulfúrico a alta temperatura o tratando en un autoclave el material de carbono en presencia de ácido sulfúrico fumante [53, 54].

Halogenación: En la halogenación se introducen elementos halógenos, principalmente flúor y bromo. El flúor es introducido poniendo el material de carbono en presencia de F_2 y aplicando temperaturas de hasta 250 ºC, o bien haciendo reaccionar carbones funcionalizados con grupos oxigenados con fluoroalquilsilano o sometiendo monómeros de fluorocarbono (CF_4 y C_3F_8) a la

acción de un plasma por microondas [55]. La funcionalización con bromo o cloro se lleva a cabo calentando el material de carbono a altas temperaturas en presencia de Br_2 o Cl_2, respectivamente [56].

Grafting: Consiste en la modificación de una funcionalidad pre-existente en la superficie del material mediante una reacción química o a través de grupos funcionales anclados directamente a la superficie [38]. Algunos de los métodos más usados se basan en la modificación de los ácidos carboxílicos superficiales para anclar otros grupos funcionales, en la reducción de sales de diazonio en presencia del material de carbono o utilizan la reacción de Prato para incorporar grupos alquilo a la superficie de éste.

Además de las dificultades experimentales para dopar materiales carbonosos en general, cuando la funcionalización se quiere realizar en materiales carbonosos ordenados la complejidad del proceso en mayor. No sólo el número disponible de precursores adecuados es menor, debido a las restricciones impuestas por los métodos de nanomoldeo, sino que además, los métodos post-síntesis no pueden ser demasiado agresivos para evitar la destrucción del orden estructural de los carbones. En la presente tesis abordamos estos retos con el objetivo general de buscar nuevos métodos de síntesis que permitan la preparación de carbones ordenados dopados con heteroátomos.

1.3. REFERENCIAS BIBLIOGRÁFICAS

[1] Sing KSW, Everett DH, Haul RAW, Moscou L, Pierotti RA, Rouquerol J, et al. Reporting physisorption data for gas solid systems with special reference to the determination of surface-area and porosity (recommendations 1984). Pure Appl Chem 1985;57(4):603-19.

[2] Lu AH, Schüth F. Nanocasting: A versatile strategy for creating nanostructured porous materials. Adv Mater 2006;18(14):1793-805.

[3] Wang J, Xin HL, Wang D. Recent progress on mesoporous carbon materials for advanced energy conversion and storage. Part Part Syst Charact 2014;31(5):515-39.

[4] Davis ME. Ordered porous materials for emerging applications. Nature 2002;417(6891):813-21.

[5] Corma A. From Microporous to Mesoporous Molecular Sieve Materials and Their Use in Catalysis. Chem Rev 1997;97(6):2373-420.

[6] Schüth F. Non-siliceous mesostructured and mesoporous materials. Chem Mater 2001;13(10):3184-95.

[7] Xia YD, Yang ZX, Mokaya R. Templated nanoscale porous carbons. Nanoscale 2010;2(5):639-59.

[8] Lozano-Castello D, Alcaniz-Monge J, de la Casa-Lillo MA, Cazorla-Amoros D, Linares-Solano A. Advances in the study of methane storage in porous carbonaceous materials. Fuel 2002;81(14):1777-803.

[9] Karavasili C, Amanatiadou EP, Sygellou L, Giasafaki DK, Steriotis TA, Charalambopoulou GC, et al. Development of new drug delivery system based on ordered mesoporous carbons: characterisation and cytocompatibility studies. J Mat Chem B 2013;1(25):3167-74.

[10] Lee J, Kim J, Hyeon T. Recent progress in the synthesis of porous carbon materials. Adv Mater 2006;18(16):2073-94.

[11] Marco-Lozar JP, Kunowsky M, Suárez-García F, Carruthers JD, Linares-Solano A. Activated carbon monoliths for gas storage at room temperature. Energy Environ Sci 2012;5(12):9833-42.

[12] Linares-Solano A, Jordá-Beneyto M, Kunowsky M, Lozano-Castelló D, Suárez-García F, Cazorla-Amorós D. Hydrogen Storage in Carbon Materials. In: Terzyk AP, Gauden PA, Kowalczyk P, eds. Carbon Materials: Theory and Practice. Kerala: Research Signpost; 2008 p. 245-81.

[13] Bansal RC, Donnet J, Stoeckli F. Active Carbon. New York: Dekker; 1988.

[14] Rodríguez-Reinoso F, Molina-Sabio M. Activated carbons from lignocellulosic materials by chemical and/or physical activation: an overview. Carbon 1992;30(7):1111-8.

[15] Puziy AM, Tascón JMD. Adsorption by phosphorous-containing carbons. In: Tascon JMD, ed. Novel Carbon Adsorbents. Amsterdam, The Netherlands: Elsevier; 2012 p. 245-67.

[16] Ahmadpour A, Do DD. The preparation of active carbons from coal by chemical and physical activation. Carbon 1996;34(4):471-9.

[17] Linares-Solano A, Lozano-Castelló D, Lillo-Ródenas MA, Cazorla-Amorós D. Carbon activation by alkaline hydroxides: preparation and reactions, porosity and performance. In: Radovic LR, ed. Chemistry and Physics of Carbon. Boca Raton: CRC Press; 2007 p. 1-62.

[18] Miura K, Hayashi J, Hashimoto K. Production of molecular sieving carbon through carbonization of coal modified by organic additives. Carbon 1991;29(4–5):653-60.

[19] Nakagawa H, Watanabe K, Harada Y, Miura K. Control of micropore formation in the carbonized ion exchange resin by utilizing pillar effect. Carbon 1999;37(9):1455-61.

[20] Villar-Rodil S, Denoyel R, Rouquerol J, Martínez-Alonso A, Tascón JMD. Fibrous carbon molecular sieves by chemical vapor deposition of benzene. Gas separation ability. Chem Mater 2002;14(10):4328-33.

[21] Villar-Rodil S, Navarrete R, Denoyel R, Albiniak A, Paredes JI, Martínez-Alonso A, et al. Carbon molecular sieve cloths prepared by chemical vapour deposition of methane for separation of gas mixtures. Microporous Mesoporous Mat 2005;77(2-3):109-18.

[22] Marsh H, Rand B. The process of activation of carbons by gasification with CO_2-II. The role of catalytic impurities. Carbon 1971;9(1):63-77.

[23] Tamai H, Kakii T, Hirota Y, Kumamoto T, Yasuda H. Synthesis of extremely large mesoporous activated carbon and its unique adsorption for giant molecules. Chem Mater 1996;8(2):454-62.

[24] Hulicova D, Oya A. The polymer blend technique as a method for designing fine carbon materials. Carbon 2003;41(7):1443-50.

[25] Pekala RW. Organic aerogels from the polycondensation of resorcinol with formaldehyde. J Mater Sci 1989;24(9):3221-7.

[26] Lewis JS, Vaidyaraman S, Lackey WJ, Agrawal PK, Freeman GB, Barefield EK. Chemical vapor deposition of boron-carbon films using organometallic reagents. Mater Lett 1996;27(6):327-32.

[27] Attard GS, Glyde JC, Goltner CG. Liquid-crystalline phases as templates for the synthesis of mesoporous silica. Nature 1995;378(6555):366-8.

[28] Ma T-Y, Liu L, Yuan Z-Y. Direct synthesis of ordered mesoporous carbons. Chem Soc Rev 2013;42(9):3977-4003.

[29] Knox JH, Kaur B, Millward GR. Structure and performance of porous graphitic carbon in liquid chromatography. J Chromatogr A 1986;352(0):3-25.

[30] Zhao DY, Feng JL, Huo QS, Melosh N, Fredrickson GH, Chmelka BF, et al. Triblock copolymer syntheses of mesoporous silica with periodic 50 to 300 angstrom pores. Science 1998;279(5350):548-52.

[31] Kim TW, Kleitz F, Paul B, Ryoo R. MCM-48-like large mesoporous silicas with tailored pore structure: Facile synthesis domain in a ternary triblock copolymer-butanol-water system. J Am Chem Soc 2005;127(20):7601-10.

[32] Beck JS, Vartuli JC, Roth WJ, Leonowicz ME, Kresge CT, Schmitt KD, et al. A new family of mesoporous molecular-sieves prepared with liquid-crystal templates. J Am Chem Soc 1992;114(27):10834-43.

[33] Ryoo R, Joo SH, Jun S. Synthesis of highly ordered carbon molecular sieves via template-mediated structural transformation. J Phys Chem B 1999;103(37):7743-6.

[34] Lee J, Yoon S, Hyeon T, Oh SM, Kim KB. Synthesis of a new mesoporous carbon and its application to electrochemical double-layer capacitors. Chem Commun 1999;(21):2177-8.

[35] Lu AH, Li WC, Schmidt W, Kiefer W, Schüth F. Easy synthesis of an ordered mesoporous carbon with a hexagonally packed tubular structure. Carbon 2004;42(14):2939-48.

[36] Kruk M, Jaroniec M, Kim T-W, Ryoo R. Synthesis and Characterization of Hexagonally Ordered Carbon Nanopipes. Chem Mater 2003;15(14):2815-23.

[37] Darmstadt H, Roy C, Kaliaguine S, Kim T-W, Ryoo R. Surface and pore structures of CMK-5 ordered mesoporous carbons by adsorption and surface spectroscopy. Chem Mater 2003;15(17):3300-7.

[38] Stein A, Wang ZY, Fierke MA. Functionalization of porous carbon Materials with designed pore architecture. Adv Mater 2009;21(3):265-93.

[39] Yasuda Ei, Inagaki M, Kaneko K, Endo M, Oya A, Tanabe Y, eds. Carbon Alloys. Novel Concepts to Develop Carbon Science and Technology. Amsterdam: Elsevier; 2003.

[40] Serp P, Figueiredo JL, eds. Carbon materials for catalysis. New Jersey: New Jersey : Wiley; 2009.

[41] Burchell TD. Carbon Materials for Advanced Technologies. Amsterdam: Pergamon; 1999.

[42] Inagaki M. New carbons. Control of structure and functions. Oxford: Elsevier; 2000.

[43] Beguin F, Frackowiak E, eds. Carbons for Electrochemical Energy Storage and Conversion Systems. Boca Raton: CRC Press, Taylor & Francis Group; 2010.

[44] Burchell TD, ed. Carbon Materials for Advanced Technologies. Amsterdam: Pergamon 1999.

[45] Tascón JMD, ed. Novel Carbon Adsorbents. Amsterdam, The Netherlands: Elsevier; 2012.

[46] Lu A, Kiefer A, Schmidt W, Schüth F. Synthesis of polyacrylonitrile-based ordered mesoporous carbon with tunable pore structures. Chem Mater 2004;16(1):100-3.

[47] Li W, Chen D, Li Z, Shi Y, Wan Y, Wang G, et al. Nitrogen-containing carbon spheres with very large uniform mesopores: The superior electrode materials for EDLC in organic electrolyte. Carbon 2007;45(9):1757-63.

[48] Xia YD, Mokaya R. Generalized and facile synthesis approach to N-doped highly graphitic mesoporous carbon materials. Chem Mater 2005;17(6):1553-60.

[49] Yang C-M, Weidenthaler C, Spliethoff B, Mayanna M, Schüth F. Facile template synthesis of ordered mesoporous carbon with polypyrrole as carbon precursor. Chem Mater 2004;17(2):355-8.

[50] Shin Y, Fryxell GE, Um W, Parker K, Mattigod SV, Skaggs R. Sulfur-functionalized mesoporous carbon. Adv Funct Mater 2007;17(15):2897-901.

[51] Pradhan BK, Sandle NK. Effect of different oxidizing agent treatments on the surface properties of activated carbons. Carbon 1999;37(8):1323-32.

[52] Cheng P-Z, Teng H. Electrochemical responses from surface oxides present on HNO3-treated carbons. Carbon 2003;41(11):2057-63.

[53] Peng L, Philippaerts A, Ke X, Van Noyen J, De Clippel F, Van Tendeloo G, et al. Preparation of sulfonated ordered mesoporous carbon and its use for the esterification of fatty acids. Catal Today 2010;150(1-2):140-6.

[54] Xing R, Liu Y, Wang Y, Chen L, Wu H, Jiang Y, et al. Active solid acid catalysts prepared by sulfonation of carbonization-controlled mesoporous carbon materials. Microporous Mesoporous Mat 2007;105(1–2):41-8.

[55] Mukhopadhyay SM, Pulikollu RV, Roy AK. Surface modification of a microcellular porous solid: carbon foam. Appl Surf Sci 2004;225(1–4):223-8.

[56] Boehm HP. Some aspects of the surface chemistry of carbon blacks and other carbons. Carbon 1994;32(5):759-69.

Capítulo 2:
Objetivos y organización de la memoria

2.1 OBJETIVOS

En la Introducción, Capítulo 1 de esta tesis, se ha destacado que para mejorar el comportamiento de un material carbonoso en una determinada aplicación es necesario adaptar y optimizar sus propiedades en base a esa aplicación específica. En este sentido, el desarrollo de materiales de carbono dopados con heteroátomos, con estructura y porosidad controladas, adquiere un especial interés debido a la mejora de propiedades que pueden presentar con respecto a los materiales no dopados.

El ordenamiento tanto de la estructura como de la textura porosa de un material presenta una serie de ventajas; por un lado, favorece la accesibilidad y difusión de las moléculas y, por otro, permite ajustar el tamaño de los poros a las dimensiones requeridas en la aplicación. La presencia de grupos funcionales superficiales es fundamental desde un punto de vista práctico, ya que esos grupos no sólo modifican las propiedades del material de carbono sino que además pueden participar activamente en el proceso. Por tanto, la síntesis de este tipo de materiales está asociada inevitablemente a la búsqueda y desarrollo de nuevos precursores y métodos de síntesis avanzados. Idealmente, éstos deben permitir el ajuste y optimización simultáneos de todas las propiedades del material, entre ellas su porosidad, estructura y química superficial.

De este modo, en la presente tesis doctoral se plantea como objetivo general la ***preparación de materiales de carbono mesoporosos dopados con heteroátomos mediante técnicas de nanomoldeo*.**

Dicho objetivo general se aborda desde dos estrategias diferentes, en base a las cuales la memoria se divide en dos bloques:

SÍNTESIS DE CARBONES MESOPOROSOS ORDENADOS DOPADOS CON HETEROÁTOMOS MEDIANTE DEPÓSITO QUÍMICO EN FASE VAPOR EN SÍLICES MESOPOROSAS (Capítulo 4):

Mediante esta primera estrategia se han preparado carbones dopados con oxígeno y/o nitrógeno. Para ello se han seguido dos aproximaciones:

i) Funcionalización mediante oxidación de carbones mesoporosos ordenados preparados por CVD

ii) Síntesis directa de carbones dopados con nitrógeno mediante la utilización de precursores que contengan dicho heteroátomo.

La introducción de grupos superficiales oxigenados en materiales de carbono es una metodología bien conocida. Sin embargo, no ha sido estudiada en profundidad para carbones mesoporosos ordenados. Los métodos de oxidación de carbones son, en general, procedimientos agresivos, que pueden modificar tanto la estructura como la porosidad del carbón. Por ello, es necesario realizar un estudio sistemático de los efectos de los tratamientos de oxidación en este tipo de materiales, centrando la atención en preservar su estructura mesoporosa ordenada a la vez que se introduce la mayor cantidad posible de funcionalidades oxigenadas.

La segunda aproximación se basa en el uso de precursores que contengan nitrógeno, como es el caso del acetonitrilo utilizado en esta tesis. En este método es esencial investigar las diferentes variables involucradas en la síntesis, de modo que no sólo se introduzcan átomos de nitrógeno, sino que la replicación de la plantilla se realice correctamente.

Los **objetivos específicos** de este bloque son los siguientes:

- Establecer las condiciones óptimas de oxidación que permitan introducir diferentes funcionalidades oxigenadas preservando la estructura mesoporosa inicial del carbón.
- Establecer las condiciones óptimas del proceso de depósito químico en fase vapor con acetonitrilo, que permitan introducir diferentes funcionalidades de nitrógeno y obtener finalmente un carbón mesoporoso ordenado.
- Identificar y cuantificar los diferentes grupos superficiales introducidos en ambos procesos.

SÍNTESIS DE CARBONES MESOPOROSOS ORDENADOS DOPADOS CON HETEROÁTOMOS POR INFILTRACIÓN EN FASE LÍQUIDA DE NUEVOS PRECURSORES (Capítulo 5):

En este bloque se aborda la búsqueda de nuevos precursores orgánicos para la síntesis de materiales de carbono mediante la técnica de nanomoldeo utilizando sílices como plantillas ("*hard-templating*"). La novedad introducida por esta tesis es el uso de poliamidas como precursores para la obtención de carbones dopados. Las poliamidas se pueden sintetizar a partir de monómeros tipo aminoácido con estructura química alifática o aromática. Dichos precursores se caracterizan por poseer nitrógeno y oxígeno, por lo que los carbones resultantes estarán dopados con ambos heteroátomos. Dada la amplia variedad de precursores disponibles y métodos sintéticos aplicables, con este trabajo se abre una nueva vía para la síntesis de carbones porosos ordenados y dopados con heteroátomos. Esta parte de la tesis constituye el bloque central de la misma, ya que en él se aborda la búsqueda de los nuevos precursores, el estudio detallado de la infiltración de las plantillas, la polimerización de los precursores en presencia de la plantilla y los procesos de carbonización bajo distintas condiciones, incluyendo el tratamiento térmico en presencia de ácido fosfórico.

Los **objetivos específicos** dentro de este segundo bloque son:

- Identificar y seleccionar los compuestos químicos más adecuados para su uso como precursores de poliamidas en la síntesis de carbones porosos ordenados
- Optimizar las condiciones de infiltración de la plantilla con el precursor para maximizar la cantidad de éste introducida.
- Optimizar las condiciones de polimerización de los precursores en presencia de la plantilla.
- Establecer las condiciones idóneas del proceso de carbonización de los materiales compuestos polímero/plantilla inorgánica, tanto en ausencia como en presencia de aditivos químicos (H_3PO_4), para la obtención de carbones ordenados y dopados con distintos heteroátomos (N, O y P).
- Identificar y cuantificar los diferentes grupos superficiales introducidos y relacionarlos con las variables de síntesis.

En los dos bloques que componen esta tesis se ha planteado como **objetivo adicional** la evaluación del efecto de los distintos heteroátomos (cantidad y naturaleza de los grupos funcionales superficiales) en distintas aplicaciones de

interés actual, como son la captura de CO_2, la eliminación de colorantes en disolución y la liberación controlada de medicamentos.

2.2 ORGANIZACIÓN DE LA MEMORIA

En el **Capítulo 1** de esta memoria se revisan las diferentes estrategias existentes para la síntesis de carbones porosos mediante la técnica de nanomoldeo. Asimismo, se presentan los métodos más relevantes para la preparación de carbones dopados con heteroátomos. En el **Capítulo 2** se plantean los objetivos del trabajo y la organización de la memoria. En el **Capítulo 3** se exponen los diferentes métodos de síntesis y técnicas de caracterización utilizadas. En los **Capítulos 4 y 5** se exponen y discuten los resultados obtenidos. La presente memoria se presenta como un compendio de artículos. El trabajo desarrollado ha dado lugar a 6 artículos que se separan en dos bloques acordes con los objetivos planteados. Los índices de calidad de las revistas en las que se han publicado los artículos, así como el puesto que ocupan dentro del área correspondiente, están recogidos en la **Tabla 2.1**.

Finalmente, el **Capítulo 7** recoge las conclusiones generales derivadas del presente trabajo.

Tabla 2.1.

Parámetros de calidad de las revistas científicas en las que han sido publicados los artículos recogidos en la memoria.

Capítulo	Publicación	Factor de Impacto	Área	Percentil (posición/ área)
IV	Surface modification of nanocast ordered mesoporous carbons through a wet oxidation method. ***Carbon 2013;62:193-203***	6.16	Materials Science, Multidiscipl.	Q1 (24/251)
	Synthesis, characterization and dye removal capacities of N-doped mesoporous carbons. ***Enviado a publicación***	--	--	--
V	Aromatic polyamides as new precursors of nitrogen and oxygen-doped ordered mesoporous carbons***. Carbon 2014;70:119-29.***	6.16	Materials Science, Multidiscipl.	Q1 (24/251)
	pH-responsive ordered mesoporous carbons for controlled ibuprofen release. ***Enviado a publicación***	--	--	--
	Evolution of the complex surface chemistry in mesoporous carbons obtained from polyaramide precursors. ***Appl Surf Sci 2014;299:19-28.***	2.538	Materials Science, Coatings and films	Q1 (1/18)
	Influence of porous texture and surface chemistry on the CO_2 adsorption capacity of porous carbons: acidic and basic site interactions. ***ACS Appl Mater Interfaces.*** **DOI: 10.1021/am506176e**	5.900	Materials Science, Multidiscipl.	Q1 (26/251)

Fuente : Journal Citation Reports 2014.

Capítulo 3:
Procedimiento experimental

3.1 SÍNTESIS DE MATERIALES

3.1.1 Síntesis de sílices mesoporosas

En este trabajo se seleccionó la sílice mesoporosa SBA-15 como plantilla. Esta sílice fue preparada siguiendo el método descrito por Zhao et al. [1]. Para ello, 10.44 g de Pluronic P123 (Mw= 5800, Aldrich) fueron añadidos a una disolución acuosa conteniendo 52.5 mL de HCl (37%, Merck). Tras disolver completamente el polímero, se añadieron gota a gota 22.64 g de tetraetilortosilicato (TEOS; 98%, Aldrich) y la mezcla fue mantenida bajo agitación a 40 °C durante 4 horas. La composición molar de la mezcla de reacción inicial fue 0.017 P123 / 1 TEOS / 145.8 H_2O / 6.04 HCl. Esta mezcla fue tratada a 125 °C en autoclave durante 72 horas. El producto obtenido fue filtrado y calcinado en aire a 550 °C durante 6 horas, constituyendo finalmente la sílice mesoporosa SBA-15. La **Figura 3.1** resume el procedimiento experimental empleado.

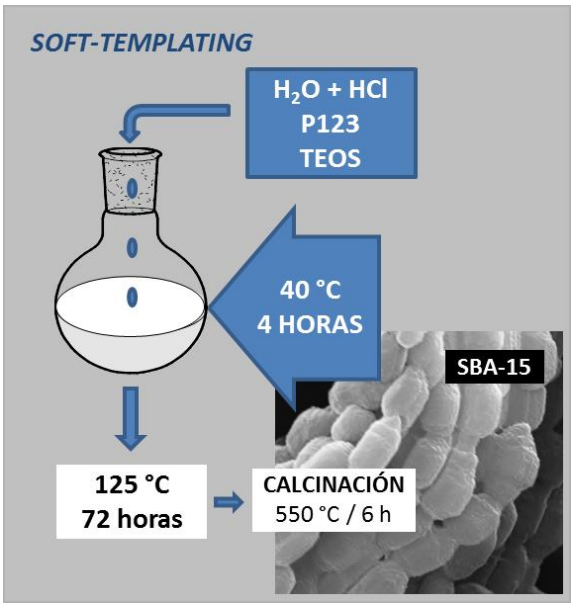

Figura 3.1.

Esquema del procedimiento experimental utilizado en la síntesis de la sílice mesoporosa SBA-15.

3.1.2 Síntesis de carbones mesoporosos

3.1.2.1 Depósito químico en fase vapor

Carbones mesoporosos ordenados no dopados

Para obtener carbones mesoporosos ordenados (CMOs) no dopados por depósito químico en fase vapor (CVD) se utilizó propileno como fuente de carbono. 1 g de SBA-15 fue colocado en la placa porosa central de un reactor vertical de cuarzo. Bajo un flujo de argón (99.999% pureza), el reactor fue calentado hasta 750 °C a razón de 10 °C/min. Una vez alcanzada dicha temperatura, se hizo pasar a través del reactor un flujo de propileno en argón (99.5% pureza; concentración 9.6% v/v) que fue mantenido durante 6 horas. Después de esta etapa de pirolisis del propileno, se llevó a cabo una etapa de carbonización adicional bajo un flujo de argón (99.999% pureza), calentando el reactor a 5 °C/min hasta 900 °C y manteniendo esta temperatura durante 2 horas.

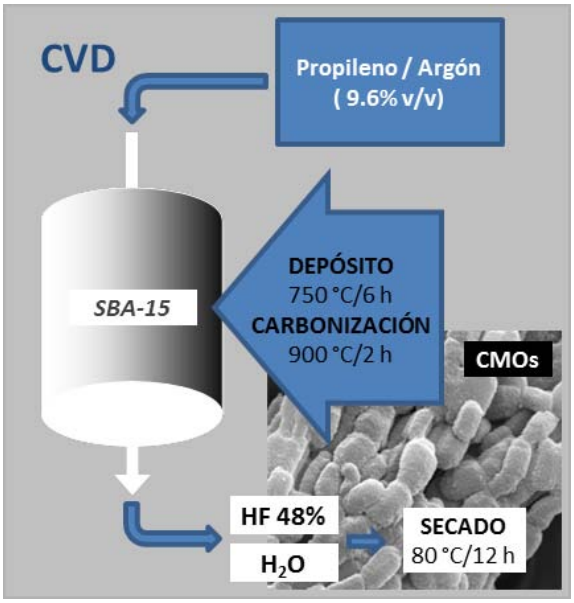

Figura 3.2.

Esquema del procedimiento experimental utilizado en la síntesis de CMOs no dopados por CVD.

El composite carbón/sílice resultante fue tratado con HF (48%, Merck) a temperatura ambiente para eliminar la plantilla de sílice. El residuo fue filtrado y lavado varias veces con agua desionizada (MilliQ) y secado a 80 °C durante 12 horas, obteniéndose finalmente un CMO tipo CMK-3. En la **Figura 3.2** se puede observar un esquema del procedimiento experimental utilizado.

Carbones mesoporosos ordenados dopados con nitrógeno

En la síntesis por CVD de carbones mesoporosos dopados con nitrógeno (N-CMOs) se utilizó acetonitrilo como fuente simultánea de carbono y nitrógeno. Típicamente, 0.5 g de SBA-15 fueron colocados en la placa porosa central de un reactor vertical de cuarzo. El sistema fue calentado hasta 850 °C bajo un flujo de argón (99.999% pureza) aplicando una velocidad de calentamiento de 10 °C/min. Tras alcanzar esta temperatura, se hizo pasar a través del reactor un flujo de argón saturado con acetonitrilo (situado en un matraz termostático a 25 °C) durante diferentes periodos de tiempo.

La concentración de acetonitrilo fue calculada a partir de la *Ecuación de* A*ntoine* (**Ecuación 3.1**):

$$\log P_{vap} = A - \frac{B}{T+C} \qquad \text{(Ecuación 3.1)}$$

, siendo P_{vap} la presión de vapor del acetonitrilo (expresada en mmHg), *A*, *B* y *C* las constantes de Antoine para el acetonitrilo (*A*= 7.0733, *B*= 1279.2 y *C*= 224.01) y T la temperatura del saturador que lo contiene (25 °C). Con estos datos, se calculó una presión de vapor para el acetonitrilo de 86.37 mmHg. Teniendo en cuenta los diferentes flujos de argón que fueron pasados por el saturador, la concentración de acetonitrilo (expresada como porcentaje en volumen) fue determinada dividiendo el volumen de acetonitrilo por el volumen total. Los valores de concentración y los tiempos de CVD a 850 ºC utilizados para cada concentración se encuentran detallados en la **Tabla 3.1**:

Tabla 3.1.

Condiciones experimentales usadas en la síntesis de N-CMOs por CVD: concentración de acetonitrilo y tiempo de depósito.

	Concentración (% v/v)		
	3.0	*6.5*	*8.8*
Tiempo de depósito (horas)	5; 6; 7	2; 3; 4	2; 3; 4

Los composites carbón/sílice obtenidos en los experimentos de CVD fueron tratados con HF (48%, Merck) a temperatura ambiente durante 12 horas, lavados

repetidamente con agua desionizada (MilliQ) y secados a 80 °C durante 12 horas. En la **Figura 3.3** se muestra un esquema detallado del procedimiento de síntesis.

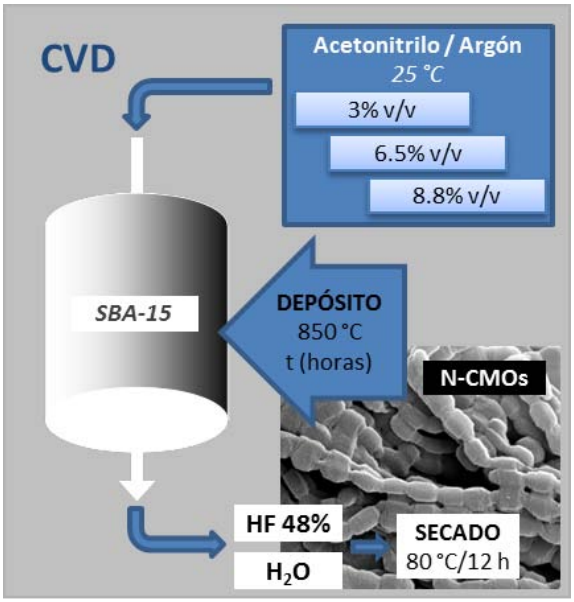

Figura 3.3.

Esquema del procedimiento experimental utilizado en la síntesis de N-CMOs por CVD.

3.1.2.2 Infiltración líquida

Los precursores de poliamidas, en concreto el ácido 3-aminobenzoico (MABA) y el ácido 4-aminobenzoico (PABA), también fueron usados por primera vez en esta tesis para la obtención de carbones mesoporosos ordenados dopados con nitrógeno y oxígeno (N,O-CMOs). En este sentido, se usaron dos métodos de infiltración en fase líquida de la plantilla, que denominaremos aquí: i) Síntesis en fase orgánica y ii) Polimerización térmica en estado sólido. Ambos métodos se basan en la infiltración de la sílice con el monómero MABA en fase líquida y su polimerización dentro de los poros de la plantilla.

Polimerización en fase orgánica: Reacción de Yamazaki

Una de las vías por las que se obtuvieron N,O-CMOs fue a través de la polimerización de precursores de poliamidas mediante la reacción de Yamazaki. Dicha reacción describe la obtendión de poli-*p*-benzamida por policondensación directa del ácido 4-aminobenzoico (PABA) usando fosfitos en presencia de sales metálicas [2]. En la presente Tesis se utilizó para la polimerización del MABA, como

se describe a continuación. La infiltración fue realizada in situ añadiendo SBA-15 al medio de reacción seguida de la reacción de Yamazaki para la síntesis del polímero (poliamida) dentro de la porosidad de la plantilla. En la **Figura 3.4** se representa esquemáticamente el procemiento experimental seguido: 1 g de SBA-15 fue colocado en un matraz de tres bocas y desgasificado a 150 °C aplicando vacío durante 2 horas. Tras ser enfriada la sílice a temperatura ambiente, se hizo pasar a través del matraz un flujo de nitrógeno (100 mL/min) para mantener el sistema en atmósfera inerte. Se añadieron 20 mL de N-metilpirrolidona (NMP; 99.99%, Sigma-Aldrich) y se agitaron vigorosamente junto con la SBA-15 hasta obtener una suspensión homogénea.

Figura 3.4.

Obtención de N,O-CMOs mediante la reacción de Yamazaki.

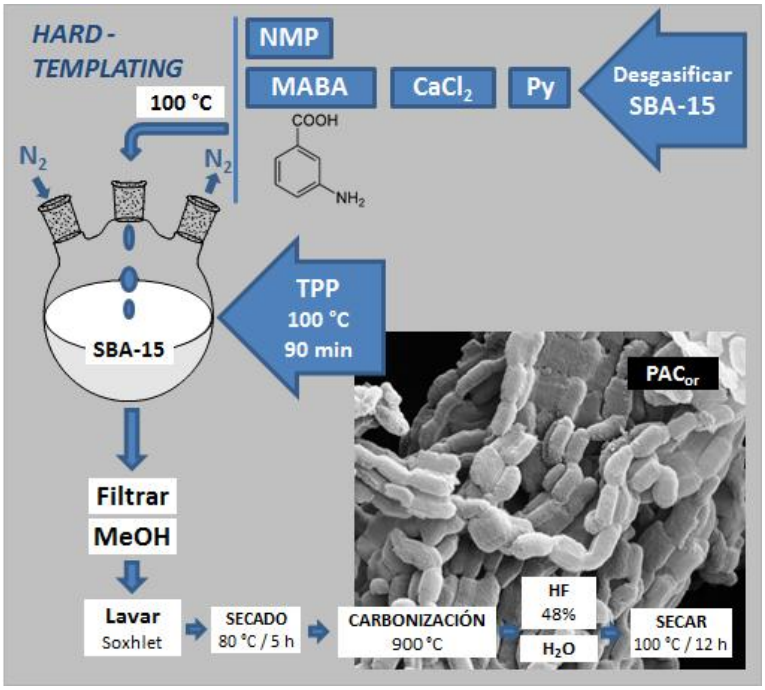

Después se añadieron sucesivamente 2.76 g de MABA (99%, Across), 1.5 g de dicloruro de calcio ($CaCl_2$; 93%, Sigma-Aldrich) y 14.5 mL de piridina (Py; 99%, Sigma-Aldrich), y se continuó agitando vigorosamente hasta que se disolvieron completamente los reactivos en el medio de reacción. Posteriormente, la mezcla fue calentada a 100 °C manteniendo la agitación constante. Una vez la disolución adquirió aspecto transparente, se añadieron 5.40 mL de trifenilfosfito (TPP; 97%, Sigma-Aldrich) para catalizar la polimerización del monómero. Cuando

transcurrieron 90 min desde la adición del catalizador, el producto final fue enfriado hasta temperatura ambiente. Se filtró para eliminar el exceso de polímero y se añadieron 100 mL de metanol (Rectapur, Prolabo) sobre el sólido filtrado. El composite polímero/sílice obtenido de esta forma fue lavado en un soxhlet con metanol durante 4 horas y fue finalmente secado a 80 °C durante 5 horas. El composite polímero/sílice seco fue carbonizado bajo un flujo de argón (500 mL/min) hasta 900 °C a 10 °C/min. La plantilla de sílice fue eliminada con HF (48%, Fluka) y el carbón final obtenido (N,O-CMO) fue secado a 100 °C durante 12 horas.

Polimerización térmica en estado sólido

El segundo método de obtención de N,O-CMOs a partir de precursores de poliamidas por infiltración líquida se basa en la polimerización térmica en estado sólido de dos monómeros: el ácido 3-aminobenzoico (MABA) y el ácido 4-aminobenzoico (PABA).

En este procedimiento de síntesis, representado esquemáticamente en la **Figura 3.5**, 1 g de SBA-15 fue colocado en un rotavapor y desgasificado a vacío calentando a 150 °C durante 2 horas. Tras enfriar la sílice hasta temperatura ambiente, se añadió sobre ella una disolución conteniendo una determinada cantidad de monómero disuelta en acetona: MABA (1.20, 1.40, 1.55, 1.70 o 1.75 g; 99%, Across) o PABA (1.20 g; 99%, Sigma-Aldrich). El volumen de disolución se seleccionó de manera que fuera adsorbido hasta humedad incipiente de la plantilla. En todos los casos, el disolvente fue eliminado a vacío y los composites sílice-MABA fueron polimerizados y carbonizados bajo un flujo de argón (500 mL/min) aplicando un tratamiento térmico en dos pasos: i) Una primera etapa isotérmica, por debajo del punto de ebullición de los monómeros (MABA o PABA), a 160 °C durante 1 hora (velocidad de calentamiento de 2 °C/min), para polimerizar térmicamente el monómero en los canales de la plantilla de sílice; ii) Una segunda etapa de carbonización, en la que se aumentó la temperatura hasta 700, 800 o 900 °C con una velocidad de calentamiento de 10 °C/min. Los composites carbonizados fueron también tratados con HF (48%, Merck) y secados a 100 °C durante 12 horas.

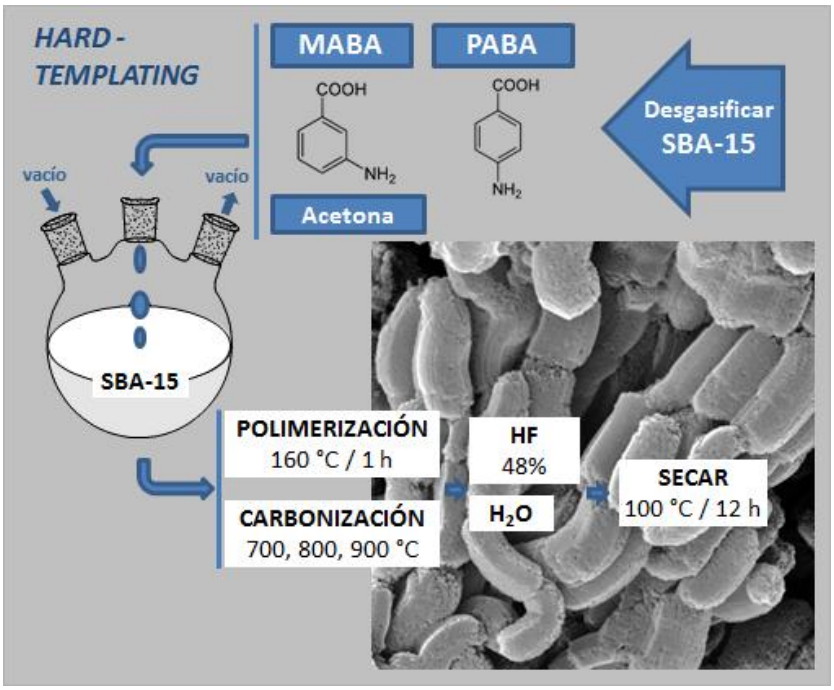

Figura 3.5.

Obtención de N,O-CMOs mediante polimerización térmica en estado sólido.

Polimerización térmica y carbonización en presencia de H_3PO_4

Este procedimiento de síntesis se basa en el de polimerización térmica en estado sólido, descrita en el apartado anterior, pero realizando la carbonización del composite MABA/sílice en presencia de H_3PO_4. Permite obtener carbones mesoporosos ordenados dopados con diferentes cantidades de nitrógeno, oxígeno y fósforo en función de la cantidad de H_3PO_4 utilizada y la temperatura de carbonización. En la **Figura 3.6** se expone un esquema del procedimiento experimental seguido.

Después de la polimerización a 160 °C durante 1 hora, se añadió sobre el composite una disolución acuosa con diferente concentración de H_3PO_4 (85%; ACS reagent, Sigma-Aldrich): 5, 50 y 150% en peso respecto el contenido de MABA en el composite. La mezcla obtenida fue carbonizada bajo un flujo de nitrógeno (150 mL/min) a la temperatura final de 700, 800 o 900 °C. Los composites carbonizados fueron lavados en un soxhlet con agua destilada hasta alcanzar un valor de conductividad inferior a 3 µS/cm, con el objetivo de eliminar el exceso de ácido fosfórico y los productos generados en su descomposición térmica o por reacción con el precursor.

Todos los composites carbonizados fueron finalmente tratados con HF (48%, Fluka) a temperatura ambiente para eliminar la plantilla de sílice, fueron lavados repetidamente con agua desionizada (MilliQ) y secados en un horno a 100 °C durante 12 horas.

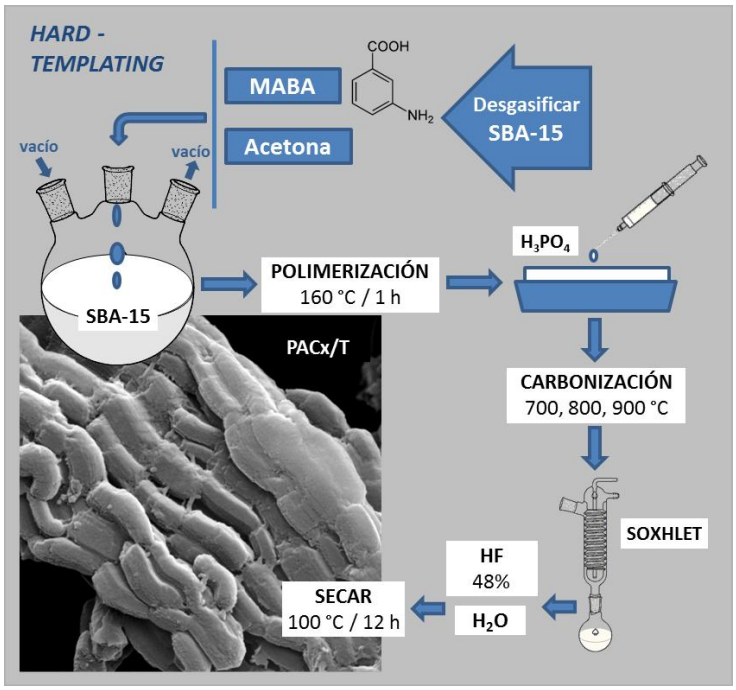

Figura 3.6.

Obtención de CMOs dopados con N, O y P mediante polimerización térmica en estado sólido en presencia de ácido fosfórico.

3.1.3 Tratamientos post-síntesis: Oxidación con HNO_3 y H_2O_2

Los tratamientos post-síntesis de oxidación fueron llevados a cabo para modificar la química superficial de los carbones mesoporosos no-dopados obtenidos por CVD. La oxidación de los carbones (CMOs) se realizó en fase líquida aplicando condiciones experimentales con diferente fuerza oxidante, tratando de evitar la modificación tanto de su estructura ordenada como de su textura porosa.

Tal y como indica el esquema experimental de la **Figura 3.8**, un CMO no dopado obtenido por CVD (síntesis detallada en el **Apartado 3.1.2.1** de este capítulo) fue sometido a dos tratamientos de oxidación en condiciones suaves y tres tratamientos en condiciones fuertes de oxidación. En todos ellos, se partió de 1 g de carbón seco (80 °C, 16 horas) al que se añadieron 150 mL de agente oxidante, H_2O_2

(30% vol, Merck) o HNO_3 (0.5; 2; 5 y 14.55 M; Sigma-Aldrich). Los carbones resultantes fueron lavados en un soxhlet con agua desionizada (MilliQ) hasta alcanzar un valor de conductividad inferior a 3 µS/cm y finalmente fueron secados a 80 °C durante 12 horas.

Figura 3.8.

Esquema experimental de los tratamientos de oxidación efectuados sobre un CMO no dopado obtenido por CVD.

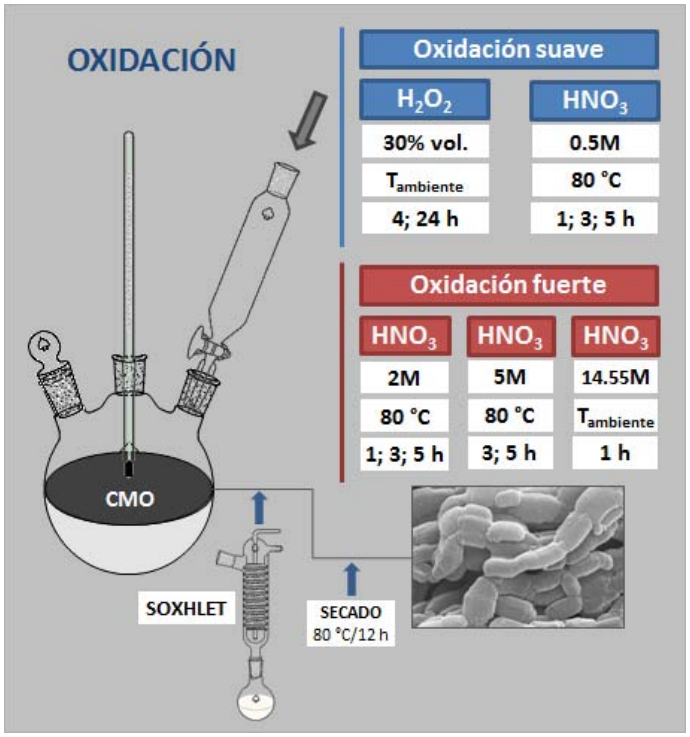

3.2 CARACTERIZACIÓN DE MATERIALES

3.2.1 Caracterización textural

3.2.1.1 Adsorción física de gases

La adsorción física de gases o fisisorción es una de las técnicas más utilizadas en la caracterización de la textura porosa de los materiales. Se trata de un fenómeno fundamentalmente superficial y termodinámico en el que intervienen dos fases: la superficie sólida (adsorbente) y el gas o vapor (adsorbato). Tras poner ambas fases en contacto, las moléculas de gas se acumulan espontáneamente ($\Delta G<0$) en la superficie del sólido y forman una interfase de espesor δ.

Tipos de isotermas y clasificación de ciclos de histéresis

Las isotermas de adsorción/desorción son curvas obtenidas a partir de las medidas de adsorción/desorción de un gas sobre un sólido a temperatura constante. En ellas se representa la cantidad adsorbida de gas (mmol o cm^3 de gas por gramo de adsorbente) en función de la presión. Cuando el gas se adsorbe en condiciones sub-críticas, la presión se suele expresar como presión relativa, P/P_0, siendo P la presión absoluta y P_0 la presión de saturación del gas (presión de vapor del adsorbato a la temperatura del experimento).

Las isotermas de adsorción se clasifican normalmente en función del criterio fijado por la IUPAC en 1985 [3]. Este criterio realiza una clasificación fenomenológica de las isotermas en función de su forma, definiendo 6 grupos.

Los diferentes tipos de isotermas pueden encontrarse en la **Figura 3.9**:

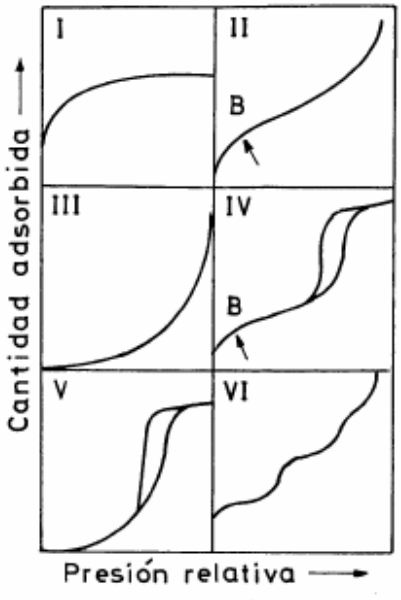

Figura 3.9.

Tipos de isotermás de adsorción según la definición IUPAC.

- La ***isoterma tipo I*** se caracteriza por el aumento de la adsorción inicial hasta alcanzar una meseta. Es característica de un proceso de fisisorción en sólidos microporosos o de un proceso de quimisorción con un determinado número de centros activos que son ocupados progresivamente por las especies adsorbidas. En el proceso de fisisorción, la adsorción máxima se corresponde con el volumen de

microporos de la muestra; cuando se llenan los microporos el proceso finaliza y la adsorción en la superficie externa se puede considerar despreciable.

- Las ***isotermas tipo II*** tienen forma sigmoidal, diferenciándose 3 tramos: un primer tramo en que se produce un rápido aumento de la adsorción, un segundo tramo casi lineal con menor pendiente y un último tramo ascendente. El denominado punto B marca el comienzo del segmento lineal. Éste indica que la monocapa está completa y comienza a adsorberse la segunda capa de moléculas de gas, por lo cual el punto B es importante en el cálculo de la superficie específica. Estas isotermas son características de sólidos macroporosos o no porosos.

- Las ***isotermas tipo III*** son convexas hacia el eje de abscisas. Se obtienen para sólidos no porosos en los que la interacción adsorbente-adsorbato es muy débil. Al principio de la isoterma se observa un ligero aumento de cantidad adsorbida con la presión, y cuando existen moléculas de gas adsorbidas, la interacción adsorbato-adsorbente hace que la curvatura de la isoterma aumente. Como este tipo de isotermas no tiene punto B, no es adecuado para el cálculo de la superficie específica del material. Un ejemplo típico es el sistema sílice-agua.

- Las ***isotermas tipo IV*** son parecidas a las de tipo II pero presentan dos diferencias importantes debido a la presencia de mesoporos:

    - La aproximación a P/P_0 no es asintótica sino que se produce con un determinado ángulo. Se debe a que los poros están llenos de líquido condensado y la adsorción tiene lugar sólo en la superficie externa, más pequeña.

    - Existe un ciclo de histéresis asociado a la condensación capilar en los mesoporos, generada cuando los mecanismos de condensación y evaporación siguen caminos diferentes.

La zona de la isoterma en la que se encuentra el punto B no se ve afectada por la condensación capilar (que normalmente ocurre para presiones relativas superiores a 0.4), y por ello son isotermas adecuadas para el cálculo de superficies específicas.

- Las ***isotermas tipo V*** se dan en sólidos mesoporosos en los que la interacción adsorbente-adsorbato es muy débil. Son raras y poco adecuadas para el análisis de superficies específicas.

- Las ***isotermas tipo VI*** se pueden considerar como una variante de las de tipo II en superficies muy homogéneas. Se obtienen para materiales con diferencias muy marcadas entre los calores de adsorción de la primera capa y el resto, y entre capas sucesivas a partir de la segunda.

De entre los 6 tipos de isotermas, las de tipo IV son especialmente importantes en la caracterización textural de los materiales mesoporosos tratados en este trabajo. En ellas se distinguen 4 zonas principales:

1) *Zona I:* A valores bajos de presión relativa, las moléculas de gas llenan la microporosidad del material y se forma una monocapa.

2) *Zona II*: Existe una relación lineal entre cantidad adsorbida y espesor de la cobertura del gas. Se forman multicapas de gas adsorbido sobre la monocapa inicial.

3) *Zona III:* A valores intermedios de presión relativa se produce la condensación capilar del gas en el interior de los mesoporos. Como se observa en la **Figura 3.9**, existe un salto en la cantidad de gas adsorbido para un pequeño aumento del espesor de la multicapa. El valor de presión relativa al que se produce dicho salto depende del tamaño medio de poro del material.

4) *Zona IV* (no mostrada en la **Figura 3.9**): Existe una relación lineal entre la cantidad adsorbida y el espesor de la multicapa. Se atribuye a la adsorción de gas sobre la superficie externa del material en forma de multicapa, que conduce finalmente a la condensación por llenado del espacio que existe entre las partículas.

En este tipo de isotermas, adsorción y desorción siguen caminos diferentes debido a la condensación capilar que tiene lugar en los mesoporos; la desorción de un determinado volumen adsorbido se da a valores más bajos de presión relativa y esto genera un ciclo de histéresis.

Los ciclos de histéresis se clasifican empíricamente según la IUPAC [3] en cuatro tipos, tal y como se muestra en la **Figura 3.10**. Esta clasificación permite correlacionar cada tipo de histéresis con la textura del adsorbente. Los ciclos de histéresis tipo ***H1*** se asocian con materiales porosos que presentan distribuciones estrechas de poros cilíndricos y relativamente uniformes, así como con materiales aglomerados o compactos de partículas esféricas. Los ciclos de histéresis ***H2*** se obtienen para óxidos inorgánicos porosos y materiales con estructuras porosas complejas. La histéresis de tipo ***H3*** no presenta una adsorción limitante próxima a la presión de saturación, asociándose a agregados de partículas con forma de plato ("platelike") o ensamblajes de poros tipo rendija. Los ciclos de histéresis ***H4*** se observan generalmente en materiales con poros estrechos en forma de rendija y que además poseen microporos.

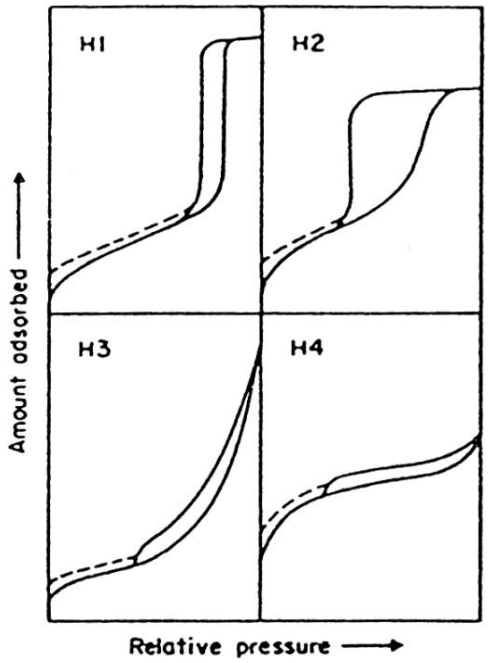

Figura 3.10. Clasificación de los ciclos de histéresis según la IUPAC.

El estudio de la textura porosa de los materiales se llevó a cabo mediante la aplicación de una serie de ecuaciones y modelos a las isotermas de adsorción de nitrógeno y dióxido de carbono. Las medidas de adsorción de N_2 se realizaron a -196 °C en dos aparatos volumétricos de adsorción: Micromeritics Asap 2010 y Quantachrome Autosorb-1. La adsorción de CO_2 fue llevada a cabo a 0 °C en un

equipo Quantachrome Nova 4200e. En ambos casos, aproximadamente 100-150 mg de muestra fueron previamente desgasificados a 150 °C (carbones) o 250 °C (sílices) durante 16 horas.

Determinación del área superficial específica. Modelo BET

La superficie específica de los materiales estudiados en esta tesis fue calculada mediante el método BET, desarrollado por Brunauer, Emmet y Teller [4]. Este método nos permite estimar el área superficial del sólido a partir de la cantidad de gas adsorbido en la monocapa y el área de cada molécula de gas. La cantidad de gas adsorbido en la monocapa (V_m) se puede calcular a partir de la **Ecuación 3.2**:

$$\frac{P}{V_{ads}\ P_0-P} = \frac{1}{V_m C} + \frac{C-1}{V_m C}\frac{P}{P_0} \qquad \text{(Ecuación 3.2)}$$

Siendo P (mmHg) la presión parcial del gas adsorbido, P_0 (mmHg) la presión de vapor del gas a la temperatura de adsorción, V_m (cm^3/g) el volumen de gas adsorbido formando la monocapa por gramo de adsorbente, C una constante que depende del calor de condensación y adsorción del adsorbato, y V_{ads} (cm^3/g) el volumen de gas adsorbido a la presión P por gramo de adsorbente. Representando $\frac{P}{V_{ads}\ P_0-P}$ frente a la presión relativa, P/P_0, se obtiene una recta con ordenada en el origen $\frac{1}{V_m C}$ y pendiente $\frac{C-1}{V_m C}$. Esta ecuación fue aplicada a los datos de adsorción contenidos en el intervalo de presiones relativas entre 0.05 y 0.3.

Determinación del volumen de microporos. Método de Dubinin-Raduskevich

La determinación del volumen de microporos se llevó a cabo aplicando el método propuesto por Dubinin-Radushkevich (DR) [5], a las isotermas de adsorción de N_2 a -196 °C y CO_2 a 0 °C en la zona de bajas presiones relativas. Se trata de un método empírico que permite estimar la microporosidad del material usando la energía de adsorción. La **ecuación DR** puede expresarse como sigue:

$$\log W = \log W_0 - 2.303 \left(\frac{RT}{\beta E_0}\right)^2 log^2 \frac{P^0}{P} \qquad \text{(Ecuación 3.3)}$$

Donde W (cm^3/g) es el volumen de gas condensado en los microporos a la temperatura T y presión relativa P/P_0 por gramo de adsorbente, W_0 (cm^3/g) es el volumen total de microporos accesibles al gas, β es el factor de afinidad adsorbato-

adsorbente respecto al benceno (β=1), que para el nitrógeno toma el valor de 0.34 y para el CO_2 el valor de 0.35, y E_0 (KJ/mol) es la energía característica de adsorción.

Representando gráficamente *log W* frente a $log^2 (P_0/P)$ se obtiene una recta cuya ordenada en el origen es $log\ W_0$. A partir del valor de la pendiente de la recta se puede calcular E_0. La región lineal de aplicabilidad de la ecuación DR a los datos de adsorción se limitó al intervalo de $P/P_0 < 0.1$ en el caso del nitrógeno y $P/P_0 < 0.03$ en el del dióxido de carbono (presión máxima medida).

El análisis conjunto de los resultados obtenidos a partir de las isotermas de adsorción de N_2 a -196 °C y CO_2 a 0 °C permitió conocer en profundidad la microporosidad de los materiales estudiados. Gracias a las isotermas de adsorción de N_2 se obtuvo información sobre la microporosidad total de los materiales, mientras que las isotermas de adsorción de CO_2 permitieron estimar el volumen de los microporos más estrechos o ultramicroporos, cuyo diámetro es inferior a 0.7 nm.

Distribuciones de tamaños de poro. Métodos BJH y DFT

La determinacion de las distribuciones de tamaños de poro (PSDs) de los materiales fue realizada a través de los métodos BJH y DFT. Los métodos usados para calcular las PSDs suponen que la isoterma obtenida experimentalmente se puede expresar como la suma de las isotermas de los poros individuales que constituyen la estructura porosa del sólido.

El método propuesto por Barrer, Joyner y Halenda (***método BJH***) [6], se basa en la ecuación de Kelvin (**Ecuación 3.4**) y considera los fenómenos de condensación capilar que aparecen para $P/P_0 > 0.4$. El aumento de la presión relativa provoca un aumento en el espesor de la capa de gas adsorbido, que puede ser calculado mediante:

$$\ln \frac{P}{P_0} = -\frac{2\gamma W_m}{RT\, r_m} \qquad \text{(Ecuación 3.4)}$$

Siendo r_m el radio para poros cilíndricos o la distancia entre láminas para poros tipo rendija, γ la tensión superficial, W_m el volumen molar y θ el ángulo de contacto. Las distribuciones de tamaños de poro se obtienen representando el volumen de poros

frente al tamaño de poro. Este método fue utilizado para analizar las PSDs de los materiales estudiados en el Artículo 2 de esta Tesis. Para ello, la **Ecuación 3.4** fue aplicada a la rama de desorción de las isotermas de N_2.

El método basado en la teoría del funcional de densidad (***método DFT***) [7, 8] supone que las moléculas adsorbidas en los poros tienden a empaquetarse según la fuerza de las interacciones con la superficie y con las otras moléculas de adsorbato. Esto hace que la densidad molar varíe en función del tamaño de poro y nos permite expresar la isoterma experimental de un sólido poroso en forma de una isoterma de adsorción generalizada (GAI). Una expresión de la misma se muestra en la **Ecuación 3.5**:

$$N\left(\frac{P}{P_0}\right) = \int_{W_{mín}}^{W_{máx}} N\left(\frac{P}{P_0}, W\right) * f(W) * dW \qquad \text{(Ecuación 3.5)}$$

, en la que $N\left(\frac{P}{P_0}\right)$ es la isoterma de adsorción experimental, *W* es la anchura de los poros, $N\left(\frac{P}{P_0}, W\right)$ es la isoterma de adsorción en un poro de anchura W, y $f(W)$ es la función de distribución de tamaños de poro.

La **Ecuación 3.5** indica que la isoterma total está formada por numerosas isotermas de poros individuales multiplicadas por su distribución relativa, aplicándola a un determinado intervalo de tamaños. Las isotermas individuales se obtienen por cálculos DFT *non-local*, definiendo primero un modelo molecular y describiéndolo mediante ecuaciones de mecánica estadística que se resuelven por métodos aproximados. Esto permite escribir una expresión aproximada para la energía libre como suma de dos contribuciones: una repulsiva de corto alcance (modelo de esferas rígidas) y otra atractiva de largo alcance. Para hallar el perfil de densidad de equilibrio, se genera un perfil de densidad, $\rho(r)$, y se minimiza la energía libre con respecto a $\rho(r)$. A partir de dicho perfil ya se puede calcular la energía libre, la isoterma de adsorción y otras propiedades de equilibrio.

El método DFT se aplica fácilmente a sistemas con geometrías sencillas y fluídos compuestos por moléculas esféricas. En las muestras analizadas en esta tesis se utilizaron los siguientes modelos DFT en condiciones de equilibrio: Non-Local Density Functional Theory (NLDFT) [9, 10], aplicado a poros con forma cilíndrica en

las sílices, y Quenching Solid Density Functional Theory (QSDFT) [11], usado en el caso de los carbones y considerando que sus poros tienen forma de rendija.

3.2.2 Caracterización estructural y morfológica

3.2.2.1 Difracción de rayos X

Mediante la técnica de difracción de rayos X (DRX) se puede caracterizar la estructura periódica o red cristalina de un sólido. Cuando un haz de rayos X incide sobre un material, parte del haz es reflejado por los átomos que conforman un mismo plano cristalográfico. La porción del haz que no es reflejada penetra hasta la siguiente capa de átomos y se repite sucesivamente el mismo proceso.

La difracción del haz incidente se produce cuando se cumplen dos condiciones:

- La distancia entre las capas de átomos es del mismo orden de magnitud que la longitud de onda de la radiación incidente.
- Los centros que provocan las reflexiones están uniformemente distribuidos.

A partir de estas dos condiciones y considerando la geometría del cristal, se puede calcular el ángulo de incidencia necesario para que se produzca una interferencia constructiva de rayos X mediante la Ley de Bragg, dada en la **Ecuación 3.6**:

$$n\lambda = 2d_{hkl} \sin\theta \qquad \text{(Ecuación 3.6)}$$

Donde *n* es el orden de difracción (número entero), λ es la longitud de onda de la radiación incidente, d_{hkl} es la distancia interplanar existente entre los planos de la red cristalina (representados por los índices de Miller, hkl) y θ el ángulo de dispersión al que aparece el máximo de difracción. Con cualquier otro ángulo distinto de θ se produce una interferencia destructiva.

Las medidas de DRX de los materiales estudiados en este trabajo fueron realizadas con un difractómetro Siemens D5000, usando radiación Cu Kα (λ=0.15405 nm), una anchura de paso de 0.01° y un tiempo de medida por paso de 1 segundo.

Difracción de rayos X a bajo ángulo

La difracción de rayos X realizada sobre materiales mesoporosos a bajo ángulo aporta información relativa al ordenamiento mesoporoso del material. Esto es posible debido a que los poros dispuestos ordenadamente producen reflexiones entre 0.5 y 5°.

Las estructuras hexagonales ordenadas, tanto de la sílice mesoporosa SBA-15 como de los carbones tipo CMK-3 obtenidos a partir de ella, han sido ampliamente estudiadas mediante difracción de rayos X a bajo ángulo [1, 12]. En ambos casos se obtienen difractogramas característicos conteniendo 3 reflexiones para valores de 2θ entre $\sim$ 0.9 y 1.8°, que se corresponden con los planos (100), (110) y (200).

A partir de la distancia interplanar resultante de la **Ecuación 3.6**, d_{100}, se puede calcular el parámetro de celda unidad, a_0, característico de un determinado ordenamiento de la mesoestructura.

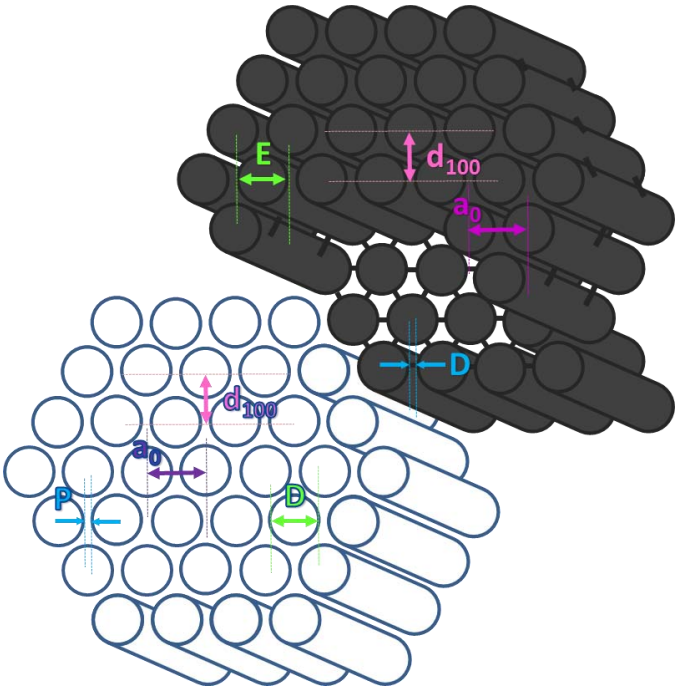

Figura 3.11

Estructura hexagonal con simetría *p6mm* de la sílice SBA-15 (izq.) y un CMO tipo CMK-3 obtenido a partir de ella (der.). a_0= parámetro de celda unidad; d_{100}= espaciado interplanar; *P*= espesor de la pared de sílice; D= diámetro de poro de la sílice o del carbón; E= diámetro de las barras de carbón.

Como se observa en la **Figura 3.11**, tanto la sílice mesoporosa SBA-15 (izquierda) como las réplicas carbonosas tipo CMK-3 (derecha) poseen un ordenamiento bidimensional hexagonal con simetría *p6mm*. El parámetro de celda unidad para el grupo espacial *p6mm* puede ser calculado a partir de la **Ecuación 3.7**:

$$a_0 = \frac{2d_{100}}{\sqrt{3}}$$ (Ecuación 3.7)

Donde a_0 es el parámetro de celda unidad (nm) y d_{100} es el espaciado interplanar (nm) obtenido a partir de la Ley de Bragg (**Ecuación 3.6**).

El espesor de la pared de sílice (P) o de las barras de carbón (E) se obtiene mediante la **Ecuación 3.8**:

$$\text{Espesor} = a_0 - D$$ (Ecuación 3.8)

Siendo a_0 el parámetro de celda unidad procedente de la **Ecuación 3.7** (nm) y D el diámetro de poro del material (nm) determinado a partir de las isotermas de adsorción de N_2 a -196 °C.

3.2.2.2 Microscopía electrónica de barrido y análisis por energía dispersiva

La microscopía electrónica de barrido (SEM) permite obtener imágenes bidimensionales de la superficie de un material. Un haz de electrones incide sobre la muestra, los átomos de ésta se ionizan y emiten electrones secundarios. Las vacantes generadas son reemplazadas por electrones de una órbita más externa, y los electrones secundarios son recogidos por el detector. Estos últimos son de baja energía (menos de 50 eV), por lo cual se detectan los electrones más cercanos a la superficie. Por ello en las fotografías SEM se obtienen zonas brillantes y sombreadas en función de la topografía de la muestra. Esta técnica se aplica en la caracterización morfológica de partículas (forma, tamaño, formación de agregados), siendo la resolución de unos pocos nanómetros.

Adicionalmente, el microscopio SEM posee una microsonda de electrones que analiza los rayos X emitidos al bombardear la muestra con el haz de electrones. El análisis mediante la microsonda de electrones (EDX) aporta información sobre los elementos químicos presentes en la muestra y puede generar un mapeado de los mismos seleccionando la longitud de onda característica de cada elemento.

En el presente trabajo se utilizó un microscopio electrónico de barrido Carl Zeiss DSM 942. Las muestras fueron fijadas sobre un portamuestras metálico mediante una lámina adhesiva de grafito. Las microfotografías SEM fueron obtenidas previa metalización de los materiales mesoporosos con iridio. De este modo se evita la

acumulación de electrones en la superficie del material que desvía el haz electrónico incidente en los barridos sucesivos.

Las medidas de EDX fueron realizadas con un detector EDAX Ametek. En este caso, las muestras no fueron metalizadas con el fin de evitar interferencias entre el iridio y los restantes elementos. A través de un mapeado de los elementos detectados en las muestras (C, N, O, P, S) se pudo determinar su concentración y distribución superficial.

3.2.2.3 Microscopía electrónica de transmisión

La microscopía electrónica de transmisión (TEM) aporta información sobre el ordenamiento, morfología y dimensiones de un determinado material. Consiste en hacer incidir un haz de electrones acelerados con un potencial de entre 100 y 200 KeV sobre una muestra cuyo espesor no debe superar los 100 nm. Al interaccionar con la materia, los electrones sufren tres tipos de fenómenos: una parte de los haces de electrones es difractada al interaccionar con las capas internas de electrones de la materia, otra parte es reflejada por las capas externas y una tercera fracción de electrones es transmitida a través de la muestra. Los electrones difractados dan información sobre la estructura cristalina del material, los electrones reflejados sobre su morfología, y finalmente los electrones transmitidos dan lugar a una imagen bidimensional TEM.

Las imágenes TEM fueron obtenidas con un microscopio JEOL 2000 EXII operando a una tensión nominal aceleradora que permite alcanzar resoluciones de hasta 3.4 Å. Las muestras fueron previamente suspendidas y diluidas en etanol; una pequeña cantidad de la suspensión fue depositada sobre una rejilla porta-muestras y tras unos minutos en que se evaporó el disolvente, se procedió a su examen al microscopio.

3.2.3 Caracterización química

3.2.3.1 Análisis termogravimétrico

El análisis termogravimétrico (TGA) y su forma derivada (DTG) permiten cuantificar la variación de masa de una muestra al aumentar progresivamente la temperatura en una atmósfera controlada. La forma derivada (DTG) es muy útil para distinguir las diferentes etapas, el intervalo de temperatura en que se producen y la temperatura a la que la velocidad de variación de masa es máxima. La atmósfera puede ser oxidante, reductora o inerte.

En el presente trabajo, las medidas fueron realizadas en una microbalanza CI Electronics. De forma general, se utilizaron en torno a 20 mg de muestra. Una excepción a esta cantidad fue el análisis termogravimétrico de precursores de poliamida en presencia de ácido fosfórico en los que, debido a la presencia de agua, la masa de muestra utilizada oscilaba alrededor de los 100 mg. En todos los casos la muestra fue sometida a un programa de calentamiento entre 25 y 900-950 °C bajo un flujo de aire o argón de 50 mL/min. La velocidad de calentamiento variaba en función del estudio a realizar, siendo 10 °C/min en la determinación del porcentaje de infiltración de los composites y pérdida de volátiles de los carbones, y 2 °C/min en el estudio del mecanismo de polimerización y pirólisis de los precursores de poliamidas.

3.2.3.2 Desorción térmica a temperatura programada

La desorción térmica programada (TPD) es un método utilizado comúnmente para caracterizar la química superficial de materiales carbonosos. Consiste en calentar progresivamente una muestra en atmósfera inerte de helio; los diferentes grupos funcionales superficiales de la muestra se van descomponiendo y se liberan en forma de gases característicos del grupo funcional del que proceden en función de la temperatura. Los gases liberados son detectados a la salida del reactor por un espectrómetro de masas; éste permite seguir los cambios de masa de la muestra, analizar la naturaleza de los gases formados durante el experimento y hacer una cuantificación de los mismos mediante un calibrado previo (H_2, CO, CO_2, NO_x o SO_x).

Los experimentos de TPD realizados en esta tesis fueron llevados a cabo en un aparato Autochem II (Micromeritics). Las muestras fueron calentadas a una velocidad constante de 10 °C/min hasta 1000 °C bajo un flujo de helio de 50

mL/min. Los gases desorbidos de los carbones (CO y CO_2) fueron monitorizados en un espectrómetro de masas Omnistar (Pfeiffer Vacuum), y sus concentraciones fueron determinadas a partir de las intensidades de la relación m/z a 28 y 44, respectivamente.

3.2.3.3 Espectroscopía infrarroja por transformada de Fourier

La espectroscopía IR es una técnica en la que se analizan las vibraciones moleculares. Dichas vibraciones se corresponden con los cambios energéticos producidos por las transiciones entre distintos estados vibracionales y rotacionales que son inducidas por la radiación de luz infrarroja en la zona del infrarrojo medio (3333 – 333 cm^{-1}). Las moléculas complejas dan lugar a espectros infrarrojos tan complicados que normalmente un análisis completo de los mismos no aporta información significativa. Sin embargo, sí puede obtenerse información sobre los grupos funcionales presentes en el material a partir de las bandas características de tensión y flexión de cada tipo de enlace químico.

En esta tesis se utilizó un espectrofotómetro Nicolet 8700 equipado con un detector MCT/A refrigerado por nitrógeno líquido. Los espectros de las muestras fueron registrados por reflectancia difusa (DRIFT) en el rango de 400-4000 cm^{-1}, recogiendo 200 barridos por espectro con una resolución de 4 cm^{-1}.

3.2.3.4 Espectroscopía fotoelectrónica de rayos X

Esta técnica permite examinar la naturaleza química y energía de enlace de los átomos de un material, permitiendo distinguir entre diferentes estados de oxidación de un mismo elemento. Cuando un sólido es irradiado con un haz de rayos X de alta energía ($h\nu$) se produce la emisión de electrones desde las capas electrónicas internas de los átomos. Los electrones cuya energía de ligadura (E_b) es inferior a la energía del haz de rayos X usados en la excitación son emitidos con un cierto valor de energía cinética (E_k). Por tanto, se debe cumplir la conocida ecuación del efecto fotoeléctrico, expresada como sigue:

$$h\nu = \mathrm{E_b} + \mathrm{E_k} + \varphi \qquad \text{(Ecuación 3.9)}$$

Siendo $h\nu$ la energía del fotón incidente, E_b la energía de enlace del electrón o energía de fotoionización, E_k la energía cinética de los electrones emitidos por los átomos del material, medida por el espectrofotómetro, y φ la función de trabajo del espectrofotómetro. Representando la intensidad de flujo de electrones emitidos por la muestra frente a su energía cinética o su energía de ligadura se obtienen los espectros XPS para un determinado nivel energético de un átomo.

Si bien un fotón de rayos X puede penetrar y excitar fotoelectrones hasta una profundidad de varios cientos de nanómetros, sólo los electrones situados en las capas más externas son capaces de abandonar el material y llegar al detector. Por ello, los análisis de XPS realizados sobre materiales sólidos aportan información limitada a una profundidad de menos de 2 nm desde la superficie del material.

Desde un punto de vista cualitativo, el análisis de los espectros XPS se basa en los desplazamientos químicos de las energías E_b que poseen los electrones internos. Las energías E_b son desplazadas por los electrones de valencia de los átomos, y por ello varían con el entorno químico de éstos. Cuando el estado de oxidación del átomo se hace más positivo, la energía de ligadura se desplaza a mayores valores. Desde el punto de vista cuantitativo, la intensidad de una línea fotoelectrónica es proporcional a la sección fotoelectrónica eficaz de un elemento determinado y al número de átomos de ese elemento presentes en la muestra.

Como análisis cualitativo, la técnica XPS aporta información acerca de los elementos presentes en la muestra y su estado de oxidación. También permite efectuar un análisis cuantitativo de los mismos, ya que la intensidad de los picos es función del número de átomos presentes en la superficie de la muestra. En general, las cantidades relativas de los elementos presentes en la superficie del material pueden ser calculadas de acuerdo con la **Ecuación 3.10**:

$$\frac{I_a}{I_b} = \frac{\sigma_a \lambda_a S_a}{\sigma_b \lambda_b S_b} \qquad \text{(Ecuación 3.10)}$$

Donde σ es la sección de fotoionización, λ es el camino libre medio de los electrones (tabulado), y S es una función instrumental que depende del espectrofotómetro y que se calcula a través de una relación provista por cada equipo. σ da una idea de la eficiencia de fotoionización, y depende del elemento

utilizado, de los rayos X incidentes y del orbital atómico. Sus valores también se encuentran tabulados.

En esta tesis, los espectros de XPS se obtuvieron en un sistema SPECS bajo una presión de 10^{-7} Pa y usando una fuente de rayos X de Al Kα (1486.3 eV, 150 W). Los electrones fotoexcitados fueron analizados en modo de energía de paso constante, usando una energía de paso de 30 eV para el espectro general y 10 eV para los espectros de niveles internos a alta resolución. Los datos fueron procesados con el software CasaXPS, y las envolventes de los espectros de niveles internos fueron ajustadas a picos mediante una función Gaussiana-Lorentziana (80/20) y una línea base tipo Shirley. Las composiciones, expresadas en porcentaje en peso, fueron determinadas a partir de los espectros generales considerando las áreas integradas de los picos de XPS principales para los diferentes elementos (C1s, N1s, O1s, P2p y S1s) y sus respectivos factores de sensibilidad.

3.2.3.5 Análisis elemental

Las concentraciones de C, N, H y S (expresadas en porcentaje en peso) de los materiales de carbono fueron medidas con un microanalizador TruSpec Micro. La concentración de oxígeno fue determinada directamente mediante un microanalizador TruSpec O. Previamente a la realización del análisis, las muestras fueron tratadas a 100 °C durante 12 horas para eliminar la humedad.

3.2.3.6 Punto de carga cero

El punto de carga cero se define como el valor de pH para el que la superficie del sólido tiene carga neta cero. En el presente trabajo, el punto de carga cero de los carbones fue determinado mediante el método de desplazamiento del pH [13] usando un pHmetro Mettler Toledo MPC227. El pH de una serie de disoluciones acuosas desoxigenadas conteniendo NaCl 0.01 M (50 mL) fue ajustado a valores iniciales de entre 2 y 12, usando HCl o NaOH 0.1 M. Sobre cada una de las disoluciones se añadieron 150 mg de carbón y las suspensiones resultantes fueron agitadas durante 24 horas en atmósfera de nitrógeno. Tras este periodo de tiempo,

el pH final de las disoluciones fue medido y representado frente al pH inicial; el punto de carga cero fue determinado para el valor en que pH inicial = pH final.

3.3 APLICACIONES

3.3.1 Captura de CO_2

Los fundamentos teóricos del estudio realizado se basan en la adsorción física de gases explicada anteriormente en la **sección 3.2.1.1**. Los detalles técnicos de las medidas se encuentran descritos brevemente en el siguiente apartado.

Isotermas de adsorción de CO_2 a 0, 25 y 50 °C

La capacidad de almacenamiento de CO_2 (mmol CO_2 / g de sorbente) de los carbones mesoporosos dopados fue calculada determinando las isotermas de adsorción de CO_2 a 0, 25 y 50 °C. Las medidas fueron realizadas en un sistema Quantachrome NOVA 4200e, previa desgasificación de los carbones a 150 °C durante 16 horas.

La intensidad de las interacciones adsorbato-adsorbente fue estimada mediante el calor isostérico de adsorción (Q_{st}). Éste fue calculado aplicando la ecuación de Clausius-Clapeyron (**Ecuación 3.11**) a las isotermas de adsorción de CO_2 a 0, 25 y 50 °C.

$$\left(\frac{\delta \ ln\, P}{\delta \ \frac{1}{T}}\right)_n = \frac{Q_{st}}{R} \qquad \text{(Ecuación 3.11)}$$

Siendo P la presión de equilibrio (Pa), T la temperatura absoluta (K), R la constante universal de los gases (8.314 J/mol K) y Q_{st} el calor isostérico de adsorción (J/mol) para un determinado recubrimiento de la superficie (n). La adsorción de CO_2 es un proceso exotérmico, por lo que el parámetro Q_{st} equivale a la entalpía de adsorción ($-\Delta H_{ads}$).

3.3.2 Adsorción de moléculas en fase líquida. Espectroscopía de absorción UV-vis

A continuación se exponen los fundamentos teóricos del proceso de adsorción que han sido considerados en este estudio, así como la descripción técnica de las medidas llevadas a cabo por espectroscopia UV-VIS.

Fundamentos teóricos del proceso de adsorción en fase líquida

En la adsorción en fase líquida se tienen los siguientes componentes: material adsorbente (sólido) y disolución, compuesta a su vez por soluto (moléculas a adsorber) y disolvente. Tanto soluto como disolvente pueden ser adsorbidos sobre la superficie del sólido formando una capa compacta, por lo que su superficie está completamente ocupada por moléculas de uno u otro. Los sistemas sólido-líquido son más complejos que los sistemas sólido-gas, puesto que existen interacciones adsorbente-adsorbato, adsorbente-disolvente, adsorbato-disolvente y adsorbato-adsorbato, siendo de gran importancia la naturaleza del disolvente.

La adsorción en fase líquida está dominada por una serie de factores:

- *Química superficial y textura porosa del adsorbente*: la química superficial influye en las interacciones adsorbente-adsorbato, mientras que las propiedades texturales (S_{BET}, volumen de poros, tamaño de poro…) afectan a la cantidad total de adsorbato adsorbida en equilibrio y la cinética del proceso [14].

- *Características físico-químicas del adsorbato (solubilidad, naturaleza iónica, grupos funcionales)*: cuanto más soluble es el soluto en el disolvente, menor será su adsorción en la superficie del sólido[15]. Si se trata de un soluto parcialmente soluble, cuanto más próxima sea su concentración a la de saturación más se adsorberá sobre el sólido[14]; en este caso, se obtienen isotermas tipo S (**Figura 3.12**). El grado de ionización de la molécula que se adsorbe determina su retención sobre el sólido [14], y la existencia de determinados grupos funcionales en la superficie de éste puede dar lugar a procesos de adsorción específica o quimisorción debido a la formación de enlaces químicos con las moléculas de soluto [14].

- *pH de la disolución*: los iones H_3O^+ y OH^- pueden competir con el soluto por la superficie del sólido. Además, el pH determina el grado de disociación del adsorbato: puede aumentar la solubilidad de especies iónicas en la fase líquida o favorecer la retención de especies neutras en la fase sólida [14].

- *Temperatura de adsorción*: la adsorción es un proceso exotérmico, por lo que un aumento de la temperatura generalmente hace disminuir la capacidad de adsorción.

- *Competencia entre adsorbatos*: puede afectar a la capacidad de adsorción y a la velocidad global de adsorción. Cuanto más parecida es la naturaleza de los adsorbatos, menor competencia existirá entre ellos y la mezcla podría comportarse como un sistema de un solo soluto [16].

- *Naturaleza química del disolvente*: influye en las interacciones con el adsorbato y hace que varíe la adsorción de éste. La tensión superficial del disolvente influye en el contacto entre el sólido y el líquido, y determina la superficie eficaz para la adsorción.

Isotermas de adsorción en fase líquida

Las isotermas de adsorción aportan información cualitativa y cuantitativa sobre el proceso de adsorción. A lo largo de éste, las moléculas de soluto se van acumulando en la superficie del sólido y su concentración en disolución disminuye progresivamente. La concentración del soluto en ambas fases se va igualando, la velocidad de adsorción disminuye y la de desorción aumenta. El equilibrio se alcanza cuando las dos velocidades alcanzan el mismo valor, y las moléculas de soluto dejan de acumularse en la superficie del sólido. En este caso, las isotermas de adsorción representan la cantidad de soluto adsorbido por unidad de masa de adsorbente frente a la concentración de equilibrio de soluto en disolución.

Modelos teóricos de isotermas en equilibrio

Las isotermas de adsorción sólido-líquido de un componente obtenidas en este trabajo fueron ajustadas a varios modelos teóricos. Los modelos aplicados en esta tesis fueron los siguientes:

Modelo de la isoterma de Langmuir [17]: este modelo asume que la adsorción tiene lugar en sitios específicos de la superficie homogénea del sólido. Es un proceso de adsorción en monocapa debido a que, una vez que una molécula de adsorbato ocupa un sitio, no se produce la adsorción de más moléculas. La capacidad máxima de adsorción se alcanza cuando la superficie del adsorbente se

satura con una monocapa de moléculas de adsorbato, en cuyo caso no se produce la migración de más moléculas hacia la superficie del material y la energía de adsorción es constante. La ecuación de Langmuir en una de sus formas lineales se expresa como indica la **Ecuación 3.12**:

$$\frac{1}{q_e} = \frac{1}{q_m} + \frac{1}{K_L q_m C_e} \qquad \text{(Ecuación 3.12)}$$

Siendo q_e la cantidad de soluto adsorbido en equilibrio por gramo de adsorbente (mg/*g*), q_m la capacidad de adsorción máxima teórica (mg/g), K_L la constante de la isoterma de Langmuir (L/mg), relacionada con la energía de adsorción, y C_e la concentración de adsorbato en equilibrio. Representando $1/q_e$ frente a $1/C_e$ se obtiene una recta, cuya ordenada en el origen nos permite calcular q_m y cuya pendiente nos da el valor de K_L.

Modelo de la isoterma de Freundlich [18]: el modelo de Freundlich considera la heterogeneidad de la superficie del sólido y las interacciones que se establecen entre éste y las moléculas de adsorbato. La adsorción se produce a través de un mecanismo en multicapa en el que la energía de adsorción decrece exponencialmente hasta que los sitios de adsorción se completan. Este modelo permite correlacionar la capacidad de adsorción con la concentración de equilibrio mediante la **Ecuación 3.13**:

$$q_e = K_F C_e^{\frac{1}{n}} \qquad \text{(Ecuación 3.13)}$$

Donde q_e es la cantidad de soluto adsorbido en equilibrio por gramo de adsorbente (mg/*g*), K_F es la constante de adsorción de Freundlich ((mg/g) (L/mg) $^{1/n}$), C_e es la concentración de adsorbato en equilibrio (mg/mL) y $1/n$ es el factor de heterogeneidad que da información sobre la intensidad de adsorción.

Modelo de la isoterma de Redlich-Peterson [19]: combina las isotermas de Langmuir y Freundlich introduciendo 3 parámetros en una ecuación empírica. La ecuación de la isoterma de Redlich-Peterson es la siguiente:

$$q_e = \frac{K_R C_e}{1 + a_R C_e^b} \qquad \text{(Ecuación 3.14)}$$

Donde q_e es la capacidad de adsorción del soluto por unidad de masa de adsorbente (mg/g), K_R y a_R son las constantes de la isoterma de Redlich-Peterson (L/g and L/mg,

respectivamente), *b* es un exponente que toma valores entre 0 y 1 y caracteriza a la isoterma: *b* = 1 indica que la isoterma es predominantemente tipo Langmuir, y *b* = 0 que es tipo Freundlich.

Modelo de la isoterma de Temkin [20]: asume que el calor de adsorción de las moléculas en una monocapa decrece linealmente con el recubrimiento, debido a la existencia de interacciones adsorbente-adsorbato y a la distribución uniforme de las energías de enlace hasta alcanzar un valor máximo. El modelo de Temkin introduce un factor que considera las interacciones indirectas entre el sólido y las moléculas de adsorbato. La expresión de la ecuación de la isoterma de Temkin se recoge en la **Ecuación 3.15**:

$$q_e = B \ln K_T + B \ln C_e \qquad \text{(Ecuación 3.15)}$$

en la que q_e es la cantidad de soluto adsorbida por unidad de masa de adsorbente (mg/g), *B* es una constante de Temkin relacionada con el calor de adsorción (J/mol), K_T es la constante de enlace en el equilibrio (L/mg) y C_e es la concentración de soluto sobrenadante en equilibrio (mg/mL). A partir de la representación gráfica de q_e frente a *ln* C_e, *B* y K_T son obtenidos de la pendiente y la ordenada en el origen de la recta, respectivamente.

Espectroscopía UV-vis

Típicamente, la espectroscopía UV-vis se basa en la absorción de radiación UV-vis por una especie química en disolución. Se hace incidir un rayo de luz, con determinada longitud de onda λ e intensidad I_0, perpendicularmente sobre una disolución. La molécula de interés contenida en la disolución debe contener un grupo funcional o especie química, denominado cromóforo, que absorbe parte de la radiación incidente (I_a) y deja pasar el resto (I_t). En este proceso se debe cumplir:

$$\mathrm{I_0 = I_a + I_t} \qquad \text{(Ecuación 3.16)}$$

La cantidad de radiación absorbida por la muestra se denomina *absorbancia*, definida por la **Ecuación 3.17**:

$$\mathrm{A = -\ln \frac{I_t}{I_0}} \qquad \text{(Ecuación 3.17)}$$

La cantidad de radiación absorbida dependerá de la distancia que atraviesa el haz a través de la disolución y de la concentración del cromóforo. Esta relación se describe mediante la Ley de Lambert-Beer dada en la **Ecuación 3.18**:

$$A = \varepsilon C L \qquad \text{(Ecuación 3.18)}$$

Siendo ε una constante denominada coeficiente de extinción específica para cada cromóforo, *C* la concentración de cromóforo en disolución y *L* la distancia que atraviesa la radiación o camino óptico.

En este trabajo, los experimentos de absorción de radiación UV-VIS fueron utilizados para medir la concentración de colorantes sintéticos o medicamentos en disolución. El equipo empleado fue un espectrofotómetro UV/VIS Thermo Spectronic Helios α. Las disoluciones de cromóforo utilizadas fueron previamente calibradas para cuantificar su concentración y los valores de absorbancia fueron seleccionados en el máximo del pico de absorción, específico de cada cromóforo.

3.4. REFERENCIAS BIBLIOGRÁFICAS

[1] Zhao DY, Feng JL, Huo QS, Melosh N, Fredrickson GH, Chmelka BF, et al. Triblock copolymer syntheses of mesoporous silica with periodic 50 to 300 angstrom pores. Science 1998;279(5350):548-52.

[2] Yamazaki N, Matsumoto M, Higashi F. Studies on reactions of the N-phosphonium salts of pyridines. XIV. Wholly aromatic polyamides by the direct polycondensation reaction by using phosphites in the presence of metal salts. J Polym Sci Pol Chem 1975;13(6):1373-80.

[3] Sing KSW, Everett DH, Haul RAW, Moscou L, Pierotti RA, Rouquerol J, et al. Reporting physisorption data for gas solid systems with special reference to the determination of surface-area and porosity (recommendations 1984). Pure Appl Chem 1985;57(4):603-19.

[4] Brunauer S, Emmett PH, Teller E. Adsorption of gases in multimolecular layers. J Am Chem Soc 1938;60(2):309-19.

[5] Rouquerol F, Rouquerol J, Sing KSW. Adsorption by powders & porous solids. Principles, methodology and applications. New York: Academic Press 1999.

[6] Barrett EP, Joyner LG, Halenda PP. The determination of pore volume and area distributions in porous substances. I. Computations from nitrogen isotherms. J Am Chem Soc 1951;73(1):373-80.

[7] Seaton NA, Walton JPRB, Quirke N. A new analysis method for the determination of the pore size distribution of porous carbons from nitrogen adsorption measurements. Carbon 1989;27(6):853-61.

[8] Ravikovitch PI, Vishnyakov A, Russo R, Neimark AV. Unified approach to pore size characterization of microporous carbonaceous materials from N_2, Ar, and CO_2 adsorption isotherms. Langmuir 2000;16(5):2311-20.

[9] Olivier JP. Improving the models used for calculating the size distribution of micropore volume of activated carbons from adsorption data. Carbon 1998;36(10):1469-72.

[10] Olivier JP. Modeling physical adsorption on porous and nonporous solids using density functional theory. J Porous Mat 1995;2(1):9-17.

[11] Neimark AV, Lin Y, Ravikovitch PI, Thommes M. Quenched solid density functional theory and pore size analysis of micro-mesoporous carbons. Carbon 2009;47(7):1617-28.

[12] Lee JS, Joo SH, Ryoo R. Synthesis of mesoporous silicas of controlled pore wall thickness and their replication to ordered nanoporous carbons with various pore diameters. J Am Chem Soc 2002;124(7):1156-7.

[13] Franz M, Arafat HA, Pinto NG. Effect of chemical surface heterogeneity on the adsorption mechanism of dissolved aromatics on activated carbon. Carbon 2000;38(13):1807-19.

[14] Radovic LR, Moreno-Castilla C, Rivera-Utrilla J. Carbon materials as adsorbents in aqueous solutions. In: Radovic LR, ed. Chemistry and Physics of Carbon; 2001 p. 227-405.

[15] Shirgaonkar IZ, Joglekar HS, Mundale VD, Joshi JB. Adsorption equilibrium data for substituted phenols on activated carbon. J Chem Eng Data 1992;37(2):175-9.

[16] Álvarez J. Adsorción de compuestos fenólicos en fase líquida sobre carbón activado. Equilibrio de mezclas multicomponentes. Tesis doctoral 1989;Universidad Complutense de Madrid.

[17] Langmuir I. The adsorption of gases on plane surfaces of glass, mica nad platinum. J Am Chem Soc 1918;40(9):1361-403.

[18] Freundlich H. Concerning adsorption in solutions. Zeitschrift Fur Physikalische Chemie--Stochiometrie Und Verwandtschaftslehre 1906;57(4):385-470.

[19] Redlich O, Peterson DL. A useful adsorption isotherm. J Phys Chem 1959;63(6):1024-.

[20] Temkin M, Pyzhev V. Kinetics of ammonia synthesis on promoted iron catalysts. Acta Physicochimica Urss 1940;12(3):327-56.

Capítulo 4:

Síntesis de carbones mesoporosos ordenados dopados con heteroátomos mediante depósito químico en fase vapor en sílices mesoporosas

4.1 Síntesis de carbones mesoporosos ordenados dopados con heteroátomos mediante depósito químico en fase vapor en sílices mesoporosas

Tal y como se comentó en el *Capítulo 1* de esta Tesis, los carbones mesoporosos ordenados (CMOs) pueden ser obtenidos mediante hard-templating a partir de plantillas sólidas mesoporosas con estructuras definidas. Estos materiales suelen presentar un escaso grado de funcionalización superficial, lo que limita su uso en aplicaciones que requieran interacciones específicas o para el anclaje de otros grupos funcionales. Si bien es cierto que existen numerosos trabajos centrados en el dopaje de materiales de carbono, la mayoría de ellos tratan sobre carbones activados, nanotubos de carbono o fibras de carbono, mientras que los métodos de funcionalización de CMOs han sido mucho menos estudiados. Además, la mayoría de los CMOs que han sido estudiados fueron obtenidos por infiltración líquida de glúcidos, pero casi no hay trabajos centrados en la funcionalización de CMOs obtenidos por CVD. También se ha comentado que las estrategias de funcionalización se pueden llevar a cabo bien en la etapa de síntesis o bien mediante tratamientos post-síntesis. Este capítulo, a través de los dos artículos que lo componen, se centra en la funcionalización de CMOs obtenidos por CVD a través de ambas estrategias:

i) En la ***Publicación 1*** se estudia el dopaje de CMOs con grupos funcionales oxigenados. Para ello, se obtuvieron CMOs por depósito químico en fase vapor de propileno, a los que posteriormente se sometió a diversos tratamientos post-síntesis de oxidación.

ii) En la ***Publicación 2*** se estudia la obtención directa de CMOs dopados con nitrógeno (N-CMOs). El dopaje fue llevado a cabo en el mismo procedimiento de síntesis, por depósito químico en fase vapor, mediante la utilización de un precursor con nitrógeno (acetonitrilo). Adicionalmente, los N-CMOs resultantes fueron utilizados para estudiar la influencia de su química superficial sobre la adsorción de colorantes sintéticos ácidos y básicos.

Tanto en la funcionalización de los materiales por síntesis directa como en la que se lleva a cabo post-síntesis no sólo es importante introducir una cierta cantidad de grupos funcionales en la superficie del material, sino que además es necesario identificar, cualitativa y cuantitativamente, el tipo de grupos funcionales que se introducen. Además, en el caso de los CMOs se debe preservar el ordenamiento de la estructura tras aplicar el método de dopaje. Por tanto, las publicaciones de este capítulo estudian tanto la evolución estructural del material como la identificación de la cantidad y tipo de grupos funcionales introducidos en el proceso de funcionalización.

PUBLICACIÓN 1:

'Surface modification of nanocast ordered mesoporous carbons through a wet oxidation method'. *Carbon 2013;62:193-203*

En este trabajo, se preparó un carbón mesoporoso ordenado (CMO) mediante CVD de propileno en una plantilla mesoporosa de sílice tipo SBA-15. Este carbón fue sometido a diversos tratamientos de oxidación en fase líquida para modificar su química superficial. Los procedimientos experimentales seguidos se encuentran detallados en los **Apartados 3.1.2.1** y **3.1.3**. Dado que los materiales de carbono en general, y los CMOs en particular, son muy sensibles a las condiciones oxidantes, las variables del tratamiento de oxidación fueron cuidadosamente seleccionadas con el fin de introducir la mayor cantidad posible de grupos funcionales oxigenados sin alterar ni el ordenamiento estructural ni la textura porosa de los materiales. Para ello, se utilizaron dos agentes con distinta fuerza oxidante (HNO_3 y H_2O_2) y se modificaron diversas variables del proceso: concentración de agente oxidante, temperatura y tiempo de oxidación. Finalmente, se llevó a cabo un estudio sistemático y exhaustivo sobre la evolución de la química superficial en función de las variables experimentales utilizadas.

Los resultados relativos a la características texturales, estructurales y morfológicas indican que la textura porosa, el ordenamiento estructural y la morfología de las partículas del material de partida se mantienen tras los tratamientos de oxidación, incluso aplicando las condiciones más severas. Sólo en el caso de la oxidación con H_2O_2 se observan ligeras modificaciones respecto la textura porosa inicial: se produce un leve aumento en el volumen total de poros y el volumen de mesoporos, ensanchándose el diámetro de éstos en torno a 10-12 nm.

El estudio de la evolución química de los materiales con los diferentes tratamientos de oxidación revela que los agentes oxidantes utilizados modifican tanto la superficie como el seno de los materiales. También se observa que las condiciones de oxidación (naturaleza y concentración del agente oxidante y tiempo de oxidación) influyen decisivamente sobre la cantidad y tipo de grupos funcionales

oxigenados introducidos. En los tratamientos efectuados con HNO_3, al aumentar la concentración de agente oxidante y el tiempo de tratamiento aumenta el grado de oxidación de los carbones, ejerciendo la primera un efecto más acusado. De hecho, los mayores contenidos de oxígeno (en torno al 9% en peso) se alcanzan para las muestras tratadas con las concentraciones más altas de ácido nítrico: 5M a 80 °C y 14.55M a temperatura ambiente. En estas condiciones, el oxígeno incorporado en los materiales se encuentra principalmente en forma de grupos funcionales carboxílicos, fenoles e hidroquinonas. Por otro lado, el peróxido de hidrógeno actúa como un agente oxidante más débil. El contenido en oxígeno introducido en los carbones tras los tratamientos con H_2O_2 tan sólo alcanza el 3% en peso, y lo hace preferentemente en forma de grupos fenólicos e hidroquinonas.

CARBON 62 (2013) 193–203

Available at www.sciencedirect.com

SciVerse ScienceDirect

journal homepage: www.elsevier.com/locate/carbon

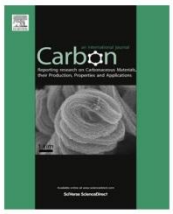

Surface modification of nanocast ordered mesoporous carbons through a wet oxidation method

A. Sánchez-Sánchez *, *F. Suárez-García*, *A. Martínez-Alonso*, *J.M.D. Tascón*

Instituto Nacional del Carbón, INCAR-CSIC, Apartado 73, 33080 Oviedo, Spain

ARTICLE INFO

Article history:
Received 22 April 2013
Accepted 5 June 2013
Available online 13 June 2013

ABSTRACT

An ordered mesoporous carbon was synthesized by chemical vapor deposition using SBA-15 silica as solid template and propylene as carbon precursor. It was submitted to several liquid oxidation treatments by means of HNO_3 and H_2O_2 under different oxidation conditions in order to modify its surface chemistry while keeping its structure and porous texture as unmodified as possible. Original and modified OMC samples were characterized using different techniques such as nitrogen adsorption at - 196 °C , X-ray diffraction, scanning electron microscopy, elemental analysis, temperature programmed desorption and X-ray photoelectron spectroscopy. A higher amount of oxygen functional groups was introduced on the material surface by using HNO_3 than by means of H_2O_2, but the original surface texture and structural arrangement were kept unchanged in both cases.

1. Introduction

Ordered mesoporous carbons (OMCs) synthesized by nanocasting method have received increasing attention in recent years because of their excellent properties such as high surface areas and pore volumes, uniform and narrow pore size distributions, high thermal stability and good electric conductivity. All these properties make them suitable materials for their application as sensors, adsorbents, catalyst supports, electrode materials or energy storage systems [1]. To this end, mesoporous silicas with variable pore size and structure have been extensively infiltrated with suitable carbon precursors via a liquid infiltration method [2] or chemical vapor deposition (CVD) [3,4]. Subsequent carbonization and removal of silica template, using HF or NaOH solutions, give rise to different OMCs that preserve the original templates' morphology and constitute inverse replicas of them. These materials contain, in general, a small amount of functional groups (i.e. oxygen-containing groups) on their surface, which could be a clear limitation, both for many applications (where functional groups are needed for developing specific interactions) [5] and for grafting their surface with other functional groups, where oxygen-containing surface groups act as anchors [6].

The introduction of oxygen-containing functional groups on the carbon surface can be attained by means of oxidation post-treatments [6–8]. Thus, oxidation treatments (typically dry, wet, plasma or electrochemical oxidation) have been frequently used because they can introduce a large amount of oxygen functional groups on the carbon surface. The behavior of the oxidizing agents generally differs with regard to the quantity and predominant type of functional groups that they introduce, and it has been widely reported that nitric acid oxidation is the most effective one in terms of surface chemistry modification of carbon materials [9]. Therefore, it is important not only to introduce a certain amount of surface functional groups (especially carbon–oxygen complexes) under specific experimental conditions, but also to indentify the nature of the functional groups generated. The functionalization of

* *Corresponding author:* Fax: +34 985 297 662.
E-mail address: ang.san@incar.csic.es (A. Sánchez-Sánchez).
0008-6223/$ - see front matter
http://dx.doi.org/10.1016/j.carbon.2013.06.011

OMCs has to be carried out carefully in order to prevent the structural collapse of their ordered framework. Different works on the oxidation/functionalization of OMCs such as CMK-3 and CMK-5 can be found in the literature [6,9–16]. In general, it was concluded that CMK-3 maintains the structural order to a large extent, while the CMK-5 structure was more sensitive and a collapse easily occurred. This is due to the differences in the 3D structure of both materials, composed of interconnected carbon rods in CMK-3 carbon and interconnected carbon pipes in CMK-5, the latter being more prone to collapse.

The aforementioned OMCs were mostly obtained via liquid impregnation using different carbon precursors [1,2,4,10–13,17–20], and only a few works have dealt with the oxidation of OMCs obtained by the CVD method [21]. In this work, a CMK-3 type OMC obtained from CVD of propylene was subjected to different liquid phase oxidation treatments using both nitric acid and hydrogen peroxide, in order to introduce an as high as possible amount of surface oxygen functional groups without disturbing the original ordered mesoporous structure. This work focuses on performing a systematic study of the surface chemistry evolution of CVD-synthesized CMK-3 carbon as a function of oxidant nature, concentration and oxidation time.

2. Experimental

2.1. Synthesis of SBA-15 template

Mesoporous SBA-15 silica was prepared by a soft-templating method using a triblock copolymer (Pluronic P123, Mw = 5800, Sigma–Aldrich) as synthesis directing agent, and TEOS (Sigma–Aldrich) as silica source, as described by Zhao et al. [22]. Typically, 10.44 g P123 was added to an aqueous solution containing 52.5 mL of 37% HCl (Merck), and stirred at 40 °C. Once the dissolution of the triblock copolymer was complete, 22.64 g 98% TEOS was added dropwise, stirring the mixture at the same temperature for 4 h. The resulting product was aged at 125 °C for 72 h, filtered and calcined in air at 550 °C during 6 h.

2.2. Synthesis of ordered mesoporous carbon

OMC was obtained following a hard-templating method via a chemical vapor deposition route, as reported elsewhere [19,23]. The calcined SBA-15 was placed in a flow-through tube furnace and heated to 750 °C under an argon flow (99.999% purity) with a heating ramp of 10 °C/min, and then maintained at this temperature for 6 h under a propylene flow (99.5% purity). Subsequent carbonization was carried out at 900 °C with a heating ramp of 5 °C/min under an argon flow. The resulting silica–carbon composite was treated with 48% HF (*Merck, Normapur*) at room temperature in order to remove the silica template, filtered and washed several times with distilled water, and dried at 80 °C. The obtained OMC was designated as X1.

2.3. Wet oxidation of ordered mesoporous carbon

The surface chemistry of mesoporous carbon X1 was modified by means of several treatments of different strength in liquid phase. Typically, 1 g dried X1 carbon was oxidized under mild conditions with 150 mL of (a) 30% (v/v) H_2O_2 (*Merck, Emsure ISO for analysis*) at ambient temperature for 4 or 24 h (named here as X1ox4A and X1ox24A, respectively); and (b) 0.5 M HNO_3 (*solution from commercial concentrated product, Sigma–Aldrich*) heating at 80 °C for 1–5 h. More severe oxidation conditions were applied using 150 mL of (c) 2 M and (d) 5 M HNO_3 (*solutions from commercial concentrated product, Sigma–Aldrich*), heating at 80 °C, from 1 to 5 h in the first case and from 3 to 5 h in the second one (carbons oxidized with HNO_3 at 80 °C were denoted as X1oxB/C, where B corresponds to the HNO_3 molarity used and C is the treatment duration in hours), and (e) 14.55 M HNO_3 (*Sigma Aldrich, commercial concentrated product*), at room temperature during 1 h (named X1oxC/1).

2.4. Characterization techniques

The porous texture of the samples was characterized through N_2 adsorption/desorption isotherms at - 196 °C using an Autosorb-1 (Quantachrome) volumetric adsorption apparatus. Porous texture parameters obtained from these isotherms were: the apparent BET surface area, S_{BET}, calculated through BET method; the total pore volume, V_t, calculated from the amount adsorbed in liquid form at $P/P_0 = 0.975$; the micropore volume, V_{micro}, calculated by applying the Dubinin–Radushkevich equation; and the mesopore volume, V_{meso}, calculated as the difference between V_t and V_{micro}. The pore size distributions (PSDs) were obtained by applying the quenched solid density functional theory method (QSDFT). The main pore size, D, was determined from these PSDs at the maximum value. Structural and morphological characterizations were carried out by X-ray diffraction and scanning electron microscopy, with a Siemens D5000 diffractometer (Cu K_α radiation; scanning range $2\theta = 0.5\text{-}5°$; step width = 0.01°; time per step = 1 second) and a Carl Zeiss DMS-942 microscope, respectively. Finally, chemical characterization was performed by elemental analysis using a LECO CHNS-932 microanalyzer and a LECO VTF-900 microanalyzer for oxygen; X-ray photoelectron spectroscopy was carried out on a SPECS system, working at a pressure of 10^{-7} Pa with a monochromatic Al K_α X-ray source (1486.3 eV, 150 W). The photo-excited electrons were analyzed in constant pass energy mode, using a pass energy of 30 eV for the survey spectra and 10 eV for the high resolution core level spectra. The CasaXPS software was used for data processing and all envelopes of core level spectra were peak-fitted with a Gaussian–Lorentzian convoluted function (80/20) and a Shirley's background. The compositions (in wt.%) were determined from the survey spectra by considering the integrated peak areas of the main XPS peaks of the different elements (C1s and O1s) and their respective sensitivity factors. Temperature programmed desorption (TPD profiles) was carried out with an Autochem II apparatus (Micromeritics). The samples were heated at a constant rate of 10 °C/min to 1000 °C under a He flow of 50 mL/min, and the evolved gases (CO and CO_2) were monitored using an Omnistar (Pfeiffer Vacuum) mass spectrometer. The amounts of released CO and CO_2 were determined from the intensities of m/z at 28 and 44, respectively.

3. Results and discussion

Nitrogen adsorption isotherms at -196 °C of original and a selection of the oxidized carbons are shown in Fig. 1A, and several textural parameters are collected in Table 1.

As we can see in Fig. 1A, both the pristine and the oxidized OMCs exhibit type IV isotherms (according to IUPAC classification), typical of mesoporous materials. Nitric acid oxidation does not apparently modify the porous texture of X1 OMC. Thus, all samples show almost the same isotherms and PSDs (see Fig. 1B) as the original carbon. In the case of H_2O_2 oxidation, the isotherm is close to that for the original carbon at low and medium P/P_0, but at high relative pressures larger N_2 uptakes are observed, which implies the presence of a greater amount of large mesoporous in the oxidized carbon (around 10 nm in size, as it can be observed in the corresponding PSD shown in Fig. 1B). This indicates that H_2O_2 has a slightly higher capacity to remove carbon atoms from the X1 surface than HNO_3. The ability of H_2O_2 for cleaving C–C bonds through oxidative degradation with the formation of small organic molecules has been demonstrated in the case of CMK-5 type carbons [13].

Despite this, the PSDs are clearly maintained after both mild and strong oxidation treatments as can be noticed in Fig. 1B. The main pore size, D, does not change following

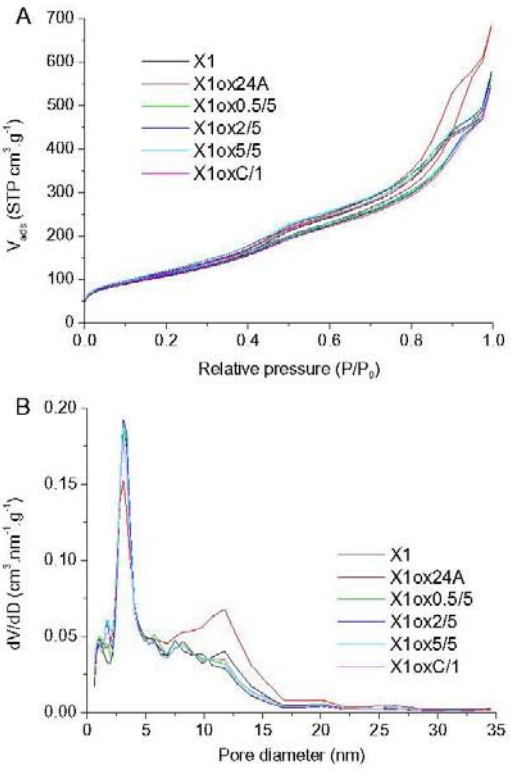

Fig. 1 – (A) Nitrogen adsorption isotherms at - 196 °C and (B) pore size distributions of raw and several oxidized carbon materials.

the post-treatments (see Table 1). As can be expected from Fig. 1A and B, textural parameters listed in Table 1 virtually do not differ between the oxidized carbons and the starting material. This suggests that, unlike other works, no introduction of oxygen functional groups that can partially block the porosity takes place. Only in the case of samples oxidized with H_2O_2, higher V_t and V_{meso} are observed, probably due to collapse of adjacent mesopores during the oxidation process by rupture of the walls that separate them. These results indicate that the porous texture of samples is unaffected after oxidation treatments with HNO_3 and only some large mesopores are produced by H_2O_2 treatments, but even in this case the main pore structure is preserved.

As concerns the structure of both oxidized and raw OMCs, the X-ray diffraction profiles (Fig. 2) show in all materials well-resolved (100), (110) and (200) peaks, corresponding to a two-dimensional hexagonal arrangement, even in the samples that were submitted to the most severe oxidation conditions. This arrangement consists of carbon rods templated from the mesoporous network of silica, plus carbon connectors originated from templating of silica wall micropores. The higher intensity of the (100) reflection in respect to that for the (110) reflection indicates that X1 sample has a CMK-3 type structure formed by carbon rods (as evidenced also by TEM, see Fig. S1 in Supporting Information) and not by carbon pipes (CMK-5 structure), which would yield a higher intensity of the (110) peak regarding the (100) peak [16]. Values of the interplanar distance, $d_{(100)}$, the unit cell parameter, a, and the diameter of carbon rods, E, are listed in Table 1. The unit cell parameter corresponding to a two-dimensional hexagonal arrangement was calculated through equation, $a = 2/(3)^{1/2} \cdot d_{(100)}$, and the diameter of the carbon rods was calculated by means of $E = a - D$[24,25], where $d_{(100)}$ is the interplanar distance obtained from Bragg's law and D is the pore diameter obtained at the maximum value of the PSDs.

As shown in Table 1, the oxidized carbons present insignificant variations in both the unit cell parameter (a) and the diameter of carbon rods (E) with respect to the raw OMC. This fact, and the presence of well-resolved peaks in the oxidized materials, indicates that oxidation treatments do not alter the two-dimensional hexagonal structure of the raw carbon.

Scanning electron micrographs of the original ordered mesoporous carbon, X1, and samples obtained from several oxidation treatments are recorded in Fig. 3.

Comparing the original carbon (Fig. 3A) with those obtained through oxidation with 5 M HNO_3/80 °C/5 h (X1ox5/5) (Fig. 3C) and H_2O_2/room temperature/24 h (X1ox24A) (Fig. 3B), no changes in particle structure can be observed following the oxidative treatments. However, the carbon treated with concentrated HNO_3/room temperature/1 h (Fig. 3D) presents isolated and scarce damaged areas, consisting in localized collapses of the structure, which generally do not alter the properties regarding the starting material. In fact, Fig. 3D shows a selected local collapse, but the overall morphology of this carbon presents similar textural and crystallographic parameters to the rest of carbons.

The results related to textural, structural and morphological characteristics of modified materials discussed thus far indicate that after oxidation treatments, under either mild

Table 1 – Textural and structural parameters obtained from nitrogen adsorption isotherms at - 196 °C and X-ray diffraction techniques, respectively.

Sample	Nitrogen adsorption isotherms at - 196 °C					XRD		
	S_{BET} ($m^2\ g^{-1}$)	V_t ($cm^3\ g^{-1}$)	V_{micro} ($cm^3\ g^{-1}$)	V_{meso} ($cm^3\ g^{-1}$)	D (nm)	$d_{(100)}$ (nm)	a (nm)	E (nm)
X1	406	0.76	0.14	0.62	3.1	10.1	11.7	8.6
X1ox4A	428	0.88	0.14	0.74	3.1	10.2	11.8	8.7
X1ox24A	401	0.85	0.15	0.70	3.1	9.9	11.4	8.3
X1ox0.5/1	393	0.72	0.15	0.57	3.1	10.1	11.7	8.6
X1ox0.5/3	396	0.74	0.15	0.59	3.1	10.2	11.8	8.7
X1ox0.5/5	413	0.73	0.16	0.57	3.1	10.2	11.8	8.7
X1ox2/1	396	0.72	0.15	0.57	3.1	10.0	11.5	8.4
X1ox2/3	410	0.73	0.16	0.57	3.1	10.1	11.7	8.6
X1ox2/5	417	0.73	0.16	0.57	3.1	10.2	11.8	8.7
X1ox5/3	440	0.77	0.14	0.63	3.1	10.1	11.7	8.6
X1ox5/5	427	0.76	0.15	0.61	3.1	10.1	11.7	8.6
X1oxC/1	415	0.73	0.15	0.58	3.1	10.1	11.7	8.6

d_{100}, Interplanar distance, obtained by means of Bragg's law; a, unit cell parameter, calculated as $2/(3)^{1/2}d_{(100)}$; E = diameter of carbon rods, calculated as the difference between the unit cell parameter (a) and the pore diameter (D).

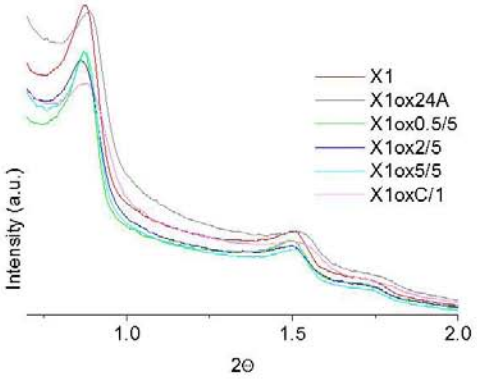

Fig. 2 – X-ray diffraction profiles of the original carbon (X1) and several oxidized materials.

or strong oxidation conditions, the original porous texture, particle morphology and structural order is preserved.

The chemical evolution, at both bulk and surface levels, was studied by means of elemental analysis, temperature programmed desorption (TPD) and X-ray photoelectron spectroscopy (XPS) techniques. The elemental contents obtained from elemental analysis and XPS, expressed as weight percentage, are collected in Table 2. The O/C ratio is also included to provide an estimate for the oxidation degree of the samples. Results obtained from both techniques are very similar to each other, indicating that the used oxidants modify both the surface and the bulk of the materials. As expected, the oxygen content, and therefore the oxidation degree of the carbons, increases with both oxidizing agent concentration and treatment time (although the former seems to have a greater effect), and reaches a maximum value around 9 wt.% for OMCs treated with 5 M and 14.55 M HNO_3 at 80 °C and room temperature.

The amount and type of oxygen functional groups introduced after the oxidation process were determined by TPD and XPS. In the interpretation of TPD measurements we assume that each type of oxygen-containing group decomposes giving rise to CO and/or CO_2 moieties at different temperatures. The deconvolution of CO and CO_2 profiles into single peaks (using multiple Gaussian functions) leads to the determination of the specific functional groups.

TPD profiles of several samples are recorded in Figs. 4 and 5. As one can see in these figures, the original carbon (X1) shows CO evolution, but does not show any CO_2 evolution. This is an indication that X1 carbon contains oxygenated functional groups that are desorbed as CO, and its low amount (804.5 μmol g^{-1}, see Table 3) indicates a low functionalization degree. The OMCs oxidized under mild conditions (H_2O_2 and 0.5 M HNO_3) yield CO profiles with a high number of peaks in the entire range of temperature. Comparing with the CO profile corresponding to X1 sample, a higher CO evolution is mainly observed between 600 and 700 °C when oxidation is carried out with H_2O_2; if oxidation is performed with 0.5 M HNO_3, in the CO evolution there are increments between 600 and 700 °C, and above 850 °C.

Using HNO_3 concentrations higher than 0.5 M (i.e. 2, 5 and 14.55 M HNO_3), or longer treatment time for a given concentration, CO desorption between 600 and 700 °C becomes clearly predominant and, additionally, the number of peaks decreases.

Deconvolution of the CO profiles corresponding to the raw material (X1) and oxidized carbon X1oxC/1 are shown in Fig. 6 as representative examples. The deconvolution of other CO profiles is given in Fig. S2 at Supporting Information. Several peaks between 250 and 500 °C are distinguished and could be assigned to the desorption of carboxylic anhydrides in different chemical environments [26] in the case of the oxidized samples, as it will be explained later. However, the shoulders at low temperatures present in the CO spectra of the X1 sample (the three small peaks at lower temperature shown in Fig. 6) cannot be justified by the desorption of carboxylic anhydride groups because this functional group decomposes by releasing both CO and CO_2, and no CO_2 evolution is observed in this carbon. Moreno-Castilla et al. [27], based in the work of Surygala et al. [28], assigned the CO peaks at low temperature to the decomposition of carbonyl groups in

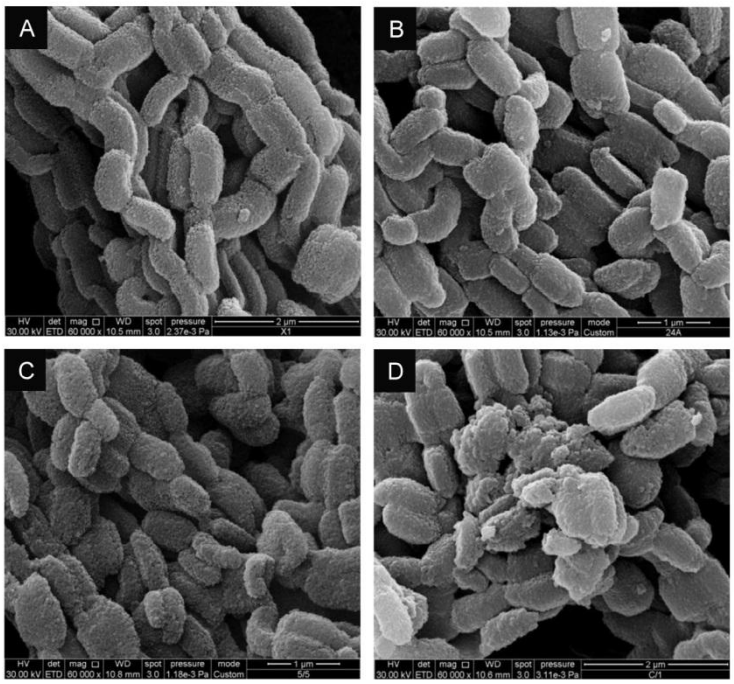

Fig. 3 – SEM micrographs of (A) raw carbon and some carbons obtained through different strength oxidation treatments: (B) 30% (v/v) H_2O_2/room temperature/24 h, (C) 5 M HNO_3/80 °C/5 h and (D) 14.55 M HNO_3/room temperature/1 h; the latter shows an isolated damaged area, but the global structure of this oxidized carbon is the same as that of the starting material.

Table 2 – Elemental analysis and XPS results for raw and oxidized carbon materials.

Sample	Elemental analysis (wt.%)					XPS (wt.%)		
	C	H	N	O	O/C	C	O	O/C
X1	97.5	0.2	0.0	2.2	0.02	97.0	3.0	0.03
X1ox4A	96.7	0.6	0.0	2.7	0.03	97.2	2.8	0.03
X1ox24A	96.4	0.6	0.0	2.7	0.03	95.4	4.6	0.05
X1ox0.5/1	97.7	0.2	0.0	2.1	0.02	97.4	2.7	0.03
X1ox0.5/3	97.4	0.2	0.0	2.5	0.03	97.3	2.7	0.03
X1ox0.5/5	95.0	0.1	0.2	4.6	0.05	94.4	5.6	0.06
X1ox2/1	94.5	0.2	0.3	5.0	0.05	94.3	6.1	0.06
X1ox2/3	93.1	0.2	0.3	6.4	0.07	93.6	6.5	0.07
X1ox2/5	92.9	0.2	0.3	6.7	0.07	93.0	7.0	0.07
X1ox5/3	90.4	0.4	0.4	8.9	0.10	91.8	8.2	0.09
X1ox5/5	90.4	0.3	0.2	9.1	0.10	91.1	8.9	0.10
X1oxC/1	90.7	0.3	0.1	8.9	0.10	91.4	8.6	0.09

α-substituted ketones and aldehydes. In a recent work, Li et al. [29] observed the evolution of CO together with H_2O at the same low temperature range, and they assigned these low-temperature CO peaks to the decomposition of carboxyl groups into CO and H_2O. However, in the case of X1 sample this low-temperature evolution of CO cannot be assigned to carboxylic groups because, as mentioned above, it presents no CO_2 evolution; for these reasons, it could be assigned to α-substituted carbonyls in ketone and aldehyde functional groups. Peaks between 600 and 700 °C, whose intensity increases dramatically as the oxidation becomes increasingly severe, can be assigned to the desorption of ethers, phenols and hydroquinones also in different chemical environments; and finally, peaks above 850 °C can be assigned to carbonyl, quinone and semiquinone groups [12,30–34]. Another peak around 1000 °C (the CO profile does not return to the base line above 1000 °C) was used for deconvolution, but it was not taken into account for the quantitative analysis; it could be assigned to basic groups, such as a pyrones and chromenes [35,39].

As concerns the CO_2 profiles (Fig. 5), and as noted before, it is clearly observed the appearance of peaks related to oxygen

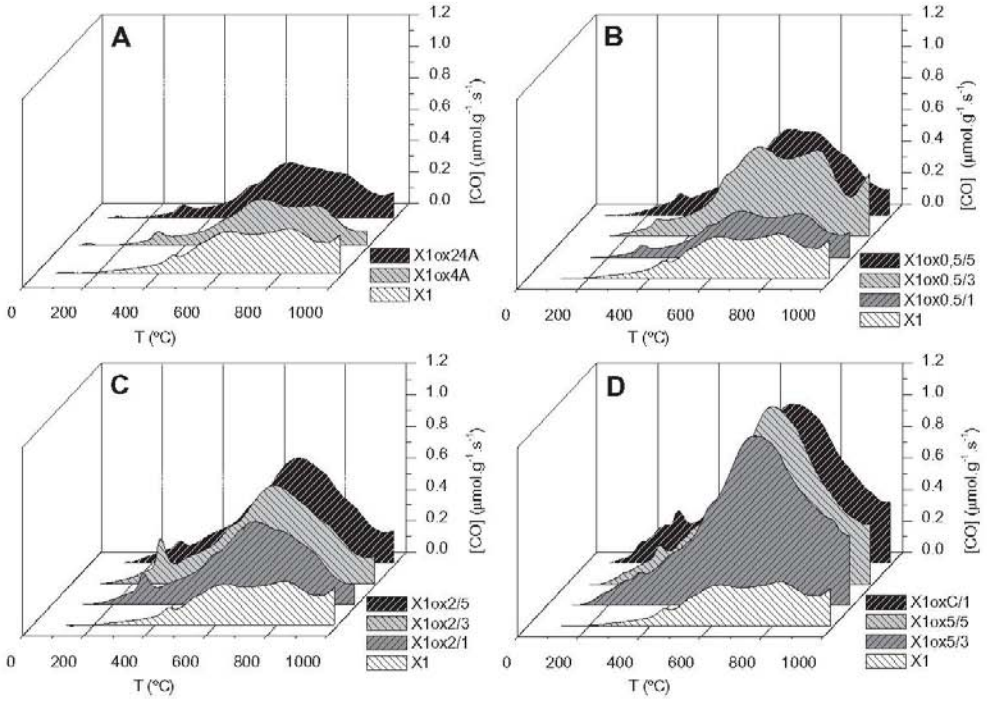

Fig. 4 – CO profiles of raw carbon (X1) and oxidized materials: (A) 30% (v/v) H_2O_2, (B) 0.5 M HNO_3, (C) 2 M HNO_3 and (D) 5 M and 14.55 M HNO_3.

functional groups, mainly acidic, even after mild oxidation treatments with hydrogen peroxide and nitric acid; their area increases with increasing oxidant concentration and oxidation time. When H_2O_2 is used as oxidizing agent, longer treatments mainly produce an increase in the area of peaks between 200 and 300 °C (strong carboxylic acids), but to a lower extent than when using 0.5 M HNO_3 (compare Fig. 5A and B). When the oxidation is carried out with higher concentrations of nitric acid (2, 5 and 14.55 M) and longer oxidation times, a great evolution of CO_2 is observed between 250 and 400 °C (weakly carboxylic acids), and the highest CO_2 peak areas are obtained for the sample oxidized with concentrated 14.55 M HNO_3 (compare Fig. 5C and D).

Deconvolution of the CO_2 profile for X1oxC/1 sample is shown in Fig. 7. Other deconvoluted profiles can be found in Fig. S3 at Supporting Information. Different peaks can be distinguished. The two small peaks (and probably a third one that is contained in the maximum of the large peak at 250 °C) correlate with the small peaks desorbed at temperatures lower than 350 °C that appear in the CO profile of this sample. Their positions and areas are almost the same, and for this reason they could be assigned to the desorption of carboxylic anhydrides in different chemical environments. The same correlation exists between the two peaks with higher areas located from 400 to 510 °C in the CO_2 profile and the corresponding peaks in the CO profile, and therefore they can also be assigned to carboxylic anhydrides in different chemical environments. The intense peak at ~250 °C could be due to the desorption of carboxylic acids and finally, the peaks that appear above 600 °C are due to lactones and lactols [12,30–34].

Globally considered, the TPD results indicate that oxidation of OMCs by means of H_2O_2 mainly introduces phenols and hydroquinones, and their concentration increases with the treatment time; through nitric acid oxidation under mild conditions, phenols, hydroquinones and carboxylic acids are mostly generated, their quantity being enhanced at higher nitric acid concentration and oxidation time.

The XPS technique is often used to identify the nature of chemical bondings in carbon material surfaces. In this way, the deconvolution of C1s and O1s high-resolution spectra provides useful information on the nature of the oxygen functional groups generated on the carbon surface. Thus, TPD and XPS techniques give complementary results to characterize the chemical evolution of the original OMC with oxidation treatments. XPS high-resolution spectra of the starting and oxidized carbons were also deconvoluted into single peaks (recorded in Fig. 8), and each peak was assigned to a certain type of chemical bonding. As expected, the main element at the surface was carbon, and its concentration decreased with increasing oxygen content when higher oxidant concentration and treatment times were used. Moreover, on the surface of all samples no elements other than carbon and oxygen were found.

The relatively low oxygen concentration at the surface of the starting material indicates that this is well ordered and with a low concentration of defects [2]. Deconvolution of its C1s high-resolution spectrum (Fig. 8A) gives rise to six peaks

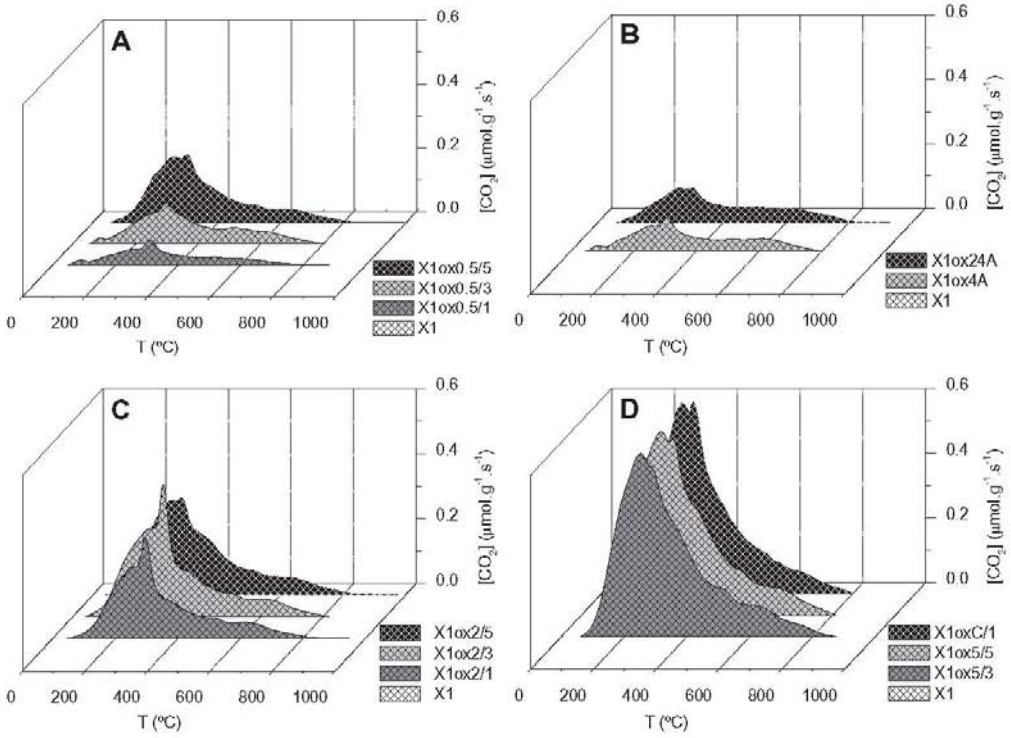

Fig. 5 – CO_2 profiles of raw carbon (X1) and oxidized materials: (A) 0.5 M HNO_3, (B) 30% (v/v) H_2O_2, (C) 2 M HNO_3 and (D) 5 M and 14.55 M HNO_3.

indicating the presence of graphitic Csp^2 at 284.39 eV, C–O and C–OH carbon species of alcohol and ether groups at 285.39 eV, C-=O bonds in carbonyl groups at 286.69 eV, carboxyl and ester functional groups at 289.09 eV, and finally, $\Pi \rightarrow \Pi^*$ transitions in highly ordered and graphitic structures at 291.39 eV. The O1s high-resolution spectrum (Fig. 8A) consists of a broad peak with low intensity; the deconvolution of O1s envelope gives three peaks: a first one at 531.8 eV, due possibly to the presence of C-=O in quinones, a second peak at 533.2 eV assigned to oxygen in phenols, non-carbonyl oxygen in carboxyls and lactones, and a contribution of single-bonded oxygen in alcohol and ether groups; and a third and small peak at 535.4 eV, which is attributed to chemisorbed/physisorbed water [2,18,32,37].

With increasing oxidant concentration and treatment times, the oxygen content and the number of peaks related to different surface oxygen functional groups increase. Broad peaks indicate the existence of different chemical states of oxygen [35,36,38]. In this way, in the sample oxidized with H_2O_2 for 24 h at room temperature (Fig. 8B), the C1s high-resolution spectrum comprises six peaks, being very similar to the starting material spectrum with the only difference that an increase in the relative intensity of the peak at 285.36 eV is produced, which is ascribable to generation of alcohol and ether groups.

Larger differences are observed in the O1s spectrum (Fig. 8B), in which the signal is considerably stronger. This spectrum presents a good fit with three peaks: two of them with similar intensities at 531.88 and 533.30 eV, assigned to C-=O bonds in esters, anhydrides and carboxyls, and single-bonded oxygen in ether and ester groups, respectively. A weak peak at 535.78 eV indicates the presence of chemisorbed water on this material surface [2,38–40].

When oxidation is carried out with 0.5 M HNO_3, C1s and O1s spectra (Fig. 8C) with stronger differences regarding the X1 spectrum are obtained; here, the C1s spectrum can be fitted to six peaks too, but the areas of the peaks at 285.33, 286.63 and 289.03 eV are higher indicating the generation of greater amounts of alcohol and ether groups, carbonyl and carboxyl groups, respectively. The O1s spectrum was fitted to three peaks, but displaying some differences with respect to the H_2O_2 treatment, too. These differences include a shift of the peak located at 532.04 eV towards higher bonding energies than the corresponding one in H_2O_2. This peak is very broad and may include several bonds, among them, C-=O in esters and anhydrides, and C–O in alcohol and ether groups, whose concentration is slightly higher than that obtained with H_2O_2 during 24 h of treatment. Moreover, this peak is predominant in area over the second one, located at 533.26 eV, and assigned to singly-bonded oxygen in ether and anhydride groups, indicating a foreground generation of these functional groups. The third peak, at 534.80 eV, is shifted to lower bonding energies, and is related to C–OH bondings in carboxylic acids [2,38,39]. Its area is slightly greater

Table 3 – CO and CO_2 concentrations (μmol g^{-1}) obtained in the TPD experiments.

Sample	[CO]	[CO_2]
X1	805	–
X1ox4A	732	175
X1ox24A	866	215
X1ox0.5/1	797	113
X1ox0.5/3	1586	211
X1ox0.5/5	1384	346
X1ox2/1	1326	384
X1ox2/3	1540	480
X1ox2/5	1596	488
X1ox5/3	2771	963
X1ox5/5	2762	935
X1oxC/1	2768	963

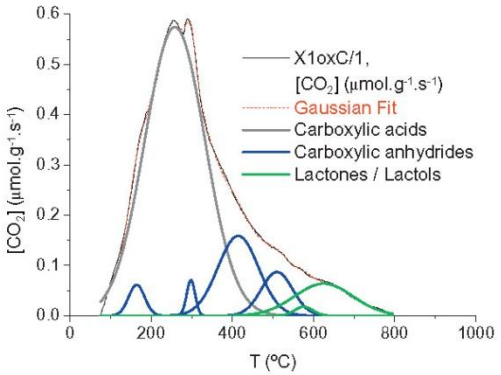

Fig. 7 – CO_2 profile deconvolution of oxidized carbon using 14.55 M HNO_3/room temperature/1 h (X1oxC/1).

than following the H_2O_2 treatment, being in agreement with TPD results shown above. Therefore, XPS spectra of 0.5 M HNO_3/5 h/80 °C-treated sample indicate the presence of higher amounts of carboxylic acids and alcohol/anhydride groups than for the carbon oxidized with H_2O_2/24 h/room temperature.

Finally, the samples treated with 5 M and 14.55 M HNO_3 (Fig. 8D and E, respectively) show C1s high-resolution spectra very similar to each other, and very different from those corresponding to milder oxidation treatments. For the last two, the XPS profiles could be fitted to six peaks, with very similar width and area values, thus indicating the similarity of their surface carbon bondings. This seems reasonable, since their carbon and oxygen mass percentages are in the same range and the TPD results showed occurrence of almost the same oxygen functional groups. The main C1s peak in both samples is placed at 284.34 eV, being assigned to highly delocalized Csp^2 bondings; the second peak, at 285.34 eV, is broader than in the previous cases, indicating the presence of greater amounts of defects on the material surface. The rest of the peaks are practically the same as those mentioned above for samples treated under milder oxidant conditions. However, interesting conclusions can be drawn when studying the corresponding O1s high-resolution spectra, which were fitted to three peaks at 531.6 ± 0.2, 533.1 ± 0.13 and 534.6 ± 0.16 eV. The most important features are the differences between the relative areas and widths of the two peaks located at lower bonding energies. Thus, in X1ox5/5 sample the first peak has higher area and is broader than the second one, and the opposite is observed in X1oxC/1 sample. Broad peaks point to the presence of different oxygen chemical states, and in both samples this is explained by the contribution of C–OH linkages in carboxylic functional groups [38–40]. This is confirmed by the fact that the first peak in sample X1ox5/5 and the first and second peaks in X1oxC/1 sample are shifted to lower bonding energies with respect to carbons treated under mild conditions.

Summarizing, when carbon is oxidized with hydrogen peroxide mainly phenols and hydroquinones are generated, but in lower amounts than using low concentration of nitric acid. Mild oxidation with nitric acid generates a wide range of functional groups. Finally, phenols, hydroquinones, anhydrides and carboxylic acids are predominantly introduced using higher concentrations of HNO_3.

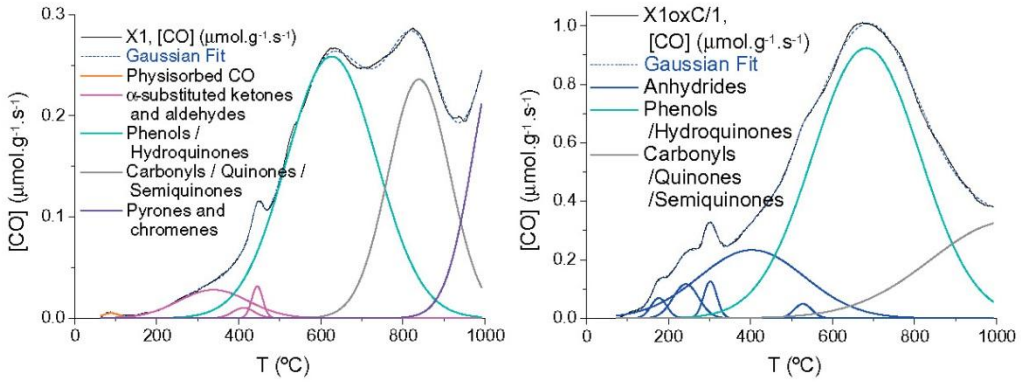

Fig. 6 – CO profile deconvolution of original carbon (X1) and the material oxidized with 14.55 M HNO_3/room temperature/1 h (X1oxC/1).

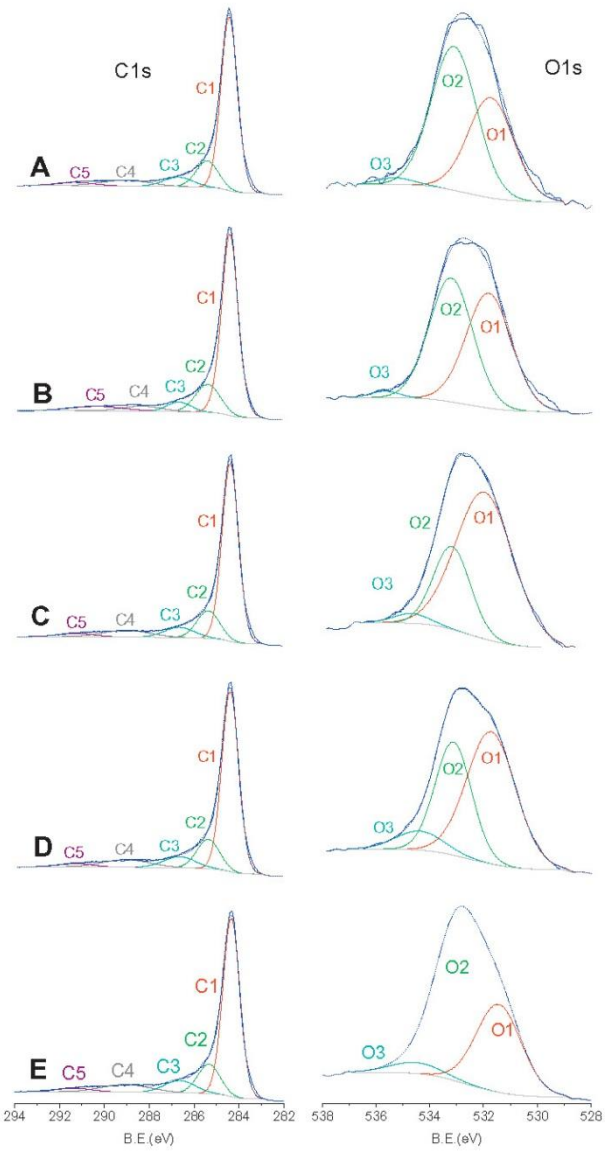

Fig. 8 – C1s and O1s high-resolution spectra of mesoporous carbons: (A) X1, (B) X1ox24A, (C) X1ox0.5/5, (D) X1ox5/5 and (E) X1oxC/1.

4. Conclusions

Through different oxidation treatments with nitric acid and hydrogen peroxide, it was possible to introduce a high variety of oxygen functional groups at the surface of an OMC. By changing the nature and concentration of the oxidizing agent and the treatment time it is possible to introduce different amounts and types of oxygen-containing functional groups, without altering neither the structural arrangement nor the porous texture of the starting OMC, even under severe oxidizing conditions. Although the original carbon is resistant to oxidative treatments, through the most severe oxidation treatments with nitric acid it is possible to introduce up to 9 wt.% oxygen on the surface, mainly in the form of carboxylic, phenol and hydroquinone functional groups. When oxidation is carried out with hydrogen peroxide at room temperature, only 3 wt.% of oxygen is incorporated, mainly by formation of phenolic groups and hydroquinones.

Appendix A. Supplementary data

Supplementary data associated with this article can be found, in the online version, at http://dx.doi.org/10.1016/j.carbon.2013.06.011.

REFERENCES

[1] Ryoo R, Joo SH, Kruk M, Jaroniec M. Ordered mesoporous carbons. Adv Mater 2001;13(9):677–81.
[2] Darmstadt H, Roy C, Kaliaguine S, Choi SJ, Ryoo R. Surface chemistry of ordered mesoporous carbons. Carbon 2002;40(14):2673–83.
[3] Choy KL. Chemical vapour deposition of coatings. Prog Mater Sci 2003;48(2):57–170.
[4] Parmentier J, Saadhallah S, Reda M, Gibot P, Roux M, Vidal L, et al. New carbons with controlled nanoporosity obtained by nanocasting using a SBA-15 mesoporous silica host matrix and different preparation routes. J Phys Chem Solids 2004;65(2–3):139–46.
[5] Radovic LR, Moreno-Castilla C, Rivera-Utrilla J. Carbon materials as adsorbents in aqueous solutions. Chemistry and physics of carbon, vol. 27. New York: Dekker; 2001. p. 227–382.
[6] Stein A, Wang Z, Fierke MA. Functionalization of porous carbon materials with designed pore architecture. Adv Mater 2009;21(3):265–93.
[7] Moreno-Castilla C, López-Ramón MV, Carrasco-Marín F. Changes in surface chemistry of activated carbons by wet oxidation. Carbon 2000;38(14):1995–2001.
[8] Pradhan BK, Sandle NK. Effect of different oxidizing agent treatments on the surface properties of activated carbons. Carbon 1999;37(8):1323–32.
[9] Jaramillo J, Álvarez PM, Gómez-Serrano V. Oxidation of activated carbon by dry and wet methods: surface chemistry and textural modifications. Fuel Process Technol 2010;91(11):1768–75.
[10] Bazula PA, Lu A-H, Nitz J-J, Schüth F. Surface and pore structure modification of ordered mesoporous carbons via a chemical oxidation approach. Microp Mesop Mater 2008;108(1–3):266–75.
[11] Li H, Xi H, Zhu S, Wen Z, Wang R. Preparation, structural characterization and electrochemical properties of chemically modified mesoporous carbon. Microp Mesop Mater 2006;96(1–3):357–62.
[12] Lázaro MJ, Calvillo L, Bordejé EG, Moliner R, Juan R, Ruiz CR. Functionalization of ordered mesoporous carbons synthesized with SBA-15 silica as template. Microp Mesop Mater 2007;103(1–3):158–65.
[13] Lu A-H, Li W-C, Muratova N, Spliethoff B, Schuth F. Evidence for C–C bond cleavage by H_2O_2 in a mesoporous CMK-5 type carbon at room temperature. Chem Commun 2005;0(41):5184–6.
[14] Vinu A, Hossian KZ, Srinivasu P, Miyahara M, Anandan S, Gokulakrishnan N, et al. Carboxy-mesoporous carbon and its excellent adsorption capability for proteins. J Mater Chem 2007;17(18):1819–25.
[15] Jun S, Joo SH, Ryoo R, Kruk M, Jaroniec M, Liu Z, et al. Synthesis of new, nanoporous carbon with hexagonally ordered mesostructure. J Am Chem Soc 2000;122(43):10712–3.
[16] Kruk M, Jaroniec M, Kim T-W, Ryoo R. Synthesis and characterization of hexagonally ordered carbon nanopipes. Chem Mater 2003;15(14):2815–23.
[17] Vinu A, Srinivasu P, Takahashi M, Mori T, Balasubramanian VV, Ariga K. Controlling the textural parameters of mesoporous carbon materials. Microp Mesop Mater 2007;100(1–3):20–6.
[18] Wang D-W, Li F, Liu M, Cheng H-M. Improved capacitance of SBA-15 mesoporous carbons after modification with nitric acid oxidation. New Carbon Mater 2007;22(4):307–14.
[19] Kim T-W, Park I-S, Ryoo R. A synthetic route to ordered mesoporous carbon materials with graphitic pore walls. Angew Chem 2003;115(36):4511–5.
[20] Joo SH, Choi SJ, Oh I, Kwak J, Liu Z, Terasaki O, et al. Ordered nanoporous arrays of carbon supporting high dispersions of platinum nanoparticles. Nature 2001;412(6843):169–72.
[21] Su F, Zeng J, Bao X, Yu Y, Lee JY, Zhao XS. Preparation and characterization of highly ordered graphitic mesoporous carbon as a Pt catalyst support for direct methanol fuel cell. Chem Mater 2005;17(15):3960–7.
[22] Zhao D, Feng J, Huo Q, Melosh N, Freidckson GH, Chmelka BF, et al. Triblock copolymer synthesis of mesoporous silica with periodic 50 to 300 Angstrom pores. Science 1998;279(5350):548–52.
[23] Enterría M, Suárez-García F, Martínez-Alonso A, Tascón JMD. Synthesis of ordered micro–mesoporous carbons by activation of SBA-15 carbon replicas. Microp Mesop Mater 2012;151:390–6.
[24] Lee J-S, Joo SH, Ryoo R. Synthesis of mesoporous silicas of controlled pore wall thickness and their replication to ordered nanoporous carbons with various pore diameters. J Am Chem Soc 2002;124(7):1156–7.
[25] Kruk M, Jaroniec M, Sakamoto Y, Terasaki O, Ryoo R, Ko CH. Determination of pore size and pore wall structure of MCM-41 by using nitrogen adsorption, transmission electron microscopy, and X-ray diffraction. J Phys Chem B 2000;104(2):292–301.
[26] Szymanski GS, Karpinski Z, Biniak S, Swiatkowski A. The effect of the gradual thermal decomposition of surface oxygen species on the chemical and catalytic properties of oxidized activated carbons. Carbon 2002;40(14):2627–39.
[27] Moreno-Castilla C, Carrasco-Marín F, Mueden A. The creation of acid carbon surfaces by treatment with $(NH_4)_2S_2O_8$. Carbon 1997;35(10–11):1619–26.
[28] Surygala J, Wandas R, Sliwka E. Oxygen elimination in the process of non-catalytic liquefaction of brown coal. Fuel 1993;72(3):409–11.
[29] Li N, Ma X, Zha Q, Kim K, Chen Y, Song C. Maximizing the number of oxygen-containing functional groups on activated carbon by using ammonium persulfate and improving the temperature-programmed desorption characterization of carbon surface chemistry. Carbon 2011;49(15):5002–13.
[30] Machado BF, Gomes HT, Serp P, Kalck P, Figueiredo JL, Faria JL. Carbon xerogel supported noble metal catalysts for fine chemical applications. Catal Today 2010;149(3–4):358–64.
[31] Pereira MFR, Soares SF, Órfao JJM, Figueiredo JL. Adsorption of dyes on activated carbons: influence of surface chemical groups. Carbon 2003;41(4):811–21.
[32] Vinke P, Van Der Eijk M, Verbree M, Voskamp AF, Van Bekkum H. Modification of the surface chemistry of a gas-activated carbon and a chemically activated carbon with nitric acid, hypochlorite, and ammonia. Carbon 1994;32(4):675–86.
[33] Calvillo L, Moliner R, Lázaro MJ. Modification of the surface chemistry of mesoporous carbons obtained through colloidal silica templates. Mater Chem Phys 2009;118(1):249–53.
[34] Gomes HT, Miranda SM, Sampaio MJ, Silva AMT, Faria JL. Activated carbons treated with sulphuric acid: catalysts for catalytic wet peroxide oxidation. Catal Today 2010;151(1–2):153–8.
[35] Zielke U, Huttinger KJ, Hoffman WP. Surface-oxidized carbon fibers: I. Surface structure and chemistry. Carbon 1996;34(8):983–98.
[36] Weidenthaler C, Lu A-H, Schmidt W, Schüth F. X-ray photoelectron spectroscopic studies of PAN-based ordered mesoporous carbons (OMC). Microp Mesop Mater 2006;88(1–3):238–43.
[37] Polzonetti G, Lucci G, Altamura P, Ferri A, Paolucci G, Goldoni A, et al. Thiophene-containing organometallic polymers

studied by near-edge X-ray absorption spectroscopy. Surf Interface Anal 2002;34(1):588–92.
[38] Dongil AB, Bachiller-Baeza B, Guerrero-Ruiz A, Rodríguez-Ramos I, Martínez-Alonso A, Tascón JMD. Surface chemical modifications induced on high surface area graphite and carbon nanofibers using different oxidation and functionalization treatments. J Colloid Interface Sci 2011;355(1):179–89.
[39] Boudou JP, Paredes JI, Cuesta A, Martínez-Alonso A, Tascón JMD. Oxygen plasma modification of pitch-based isotropic carbon fibres. Carbon 2003;41(1):41–56.
[40] Seredych M, Hulicova-Jurcakova D, Lu GQ, Bandosz TJ. Surface functional groups of carbons and the effect on their chemical character, density and accessibility to ions on electrochemical performance. Carbon 2008;46(11):1475–88.

Supporting information

Surface modification of nanocast ordered mesoporous carbons through a wet oxidation method

A. Sánchez-Sánchez[1], F. Suárez-García, A. Martínez-Alonso, J. M. D. Tascón.

Instituto Nacional del Carbón, INCAR-CSIC, Apartado 73, 33080 Oviedo, Spain.

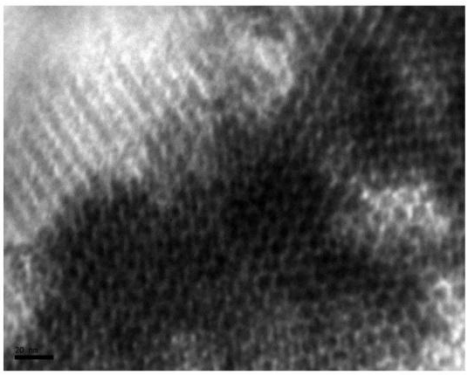

Figure S1: TEM micrograph taken along the channel direction of the X1 carbon. It confirms the CMK-3 type structure of X1 as carbon rods are clearly seen.

[1] Corresponding autor: Fax Number: +34 985 297 662; E-mail adress: ang.san@incar.csic.es

(A. Sánchez-Sánchez)

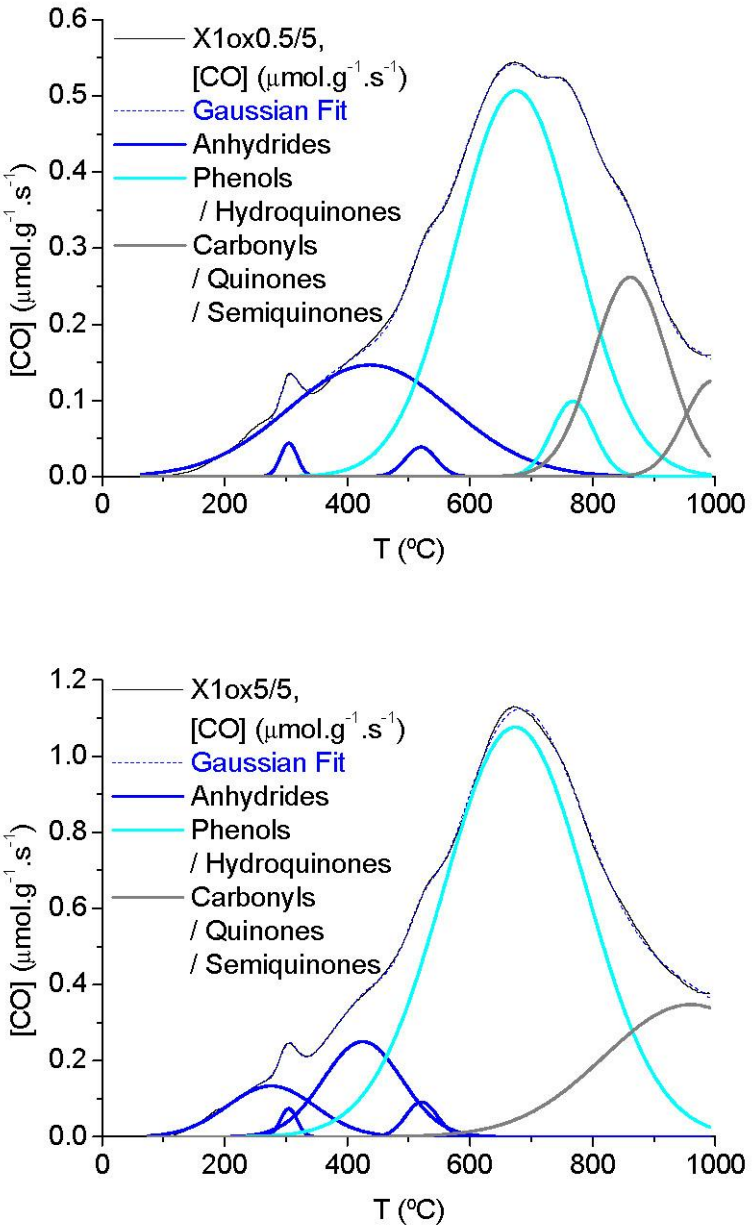

Figure S2: CO profile deconvolution for carbons oxidized with 0.5 and 5 M HNO_3 during 5 h.

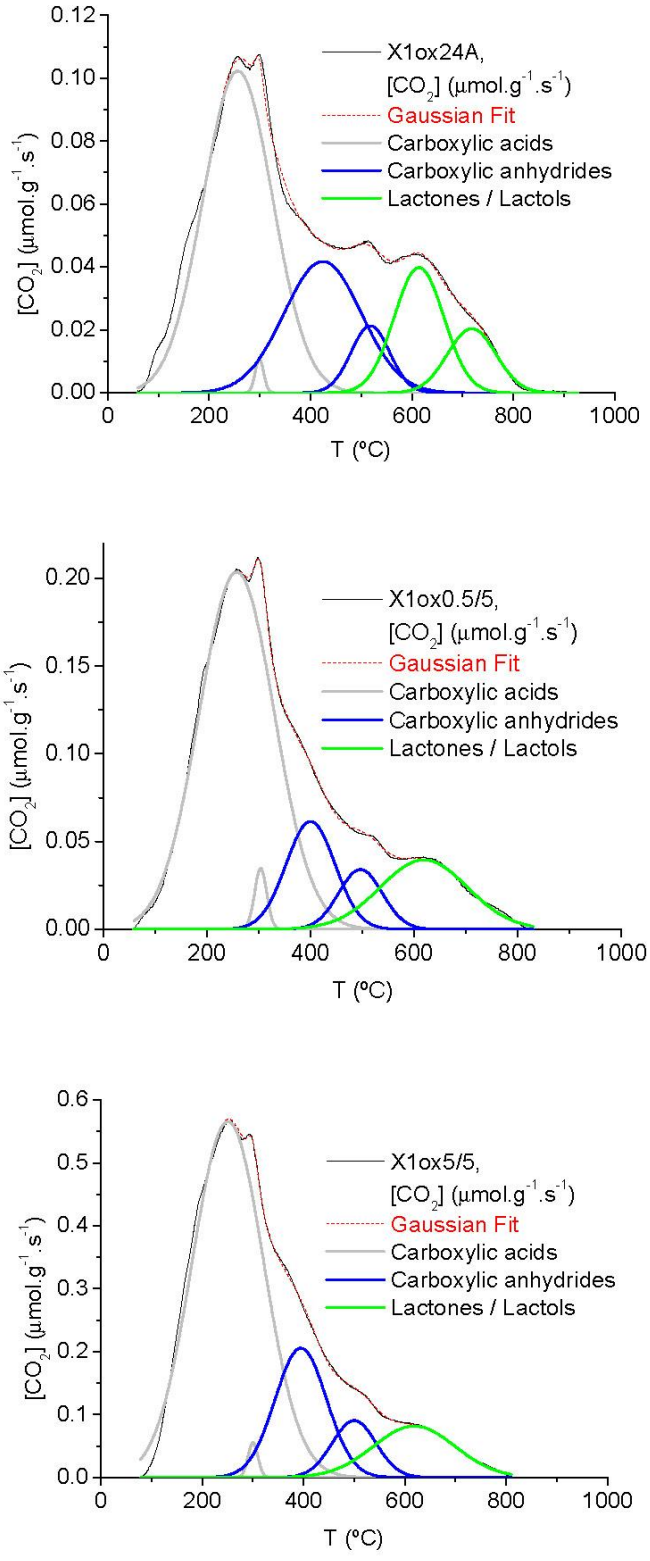

Figure S3: CO_2 profile deconvolution of carbons oxidized with 30 % (v/v) H_2O_2 during 24 h and 0.5 and 5 M HNO_3 during 5 h.

PUBLICACIÓN 2:

'Synthesis, characterization and dye removal capacities of N-doped mesoporous carbons'. *Enviado a publicación*

Diversos CMOs dopados con nitrógeno fueron sintetizados por CVD usando acetonitrilo como fuente simultánea de carbono y nitrógeno y SBA-15 como plantilla de sílice mesoporosa. Posteriormente, se llevó a cabo la caracterización textural, estructural y de la química superficial de dichos materiales y se relacionó su evolución con las condiciones experimentales utilizadas, esto es, la concentración de la corriente de acetonitrilo y el tiempo de depósito. Los detalles del procedimiento experimental utilizado se encuentran en el **Apartado 3.1.2.1**. Examinando los usos potenciales de estos materiales, nos dimos cuenta de que la influencia de las funcionalidades de nitrógeno sobre la adsorción de colorantes por carbones había sido poco estudiada en comparación con los numerosos trabajos dedicados a las funcionalidades oxigenadas. Por tanto, utilizamos estos materiales para estudiar la influencia de grupos funcionales nitrogenados sobre la adsorción de colorantes ácidos y básicos. Para ello se utilizó un CMO no dopado con fines comparativos, obtenido por CVD de propileno tal y como se indica en el **Apartado 3.1.2.1**. Como compuestos para la adsorción se seleccionaron tres colorantes con diferente tamaño molecular y conteniendo grupos funcionales ácidos o básicos: el azul de metileno, el naranja de metilo y la fucsina ácida. Los dos primeros poseen tamaños moleculares semejantes y diferente carácter ácido-base, y el último es de mayor tamaño y posee grupos funcionales ácidos.

El grado de infiltración (esto es, la cantidad de carbón depositado en la plantilla) depende de la concentración de acetonitrilo en la corriente de síntesis y del tiempo de infiltración. De este modo, aumentando cualquiera de estas variables se produce un incremento del primero.

La textura porosa y el ordenamiento estructural dependen del grado de infiltración de la plantilla y no de las condiciones experimentales, esto es, concentración de precursor y tiempo de depósito. A medida que aumenta el grado de infiltración, las áreas superficiales y los volúmenes de poros de los N-CMOs disminuyen y aumenta

el ordenamiento de largo alcance. Esto se explica por una infiltración más homogénea y una mejor replicación de la plantilla. Las distribuciones de tamaños de poro de los materiales muestran claramente esta evolución: a medida que aumenta el grado de infiltración, las distribuciones se hacen progresivamente más estrechas y presentan un solo tamaño de mesoporos a 3.4 nm, que se corresponde con el espesor de las paredes de la plantilla utilizada. Asimismo, la replicación correcta de ésta, desde el punto de vista del ordenamiento de largo alcance y de la morfología de las partículas, se produce para porcentajes de infiltración superiores al 40% en peso.

La composición química de los N-CMOs es independiente de las condiciones experimentales y del grado de infiltración de la plantilla, y depende casi exclusivamente de la temperatura de carbonización. Los N-CMOs obtenidos presentan una naturaleza química muy rica en grupos funcionales nitrogenados y oxigenados. La concentración superficial de nitrógeno alcanza el 9.42% en peso, encontrándose principalmente en forma de nitrógeno cuaternario. El contenido superficial de oxígeno varía inversamente con el contenido de nitrógeno. Su concentración oscila entre el 3 y el 5% en peso, formando parte de ésteres, anhídridos y alcoholes en mayor medida, y carbonilos y ácidos carboxílicos en menor proporción.

Por el contrario, y tal como era de esperar, el CMO no dopado presenta un grado de funcionalización muy pobre: su contenido en oxígeno es inferior al 3% en peso y no se encuentra nitrógeno dentro de los límites de detección de los equipos utilizados.

A partir de los datos de adsorción de los tres colorantes mencionados anteriormente, se concluye que la presencia de grupos funcionales nitrogenados es desfavorable para la adsorción de colorantes catiónicos como el azul de metileno. Sin embargo, la adsorción de colorantes aniónicos, naranja de metilo y fucsina ácida, no se ve afectada por la presencia de dichas funcionalidades, sino que depende principalmente de la porosidad de los carbones. Por otro lado, la presencia de funcionalidades nitrogenadas está asociada con una mejora en las cinéticas de adsorción de ambos tipos de colorantes, ácidos y básicos: los N-OMCs alcanzan

virtualmente el 100% de las capacidades máximas de adsorción en menos de 15 minutos. Dichas mejoras pueden ser explicadas por la mayor hidrofilia de la superficie de los N-OMCs debido a la presencia de una gran cantidad de grupos funcionales polares, que promueven el contacto de los carbones con la disolución y aumentan la velocidad del proceso de adsorción.

Synthesis, characterization and dye removal capacities of N-doped mesoporous carbons

Á. Sánchez-Sánchez, F. Suárez-García*, A. Martínez-Alonso, J. M. D. Tascón

Instituto Nacional del Carbón, INCAR-CSIC, Apartado 73, 33080 Oviedo, Spain.

Abstract

Nitrogen-doped ordered mesoporous carbons (N-OMCs) were synthesized by chemical vapor deposition, using acetonitrile as carbon and nitrogen source and SBA-15 as mesoporous silica template. Their porous texture, structural order and surface chemistry were studied as a function of the experimental conditions (acetonitrile stream concentration and deposition time). A non-doped OMC was prepared by the same procedure using propylene as carbon source. Methylene blue (MB), methyl orange (MO) and fuchsin acid (FA) were selected as probe molecules to investigate the dye adsorption behavior on the OMCs. Both N-doped and non-doped OMCs adsorbed large amounts of these three dyes demonstrating the importance of mesoporosity, especially for the adsorption of larger dyes (e.g. FA). Nitrogen functional groups were detrimental for the adsorption of the basic dye (MB). On the other hand, the nitrogen functionalities improved the adsorption kinetics for both acid and basic dyes, and the N-doped samples achieved 100% of their maximum adsorption capacities in less than 15 min.

Key words

Ordered mesoporous carbon; N-doped carbons; dye adsorption; adsorption kinetics

* Corresponding author: Fax number: +34 985 297 662; e-mail address: fabian@incar.csic.es

1. INTRODUCTION

Dyes are a kind of synthetic compounds with high chemical stability and usually large size that are extensively used in textile, printing, paper, plastic and other industries [1, 2]. Many of them are not particularly toxic, but are very difficult to biodegrade and in small amounts they can color large bodies of water to which they are dumped, reduce the penetration of sunlight, consume dissolved oxygen and destroy life ecosystem. Numerous studies show that these compounds can be efficiently removed by adsorption [1-6]; this method has a lower cost than other techniques, it affords a high efficiency and capacity to adsorb a wide variety of chemical compounds, the operational design is very simple and a variety of adsorbent materials is available [2-4, 6], including zeolites [7-9], mesoporous silicas [10, 11], clay materials [4] and especially low-cost adsorbents (i.e. agriculture and industrial residues) [1, 3, 12, 13] and activated carbons [2, 5-7, 14-18]. Activated carbons present advantages over other adsorbents, not only in terms of higher adsorption capacities but also as catalysts for dye degradtion [5, 6, 19]. Nevertheless, most dyes are bulky molecules, usually with molecular sizes > 1 nm, while the porosity of many classical activated carbons is mainly composed by micropores (pore width < 2 nm), which results in pore blockage and slow adsorption kinetics. Therefore, mesoporous carbons (pore size between 2 and 50 nm) would be more suitable than other adsorbents for removing bulky dyes from water, as it was recently demonstrated [14, 20-27]. Among them, ordered mesoporous carbons (OMCs) are expected to have a better performance for dye adsorption than amorphous mesoporous carbons. Thus, it was demonstrated that the spatial ordered arrangement of their porosity, the existence of hierarchical porosity in some of them, the narrow pore size distributions (consisting of a single pore size in many cases) and their high pore volumes and tunable pore size and structure, determine a faster adsorption kinetics, higher selectivity and larger adsorption capacities than for other more conventional mesoporous materials in different applications [28-30].

Besides porosity, surface chemistry is another important factor in adsorption since

it determines the acid or basic character of the adsorbent, modifies its hydrophilicity and specific interactions can be established between the functional groups of the adsorbent surface and those of the adsorbate [6, 31, 32]. In the context of dye adsorption, Pereira et al. [33] modified an activated carbon by different treatments and studied the influence of surface chemistry on adsorption of anionic and cationic dyes. In the case of anionic dyes the adsorption capacity was clearly related with the surface basicity of the carbon. For cationic dyes the presence of acid groups had a positive effect, but these dyes were mainly adsorbed by dispersive interactions between free electrons of the dye molecule and delocalized electrons of the graphene layer. The presence of oxygen-containing (acid) groups on the surface of a CMK-3 type OMC [34] also enhanced the adsorption capacity of reactive (anionic) dyes [35]. This was attributed to the increase of the surface hydrophilicity and the better dispersion of the adsorbent in an aqueous medium. Other works on the effect on dye adsorption of the surface chemistry of activated carbons modified by oxidation and/or thermal treatments can be found in the literature [5, 6, 32].

In connection with the beneficial effects of surface functionalities in carbons [5, 6, 16, 31-33, 35, 36] for dye removal, the presence of nitrogen functionalities is expected to improve the behavior of doped carbons by increasing their basic character and also by establishing specific interactions with certain dyes. The functionalization of OMCs with oxygen-containing groups can be easily carried out by oxidation post-treatments [37-39], but the preparation of N-doped OMCs still constitutes a major challenge. A suitable selection of both the precursor and the experimental conditions has to be done in order to achieve N-doped carbons having an ordered porous structure [40-46].

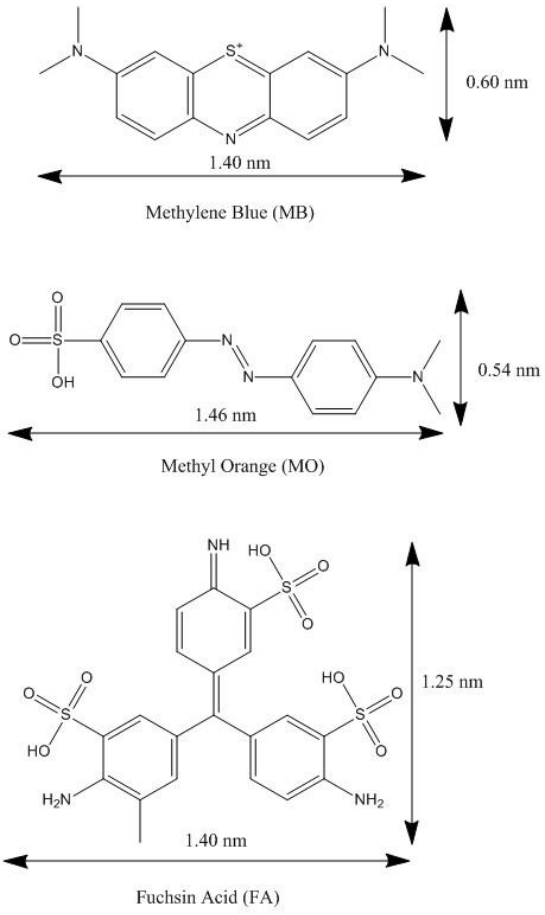

Figure 1. Molecular structure of the three dyes used in this work. Molecular sizes estimated with ChemBioDraw® software.

The influence of nitrogen functionalities on dye adsorption by carbons has been comparatively little studied. To our knowledge, the only available results are those from Peng et al. [47], who very recently studied the effect of N-doping of CMK-3 by ammonia treatment on the adsorption of an acid dye (acid black 1). In the present work, N-doped OMCs were synthesized through chemical vapor deposition (CVD) using acetonitrile as precursor and SBA-15 silica as mesoporous template. The effect of experimental conditions on the structural, textural and surface chemical properties of the obtained carbon materials was studied. These N-OMCs, and an un-doped carbon also obtained by CVD (using propylene as precursor and the same silica template), were then used as adsorbents for acidic and cationic dyes. Three dyes with different molecular sizes and containing acidic or basic functional groups were used as model compounds (Figure 1): methylene blue (MB, cationic dye; ~1.40

x 0.60 x 0.25 nm), methyl orange (MO, azo dye possessing an anionic group, SO_3^-; ~1.46 x 0.54 x 0.20 nm) and fuchsin acid (FA, anionic dye; ~1.40 x1.25x0.50 nm). The two first dyes have similar molecular sizes but different acid-base character and the last one has a larger molecular size.

2. EXPERIMENTAL SECTION

2.1. Synthesis of SBA-15 silica template

Mesoporous SBA-15 silica was prepared following a soft-templating method described by Zhao et al. [48]. Pluronic P123 (Mw= 5800, Aldrich) was dissolved in an aqueous solution of HCl (Merck). After that, tetraetoxysilane (TEOS, Aldrich) was added dropwise and the mixture was kept under stirring (40 ºC, 4 h). The molar composition of the starting reaction mixture was 0.017 P123 / 1 TEOS / 145.8 H_2O / 6.04 HCl. The resulting product was aged (125 ºC, 72 h), filtered and calcined in air (550 ºC, 6 h).

2.2. Synthesis of nitrogen-doped mesoporous carbons (N-OMCs)

N-doped OMCs (CMK-3 type) were synthesized via CVD using acetonitrile as source for both carbon and nitrogen. Typically, 0.5 g SBA-15 was heated to 850 ºC under an argon flow (99.999% purity); once this temperature was reached, an argon flow saturated with acetonitrile (placed in a flask thermostated at 25 ºC) was passed through the reactor for different times. The acetonitrile concentration was calculated from Antoine equation (1):

$$\log P_{vap} = A - \frac{B}{T+C} \qquad (1)$$

, where P_{vap} is the vapor pressure of acetonitrile (expressed in mmHg), *A*, *B* and *C* the constants for acetonitrile (*A*= 7.0733, *B*= 1279.2 and *C*= 224.01) and T the temperature of the thermostatic saturator (in ºC). For a temperature of 25 ºC, the acetonitrile P_{vap} was 86.37 mmHg. The acetonitrile concentration (in v/v %) was calculated taking into account the different argon flows that were saturated with the precursor. The resulting values are listed in Table 1.

The synthesized silica-carbon composites were treated with 48% HF at room

temperature for 12 hours in order to remove the silica template, then filtered and washed several times with distilled water and finally dried at 100 ºC. The resulting N-OMCs were called *Nx/t*, where *x* indicates the acetonitrile concentration in v/v % and *t* the CVD time in hours. Besides the N-doped OMCs, a non-doped CMK-3 carbon (named *X3*) was also synthesized by CVD using propylene as carbon source as described elsewhere [37].

2.3. Materials characterization

Porous texture characterization was done from nitrogen adsorption isotherms at -196 ºC measured in a volumetric apparatus ASAP 2010 (Micromeritics). The samples were degassed at 250 ºC for 15 h prior to measurements. Applying the BET equation we obtained the apparent surface area, S_{BET}; the total pore volume, V_t, was calculated from the adsorbed amount at the relative pressure of 0.975; the micropore volume, V_{micro}, was determined using the Dubinin-Raduskevich equation; by subtraction of V_{micro} from V_t, the mesopore volume, V_{meso}, was obtained. Pore size distributions (PSDs) were obtained by applying the non-local density functional theory (NLDFT).

The infiltration degree (wt.%) (i.e., the carbon content in the carbon/silica composite) was determined by thermogravimetric analysis in a CI Electronics microbalance, using an air flow of 50 mL/min.

Structural and morphological characterizations were carried out by X-ray diffraction (XRD), scanning electron microscopy (SEM) and transmission electron microscopy (TEM), using a Siemens D5000 diffractometer (Cu K_α radiation; scanning range 2θ = 0.5-5º; step width = 0.01º; time per step = 1 second), a Carl Zeiss DMS-942 microscope and a JEOL 2000 EX/II microscope (operating potential of 160 KV), respectively.

The surface chemical characterization was carried out by elemental analysis and X-ray photoelectron spectroscopy (XPS). Elemental analysis was done on a TruSpec Micro analyzer provided with a TruSpec O accessory for oxygen. XPS analysis was performed on a SPECS system, working at a pressure of 10^{-7} Pa with a

monochromatic Al K_α X-ray source (1486.3 eV, 150 W).

2.4. Dye adsorption experiments

2.4.1. Batch equilibrium studies

Batch experiments were performed in a set of erlenmeyer flasks, each one containing 20 mL of different initial concentrations of dye (25-500 mg/L) and 20 mg of carbon, without any pH adjustment. The flasks were kept at 25 ºC in a thermostatic bath shaker. A contact time of 24 hours was set to reach complete equilibrium; after that, the sample solutions were filtered and the residual concentrations were determined by duplicate using a UV/Vis spectrophotometer at the maximum wavelengths (λ_{max}) of light absorption for each dye (665, 465 and 546 nm for MB, MO and Fa, respectively). The adsorbed amount at equilibrium was calculated through equation (2):

$$q_e = C_0 - C_e \frac{V}{m_s} \qquad (2)$$

, being C_0 the initial dye concentration (mg/L), C_e the equilibrium dye concentration (mg/L), V the volume of dye solution (L) and m_s the weight of carbon adsorbent (g).

The maximum adsorption capacity of carbons for each dye was measured using a large excess of adsorbate. Experiments were made in the same manner as for the adsorption isotherms, but using an initial dye concentration of 2 g/L.

2.4.2. Batch kinetic studies

The kinetic experiments were carried out using a set of different erlenmeyer flasks placed in a thermostatic bath shaker at 25 ºC and without any pH adjustment. Each flask contained 20 mg of carbon and 20 mL of fixed initial dye concentration. The solutions were shaken during time intervals from 15 to 450 min, withdrawn and filtered using 0.1 µm syringe filters. The residual concentrations were also measured by duplicate by UV/Vis spectrophotometry at the λ_{max} of light absorption, and the amount of dye adsorbed at time t was calculated using equation (3):

$$q_t = C_0 - C_t \frac{V}{m_s} \quad (3)$$

, being C_t the dye concentration at any time *t* (mg/L).

3. RESULTS AND DISCUSSION

3.1. Characterization of the OMCs

The nitrogen adsorption/desorption isotherms on the obtained OMCs are recorded in Figure 2; the one for the SBA-15 template is also included for comparison with the carbon replicas. The PSDs of the carbon materials are recorded in Figure 3, and porous textural texture parameters are listed in Table 1. As shown in Figure 2, the silica template presents a type IV isotherm with a type-H1 hysteresis loop according to the IUPAC classification, which is characteristic of mesoporous materials with a narrow distribution of uniform pores [49, 50]. As expected, hard-templating of SBA-15 silica gave rise to CMK-3 type mesoporous carbons [34] whose structure is an inverse replica of the former: carbon rods templated from the silica mesoporous channels, and carbon connectors originated from the silica micropores. Therefore, OMCs have mesopores derived from the silica wall and type-IV nitrogen adsorption isotherms are expected from them. As shown in Figure 2, the OMCs prepared in this work exhibit type IV isotherms but with different hysteresis loops. The evolution of the hysteresis loops is related to the different infiltration degree of the silica template (i.e. the amount of carbon present in the composite, see Table 1). Thus, the shape of the hysteresis loops varies from H3 type to H4 type and the nitrogen uptakes at high relative pressures decrease with increasing infiltration degree of the template. Moreover, as the infiltration degree increases the shape of the isotherms tends to take the expected shape for CMK-3 carbon prepared by CVD with propylene [37, 51, 52], as can be seen in Figure 2.

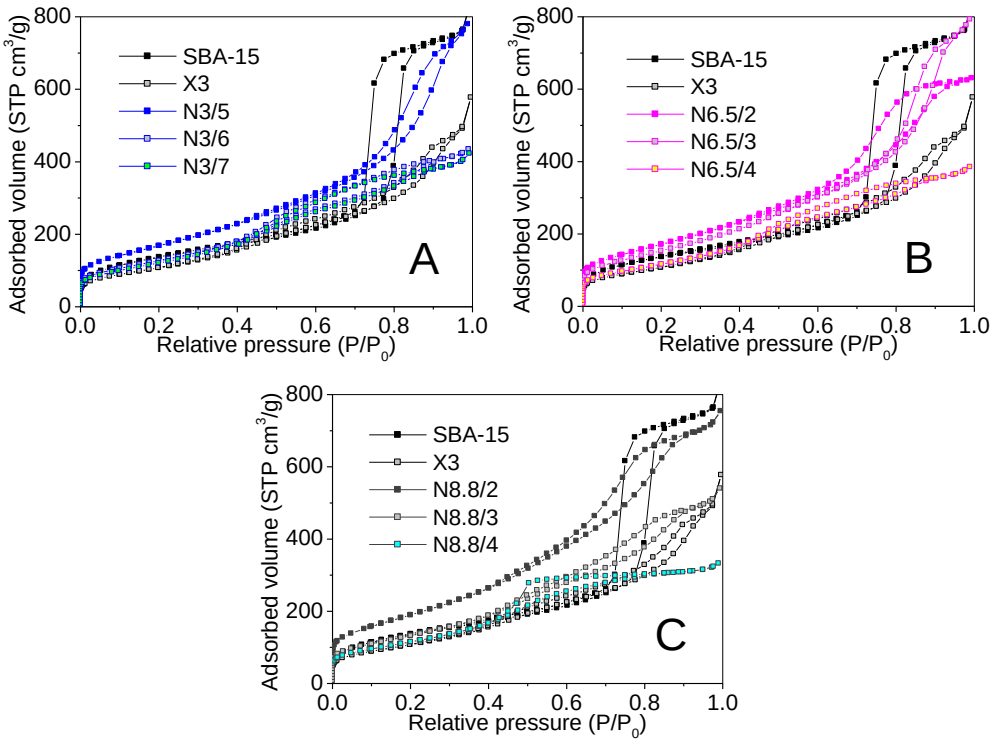

Figure 2. Nitrogen adsorption/desorption isotherms at – 196 ºC on SBA-15 silica template and OMCs prepared by CVD with propylene (sample X3) and N-OMCs synthesized with different acetonitrile concentrations: A) 3.0 % v/v, B) 6.5 % v/v and C) 8.8 % v/v.

The evolution of the PSDs of the carbon materials (Figure 3) agrees with the aforementioned change in the shape of the isotherms, which is connected with the achieved infiltration degree. The PSDs of the OMCs with low infiltration degrees (samples N3/5, N6.5/2, N6.5/3 and N8.8/2) show two maxima in the mesopore range (at 3.36 nm and between 5 and 10 nm). As the infiltration degree increases (see Table 1), the second maximum shifts to a lower pore size; the PSDs become narrower and exhibit only a mesopore size at 3.36 nm for the highest degrees of infiltration, which corresponds to the silica wall thickness [52]. The sample prepared by propylene CVD (sample X3) has a pore size distribution similar to those of the N-doped carbons with a similar infiltration degree (samples N3/7, N6.5/4 and N8.8/4). The results collected in Table 1 demonstrate that increasing acetonitrile concentrations are needed to shorten the CVD time in order to obtain equivalent infiltration degrees.

Table 1. Experimental conditions used in the CVD process, textural parameters calculated from the N_2 adsorption/desorption isotherms measured at -196 ºC, infiltration degree of the composites and structural data from low-angle XRD.

Sample	Experimental conditions		Nitrogen adsorption isotherms at -196 ºC				Infiltration (wt.%)	XRD	
	[CH_3CN] (% v/v)	t (h)	S_{BET} (m^2/g)	V_t (cm^3/g)	V_{micro} (cm^3/g)	V_{meso} (cm^3/g)		$d_{(100)}$ (nm)	a (nm)
SBA-15	--		513	1.24	0.22	1.02	--	9.8	11.3
X3	--		406	0.76	0.14	0.62	55.5	10.1	11.7
N3/5	3.0	5	616	1.16	0.20	0.96	22.5	--	--
N3/6		6	473	0.65	0.15	0.50	46.8	10.0	11.5
N3/7		7	457	0.62	0.14	0.48	50.5	9.9	11.4
N6.5/2	6.5	2	629	0.97	0.20	0.77	23.1	--	--
N6.5/3		3	570	1.18	0.18	1.00	46.9	10.1	11.7
N6.5/4		4	437	0.58	0.14	0.44	55.2	10.0	11.5
N8.8/2	8.8	2	704	1.11	0.23	0.88	42.6	10.1	11.6
N8.8/3		3	494	0.78	0.16	0.62	47.6	10.1	11.6
N8.8/4		4	432	0.50	0.14	0.36	56.4	9.8	11.3

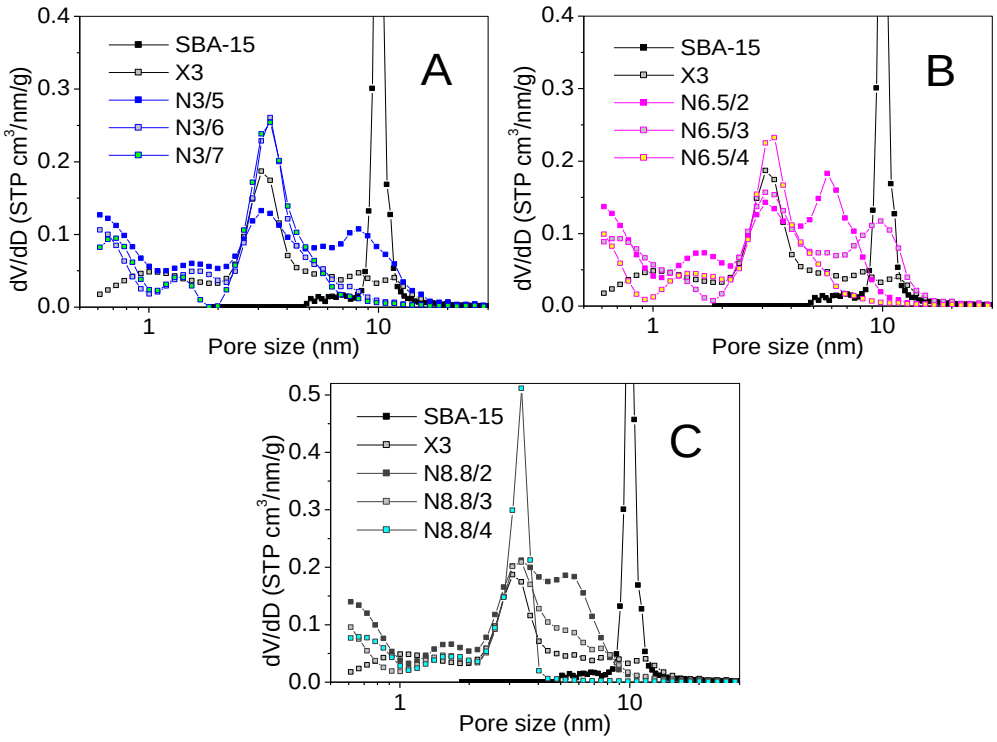

Figure 3. PSDs of the SBA-15 silica template, OMC prepared by CVD with propylene (sample X3) and N-OMCs synthesized with different acetonitrile concentrations: A) 3.0 % v/v, B) 6.5 % v/v and C) 8.8 % v/v.

Also, comparing the pore textural parameters of samples with similar infiltration degrees, it seems clear that porosity development depends on the infiltration degree rather than on the experimental conditions (e.g., acetonitrile concentration). Additionally, OMCs prepared with acetonitrile as precursor and having infiltration degrees around 55 wt.% have a porous texture similar to that of the X3 carbon, obtained using propylene as carbon source.

Similar conclusions can be drawn from the evolution of the XRD patterns (Figure 4): carbons exhibiting similar infiltration degrees of the SBA-15 template yield similar low-angle XRD patters. Three well-resolved peaks, which correspond to the (100), (110) and (200) reflections of a p6mm hexagonal symmetry, are clearly observed in the patterns of the SBA-15 template and the OMCs prepared with an infiltration degree higher than 40 wt.%. Figure 4 clearly shows that, for a given acetonitrile concentration, the intensity of the peaks increases with increasing infiltration degree; this suggests that a better long-term ordering of the mesoporous structure is achieved with high infiltration degrees. No peaks can be distinguished in the XRD profiles of the carbons with an infiltration degree < 24 wt.% (N3/5 and N6.5/2), so they are mesoporous (see their porous texture characterization) but not long-term ordered. Two possible reasons could explain this: i) the silica-carbon composites with low carbon content do not withstand the high temperatures of CVD treatment; ii) a poor infiltration process fails to fully replicate the silica template, and the ordered structure partially collapses after silica etching with HF. In order to clarify this, low-angle XRD profiles were measured for several silica-carbon composites with carbon contents of 23 and 47 wt.% (Fig. 4D). The presence of well-defined peaks in the XRD profiles of these composites demonstrates that structural order is lost in the etching step because of the low infiltration degree of the template with carbon.

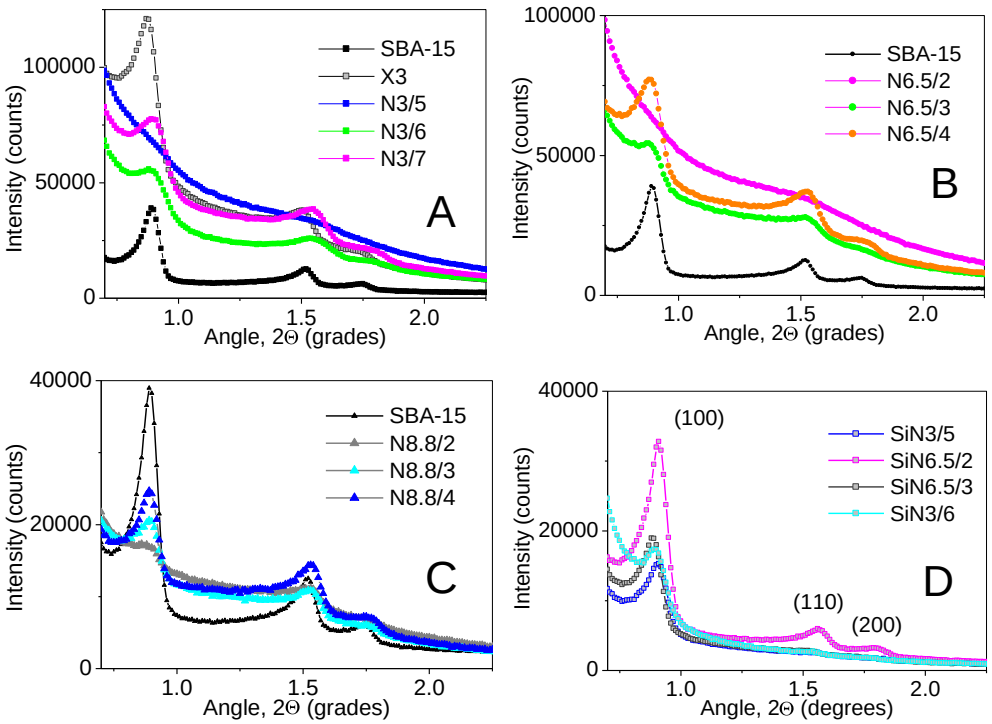

Figure 4. Low-angle XRD patterns of parent SBA-15 template, OMCs prepared by CVD with propylene (sample X3) and carbon replicas synthesized with different acetonitrile concentrations: A) 3.0 % v/v, B) 6.5 % v/v and C) 8.8 % v/v. D) Low-angle XRD patterns of different silica-carbon composites.

Finally, SEM and TEM images (Figure 5) corroborate that infiltration degrees > 40 wt.% are needed to get a proper replication of the template. The SEM micrograph of the lowest infiltrated carbon (N3/5, Figure 5A) shows that particles with a better defined shape coexist with unstructured zones, probably due to a small and heterogeneous filling of silica pores that is insufficient to generate complete replicas of the mesoporous template. By contrast, the SEM micrograph of the most infiltrated carbon (N8.8/4, Figure 5B) presents well-structured particles whose shape is the same as that of the parent silica template (not shown here); this suggests that a high and more homogeneous filling of silica pores was attained. This is also supported by the high-resolution TEM images. Heterogeneous filling of silica pores with carbon can be deduced from the TEM image of N3/5 carbon (Figure 5C) where ill-defined parts coexist with others formed by parallel carbon bars. However, the TEM image of N8.8/4 sample exhibits a well-defined and highly ordered

structure (Figure 5D).

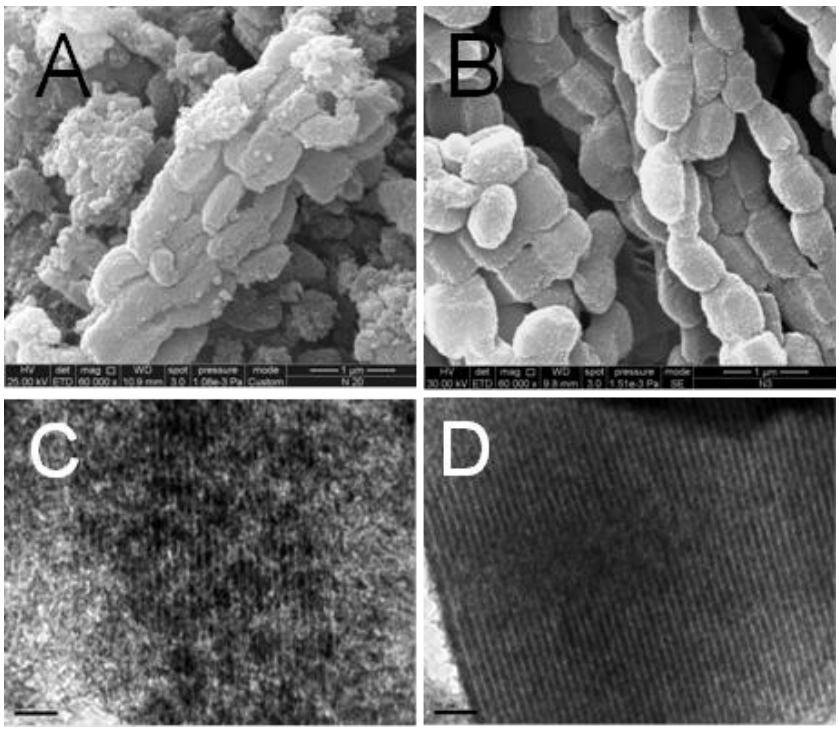

Figure 5. SEM (top) and TEM (bottom) images corresponding to: (A and C) the lowest infiltrated carbon (N3/5) and (B and D) the highest infiltrated carbon (N8.8/4).

Table 2 collects results from elemental analysis and XPS, expressed as weight percentages of carbon, nitrogen and oxygen. No clear relationship is observed between the results obtained by these two techniques. As expected, the most abundant element on the surface and the bulk of materials is carbon, but significant nitrogen amounts were introduced as well. Thus, the nitrogen content in the bulk of the doped carbons ranges from 7.26 to 8.79 wt.%, as measured by elemental analysis; however, the surfaces nitrogen content reached a maximum value of 9.42 wt.% (in the most infiltrated carbon, N8.8/4), as measured by XPS. Moreover, data obtained by both techniques show an inverse trend for nitrogen and oxygen: the greater the nitrogen content, the lower the oxygen content.

Table 2. Chemical composition of the OMCs as obtained by elemental analysis and XPS.

Sample	Elemental analysis (wt.%)			XPS (wt.%)		
	C	N	O	C	N	O
X3	97.54	0.02	2.21	97.04	0.00	2.96
N3/5	83.92	7.26	5.42	88.88	6.98	4.15
N3/6	82.91	7.62	4.76	88.45	8.03	3.52
N3/7	82.38	7.53	5.17	88.61	6.37	5.02
N6.5/2	83.49	7.96	4.68	87.27	9.13	3.61
N6.5/3	83.22	8.68	4.07	87.02	8.43	4.55
N6.5/4	81.01	7.49	5.34	88.06	8.92	3.01
N8.8/2	79.27	8.37	4.87	88.92	8.48	2.61
N8.8/3	82.62	8.62	3.68	87.54	8.55	3.91
N8.8/4	82.55	8.79	3.37	87.23	9.42	3.35

The sample prepared by propylene CVD exhibits a very poor functionalization degree, as deduced from the very low oxygen content (both in the bulk and at the surface). Nitrogen was not found in that sample (X3) within the detection limits of the two used techniques.

Deconvolution of the C1s, N1s and O1s high resolution XPS spectra into single peaks was carried out in an attempt to better understand the carbon surface chemistry in terms of amount and type of different functional groups. Comparing the high-resolution spectra of the different samples (not shown here), only small differences were found. This is consistent with the similar surface compositions of the studied carbons. As an illustration, the high-resolution spectra (C1s, N1s and O1s) of a representative carbon (N8.8/3) are shown in Figure 6. Data from the deconvolution of the peaks and assignment to specific functional groups can be found in Supporting Information (Table S1).

All the carbons displayed asymmetric C1s profiles. Thus, the C1s high resolution spectrum of N8.8/3, shown in Figure 6A, exhibits a tail towards high binding energies (BE), due to the presence of nitrogen and oxygen functionalities in the material surface. The C1s profiles were fitted to six peaks, as shown in Figure 6A;

taking into account the high area and narrow width of the C1and high area of the C6 components, we can say that carbon atoms belong mainly to an ordered and graphitic structure [41, 53, 54].

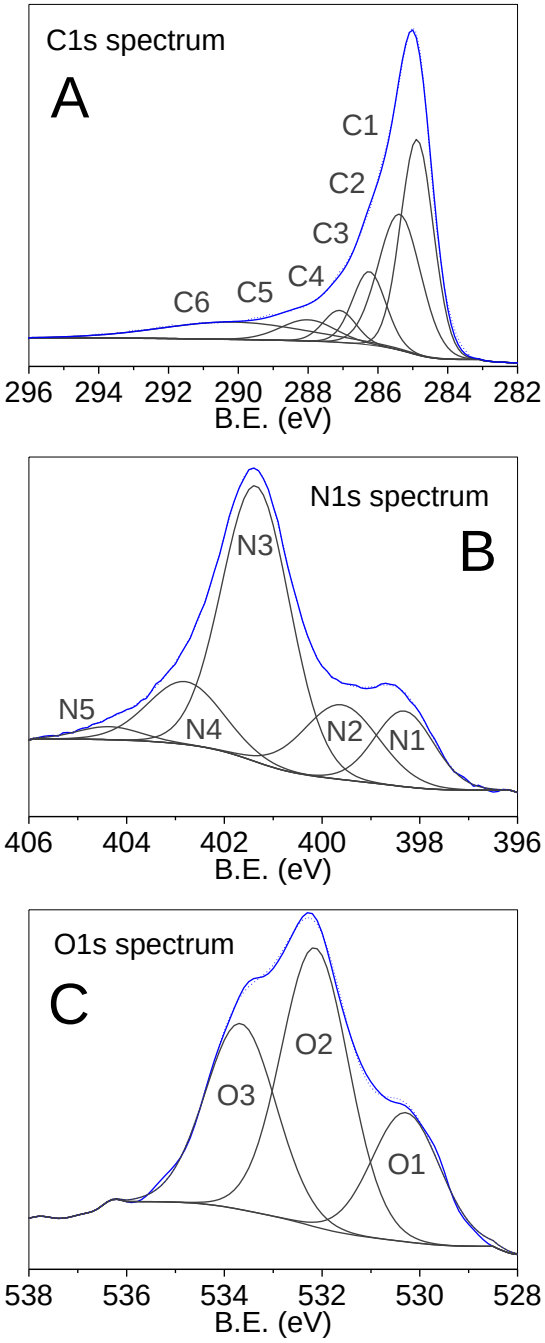

Figure 6. Deconvoluted profiles of the high-resolution spectra for N8.8/3 carbon: A) C1s, B) N1s and C) O1s.

The N1s high resolution spectra of the carbons were broad, as illustrated for N8.8/3

sample in Figure 6B. A satisfactory fit was obtained by means of five broad components, which indicates the existence of numerous local bonding environments giving rise to overlapped peaks. The peak possessing the largest area is N3, assigned to quaternary nitrogen (substitutional nitrogen in condensed polyaromatic systems) [55-57]. Finally, the O1s high resolution spectra of the carbons were also broad. Thus, for sample N8.8/3 (Figure 6C) a satisfactory fit was achieved by means of three peaks; this indicates the main presence of esters, anhydrides and alcohols, as well as carbonyls and carboxylic acids in smaller amounts [41, 54, 55].

3.2. Dye adsorption

The uptake values of the tested dyes by several OMCs are plotted in Figure 7 as a function of the BET surface area. Generally speaking, the studied N-doped mesoporous carbons adsorb a higher amount of MO (up to 1.2 mmol/g) than that of the two other dyes. These carbons (except N8.8/2 sample) adsorb similar amounts of MB and FA despite the different molecular sizes of these two dyes (see Figure 1). The non-doped carbon X3 adsorbs slightly more MB than MO. Taking into account the molecular size of the dyes (Figure 1), the uptake values could be expected to follow the trend MB ~ MO > FA, which is the case for the non-doped carbon. Thus, the amount of each dye required for covering the entire BET surface area of the carbons (namely, the monolayer capacity straight lines in Figure 7) was estimated from the S_{BET} of the material and the dyes' molecular areas, according to equation (4) [32]:

$$Monolayer\ Capacity\ = \frac{S_{BET}}{Dye\ Molecular\ area \times N_A} \qquad (4)$$

, where S_{BET} is the BET surface area recorded in Table 1; N_A is the Avogadro's number; the molecular areas of the dyes were calculated from their molecular sizes (Figure 1).

The value of the monolayer capacity obtained here is only an estimate and can be far from the real one because it is assumed that: i) the entire BET surface area of the material is accessible to the dye (which is not possible due to the molecular size

of the dyes, which will be unable to reach some narrow micropores) and ii) the area occupied by the dye molecules in the adsorbed phase is assumed to be the dye molecular area calculated form their molecular size (this assumption implies that dye molecules are compactly adsorbed in a horizontal orientation and that they are not solvated with water molecules).

Despite these limitations, the monolayer capacity concept is useful for discussion. Thus, as one can see in Figure 7, MO and MB have similar monolayer capacities as a function of the BET surface area in agreement with their similar molecular areas. The monolayer capacity increases linearly with increasing BET surface area for the three dyes, as expected from equation (4). Taking this into account, we can conclude from Figure 7 that the adsorption of acid dyes (i.e. MO and FA) is mainly connected with the porosity of the carbons, while the adsorption of basic dyes (i.e. MB) is clearly hindered by the presence of nitrogen surface functionalities in the adsorbent.

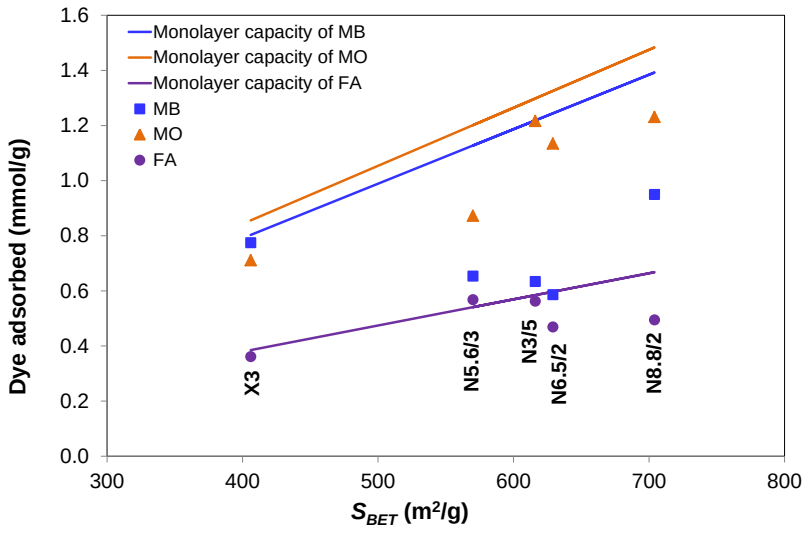

Figure 7. Maximum adsorption capacity of MB, MO and FA on selected N-doped OMCs and on sample X3 (non-doped carbon). Initial dye concentration, 2g/L. The solid lines correspond to the theoretical monolayer adsorption capacity for each dye as function of S_{BET}.

3.2.1. Equilibrium isotherms

The adsorption isotherms for the three dyes at 25 ºC on the non-doped carbon (X3) and two N-doped carbons (N8.8/4 and N8.8/3) were measured in the interval of initial concentrations from 0.025 to 0.5 mg/L (Figure 8). The shape of the resulting isotherms is H4 type according to Giles classification [58]. An H-type isotherm is indicative of a high affinity between the carbon surface and the dye molecules, while the presence of two plateaus indicates the formation of two layers. Figure 8A shows a higher adsorption capacity of MB by X3 sample than by the N-doped carbons in spite of their similar S_{BET}. The non-doped and N-doped carbons have similar adsorption capacities (at least for the first layer, i.e. equilibrium concentration, Ce, around 0.1 mg/mL) for the two other dyes (Figure 8 B and C). These results agree with the previous findings for the maximum adsorption capacities and confirm that the adsorption of MB is hindered by the presence of N-containing surface groups, whereas the adsorption of acid dyes is mainly determined by sample porosity and not by surface functional groups.

The adsorption isotherms were fitted to different theoretical isotherms (Langmuir, Freundlich, Redlich-Peterson and Temkin). For these fits only data up to the first layer formation were used. The values of the correlation coefficient, R^2, and the different constants obtained after fitting the experimental isotherms to the theoretical models are collected in Table 3. The data reported in this table confirm the previous statements about the adsorption of basic and acid dyes in non-doped or N-doped carbons. The Langmuir model yields the best fit for the adsorption of the three studied dyes and carbons, while Temkin equation gives the worst fit. The *b* parameter from the Redlich-Peterson equation is close to 1 in all cases, which indicates that the adsorption isotherms are preferably Langmuirian.

In the case of MB a higher affinity is exhibited by the non-doped carbon (higher Langmuir constant, K_L, and Freundlich exponent, *n,* than for the N-doped carbons). The B constant in the Temkin equation relates to the adsorption energy, therefore it would be expected to be greater for carbon X3 than for the other ones. However it is smaller, which may be due to the very poor fit of the data by Temkin equation.

MO shows an opposite behavior, as K_L and n are much higher for sample N8.8/4 than for sample X3, indicating that the adsorption of this small acid dye is favored by the presence of N-functional groups, although it is not reflected in the maximum adsorption capacities. Finally, in the case of FA both non-doped and doped carbons exhibit comparable parameters (although slightly higher for the doped sample) indicating that for this dye the surface chemistry is less influential than the porosity, probably due to the very large molecular size of FA.

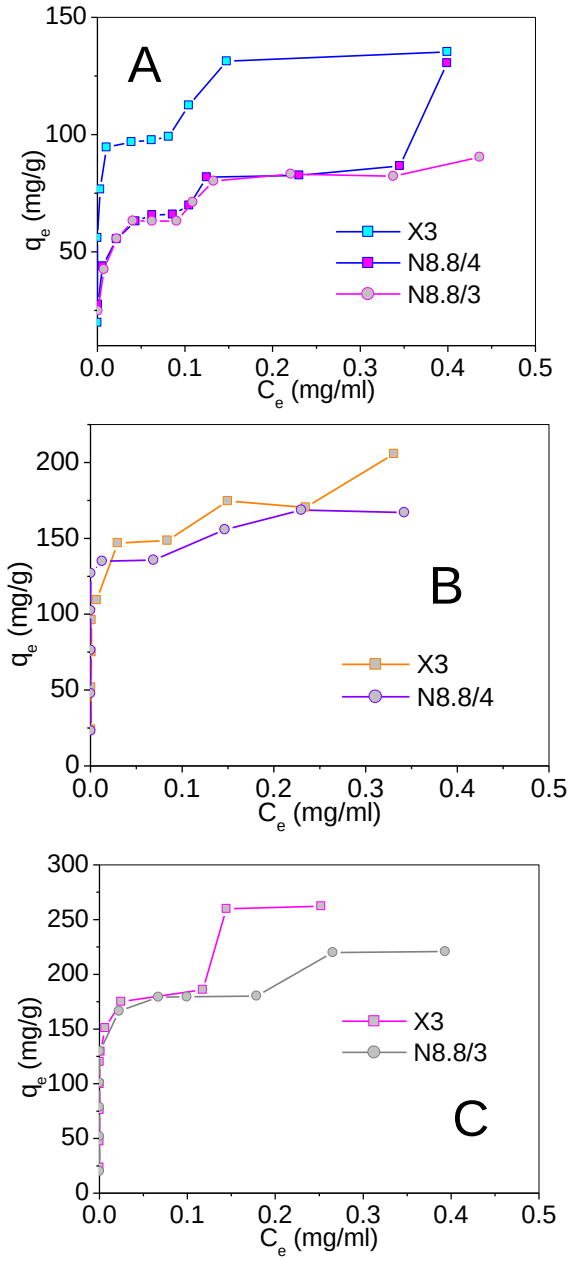

Figure 8. Adsorption isotherms of dyes on X3 and doped carbons: A) MB, B) MO and C) AF.

Table 3. Equilibrium parameters for the adsorption of MB, MO and FA onto X3, N8.8/4 and N8.8/3 samples obtained by applying four theoretical models

Isotherm models		Methylene blue (MB)			Methyl orange (MO)		Fuchsin Acid (FA)	
		X3	N8.8/4	N8.8/3	X3	N8.8/4	X3	N8.8/3
Langmuir	q_m (mg/g)	98.99	67.94	65.21	150.85	135.76	186.50	180.32
	K_L (L/mg)	2.32	0.35	0.40	0.82	15.35	1.75	2.45
	R^2	0.9998	0.9983	0.9986	0.9996	0.9996	0.9998	0.9999
Freundlich	K_F (mg/g)(L/mg)$^{1/n}$	75.24	30.92	28.04	84.67	122.32	130.60	136.27
	n	15.07	5.35	4.77	7.07	32.76	12.67	16.78
	R^2	0.9646	0.9980	0.9907	0.9372	0.6269	0.9818	0.9782
Redlich-Peterson	K_R (L/g)	$2.81x10^6$	$1.72x10^6$	$1.62 x10^6$	$6.32x10^5$	$8.18x10^5$	$8.74 x10^5$	$8.97 x10^5$
	a_R (L/mg)	$4.02x10^4$	$5.30x10^4$	$5.56x10^4$	8518.25	8834.96	6845.25	6630.65
	b	0.92	0.83	0.81	0.82	0.91	0.91	0.93
	R^2	0.9954	0.9980	0.9959	0.9945	0.9909	0.9963	0.9939
Temkin	K_T (L/mg)	$5.17x10^6$	46.50	26.37	166.17	$3.87x10^{14}$	3474.50	$3.13x10^6$
	B (J/mol)	5.01	8.13	8.66	16.43	3.67	14.97	9.15
	R^2	0.9504	0.9934	0.9802	0.9471	0.6516	0.9367	0.9815

3.2.2. Adsorption kinetics

The adsorption kinetics is another important factor for the practical application of an adsorbent to the elimination of pollutants from solutions because it determines the contact time. The time-resolved adsorption capacities of the dyes on the tested carbons are shown in Figure 9. The initial concentrations of the dyes (i.e. 300 mg/ml of MB and FA, and 200 mg/ml of MO) were selected according to the monolayer formation in the respective adsorption isotherms (Figure 8). The adsorption rates are very fast in all of the studied cases, and adsorption capacities > 80% are reached in less than 15 minutes.

As shown in Figure 9, the N-doped carbons have much faster adsorption kinetics than the non-doped one for the three dyes. Thus, N-doped samples achieved virtually 100% of their adsorption capacity at the first measured point (15 minutes in our experiments). Note that the N-doped carbons also exhibit a higher adsorption rate for MO although the adsorption of this dye is disfavored in these samples. This is probably due to a higher hydrophilicity of the doped carbons thanks to a greater number of polar functional groups, which promotes the contact of the carbons with the solution leading to a faster process.

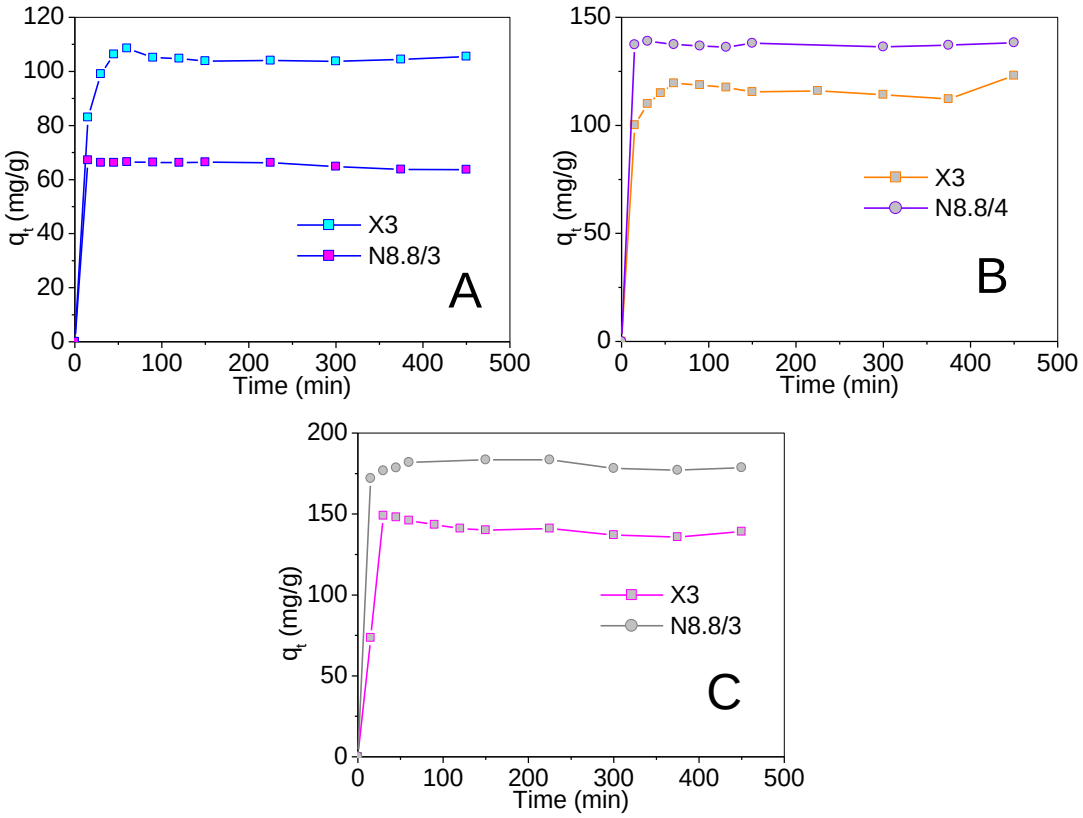

Figure 9. Time-resolved adsorption capacities of the tested dyes on X3 and N-doped carbons (N8.8/4 and N8.8/3) for: A) MB, B) MO and C) AF.

4. CONCLUSIONS

OMCs doped with nitrogen (up to 9.4 wt.%) were successfully prepared by CVD at 850 ºC using acetonitrile as simultaneous carbon and nitrogen source and SBA-15

silica as template. By increasing the acetonitrile concentration in the stream used in CVD, shorter deposition times were needed to achieve equivalent infiltration degrees. The porous texture and the structural order of the N-doped carbons mainly depend on the infiltration degree of the template and not on the experimental conditions (acetonitrile concentration, deposition time). As the infiltration degree increases, the surface areas and pore volumes of the OMCs decrease due to a more homogenous infiltration and a better replication of the template. This is clearly observed in the corresponding PSDs, which become progressively narrower with mesopore sizes centered at 3.36 nm, which corresponds to the silica wall thickness.

Three dyes with different molecular sizes and containing acidic or basic functional groups were used to investigate the effect of the N-containing functional groups. The presence of nitrogen functional groups was detrimental for the adsorption of the cationic dye (i.e., MB). On the other hand, the adsorption of anionic dyes was not affected by the presence of N-containing groups and mainly depended on the porosity of the OMCs. Finally, the presence of nitrogen functionalities improved the adsorption kinetics for both acid and basic dyes, and the N-doped samples achieved 100% of their maximum adsorption capacities in less than 15 min.

ACKNOWLEDGMENTS

The authors gratefully acknowledge the Spanish MINECO and FEDER (project MAT2012-34011) for financial support.

5. REFERENCES

[1] V.K. Gupta, Suhas, Application of low-cost adsorbents for dye removal - A review, J. Environ. Manage., 90 (2009) 2313-2342.

[2] E. Forgacs, T. Cserháti, G. Oros, Removal of synthetic dyes from wastewaters: a review, Environ. Int., 30 (2004) 953-971.

[3] G. Crini, Non-conventional low-cost adsorbents for dye removal: A review, Bioresource Technol., 97 (2006) 1061-1085.

[4] M. Rafatullah, O. Sulaiman, R. Hashim, A. Ahmad, Adsorption of methylene blue on low-cost adsorbents: A review, J. Hazard. Mater., 177 (2010) 70-80.

[5] G. Mezohegyi, F.P. van der Zee, J. Font, A. Fortuny, A. Fabregat, Towards advanced aqueous dye removal processes: A short review on the versatile role of activated carbon, J.

Environ. Manage., 102 (2012) 148-164.

[6] J. Rivera-Utrilla, M. Sánchez-Polo, V. Gómez-Serrano, P.M. Álvarez, M.C.M. Alvim-Ferraz, J.M. Dias, Activated carbon modifications to enhance its water treatment applications. An overview, J. Hazard. Mater., 187 (2011) 1-23.

[7] V. Meshko, L. Markovska, M. Mincheva, A.E. Rodrigues, Adsorption of basic dyes on granular acivated carbon and natural zeolite, Water Res., 35 (2001) 3357-3366.

[8] S. Wang, Y. Peng, Natural zeolites as effective adsorbents in water and wastewater treatment, Chem. Eng. J., 156 (2010) 11-24.

[9] X. Jin, B. Yu, Z. Chen, J.M. Arocena, R.W. Thring, Adsorption of Orange II dye in aqueous solution onto surfactant-coated zeolite: Characterization, kinetic and thermodynamic studies, J. Colloid Interface Sci., 435 (2014) 15-20.

[10] X. Gu, H. Xu, L. Luo, J. Wu, H. Lin, J. Chen, Adsorption of Methyl Violet Onto Mesoporous MCM-48 from Aqueous Solution, J. Nanosci. Nanotechnol., 14 (2014) 4655-4663.

[11] Y.Z. Liu, Z.X. Wu, X. Chen, Z.Z. Shao, H.T. Wang, D.Y. Zhao, A hierarchical adsorption material by incorporating mesoporous carbon into macroporous chitosan membranes, J. Mater. Chem., 22 (2012) 11908-11911.

[12] M. Ahmaruzzaman, A review on the utilization of fly ash, Prog. Energy Combust. Sci., 36 (2010) 327-363.

[13] E.L.K. Mui, W.H. Cheung, M. Valix, G. McKay, Dye adsorption onto activated carbons from tyre rubber waste using surface coverage analysis, J. Colloid Interface Sci., 347 (2010) 290-300.

[14] X. Yuan, W. Xing, S.-P. Zhuo, W. Si, X. Gao, Z. Han, Z.-F. Yan, Adsorption of bulky molecules of nonylphenol ethoxylate on ordered mesoporous carbons, J. Colloid Interface Sci., 322 (2008) 558-565.

[15] M. Dai, Mechanism of Adsorption for Dyes on Activated Carbon, J. Colloid Interface Sci., 198 (1998) 6-10.

[16] M.M. Mohamed, Acid dye removal: comparison of surfactant-modified mesoporous FSM-16 with activated carbon derived from rice husk, J. Colloid Interface Sci., 272 (2004) 28-34.

[17] I.A.W. Tan, A.L. Ahmad, B.H. Hameed, Adsorption of basic dye on high-surface-area activated carbon prepared from coconut husk: Equilibrium, kinetic and thermodynamic studies, J. Hazard. Mater., 154 (2008) 337-346.

[18] F.-C. Wu, R.-L. Tseng, High adsorption capacity NaOH-activated carbon for dye removal from aqueous solution, J. Hazard. Mater., 152 (2008) 1256-1267.

[19] L. Gu, N. Zhu, H. Guo, S. Huang, Z. Lou, H. Yuan, Adsorption and Fenton-like degradation of naphthalene dye intermediate on sewage sludge derived porous carbon, J. Hazard. Mater., 246–247 (2013) 145-153.

[20] X. Yuan, S.-P. Zhuo, W. Xing, H.-Y. Cui, X.-D. Dai, X.-M. Liu, Z.-F. Yan, Aqueous dye adsorption on ordered mesoporous carbons, J. Colloid Interface Sci., 310 (2007) 83-89.

[21] Y. Tian, P. Liu, X. Wang, H. Lin, Adsorption of malachite green from aqueous solutions onto ordered mesoporous carbons, Chem. Eng. J., 171 (2011) 1263-1269.

[22] Y. Dong, H. Lin, Q. Jin, L. Li, D. Wang, D. Zhou, F. Qu, Synthesis of mesoporous carbon fibers with a high adsorption capacity for bulky dye molecules, J. Mater. Chem. A, 1 (2013) 7391-7398.

[23] G.P. Hao, W.C. Li, S.A. Wang, S.F. Zhang, A.H. Lu, Tubular structured ordered mesoporous carbon as an efficient sorbent for the removal of dyes from aqueous solutions,

Carbon, 48 (2010) 3330-3339.

[24] X. Zhuang, Y. Wan, C. Feng, Y. Shen, D. Zhao, Highly Efficient Adsorption of Bulky Dye Molecules in Wastewater on Ordered Mesoporous Carbons, Chem. Mater., 21 (2009) 706-716.

[25] Y. Zhai, Y. Dou, X. Liu, B. Tu, D. Zhao, One-pot synthesis of magnetically separable ordered mesoporous carbon, J. Mater. Chem., 19 (2009) 3292-3300.

[26] Y.P. Zhai, Y.Q. Dou, X.X. Liu, S.S. Park, C.S. Ha, D.Y. Zhao, Soft-template synthesis of ordered mesoporous carbon/nanoparticle nickel composites with a high surface area, Carbon, 49 (2011) 545-555.

[27] X. Peng, D. Huang, T. Odoom-Wubah, D. Fu, J. Huang, Q. Qin, Adsorption of anionic and cationic dyes on ferromagnetic ordered mesoporous carbon from aqueous solution: Equilibrium, thermodynamic and kinetics, J. Colloid Interface Sci., 430 (2014) 272-282.

[28] A.H. Lu, F. Schüth, Nanocasting: A versatile strategy for creating nanostructured porous materials, Adv. Mater., 18 (2006) 1793-1805.

[29] C.D. Liang, Z.J. Li, S. Dai, Mesoporous carbon materials: Synthesis and modification, Angew. Chem. Int. Ed., 47 (2008) 3696-3717.

[30] J. Lee, J. Kim, T. Hyeon, Recent progress in the synthesis of porous carbon materials, Adv. Mater., 18 (2006) 2073-2094.

[31] L.R. Radovic, Surface chemistry of activated carbon materials: state of the art and implications for adsorption, in: J.A. Schwarz, C.I. Contescu (Eds.) Surfaces of nanoparticles and porous materials, Marcel Dekker, New York, 1999.

[32] L.R. Radovic, C. Moreno-Castilla, J. Rivera-Utrilla, Carbon materials as adsorbents in aqueous solutions, in: L.R. Radovic (Ed.) Chemistry and Physics of Carbon, 2001, pp. 227-405.

[33] M.F.R. Pereira, S.F. Soares, J.J.M. Órfão, J.L. Figueiredo, Adsorption of dyes on activated carbons: influence of surface chemical groups, Carbon, 41 (2003) 811-821.

[34] R. Ryoo, S.H. Joo, M. Kruk, M. Jaroniec, Ordered mesoporous carbons, Adv. Mater., 13 (2001) 677-681.

[35] X. Dong, J. Fu, X. Xiong, C. Chen, Preparation of hydrophilic mesoporous carbon and its application in dye adsorption, Mater. Lett., 65 (2011) 2486-2488.

[36] J.J.M. Órfão, A.I.M. Silva, J.C.V. Pereira, S.A. Barata, I.M. Fonseca, P.C.C. Faria, M.F.R. Pereira, Adsorption of a reactive dye on chemically modified activated carbons—Influence of pH, J. Colloid Interface Sci., 296 (2006) 480-489.

[37] A. Sánchez-Sánchez, F. Suárez-García, A. Martínez-Alonso, J.M.D. Tascón, Surface modification of nanocast ordered mesoporous carbons through a wet oxidation method, Carbon, 62 (2013) 193-203.

[38] P.A. Bazula, A.-H. Lu, J.-J. Nitz, F. Schueth, Surface and pore structure modification of ordered mesoporous carbons via a chemical oxidation approach, Microporous Mesoporous Mat., 108 (2008) 266-275.

[39] M.J. Lázaro, L. Calvillo, E.G. Bordejé, R. Moliner, R. Juan, C.R. Ruiz, Functionalization of ordered mesoporous carbons synthesized with SBA-15 silica as template, Microporous Mesoporous Mat., 103 (2007) 158-165.

[40] A. Lu, A. Kiefer, W. Schmidt, F. Schüth, Synthesis of polyacrylonitrile-based ordered mesoporous carbon with tunable pore structures, Chem. Mater., 16 (2004) 100-103.

[41] C. Weidenthaler, A.H. Lu, W. Schmidt, F. Schüth, X-ray photoelectron spectroscopic studies of PAN-based ordered mesoporous carbons (OMC), Microporous Mesoporous Mat., 88 (2006) 238-243.

[42] W. Kim, J.B. Joo, N. Kim, S. Oh, P. Kim, J. Yi, Preparation of nitrogen-doped mesoporous carbon nanopipes for the electrochemical double layer capacitor, Carbon, 47 (2009) 1407-1411.

[43] Y.D. Xia, R. Mokaya, Synthesis of ordered mesoporous carbon and nitrogen-doped carbon materials with graphitic pore walls via a simple chemical vapor deposition method, Adv. Mater., 16 (2004) 1553-1558.

[44] Y.D. Xia, R. Mokaya, D.M. Grant, G.S. Walker, A simplified synthesis of N-doped zeolite-templated carbons, the control of the level of zeolite-like ordering and its effect on hydrogen storage properties, Carbon, 49 (2011) 844-853.

[45] S. Giraudet, Z. Zhu, X. Yao, G. Lu, Ordered mesoporous carbons enriched with nitrogen: application to hydrogen storage, J. Phys. Chem. C, 114 (2010) 8639-8645.

[46] A. Sánchez-Sánchez, F. Suárez-García, A. Martínez-Alonso, J.M.D. Tascón, Aromatic polyamides as new precursors of nitrogen and oxygen-doped ordered mesoporous carbons, Carbon, 70 (2014) 119-129.

[47] X. Peng, X. Hu, D. Fu, F.L.Y. Lam, Adsorption removal of acid black 1 from aqueous solution using ordered mesoporous carbon, Appl. Surf. Sci., 294 (2014) 71-80.

[48] D.Y. Zhao, J.L. Feng, Q.S. Huo, N. Melosh, G.H. Fredrickson, B.F. Chmelka, G.D. Stucky, Triblock copolymer syntheses of mesoporous silica with periodic 50 to 300 angstrom pores, Science, 279 (1998) 548-552.

[49] K.S.W. Sing, D.H. Everett, R.A.W. Haul, L. Moscou, R.A. Pierotti, J. Rouquerol, T. Siemieniewska, Reporting Physisorption Data for Gas Solid Systems with Special Reference to the Determination of Surface-Area and Porosity (Recommendations 1984), Pure Appl. Chem., 57 (1985) 603-619.

[50] F. Rouquerol, J. Rouquerol, K.S.W. Sing, Adsorption by Powders & Porous Solids. Principles, Methodology and Applications, Academic Press New York, 1999.

[51] M. Enterría, F. Suárez-García, A. Martínez-Alonso, J.M.D. Tascón, Synthesis of ordered micro–mesoporous carbons by activation of SBA-15 carbon replicas, Microporous Mesoporous Mat., 151 (2012) 390-396.

[52] J. Parmentier, S. Saadhallah, M. Reda, P. Gibot, M. Roux, L. Vidal, C. Vix-Guterl, J. Patarin, New carbons with controlled nanoporosity obtained by nanocasting using a SBA-15 mesoporous silica host matrix and different preparation routes, J. Phys. Chem. Solids, 65 (2004) 139-146.

[53] A.B. Dongil, B. Bachiller-Baeza, A. Guerrero-Ruiz, I. Rodríguez-Ramos, A. Martínez-Alonso, J.M.D. Tascón, Surface chemical modifications induced on high surface area graphite and carbon nanofibers using different oxidation and functionalization treatments, J. Colloid Interface Sci., 355 (2011) 179-189.

[54] J.P. Boudou, P. Parent, F. Suárez-García, S. Villar-Rodil, A. Martínez-Alonso, J.M.D. Tascón, Nitrogen in aramid-based activated carbon fibers by TPD, XPS and XANES, Carbon, 44 (2006) 2452-2462.

[55] A. Sánchez-Sánchez, F. Suárez-García, A. Martínez-Alonso, J.M.D. Tascón, Evolution of the complex surface chemistry in mesoporous carbons obtained from polyaramide precursors, Appl. Surf. Sci., 299 (2014) 19-28.

[56] W. Kim, M.Y. Kang, J.B. Joo, N.D. Kim, I.K. Song, P. Kim, J.R. Yoon, J. Yi, Preparation of ordered mesoporous carbon nanopipes with controlled nitrogen species for application in electrical double-layer capacitors, J. Power Sources, 195 (2010) 2125-2129.

[57] H.F. Gorgulho, F. Goncalves, M.F.R. Pereira, J.L. Figueiredo, Synthesis and characterization of nitrogen-doped carbon xerogels, Carbon, 47 (2009) 2032-2039.

[58] C.H. Giles, D. Smith, A. Huitson, General treatment and classification of solute

adsorption-isotherm. 1. Theoretical, J. Colloid Interface Sci., 47 (1974) 755-765.

Synthesis, characterization and dye removal capacities of N-doped mesoporous carbons

Á. Sánchez-Sánchez, F. Suárez-García, A. Martínez-Alonso, J. M. D. Tascón

Instituto Nacional del Carbón, INCAR-CSIC, Apartado 73, 33080 Oviedo (Spain)

Supporting information:

Table S1. Data deduced from the deconvoluted high-resolution spectra of N8.8/3 sample: Binding energies (BE), peak areas (A) and functional group assignments.

Spectrum	*Peak*	*BE (eV)*	*A (%)*	*Assignments*
C1s	C1	284.88	35.36	C=C ($\pi\rightarrow\pi^*$delocated bondings)
	C2	285.38	28.99	C=C (located bondings)
	C3	286.25	12.16	C-O (ether, phenol, anhydride), Csp^3, C=N (aromatic rings), C-N
	C4	287.10	5.25	C=O, C=N $\pi\rightarrow\pi^*$ shake-up satellite of C2
	C5	288.01	5.81	Carboxylic C-O (-COOH) N component
	C6	290.14	12.44	C=C ($\pi\rightarrow\pi^*$delocated bondings)
N1s	N1	398.32	13.03	Pyridinic nitrogen (N_6), C≡N
	N2	399.60	16.31	Pyrrolic nitrogen (N_5), Ph-C≡N
	N3	401.35	54.66	Quaternary nitrogen (N_Q)
	N4	402.80	13.65	Nitrogen oxides (NOx)
	N5	404.35	2.37	Nitrogen oxides (NOx)
O1s	O1	530.29	21.61	O=C (carbonyls, carboxylic acids)
	O2	532.14	46.29	C=O (esters, anhydrides) -OH (alcohols), O-C (esters)
	O3	533.66	32.10	Non-carbonylic O-C (esters, anhydrides)

Capítulo 5:

Síntesis de carbones mesoporosos dopados con heteroátomos por infiltración en fase líquida de nuevos precursores

5.1 Síntesis de carbones mesoporosos ordenados dopados con heteroátomos por infiltración en fase líquida de nuevos precursores

A lo largo del *Capítulo 1* de esta tesis se ha destacado la importancia de optimizar el comportamiento de un material de carbono en una aplicación determinada, adaptando tanto su textura porosa como su química superficial. También se ha expuesto la dificultad de dopar los materiales de carbono con grupos funcionales nitrogenados, los cuales pueden ser necesarios para desarrollar una función específica dentro de una aplicación. De hecho, a día de hoy, la síntesis de materiales de carbono dopados con estructuras de poro bien definidas, porosidad elevada y alto contenido en heteroátomos sigue constituyendo todo un reto. Muchos métodos convencionales de dopaje presentan inconvenientes, relacionados principalmente con los largos períodos de tiempo que son necesarios para sintetizar y modificar los materiales, la ausencia de un control estricto sobre los grupos funcionales nitrogenados que se introducen o la escasez de precursores apropiados. Por tanto, es imprescindible desarrollar nuevos procedimientos de síntesis y descubrir nuevos precursores que nos ayuden a superar estas limitaciones y permitan diseñar materiales ejerciendo un control estricto sobre su textura porosa y su composición química.

En el capítulo que nos ocupa, se describe el uso de monómeros de poliamidas aromáticas como **nuevos precursores** para la síntesis de CMOs dopados con nitrógeno y oxígeno (N,O-CMOs). La amplia variedad de poliamidas, tanto alifáticas como aromáticas, y métodos sintéticos existentes nos permite disponer de una gran variedad de precursores. Por tanto, esta tesis abre una nueva vía de obtención de CMOs dopados con multitud de posibilidades por explorar.

Este capítulo se compone de cuatro artículos, a través de los cuales se estudia la síntesis, caracterización y aplicaciones de CMOs dopados con nitrógeno y oxígeno derivados de precursores de poliamidas aromáticas:

i) En la ***Publicación 3*** se muestran los resultados relativos a la preparación y caracterización de CMOs dopados con nitrógeno y oxígeno obtenidos mediante dos

métodos de síntesis basados en la infiltración líquida de la sílice mesoporosa SBA-15 con un precursor de poliamidas aromáticas.

ii) La ***Publicación 4*** se centra en la síntesis y caracterización de N,O-CMOs derivados de dos precursores de poliamidas aromáticas: un monómero meta-sustituido, que da lugar a CMOs tipo CMK-3, y otro para-sustituido, que genera CMOs tipo CMK-5. Adicionalmente, los dos materiales obtenidos se utilizaron como portadores de ibuprofeno y se llevó a cabo un estudio de la liberación controlada de este fármaco en función del pH.

iii) En la ***Publicación 5*** se muestran los resultados correspondientes a la caracterización de la química superficial mediante XPS de CMOs dopados con grupos funcionales de nitrógeno, oxígeno y fósforo, cuya síntesis se recoge en la publicación 6.

iv) La ***Publicación 6*** se centra en la obtención y caracterización fisicoquímica de CMOs dopados con nitrógeno, oxígeno y fósforo, preparados mediante carbonización en presencia de H_3PO_4 de composites poliamida/SBA-15. Adicionalmente, estos materiales fueron utilizados como adsorbentes para estudiar la influencia de la textura porosa y la química superficial sobre la adsorción de CO_2.

PUBLICACIÓN 3:

'Aromatic polyamides as new precursors of nitrogen and oxygen-doped ordered mesoporous carbons'. *Carbon 2014;70:119-29*

En este trabajo se utilizan por primera vez precursores de poliamidas aromáticas para la síntesis de carbones mesoporosos ordenados. La obtención fue llevada a cabo mediante *hard-templating* aplicando dos métodos diferentes, a los que denominamos:

1. ***Síntesis en fase orgánica:*** La infiltración se realizó in situ añadiendo la plantilla de sílice al medio de reacción, en el que se encontraba el monómero, para la síntesis de poliamidas mediante la reacción de Yamazaki.
2. ***Polimerización térmica en estado sólido:*** La infiltración de la plantilla fue llevada a cabo mediante impregnación a humedad incipiente de una cierta cantidad de monómero (1.40, 1.55, 1.70 o 1.75 gramos de MABA por gramo de SBA-15) disuelta en un disolvente orgánico, seguido por la eliminación del disolvente a vacío. Posteriormente se llevó a cabo una etapa de polimerización térmica a 160 °C durante 1 hora.

En ambos casos se utilizó como precursor el ácido 3-aminobenzoico (MABA) y SBA-15 como plantilla de sílice mesoporosa, y la infiltración fue realizada en un solo paso. Tras carbonizar a 900 °C y eliminar la plantilla de sílice se obtuvieron diversos CMOs dopados con nitrógeno y oxígeno (N,O-CMOs). Los procedimientos experimentales seguidos en ambos métodos se encuentran detallados en el **Apartado 3.1.2.2**. Finalmente, las características de los N,O-CMOs obtenidos relativas a su textura porosa, el ordenamiento de su estructura y su química superficial fueron examinadas en detalle y relacionadas con los métodos de síntesis utilizados.

El grado de polimerización de los polímeros preparados por el método de síntesis en fase orgánica fue mayor que el de los obtenidos por polimerización térmica en estado sólido. Por ello, se obtienen valores más altos de rendimientos de carbonización y de contenidos de carbono en los composites carbón/sílice preparados por el primer método. Es destacable que tanto los rendimientos de

carbonización como los contenidos de carbono obtenidos en ambos métodos eran relativamente altos en comparación con otros procedimientos descritos y, por ello, fue posible realizar el proceso de infiltración en una sola etapa. Por tanto, los métodos expuestos en este trabajo presentan claras ventajas respecto a otros en los que se utilizan precursores que requieren más de una etapa de infiltración (sacarosa, amino-sacarosa o alcohol furfurílico) o tiempos muy largos de polimerización/estabilización (alcohol furfurílico o acrilonitrilo).

Los CMOs dopados obtenidos por polimerización térmica en estado sólido poseen PSDs estrechas centradas en un solo tamaño de mesoporos. Conforme aumenta el grado de infiltración de los composites, disminuye el área superficial específica de los carbones. De este modo, el carbón menos infiltrado presenta los valores máximos de área superficial específica (~1100 m^2/g) y de volumen total de poros (1.05 cm^3/g). Una ventaja interesante de este método es la ausencia de carbono amorfo en la superficie externa de las partículas. Esto se debe a que el monómero depositado fuera de los canales de la plantilla es arrastrado por la corriente de gas fuera del reactor durante la etapa de polimerización térmica a 160 ºC. Por otro lado, el carbón obtenido por la reacción de Yamazaki presenta dos diámetros de mesoporos y su valor de área superficial específica es inferior al de los carbones obtenidos por el método de polimerización térmica en estado sólido. Esto se debe a su mayor grado de polimerización, por el que se produce la evolución de menos compuestos volátiles y, en consecuencia, se desarrolla menos la microporosidad.

Los resultados estructurales indican que los carbones obtenidos por los dos métodos presentan ordenamiento de largo alcance. A pesar de ello, el carbón obtenido a partir de la reacción de Yamazaki está constituido por zonas con diferente grado de infiltración. Por otro lado, en ambos casos se mantiene la morfología de las partículas de sílice en los carbones finales sin presencia de carbono amorfo. Junto a los resultados de textura porosa, estos datos apuntan a que en el método de síntesis en fase orgánica tiene lugar una infiltración heterogénea de la plantilla, mientras que en el de polimerización térmica en estado sólido la infiltración se realiza homogéneamente.

Las funcionalidades nitrogenadas se distribuyen homogéneamente entre el seno y

la superficie de los materiales de carbono, mientras que los grupos funcionales de oxígeno se encuentran principalmente localizados en su seno. En los materiales de carbono obtenidos por los dos métodos, aproximadamente el 50% del nitrógeno se encuentra en forma de nitrógeno cuaternario, un 40% como nitrógeno piridínico y pirrólico, y sólo un 7% del nitrógeno está unido al oxígeno. En cuanto a las funcionalidades oxigenadas, en ambos casos se obtienen mayores concentraciones de ésteres y anhídridos. Sin embargo, existen ligeras diferencias en las proporciones del resto de grupos de oxígeno que pueden ser debidas a los diferentes grados de polimerización conseguidos con los dos métodos: los materiales obtenidos por polimerización térmica en estado sólido presentan una cantidad ligeramente mayor de carbonilos y ácidos carboxílicos, y el carbón obtenido mediante síntesis en fase orgánica posee una concentración de ésteres, anhídridos y alcoholes casi 5 veces superior a la de carbonilos y ácidos carboxílicos.

Por tanto, el método de polimerización térmica en estado sólido presenta una serie de ventajas con respecto al de síntesis en fase orgánica: los CMOs poseen porosidades más desarrolladas, mayor ordenamiento estructural de largo alcance, la infiltración es más homogénea y el procedimiento experimental es más sencillo y menos contaminante. Además, estas características lo convierten en una ruta atractiva para la preparación de N,O-CMOs en comparación con la técnica de CVD u otros procesos de infiltración liquida llevados a cabo con otros precursores.

CARBON 70 (2014) 119–129

Available at www.sciencedirect.com

ScienceDirect

journal homepage: www.elsevier.com/locate/carbon

Aromatic polyamides as new precursors of nitrogen and oxygen-doped ordered mesoporous carbons

*Angela Sánchez-Sánchez, Fabián Suárez-García *, Amelia Martínez-Alonso, Juan M.D. Tascón*

Instituto Nacional del Carbón, INCAR-CSIC, Apartado 73, Oviedo 33080, Spain

ARTICLE INFO

Article history:
Received 30 October 2013
Accepted 27 December 2013
Available online 7 January 2014

ABSTRACT

Polyamides are used for the first time as precursors in the synthesis of nitrogen- and oxygen-doped ordered mesoporous carbons (OMCs) by applying two synthetic methods, named here as: (i) organic phase synthesis (infiltration *in situ* by Yamazaki reaction-based method) and (ii) solid-state thermal polymerization (liquid infiltration and thermal polymerization of the monomer into the porosity of the template). In both cases, 3-aminobenzoic acid (MABA) and SBA-15 mesoporous silica are used as precursor and template, respectively, and the infiltration takes place in one single step. In the first method, the infiltration process is accomplished in situ through Yamazaki reaction of the MABA; in the second one, the MABA monomer is introduced into the channels of the silica template by incipient wetness dissolved in a common and low polluting organic solvent. After carbonization at 900 °C and removal of the template, OMCs with very narrow pore size distributions and nitrogen and oxygen contents as large as ~6 and 6.4–11.5 wt.%, respectively, are obtained. This work opens a new way to prepare advanced carbon materials, due to the wide variety of polyamides that can be synthesized by applying the two proposed methods to a large number of both aliphatic and aromatic precursors.

1. Introduction

Porous carbon materials are solids constituted principally by carbon, having a well-developed porous texture (surface area, pore volume, etc.) and deserving a number of applications in different fields such as gas and liquid purification, mixture separation, catalysis, etc. [1–4]. Besides the classic uses, these materials are potentially useful for emerging applications of great interest such as storage of combustible gases (hydrogen, methane) or electrical energy storage (anodes in Li-ion batteries or electrodes in supercapacitors) [5–8]. These increasingly specific applications require that the involved materials have some specific properties concerning their porous texture, surface chemistry, crystalline order and morphology, in such a way that their behavior can be optimized for a given utilization. Porous texture is the main determining factor for most of the applications, and therefore many research efforts have been made to develop preparative methods leading to carbonaceous materials exhibiting an optimal porosity for a given application. In this sense, nanocasting is a powerful method for creating materials with a closely controlled porous nanostructure [8–12] that is being intensively applied for preparing ordered porous carbons. Within the nanocasting method, hard templating is one of the most used synthetic routes; based on the use of crystalline inorganic solids (such as zeolites, ordered mesoporous silica, etc.) as templates and the infiltration of the template porosity with a carbon precursor, a negative replica is obtained after the carboniza-

* *Corresponding author.*
E-mail address: Fabian@incar.csic.es (F. Suárez-García).
0008-6223/$ - see front matter
http://dx.doi.org/10.1016/j.carbon.2013.12.080

tion of the resulting composite and the removal of the solid template. Thereby, depending on the template used, carbon materials with different structure and porosity can be obtained [8–11].

In order to optimize the behavior of a carbonaceous adsorbent in a given application, besides porosity, the surface chemistry can play a determining role. For instance, the incorporation of heteroatoms such as boron, nitrogen or oxygen in a carbon network can improve its electrical, mechanical, semiconductor and field emission properties [4,6,13–18]; this improvement of properties makes the synthesis of doped ordered porous carbons an interesting target, especially in the case of the mentioned heteroatoms. As concerns N-doped carbons, some works report their preparation by infiltration/polymerization and subsequent carbonization, using polyacrilonitrile [19,20], quinolone [17], diaminobenzene [21], aminoglucose [22] or ethylenediamine and carbon tetrachloride [23–25], as precursors. Other works accomplish the synthesis of N-doped carbons through chemical vapor deposition of acetonitrile [26,27] or by means of a post-treatment with NH_3 over an ordered mesoporous carbon (OMC) [25]. These works show that it is possible to obtain N-doped ordered porous carbon by selecting suitable synthesis conditions, but in some cases, multistep processes are required or a limited variety of precursors is available.

In the present work, we report for the first time on two different methods for preparing carbons doped with both nitrogen and oxygen by using aromatic polyamides (polyaramides) as precursors. Polyamides are condensation polymers constituted by macromolecular chains where the amide functional group (–CONH–) is sequentially repeated. The wide variety of precursors and synthetic methods applicable leads to a great variety of polyamides, both aliphatic and aromatic. In previous works from our research group, we have used polyaramide fibers, poly (p-phenylene terepthalamide) (PPTA) and poly (m-phenylene isophthalamide) (PMIA), as precursors for preparing activated carbon fibers (ACFs) [28–34]. From these aromatic polyamides, ACFs with a considerably large amount of heteroatoms (N and O), high specific surface areas and pore volumes and uniform and narrow pore size distributions were obtained. In addition, their high carbonization yields pointed to the polyaramides as suitable precursors of ordered porous materials with interesting properties [33].

Here, nitrogen- and oxygen-doped ordered mesoporous carbons were synthesized through polymerization reactions of 3-aminobenzoic acid (MABA) within the porous network of a mesoporous silica template, SBA-15, and subsequent carbonization and removal of the latter. Two different methods of infiltration/polymerization were studied. In the first one, the infiltration was carried out in situ by adding SBA-15 to the reaction medium for polyamide synthesis, as described by Yamazaki et al. [35]. In the second method, the infiltration of the SBA-15 silica was carried out by incipient wetness impregnation of a certain amount of monomer dissolved in an organic solvent, followed by removal of the latter under vacuum. The porous texture, the structure and the surface chemistry of the resulting OMCs were studied in detail and they were related to the synthesis method used.

2. Experimental

2.1. Synthesis of the SBA-15 template

The mesoporous silica SBA-15 was used as template. This silica was prepared following the method described by Zhao et al. [36]. Pluronic P123 (Mw = 5800, Aldrich) (10.44 g) was dissolved in an aqueous solution containing 52.5 mL of 37% HCl (Merck). After complete polymer dissolution, tetraetoxysilane (TEOS, Aldrich) (22.64 g) was added dropwise and the mixture was kept under stirring (40 °C, 4 h). The molar composition of the starting reaction mixture was 0.017 P123/1 TEOS/145.8 H_2O/6.04 HCl. The resulting product was aged (125 °C, 72 h), filtered and calcined in air (550 °C, 6 h).

2.2. Synthesis of the ordered mesoporous carbons

The polymerization of the polyamide precursor in the SBA-15 porosity was carried out through two different routes, designated here as: (i) organic phase synthesis and (ii) solid-state thermal polymerization. In both cases, the monomer 3-aminobenzoic acid (MABA) (99%, Across) was used as polyaramide precursor. In the first case, the infiltration was done in situ by adding SBA-15 to the reaction medium, and following the Yamazaki reaction for polyamide synthesis [27,37]. In our case, the reaction was accomplished in a three-neck conical-shape flask equipped with a magnetic stirrer and a temperature controller. After placing SBA-15 mesoporous silica (1 g) in the reactor, this was connected to a vacuum line and heated (150 °C, 2 h); then, it was cooled down to room temperature and a nitrogen flow (100 mL/min) was continuously passed through the reactor in order to maintain an inert atmosphere during the process. N-methylpyrrolidone (99.99%, Sigma–Aldrich) (20 mL) was added to the reactor under vigorous stirring. Afterwards, MABA (2.76 g), calcium dichloride (93%, Sigma–Aldrich) (1.50 g) and pyridine (99%, Sigma–Aldrich) (14.5 mL) were added, and the final mixture was heated (100 °C) until complete dissolution of the solid reagents. Both the temperature (100 °C) and the vigorous stirring were kept constant until the completion of the reaction. Once the mixture became clear, triphenyl phosphite (97%, Sigma–Aldrich) (5.40 mL) was added to catalyze the monomer polymerization; when a time of 90 min had elapsed since catalyst addition, the final product was cooled to room temperature, filtered in order to remove the polymer excess, and then methanol (Rectapur, Prolabo) (100 mL) was added to precipitate it. The polymer/silica composite obtained in this way was washed in a Soxhlet apparatus with methanol for 4 h and dried (80 °C, 5 h). The dried polymer/silica composite was carbonized (heating rate of 10 °C/min to 900 °C, then kept for 30 min at this temperature) under argon (500 mL/min). The silica template was removed from the carbonized composite by treatment with hydrofluoric acid (48%, Fluka) and the final carbon was dried (100 °C, 12 h), being designated as PACor.

In the second case preparation method, the solid-state thermal polymerization was performed as follows: SBA-15 (1 g) was placed in a rotary evaporator and degassed under vacuum (150 °C, 2 h). After being cooled down to room temperature, different amounts of MABA dissolved in acetone (1.40, 1.55, 1.70 and 1.75 g) were added in order to infiltrate the porosity of the silica template. The volume of solution was selected so as to fill the porosity of the silica template to incipient wetness. In all cases, the solvent was removed under vacuum and the monomer–silica composites were both polymerized and carbonized under argon (500 mL/min) by means of a two-step thermal procedure: a first isothermal stage (160 °C, 1 h), below the boiling point of the MABA monomer, was applied to produce the thermal polymerization of the monomer into the channels of the SBA-15 silica template. This was followed by carbonization at the target temperature (heating rate of 10 °C/min to 900 °C, then kept for 30 min at this temperature). The carbonized composites were also treated with HF and dried (100 °C, 12 h). The obtained mesoporous carbons were denoted as PAC_x, where the *subscript x* indicates the amount of MABA (1.40, 1.55, 1.70 or 1.75 g) introduced per gram of SBA-15 silica template.

2.3. *Characterization techniques*

The porous texture of the samples was characterized through N_2 adsorption/desorption isotherms at −196 °C using a volumetric adsorption apparatus ASAP 2010 (Micromeritics). From these isotherms, we obtained porous texture parameters such as: the apparent BET surface area, S_{BET}, calculated by means of the BET method applied in the relative pressure range of 0.05–0.25; the total pore volume, V_T, calculated from the amount of nitrogen adsorbed in liquid form at the relative pressure of 0.95; the micropore volume, V_{micro}, calculated by applying the Dubinin–Radushkevich equation; and the mesopore volume, V_{meso}, calculated as the difference between V_T and V_{micro}. The pore size distributions (PSD) were obtained by applying the Barret–Joyner–Hallenda (BJH) method to the desorption branch of the isotherms. The main pore size, D, was determined from the PSDs at the maximum value of the distribution.

The carbon fraction in the carbonized composites (infiltrated carbon) was evaluated by thermogravimetric analysis using a CI Electronics microbalance, by heating the carbon/silica composite (20 mg) to the target temperature (950 °C) under air flow (50 mL/min).

The structural and morphological characterizations were carried out by X-ray diffraction, transmission electron microscopy and scanning electron microscopy, with a Siemens D5000 diffractometer (Cu Kα radiation; scanning range $2\theta = 0.5–5°$; step width = 0.01°; time per step = 1 s), a JEOL 2000 EX/II microscope (operating potential of 160 kV) and a Carl Zeiss DMS-942 microscope, respectively.

The chemical characterization was performed by means of three techniques. FT-IR spectra were obtained in a Nicolet 8700 instrument equipped with a high sensitivity MCT/A detector in the range of 400–4000 cm^{-1}, and recording 200 scans per spectrum at a resolution of 4 cm^{-1}. Elemental analysis was carried out using a LECO CHNS-932 microanalyser provided with a LECO VTF-900 accessory for oxygen. X-ray photoelectron spectroscopy was carried out in a SPECS system, working at a pressure of 10^{-7} Pa with a monochromatic Al Kα X-ray source (1486.3 eV, 150 W); the photo-excited electrons were analyzed in constant pass energy mode, using a pass energy of 30 eV for the survey spectra and 10 eV for the high-resolution core level spectra. The CasaXPS software was used for data processing and all envelopes of core level spectra were peak-fitted with a Gaussian–Lorentzian convoluted function (80/20) and a Shirley's background. The compositions in wt.% were determined from the survey spectra by considering the integrated areas of the main XPS peaks of the different elements (C1s, N1s and O1s) and their respective sensitivity factors.

3. Results and discussion

As shown in Table 1, the carbonization yields of the aromatic polyamide-derived carbons are high, ranging from 41.2 to 46.8 wt.% for the materials obtained by the solid-state thermal polymerization method, and 51.4 wt.% for the sample PAC_{OR} prepared through the Yamazaki reaction. Such carbonization yields, calculated relative to the initial mass of polymer, are considerably high if we take into account that the carbonization temperature reached 900 °C, and agree with previous results for other carbons derived from polyaramides such as PPTA and PMIA, which exhibited carbonization yields at the same temperature of about 40 [34,36] and 55 wt.% [37] on dry basis, respectively. As noted from these results, the meta-substituted polymer, PMIA, presented a higher carbonization yield than the para-substituted polymer, PPTA, which has been associated with their different mechanisms of thermal degradation [33].

In the present work, the differences between the two synthesis routes in terms of carbonization yields can be explained taking into account the different polymerization degrees achieved. An estimation can be accomplished by following the chemical evolution of the amide, amine and carboxylic functional groups in the parent precursor before and after being polymerized through both methods. For this purpose, we have compared in Fig. 1 the FT-IR spectra of the monomer (MABA), this one submitted to thermal polymerization at 160 °C/1 h under inert atmosphere and the polymer resulting from the organic phase synthesis of such MABA monomer. FT-IR bands were assigned based on [38].

The FT-IR spectrum of the parent monomer (MABA) presents absorption bands corresponding to the amine and carboxylic acid terminal groups: a broad band between 2850 and 3300 cm^{-1} due to the N—H stretching in amines and the O—H stretching in carboxylic acids, and a strong band at 1655 cm^{-1} that corresponds to the C=O stretching vibration of aromatic carboxylic acids. Polymerization of MABA takes place following the two used methods as well-resolved bands corresponding to the amide group are clearly observed in the FT-IR spectra of the two resulting products. Thus, three strong bands usually designated as amide I band at 1653 cm^{-1} (related to the C=O stretching of amides), amide II band at 1558 cm^{-1} (due to the N—H deformation of solid or condensed secondary amides), and amide III band at 1332 and 1267 cm^{-1} (due to the cis and trans N—H deformations in secondary

Table 1 – Porous texture parameters obtained from the nitrogen adsorption isotherms and carbon and carbonization yields.

Sample	S_{BET} (m^2/g)	V_T (cm^3/g)	V_{micro} (cm^3/g)	V_{meso} (cm^3/g)	D (nm)	Infiltrated carbon (wt.%) [a]	Carbonization yield (wt.%) [b]
SBA-15	513	1.15	0.22	0.93	8.1	–	–
PACor	396	0.50	0.15	0.35	3.8 6.9–11.1	49.4	51.4
PAC1.40	1084	1.05	0.43	0.62	4.0	37.8	41.2
PAC1.55	980	0.96	0.36	0.60	4.4	42.2	44.5
PAC1.70	909	0.93	0.34	0.59	4.4	41.3	46.8
PAC1.75	864	0.85	0.32	0.53	4.4	41.2	42.5

[a] Infiltrated carbon calculated by TG in air as the fraction of carbon in the carbon/silica composites after the carbonization step.
[b] Carbonization yield of the carbon/silica composites.

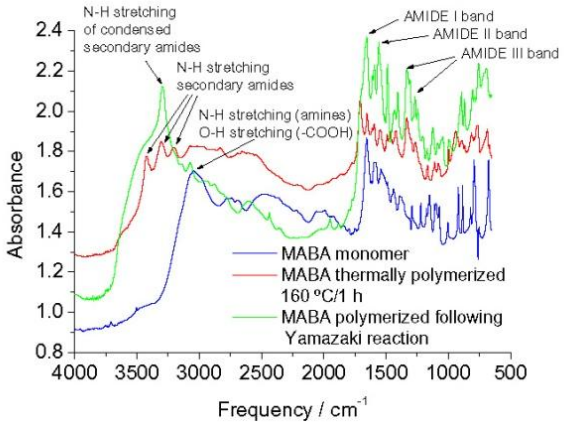

Fig. 1 – FT-IR spectra of the MABA precursor and the polymerized products obtained through two different synthesis methods. (A colour version of this figure can be viewed online.)

amides, respectively), can be seen in Fig. 1. In the case of the polymer prepared following the Yamazaki reaction, a sharp and strong band at 3294 cm^{-1} and a weaker one at 3070 cm^{-1}, both due to the N—H stretching in condensed secondary amides, are also observed. Additionally, the polymer prepared by thermal treatment at 160 °C during 1 h gives an FT-IR spectrum with other bands ascribable to a significant amount of terminal groups (mainly, a broad band between 3100 and 2800 cm^{-1} assigned to the N—H stretching of amines or O—H stretching of —COOH, and a narrow one at 1705 cm^{-1} due to the C=O stretching of —COOH). This indicates that the thermally polymerized product presents a lower degree of polymerization than the one obtained through the organic phase synthesis, in which the terminal group bands are hardly discernible and those related to the amide functional groups exhibit the highest intensities and are clearly predominant, indicating the higher polymerization degree reached. Such a high polymerization degree allowed us to reach particularly high carbonization and carbon yields in the carbon/silica composites (Table 1), especially if we consider that the infiltration process is accomplished in one single step. The preparation methods proposed here have clear advantages with regard to others based on precursors that need more than one infiltration step (e.g. sucrose [39,40], amino sucrose [22] and furfuryl alcohol [40,41]) or very long polymerization/stabilization times (e.g. furfuryl alcohol [42] and acrylonitrile [19,20]). Thus, the fraction of carbon material in the composite of PACor amounts to 49.4 wt.%, which is considerably higher than those previously reported for other carbon precursors (e.g. 30 wt.% by means of a single infiltration step with furfuryl alcohol, or about 36 wt.% when the infiltration is carried out in one single step using a pitch [43]). In the case of the OMC series prepared following solid-state thermal polymerization, the carbon fraction in the composites reaches a maximum value of 42.2 wt.% for sample PAC1.55. As indicated by the constant infiltration percentages attained for the PAC1.70 and PAC1.75 carbons, an amount of MABA monomer higher than 1.55 g/g silica does not increase significantly the carbon fraction in the composites. Thus, these results point to 1.55 g MABA/g SBA-15 template as the maximum amount of polyaramide precursor that could fill the entire porosity of the silica template. Moreover, a very interesting fact is observed in the thermal polymerization of this polymer precursor, that is, it takes place almost exclusively inside the pores of the SBA-15 template. Thereby, we studied the thermal polymerization of different amounts of MABA under the same carbonization conditions (160 °C/1 h/500 mL min^{-1} argon flow), and found that the monomer located outside the silica pores was swept along and deposited on the cold side of the reactor. This means that

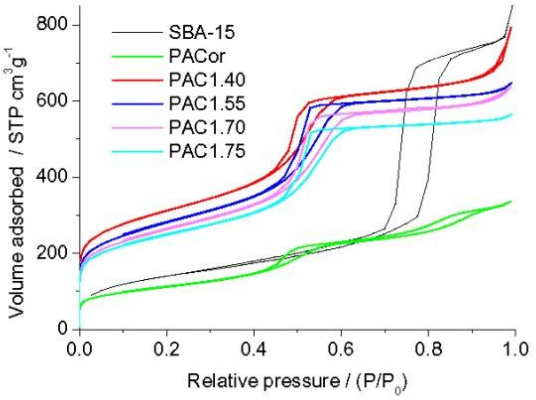

Fig. 2 – Nitrogen adsorption–desorption isotherms at −196 °C on the SBA-15 silica template and the ordered mesoporous carbons. (A colour version of this figure can be viewed online.)

no amorphous carbon is deposited on the surface particles, as we can observe in the SEM micrographs that are shown below.

The pore textural characterization of samples was accomplished through nitrogen physisorption at −196 °C, and the resulting adsorption–desorption isotherms are plotted in Fig. 2. The BJH method applied to the desorption branch of the isotherms was used for obtaining the pore size distributions (PSD) and for estimating the main pore diameter of the OMCs (D) at the maximum of the distribution. As one can see in Fig. 2, the OMCs obtained through the solid thermal polymerization method yield type IV isotherms with type H1 hysteresis loops (characteristics of mesoporous materials) and narrow pore size distributions of uniform pore size. This fact is clearly confirmed by the PSDs that are shown in Fig. 3.

These carbon materials exhibit very narrow PSD centered between 4 and 4.4 nm pore diameter values, which correspond to the thickness of the silica walls that were removed by dissolution in HF. The maximum values of apparent surface area and total pore volume (1084 $m^2\ g^{-1}$ and 1.05 $cm^3\ g^{-1}$, respectively) are obtained for the lowest infiltrated sample (PAC1.40) and they decrease as a greater MABA amount is used in infiltration, mainly due to a decrease in the micropore volume.

The Yamazaki reaction-based method yielded an OMC with a very different porous texture. The adsorption–desorption isotherm of the PACor carbon presents two hysteresis loops that point to the existence of two mesopore diameters (one at 3.8 nm, plus a wider distribution from 6.9 to ~11 nm, see Fig. 3) that could be explained by a heterogeneous infiltration of the silica template. The first maximum value of 3.8 nm is nearly the same as in the other carbons and is related to the replication of the silica walls; the second one corresponds with the non-infiltrated pores of the SBA-15 (8.1 nm) plus the thickness of the silica walls that were removed by HF treatment (3.1 nm). This sample possesses small micropore and mesopore volumes that give rise to the lowest S_{BET} among the studied carbon materials. As previously mentioned, the high polymerization degree of the MABA precursor in the synthesis step gives rise to a high carbon content (about 50 wt.%) due to a lower evolution of volatiles during the carbonization step, which produces a lower micropore development and therefore a low S_{BET} value. Additionally, this low porosity development in comparison with thermal polymerization carbons could be explained by the lower infiltration degree of the organic phase synthesis (as it is demonstrated by the adsorption characterization and also by TEM studies, see below at Fig. 6).

The ordered mesoporous carbons and the silica template were structurally characterized by small-angle X-ray diffraction, and the resulting diffractograms are recorded in Fig. 4. Both the SBA-15 template and the carbon replicas present three well-resolved peaks related to the (100), (110) and (200) reflections of the bidimensional hexagonal space group *p6mm*. The unit cell parameter, *a*, has been calculated from the (100) reflection according to the equation:

$$a = (2/3^{1/2})d_{100} \quad (1)$$

A greater broadness and the displacement of OMC peaks towards higher 2θ values regarding those of the silica template are observed. Data in Table 2 confirm the decreases of the interplanar distance d_{100} and the unit cell parameter *a*. Such findings agree with previous results [44], and may be ascribed to the lattice contraction of the framework during the carbonization process at high temperatures and upon silica template dissolution with HF. The synthesis method exerts a negligible influence on the d_{100} and *a* parameters, as their variation among the OMC samples is not significant. On the other hand, the diffractograms of all carbons present (110) and (200) reflections indicative of long range order. Among the obtained materials, PAC1.55 seems to possess the most ordered arrangement as suggested by the highest intensity of such reflections. For this reason and taking into account the maximum carbon content of this sample (42.2 wt.%, see Table 1), it is reasonable to consider that an infiltration process with 1.55 g MABA/g silica template through the thermal polymerization method gives rise to a homogeneously infiltrated and highly ordered carbon.

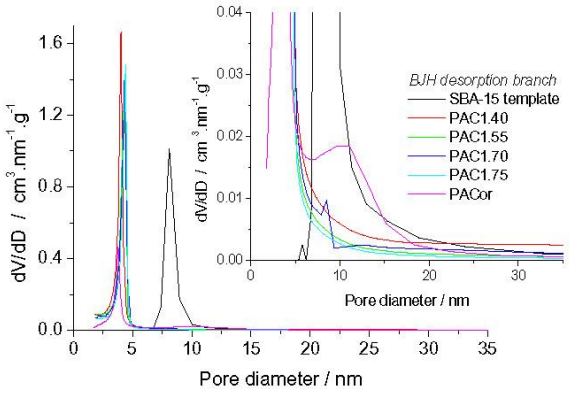

Fig. 3 – Pore size distributions of the SBA-15 template and the ordered mesoporous carbons obtained by BJH method applied to the desorption branches of the isotherms. An inset between 0.00 and 0.04 values of dV/dD is presented. (A colour version of this figure can be viewed online.)

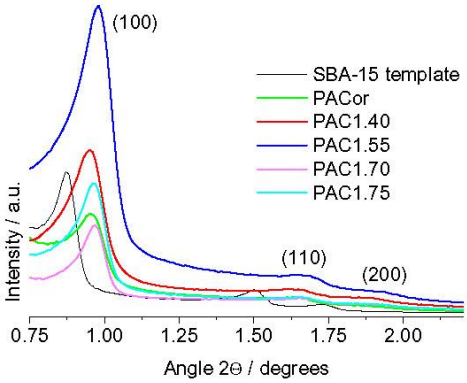

Fig. 4 – Low-angle XRD patterns for the SBA-15 silica template and the ordered mesoporous carbons obtained by the two synthetic routes. (A colour version of this figure can be viewed online.)

Table 2 – Structural parameters of the parent silica (SBA-15) and the OMCs, obtained by means of XRD.

Sample	d_{100} (nm) [a]	a (nm) [b]
SBA-15	9.92	11.5
PACor	9.29	10.7
PAC1.40	9.29	10.7
PAC1.55	9.01	10.4
PAC1.70	9.10	10.5
PAC1.75	9.17	10.6

[a] d_{100} = interplanar distance calculated by Bragg's law.
[b] a = unit cell parameter for the *p6mm* space group, calculated through Eq. (1).

The particle morphology and the nanostructure of the silica and carbon samples were examined by SEM and TEM, respectively. SEM micrographs of SBA-15 template and several carbon materials are recorded in Fig. 5, and indicate that the silica particle morphology is maintained after the nanotemplating process regardless of the synthesis method used.

Although no distinctive morphological features are apparent between the OMC synthesized through the Yamazaki reaction-based method and those thermally polymerized, some differences related to surface roughness can be highlighted among the latter. Thus, the PAC1.75 carbon presents a smoother surface compared to PAC1.55 sample in spite of having similar infiltration percentages, which is consistent with the porosity decrease at a higher amount of MABA precursor per gram of silica template used in the infiltration process. The absence of any amorphous carbon on the external surface of the particles supports the idea that the monomer polymerization takes place preferably inside the silica pores, and the MABA excess is swept out by the argon flow towards the cold end of the reactor.

TEM micrographs of the silica template and the OMCs obtained through both synthesis methods are shown in Fig. 6. As one can see, the nanostructure of the carbons is similar to that of the parent SBA-15 silica. A view of the silica template under the (100) direction is presented in Fig. 6(a), where linear arrays of mesopore channels are separated by an average distance of about 8 nm, as previously mentioned. TEM micrographs of thermally polymerized OMCs, shown in Fig. 6(c)–(f), exhibit highly-ordered nanostructures that are constituted by domains with long-range ordered mesopores. Taking into account the cross-sectional TEM images and those taken under the (100) direction, it is possible to estimate an average diameter of the mesopores at around 4 nm, a distance between two adjacent mesopores of about 10 nm and a diameter of the carbon rods of nearly 6 nm, confirming the results derived from the N_2 adsorption and XRD experiments. However, a precise determination of such parameters in PACor sample is more complicated. The high-resolution image shown in Fig. 6(b) presents ordered but heterogeneously distributed domains, where areas with different infiltration degrees coexist. These results are also consistent with those derived from the nitrogen adsorption–desorption isotherms and XRD patterns discussed above.

As concerns the chemical composition of the OMCs, the carbon, nitrogen and oxygen contents were determined by elemental analysis and XPS, and are listed in Table 3. In the case of the XPS data, the weight percentage of the elements was calculated in order to provide the same basis for comparison.

Despite the limitations of both analysis techniques, it would seem that the nitrogen functionalities are homogeneously

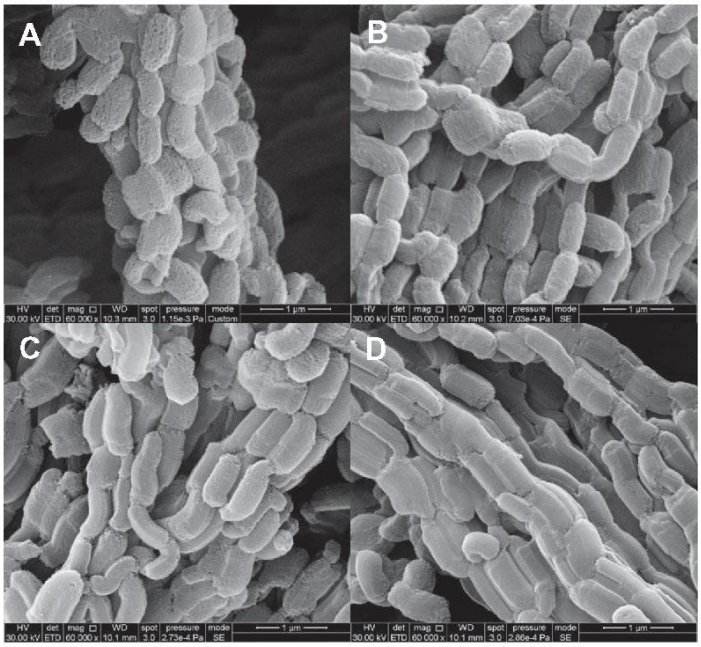

Fig. 5 – SEM micrographs of representative samples: (A) SBA-15 silica template, (B) PACor, (C) PAC1.55 and (D) PAC1.75.

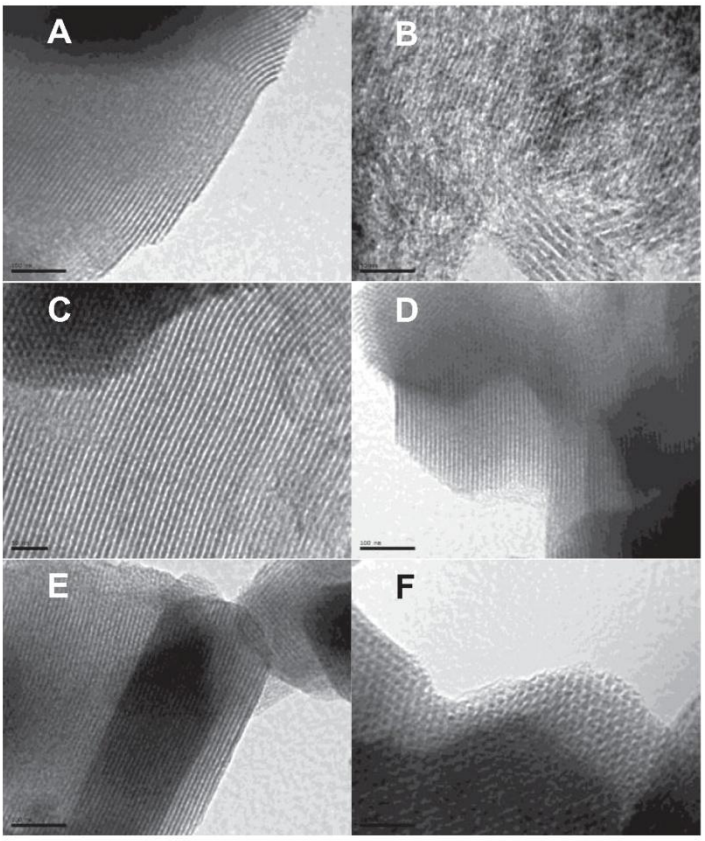

Fig. 6 – TEM micrographs of the parent silica and OMCs: (A) SBA-15 silica template (scale bar: 100 nm), (B) PACor (scale bar: 100 nm), (C) PAC1.40 (scale bar: 50 nm), (D) PAC1.55 (scale bar: 100 nm), (E) PAC1.70 (scale bar: 100 nm) and (F) PAC1.75 (scale bar: 50 nm).

Table 3 – Chemical composition of OMCs obtained from elemental analysis and XPS.

Sample	Elemental analysis (wt.%)			XPS (wt.%)		
	C	N	O	C	N	O
PACor	83.8	5.3	10.0	88.0	5.6	6.4
PAC1.40	81.7	5.5	11.5	89.2	5.2	5.6
PAC1.55	81.9	5.3	8.7	90.2	5.4	4.4
PAC1.70	81.2	6.0	7.5	90.1	5.6	4.4
PAC1.75	81.1	5.4	9.1	90.8	5.6	3.6

distributed in the bulk and the surface of the OMCs, as the weight percentages are almost the same in both cases. However, the oxygen contents obtained from elemental analysis are much higher than the corresponding values from XPS, indicating that the oxygen functional groups are mainly located in the bulk of the carbons. Moreover, the nitrogen content is very similar in all the samples, ranging from 5 to 6 wt.%, and seems to be unaffected by the synthesis method used. On the other hand, while the oxygen percentage varies from 11.5 to 7.5 wt.% in the bulk of the carbons without a clear tendency, in the surface it ranges from a maximum value of 6.4 wt.% for PACor to a minimum of 3.6 wt.% for PAC1.75. In the case of thermally polymerized samples, a slight decrease of the oxygen content can be observed as a higher amount of MABA per gram of silica was used in the infiltration process. A comparison with the composition of the starting polymer (70.6 wt.% C; 4.2 wt.% H; 11.8 wt.% N and 13.43 wt.% O) shows that about 50% of the N is retained after carbonization. The fraction of O retained ranges from 56% to 86% in respect to the polymer, but in this case, some of the oxygen can be introduced during the manipulation after carbonization (ambient exposure, HF treatment, drying, etc.). In both cases, this polymer yields high heteroatom retention after carbonization, even at the high temperature used here.

In order to obtain further information about the nature and the chemical coordination of carbon, nitrogen and oxygen in the material surface, the high-resolution XPS spectra of these elements were deconvoluted into single peaks that were assigned to specific functional groups. The

samples synthesized following the thermal polymerization method exhibit chemical compositions with very few differences among them; for this reason, PAC1.55 has been selected as representative sample of such method and compared with PACor carbon, obtained through the Yamazaki reaction-based synthesis. The C1s, N1s and O1s high-resolution spectra of the two representative OMCs have been plotted in Fig 7.

The deconvolution of the C1s-high resolution spectra yielded six peaks, as indicated in Fig. 7, whose binding energies (BE), area percentages (A) and functional group assignments are listed in Table 4. The BE and A values are almost the same in the C1s high-resolution spectra of the two samples, indicating that the carbon atoms are involved in the same types of surface chemical bonds. The N1s high resolution spectra, also shown in Fig. 7, are also very similar to each other, and their BE intervals are broad due to the presence of different functionalities or chemical environments. A satisfactory fitting was obtained by means of five broad components, which indicate the existence of numerous local bonding environments giving rise to overlapped peaks.

The most distinctive feature in the N1s high-resolution spectra is that the peak exhibiting the largest area is N3, assigned to substitutional nitrogen in condensed polyaromatic systems; in fact, as shown in Table 4, around 50% of the nitrogen contained in the OMCs is in the form of quaternary nitrogen, followed by a 40% of pyridinic and pyrrolic nitrogen and nitrile functional groups. Only about 7% of nitrogen is forming part of functionalities bonded to oxygen. Finally, the deconvolution of the O1s high resolution spectra was accomplished into three peaks, as shown in Fig. 7. These spectra present the most significant differences between the two studied carbons, as the BEs and the areas of the peaks differ considerably from each other. In the O1s high-resolution spectra of the two representative carbons plotted in Fig. 7, O3 is clearly predominant over the other peaks, and around 50% of oxygen is forming part of non-carbonylic C—O bondings in esters and anhydrides (see Table 4).

As concerns the other peaks, the O2 area in the PACor carbon is nearly five times higher than the O1 area, pointing to a greater abundance of ester, anhydride and alcohol functional groups in the material surface regarding carbonyls and carboxylic acids. By contrast, the PAC1.55 carbon exhibits a slightly higher contribution of the O1 area, which results in a major occurrence of the carbonyl and carboxylic functional groups in its surface. This could agree with the greater polymerization degree of the carbon synthesized trough the

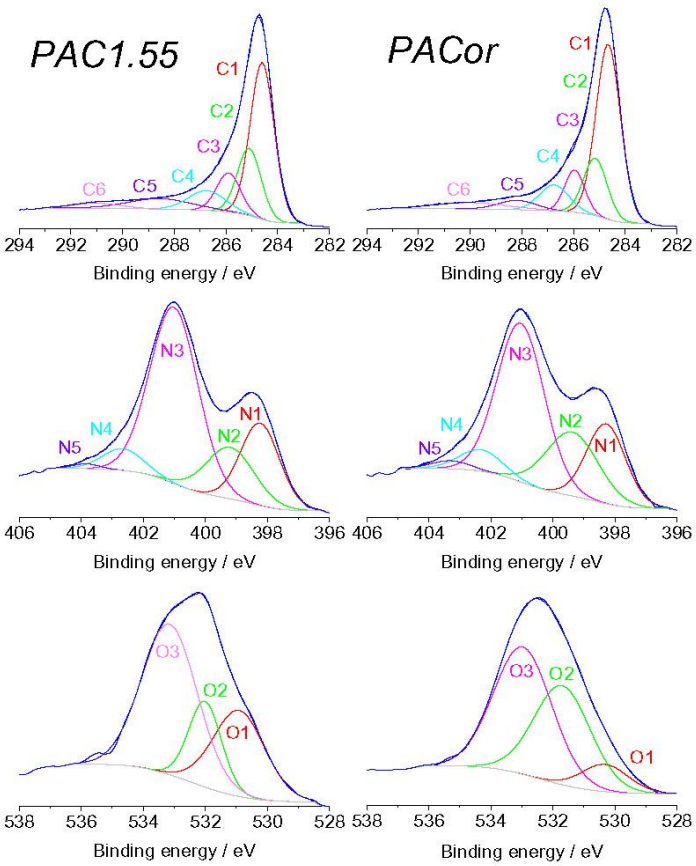

Fig. 7 – Deconvoluted profiles of the C1s, N1s and O1s high-resolution XPS spectra of two representative ordered mesoporous carbons: PAC1.55 and PACor. (A colour version of this figure can be viewed online.)

Table 4 – XPS data and functional group assignments for PACor and PAC1.55 carbons. Functional groups assignments were done based on [28,45–50].

Spectrum	Peak	PAC1.55		PACor		Functional groups
		BE (eV) [a]	A (%) [b]	BE (eV) [a]	A (%) [b]	
C1s	C1	284.60	47.27	284.66	53.19	C=C ($\pi\rightarrow\pi^*$ delocalized bondings)
	C2	285.10	20.24	285.16	16.77	C=C (localized bondings)
	C3	285.90	11.83	285.96	10.43	C—O (ethers, phenols, anhydrides), Csp^3, C=N (aromatic rings), C—N
	C4	286.74	9.24	286.75	9.50	C=O, C=N, $\pi\rightarrow\pi^*$ shake-up satellite of C2
	C5	288.55	8.41	288.18	4.41	Carboxylic C—O (—COOH), N component
	C6	291.00	3.01	289.97	5.72	C=C ($\pi\rightarrow\pi^*$ bonding, in highly ordered and graphitic structures)
N1s	N1	398.23	21.15	398.28	20.57	N_6, C≡N
	N2	399.19	16.37	399.37	21.99	N_5, Ph—C≡N
	N3	401.01	55.84	401.03	49.36	N_Q (quaternary nitrogen)
	N4	402.65	5.81	402.32	6.10	Nitrogen oxides
	N5	403.83	0.83	403.28	1.97	Nitrogen oxides
O1s	O1	530.91	28.53	530.32	8.93	O=C (carbonyls, carboxylic acids)
	O2	532.00	18.01	531.70	39.24	C=O (esters, anhydrides), —OH (alcohols), O—C (esters)
	O3	533.15	53.46	532.97	51.83	Non-carbonylic O—C (esters and anhydrides)

[a] BE = binding energy.
[b] A = relative area percentage.

Yamazaki reaction, which gives rise to a lower amount of terminal functional groups such as carboxylic acids. As concerns to the binding energies (BEs), listed in Table 4, the peaks in the PAC1.55 sample are displaced towards higher values with respect to those in the PACor sample, indicating that oxygen is in a less electronegative chemical environment.

Considering the overall results for the two representative samples, they are consistent with the obtaining of the same polymer chains from the same precursor (MABA), irrespective of the synthesis method used, but giving rise to different oxygen surface functionalities. A plausible explanation could be found in the different degree of polymerization achieved by the two synthetic methods, resulting in a different thermal degradation mechanism, which yields a carbon material with lower aromatization degree and higher amount of edges and therefore high surface area in the PAC_x series (as it was shown before), where oxidation during the acid etching and washing steps could take place in greater extent.

4. Conclusions

Using aromatic polyamides as OMC precursors, highly-ordered and nitrogen- and oxygen-rich materials with large surface areas and pore volumes have been obtained. Solid-state thermal polymerization and organic phase synthesis succeeded as innovative methods for the polyamide-derived OMC synthesis, in which 3-aminobenzoic acid was the polyaramide precursor and SBA-15 silica was the mesoporous template. In both procedures, the MABA monomer was introduced in the pore system of the silica template in a single step and the carbonization was accomplished at 900 °C. The solid-state thermal polymerization method presents additional advantages related to the highly homogeneous infiltration of the polymer precursor, the simultaneity of the polymerization/carbonization stages and the absence of any amorphous carbon on the external surface of the particles. Moreover, it is a low polluting and easy to perform procedure. All these characteristics make the solid-state thermal polymerization a more advantageous method than the Yamazaki reaction-based synthesis. Moreover, it represents an attractive pathway for the preparation of N- and O-doped OMCs in comparison with the chemical vapor deposition technique or liquid infiltration processes using other carbon precursors. The resulting OMCs not only display highly-ordered arrangements but also high nitrogen (around 6 wt.%) and oxygen contents (maximum value of 11.5 wt.% in the materials bulk and 6.4 wt.% on their surface), in spite of the high carbonization temperatures; such heteroatoms occur in a wide variety of functional groups, which makes their surface chemistry a very interesting feature for many applications. With the aim of increasing the nitrogen content in the ordered carbon structures and to better understand the involved mechanistic events, deeper studies are under way to optimize the experimental conditions and to use other available polyamide precursors.

Acknowledgements

The authors gratefully acknowledge the Spanish Ministerio de Ciencia e Innovación (project MAT2009-11375) and Ministerio de Economía y Competitividad and FEDER (project MAT2012-34011) for financial support.

REFERENCES

[1] Burchell TD. Carbon materials for advanced technologies. Amsterdam: Pergamon; 1999.
[2] Bottani EJ, Tascon JMD, editors. Adsorption by carbons. Amsterdam: Elsevier; 2008.

[3] Terzyk AP, Gauden PA, Kowalczyk P, editors. Carbon materials: theory and practice. Kerala: Research Signpost; 2008.
[4] Yasuda EI, Inagaki M, Kaneko K, Endo M, Oya A, Tanabe Y, editors. Carbon alloys, novel concepts to develop carbon science and technology. Amsterdam: Elsevier; 2003.
[5] Sun B, Liu H, Munroe P, Ahn H, Wang G. Nanocomposites of CoO and a mesoporous carbon (CMK-3) as a high performance cathode catalyst for lithium–oxygen batteries. Nano Res 2012;5(7):460–9.
[6] Beguin F, Frackowiak E, editors. Carbons for electrochemical energy storage and conversion systems. Boca Raton: CRC Press, Taylor & Francis Group; 2010.
[7] Pumera M. Graphene-based nanomaterials for energy storage. Energy Environ Sci 2011;4(3):668–74.
[8] Nishihara H, Kyotani T. Templated nanocarbons for energy storage. Adv Mater 2012;24(33):4473–98.
[9] Xia YD, Yang ZX, Mokaya R. Templated nanoscale porous carbons. Nanoscale 2010;2(5):639–59.
[10] Lu AH, Schüth F. Nanocasting: a versatile strategy for creating nanostructured porous materials. Adv Mater 2006;18(14):1793–805.
[11] Lee J, Kim J, Hyeon T. Recent progress in the synthesis of porous carbon materials. Adv Mater 2006;18(16):2073–94.
[12] Xue C, Tu B, Zhao D. Facile fabrication of hierarchically porous carbonaceous monoliths with ordered mesostructure via an organic–organic self-assembly. Nano Res 2009;2(3):242–53.
[13] Liu Z, Zhang G, Lu Z, Jin X, Chang Z, Sun X. One-step scalable preparation of N-doped nanoporous carbon as a high-performance electrocatalyst for the oxygen reduction reaction. Nano Res 2013;6(4):293–301.
[14] Lei Z, Bai D, Zhao XS. Improving the electrocapacitive properties of mesoporous CMK-5 carbon with carbon nanotubes and nitrogen doping. Micropor Mesopor Mater 2012;147(1):86–93.
[15] Su DS, Zhang J, Frank B, Thomas A, Wang X, Paraknowitsch J, et al. Metal-Free heterogeneous catalysis for sustainable chemistry. ChemSusChem 2010;3(2):169–80.
[16] Shrestha S, Mustain WE. Properties of nitrogen-functionalized ordered mesoporous carbon prepared using polypyrrole precursor. J Electrochem Soc 2010;157(11):B1665–72.
[17] Kim W, Joo JB, Kim N, Oh S, Kim P, Yi J. Preparation of nitrogen-doped mesoporous carbon nanopipes for the electrochemical double layer capacitor. Carbon 2009;47(5):1407–11.
[18] Kwon T, Nishihara H, Itoi H, Yang Q-H, Kyotani T. Enhancement mechanism of electrochemical capacitance in nitrogen-/boron-doped carbons with uniform straight nanochannels. Langmuir 2009;25(19):11961–8.
[19] Lu A, Kiefer A, Schmidt W, Schüth F. Synthesis of polyacrylonitrile-based ordered mesoporous carbon with tunable pore structures. Chem Mater 2004;16(1):100–3.
[20] Weidenthaler C, Lu AH, Schmidt W, Schüth F. X-ray photoelectron spectroscopic studies of PAN-based ordered mesoporous carbons (OMC). Micropor Mesopor Mater 2006;88(1–3):238–43.
[21] Liu N, Yin L, Wang C, Zhang L, Lun N, Xiang D, et al. Adjusting the texture and nitrogen content of ordered mesoporous nitrogen-doped carbon materials prepared using SBA-15 silica as a template. Carbon 2010;48(12):3579–91.
[22] Gadiou R, Didion A, Gearba RI, Ivanov DA, Czekaj I, Koetz R, et al. Synthesis and properties of new nitrogen-doped nanostructured carbon materials obtained by templating of mesoporous silicas with aminosugars. J Phys Chem Solids 2008;69(7):1808–14.
[23] Vinu A, Ariga K, Mori T, Nakanishi T, Hishita S, Golberg D, et al. Preparation and characterization of well-ordered hexagonal mesoporous carbon nitride. Adv Mater 2005;17(13):1648–52.
[24] Jiang J, Gao Q, Xia K, Hu J. Enhanced electrical capacitance of porous carbons by nitrogen enrichment and control of the pore structure. Micropor Mesopor Mater 2009;118(1–3):28–34.
[25] Giraudet S, Zhu Z, Yao X, Lu G. Ordered mesoporous carbons enriched with nitrogen: application to hydrogen storage. J Phys Chem C 2010;114(18):8639–45.
[26] Xia YD, Mokaya R. Synthesis of ordered mesoporous carbon and nitrogen-doped carbon materials with graphitic pore walls via a simple chemical vapor deposition method. Adv Mater 2004;16(17):1553–8.
[27] Xia YD, Mokaya R, Grant DM, Walker GS. A simplified synthesis of N-doped zeolite-templated carbons, the control of the level of zeolite-like ordering and its effect on hydrogen storage properties. Carbon 2011;49(3):844–53.
[28] Boudou JP, Parent P, Suárez-García F, Villar-Rodil S, Martinez-Alonso A, Tascon JMD. Nitrogen in aramid-based activated carbon fibers by TPD XPS and XANES. Carbon 2006;44(12):2452–62.
[29] Castro-Muñiz A, Suárez-García F, Martínez-Alonso A, Tascón JMD. Activated carbon fibers with a high content of surface functional groups by phosphoric acid activation of PPTA. J Colloid Interface Sci 2011;361(1):307–15.
[30] Leitner K, Lerf A, Winter M, Besenhard JO, Villar-Rodil S, Suárez-García F, et al. Nomex-derived activated carbon fibers as electrode materials in carbon based supercapacitors. J Power Sources 2006;153(2):419–23.
[31] Suárez-García F, Paredes JI, Martinez-Alonso A, Tascon JMD. Preparation and porous texture characteristics of fibrous ultrahigh surface area carbons. J Mater Chem 2002;12(11):3213–9.
[32] Villar-Rodil S, Denoyel R, Rouquerol J, Martinez-Alonso A, Tascon JMD. Fibrous carbon molecular sieves by chemical vapor deposition of benzene gas separation ability. Chem Mater 2002;14(10):4328–33.
[33] Villar-Rodil S, Suárez-García F, Paredes JI, Martinez-Alonso A, Tascon JMD. Activated carbon materials of uniform porosity from polyaramid fibers. Chem Mater 2005;17(24):5893–908.
[34] Castro-Muñiz A, Martinez-Alonso A, Tascon JMD. Modification of the pyrolysis/carbonization of PPTA polymer by intermediate isothermal treatments. Carbon 2008;46(7):985–93.
[35] Yamazaki N, Matsumoto M, Higashi F. Studies on reactions of the N-phosphonium salts of pyridines. XIV. Wholly aromatic polyamides by the direct polycondensation reaction by using phosphites in the presence of metal salts. J Polym Sci Pol Chem 1975;13(6):1373–80.
[36] Mosquera MEG, Jamond M, Martinez-Alonso A, Tascon JMD. Thermal transformations of Kevlar aramid fibers during pyrolysis: infrared and thermal analysis studies. Chem Mater 1994;6(11):1918–24.
[37] Villar-Rodil S, Martinez-Alonso A, Tascon JMD. Studies on pyrolysis of Nomex polyaramid fibers. J Anal Appl Pyrol 2001;58:105–15.
[38] Socrates G. Infrared and Raman characteristic group frequencies: tables and charts. Chichester (UK): John Wiley and Sons; 2001.
[39] Jun S, Joo SH, Ryoo R, Kruk M, Jaroniec M, Liu Z, et al. Synthesis of new, nanoporous carbon with hexagonally ordered mesostructure. J Am Chem Soc 2000;122(43):10712–3.
[40] Gierszal KP, Jaroniec M, Kim T-W, Kim J, Ryoo R. High temperature treatment of ordered mesoporous carbons prepared by using various carbon precursors and ordered mesoporous silica templates. New J Chem 2008;32(6):981–93.

[41] Lu AH, Schmidt W, Spliethoff B, Schüth F. Synthesis of ordered mesoporous carbon with bimodal pore system and high pore volume. Adv Mater 2003;15(19):1602–6.
[42] Lu A-H, Li W-C, Schmidt W, Schüth F. Template synthesis of large pore ordered mesoporous carbon. Micropor Mesopor Mater 2005;80(1–3):117–28.
[43] Parmentier J, Saadhallah S, Reda M, Gibot P, Roux M, Vidal L, et al. New carbons with controlled nanoporosity obtained by nanocasting using a SBA-15 mesoporous silica host matrix and different preparation routes. J Phys Chem Solids 2004;65(2–3):139–46.
[44] Lee JS, Joo SH, Ryoo R. Synthesis of mesoporous silicas of controlled pore wall thickness and their replication to ordered nanoporous carbons with various pore diameters. J Am Chem Soc 2002;124(7):1156–7.
[45] Cuesta A, Martinez-Alonso A, Tascon JMD, Bradley RH. Chemical transformations resulting from pyrolysis and CO2 activation of Kevlar flocks. Carbon 1997;35(7):967–76.
[46] Hueso JL, Espinós JP, Caballero A, Cotrino J, González-Elipe AR. XPS investigation of the reaction of carbon with NO, O_2, N_2 and H_2O plasmas. Carbon 2007;45(1):89–96.
[47] Dementjev AP, de Graaf A, van de Sanden MCM, Maslakov KI, Naumkin AV, Serov AA. X-ray photoelectron spectroscopy reference data for identification of the C_3N_4 phase in carbon–nitrogen films. Diam Relat Mater 2000;9(11):1904–7.
[48] Xiao B, Boudou JP, Thomas KM. Reactions of nitrogen and oxygen surface groups in nanoporous carbons under inert and reducing atmospheres. Langmuir 2005;21(8):3400–9.
[49] Briggs D. Surface analysis of polymers by XPS and static SIMS. Cambridge: Cambridge University Press; 1998.
[50] Briggs D, Grant JT. Surface analysis by Auger and X-ray photoelectron spectroscopy. Chichester: IM Publications; 2003.

PUBLICACIÓN 4:

'pH-responsive ordered mesoporous carbons for controlled ibuprofen release'. *Enviado a publicación.*

Diferentes tipos de materiales porosos han sido utilizados como portadores para la liberación controlada de medicamentos, incluyendo polímeros, péptidos, hidrogeles, sílices y carbones mesoporosos y estructuras orgánicas metálicas. Sin embargo, muchos de ellos presentan desventajas relacionadas con su inestabilidad en las condiciones fisiológicas o una baja biocompatibilidad. Liberar un medicamento de forma controlada es importante por dos razones principales: i) Se pueden utilizar medicamentos poco solubles; ii) Se controla dónde es liberado el medicamento, cuándo lo hace y en qué cantidad se libera. En este sentido, la química superficial de los materiales portadores es un factor clave para la adsorción y liberación de medicamentos. Teniendo en cuenta los resultados expuestos en la **Publicación 3**, los CMOs obtenidos por polimerización térmica en estado sólido a partir de precursores de poliamidas presentan propiedades muy interesantes para su aplicación como portadores de medicamentos: poseen porosidades desarrolladas conteniendo micro y mesoporos, estructuras altamente ordenadas y químicas superficiales muy ricas en nitrógeno y oxígeno.

En el presente trabajo se utilizaron dos precursores diferentes de poliamidas aromáticas: el ácido *m*-aminobenzoico (MABA) y el ácido *p*-aminobenzoico (PABA). La infiltración se realizó con 1.20 g de MABA o PABA/g SBA-15, siguiendo las etapas detalladas en el procedimiento experimental del **Apartado 3.1.2.2**. Un resultado destacable de este trabajo es la obtención de CMOs dopados con diferente tipo de estructura en función del precursor utilizado. Así, a partir de MABA se obtienen CMOs tipo CMK-3, mientras que el monómero PABA da lugar a CMOs tipo CMK-5. La estructura tipo CMK-3 consiste en barras de carbón separadas por pequeños conectores; los microporos se localizan en la superficie de las barras, mientras que los mesoporos se corresponden con la distancia que existe entre las barras de carbón. Por otro lado, la estructura tipo CMK-5 es similar a la de tipo CMK-3 pero

está constituida por tubos en lugar de barras. En esta estructura tenemos dos tipos de mesoporos: entre los tubos (equivalentes a los de la estructura CMK-3 y que proceden de las paredes de la plantilla) y en el interior de los tubos. El contenido de nitrógeno y oxígeno en ambos materiales es elevado. Sin embargo, su distribución en los carbones es diferente: el carbón obtenido a partir de MABA presenta una mayor proporción de funcionalidades de nitrógeno pirrólico y nitrógeno cuaternario, así como grupos oxigenados predominantemente en forma de anhídridos, alcoholes y éteres; en el segundo carbón (obtenido a partir de PABA), la proporción de nitrógeno pirrólico y cuaternario es menor y el oxígeno se encuentra formando parte principalmente de anhídridos y ésteres.

Las diferencias texturales, estructurales y, especialmente, de química superficial que existen entre los dos materiales estudiados se reflejan en su diferente comportamiento de adsorción y liberación de ibuprofeno. Ambos CMOs actúan como buenos adsorbentes de ibuprofeno, pero el carbón tipo CMK-5 es más eficaz como sistema de liberación controlada. Las cinéticas de liberación del fármaco son muy rápidas para los dos carbones, manteniéndose un nivel constante de ibuprofeno en disolución desde los primeros 15 minutos hasta las 24 horas. Además, la química superficial de los materiales induce una respuesta específica al pH del medio, puesto que el aumento del pH de 2 a 7.4 produce un incremento de la cantidad liberada. Esta propiedad de respuesta inducida por el pH es más evidente para el carbón derivado del monómero PABA, ya que a pH=2 la concentración de fármaco en equilibrio se mantiene en el 8% en peso y aumenta hasta el 30% en peso para un valor de pH de 7.4. Teniendo en cuenta los cortos periodos de tiempo necesarios para alcanzar la concentración de equilibrio, la liberación controlada del fármaco y la respuesta de liberación inducida por el pH, podemos concluir que los CMOs obtenidos a partir de precursores de poliamidas aromáticas son materiales muy prometedores como portadores para la liberación controlada de medicamentos poco solubles como el ibuprofeno.

pH-Responsive Ordered Mesoporous Carbons for Controlled Ibuprofen Release

Á. Sánchez-Sánchez[†], F. Suárez-García, A. Martínez-Alonso, J. M. D. Tascón

Instituto Nacional del Carbón, INCAR-CSIC, Apartado 73, 33080 Oviedo (Spain)

ABSTRACT

Nitrogen-doped ordered mesoporous carbons (OMCs) were synthesized by nanocasting using SBA-15 mesoporous silica as template and two polyaramide precursors: *m*-aminobenzoic acid (MABA) and *p*-aminobenzoic acid (PABA). The structure of the resulting OMCs was greatly influenced by the precursor used, since MABA yields a CMK-3 type OMC, while PABA gives a CMK-5 one. Both carbons displayed differences in the textural parameters, structural characteristics and surface chemical functionalities, which was reflected in a different behavior in the adsorption and release of ibuprofen as a function of the pH. Although the two carbons exhibited a good behavior as drug adsorbents, the PAMA-derived carbon was more efficient, in terms of drug delivery, than the carbon prepared from MABA, which was associated to the tube-like structure of the former. The studies on ibuprofen release revealed that both carbons have very fast desorption kinetics, and the maximum ibuprofen delivery was reached in the first 15 min and remained constant up to 24 hours. Both carbons also exhibited a specific response towards the pH, which was associated to the presence of nitrogen functionalities on the carbon surfaces. This pH-responsive property was most evident for the PAMA derived carbon, which allowed a sustained drug level of 8 wt.% at pH=2 and of 30 wt.% at pH=7.4.

[†] Corresponding author: Fax number: +34 985 297 662; e-mail adress: ang.san@incar.csic.es

1. INTRODUCTION

Ibuprofen (2-(4-isobutylphenyl) propionic acid) is a non-steroidal anti-inflammatory drug, which has a molecular size of about 1.03 x 0.53 nm and is a well characterized drug commonly used as a release drug model [1-3]. Ibuprofen is also one of the most consumed medicines all over the world. The usual therapeutic concentration of ibuprofen in human blood is around 50 mg/L, and the toxic effect appears above 250 mg/L [4]. Overdose of ibuprofen occurs with depression of central nervous system, respiratory and gastrointestinal problems and acute renal failure [4]. The use of drug delivery systems allows the control of the drug release (where, when and how much drug is delivered) and also allows the use of poorly soluble drug [1]. Different materials have been studied as systems for controlled delivery, including polymers, peptides, hydrogel, mesoporous silicas and carbons, metal-organic frameworks (MOFs), etc. [1, 2, 5-9]. Polymers, peptides, hydrogel and related materials are being extensively studied as drug delivery systems because of their biocompatibility, their capacity to imbibe high amounts of solutions and the possibility of synthesizing them to respond to several stimuli as pH, temperature, etc. [5, 6, 10-14]. The porous materials having been most often used in this application are MOFs, mesoporous silicas and carbons. Thus, different drugs, such as ibuprofen, antitumor and retroviral agents, have been supported onto MOFs [8, 9]. Despite their versatility, these materials have several drawbacks for their use as drug carriers such as the progressive delivery of toxic metals (e.g. ruthenium or chromium) and the structural instability in acidic and alkaline media. Another important family of materials studied as controlled drug delivery systems are mesoporous silicas [1, 15-19]. Mesoporous silicas are interesting materials for this application thanks to their properties such as adjustable pore size, interconnected pore structure, high pore volumes and surface areas and also to the possibility of grafting and functionalization with suitable groups and molecules [16, 19]. However, they have some drawbacks as their weak stability under extreme pH conditions or the fact that long-term exposure to silica compounds can exert a cytotoxic effect and weaken the immune system [20, 21]. Ordered mesoporous

carbons (OMCs) overcome the drawbacks of these materials and emerge as highly valuable drug delivery systems because of their well-ordered and tunable pore structure, high pore volumes and specific surface areas, high stability in aqueous media and excellent biocompatibility [22, 23]. The surface chemistry of materials used as drug carriers is a key factor in adsorption and release of drugs. Introduction of oxygen functionalities has been proved to influence the adsorption of aromatic molecules through interactions between the former and the aromatic ring of the latter [24] or the formation of hydrogen bonds [25]. Mestre et al. [26] showed that the presence of basic functionalities is also important, as well as the mesoporous texture of the carbons. Carbon materials have also been grafted with polymers and their performace for ibuprofen adsorption and release has been recently studied [27]. Thus, a CMK-3 type OMCs was functionalized with a thermal-response polymer (i.e. poly-(N-isopropyl acrylamide). The resulting composite material was applied for ibuprofen release and exhibited a thermo-sensitive release property at around 20-25 °C [27]. Apart from this work, to the best of our knowledge, there are no studies on the effect of nitrogen surface groups in carbon materials in the controlled release of drugs. So in this work, nitrogen-doped ordered mesoporous carbons (N-OMCs) were obtained by nanocasting from two different polyaramide precursors, 3-aminobenzoic acid (MABA) or 4-aminobenzoic acid (PABA). The resulting carbons exhibited different structures depending on the precursor used, being CMK-3 type in the material obtained from MABA and CMK-5 in the one obtained from PABA. The effect of both the type of ordered structure and the surface chemistry on ibuprofen release was investigated as a function of the pH at two physiologic values, pH = 2 (i.e., stomach) and 7.5 (i.e., small intestine).

2. EXPERIMENTAL SECTION

2.1. Synthesis of SBA-15 silica template

Mesoporous SBA-15 silica was prepared using the method described by Zhao et al. [28]. In this case, Pluronic P123 (Mw= 5800, Aldrich) was dissolved in an aqueous solution of HCl (Merck). After complete polymer dissolution, tetraetoxysilane (TEOS,

Aldrich) was added dropwise and the mixture was kept under stirring (40 ºC, 4 h). The molar composition of the starting reaction mixture was 0.017 P123 / 1 TEOS / 145.8 H_2O / 6.04 HCl. The resulting product was aged (125 ºC, 72 h), filtered and calcined in air (550 ºC, 6 h).

2.2. Synthesis of nitrogen-doped mesoporous carbons (N-OMCs)

The N-OMCs were synthesized following a solid-state thermal polymerization method proposed previously [29]. Here, briefly. SBA-15 mesoporous silica (1 g) was placed in a rotatory evaporator and degassed under vacuum (150 ºC, 2 h). After being cooled down to room temperature, 3-aminobenzoic acid (MABA, 1.20 g; *Across*) or 4-aminobenzoic acid (PABA, 1.20 g; Sigma-Aldrich) dissolved in acetone (45 mL; *Sigma-Aldrich*) was added to the SBA-15 template. The solvent was removed under vacuum and the resulting composite was carbonized under a nitrogen flow (150 mL / min) under a two-step program. First step (1 ºC/min) was at 160 ºC for 1 h, in order to promote the thermal polymerization of the monomers, and the second one (10 ºC/min) was carried out up to the target temperature (700 ºC and keeping this temperature for 30 min). The carbonized composites were treated with hydrofluoric acid (40 %, *Fluka*) at room temperature to remove the silica template, filtered and dried in an oven (80 ºC, 12 h). The resulting OMCs were named as MA and PA, which indicate the monomer used in the synthesis (MABA and PABA, respectively).

2.4. Characterization Techniques

Nitrogen adsorption isotherms were measured at –196 ºC with a volumetric adsorption apparatus Autosorb-1 (Quantachrome). The samples were degassed at 150 ºC for 16 h prior to measurements. The specific surface area (S_{BET}) of the carbons was obtained by using the BET equation. The total pore volume (V_t) was calculated from the amount adsorbed at the relative pressure of 0.975, and the micropore volume ($V_{\mu p}$) was determined from Dubinin-Raduskevich equation in the relative pressure range of 10^{-3} to 10^{-1}. The mesopore volume (V_{mp}) was calculated from the pore size distributions (PSDs), obtained by applying the QSDFT method

[30] to the nitrogen adsorption isotherms.

The zero charge point (pH_{ZCP}) of each carbon was determined through the pH drift method [25, 31] using a Mettler Toledo MPC227 pHmeter The pH of deoxygenized 0.01 M NaCl aqueous solutions (50 mL) was adjusted to successive initial values between 2 and 12 by adding 0.1 M HCl or NaOH. Mesoporous carbon (MA or PA, 150 mg) was added to each solution and the resulting suspensions were stirred for 24 hours under a nitrogen atmosphere. After that, the final pH was measured and plotted versus the initial pH, and the pH_{ZCP} was determined as the value for which both pH are equals.

The X-ray diffraction (XRD) patterns were recorded with a Siemens D5000 diffractometer, using Cu K_{α} radiation in the scanning range of 2θ = 0.5-5º, with a step width of 0.01º and a time per step of 1 second. Scanning electron microscopy (SEM) was performed on a Carl Zeiss DMS-942 microscope. Carbon content in the carbonized composites was determined as the weight loss at 900 ºC by thermogravimetric analysis in a CI Electronics microbalance using an air flow of 50 ml/min, a sample mass of 20 mg and a heating rate of 5 ºC/min. Elemental analysis was carried out on a TruSpec Micro analyzer provided with a TruSpec O accessory for oxygen. XPS analysis was performed on a SPECS system, working at a pressure of 10^{-7} Pa with a monochromatic Al K_{α} X-ray source (1486.3 eV, 150 W). The photo-excited electrons were analyzed in constant pass energy mode, using pass energy of 30 eV for the survey spectra and 10 eV for the high resolution core level spectra. The CasaXPS software was used for data processing and all envelopes of core level spectra were peak-fitted with Gaussian-Lorentzian convoluted functions (80/20) and a Shirley's background. The compositions (expressed in wt.%) were determined from the survey spectra by considering the integrated peak areas of the main XPS peaks for the different elements (C1s, N1s and O1s) and their respective sensitivity factors. No corrections were made in the N1s binding energy as the carbons showed no charging effects.

2.5. Ibuprofen release

For ibuprofen loading, MA or PA carbons (10 mg) were suspended into an ibuprofen solution in ethanol (30 mg/mL; 10 mL), contained in a closed batch to prevent solvent evaporation. The mixture was maintained under stirring and constant temperature (25 ºC) in a thermostatic bath shaker. After the contact time (24 h) was elapsed, the loaded carbons were filtered and dried (60 ºC; 12 hours). The residual concentrations of ibuprofen were determined by triplicate using a double-beam UV/VIS spectrophotometer (Thermo Spectronic Heλios α) at the wavelength of the maximum absorption (i.e. 202 nm). The adsorbed amount at equilibrium was calculated through equation 1:

$$q_e = C_0 - C_e \frac{V}{m_s} \qquad \text{Equation (1)}$$

where C_0 is the initial ibuprofen concentration (mg/L), C_e is the equilibrium ibuprofen concentration (mg/L), V the volume of solution (L) and m_s the weight of carbon adsorbent (g).

The resulting loaded carbons (MA-IBU and PA-IBU) were used to study the ibuprofen release through kinetic experiments. The samples (20 mg) were immersed into buffer solutions (50 mL) thermostated at 36 ºC and with the pH values adjusted at 2 (i.e. simulating the stomach pH) or 7.4 (i.e. simulating the small intestine pH). At given time intervals, 2 mL of solution were removed using a syringe filter (used for measuring the ibuprofen concentration) and replaced with the same volume of preheated fresh buffer. The concentration of ibuprofen was measured by triplicate through UV/VIS spectrophotometry at the wavelength of the maximum absorption (i.e. 202 nm). The amount of released ibuprofen at time *t*, calculated through equation 1**,** was expressed as mg (ibuprofen) / g (carbon).

3. RESSULTS AND DISCUSSION

3.1. Sample characterization

The low-angle XRD patterns of the carbons are shown in Figure 1. The MA carbon exhibits three well-resolved peaks at 2θ = 0.949º, 1.627º and 1.870º, which can be indexed to the (100), (110) and (200) reflections, respectively, of the *p6mm*

hexagonal symmetry group. However, the PA sample displays a rather different diffractogram. The (100) reflection peak at around 0.937° is hardly noticeable and the (110) and (200) peaks (found at 1.590º and 1.840º, respectively) are more intense that those of MA carbon. Moreover, a fourth peak appears at 2 = 2.449º, which can be indexed to the (210) reflection. These data indicate that MA is a mesoporous CMK-3 type carbon, while PA carbon possesses a tube-like mesoporous CMK-5 structure [32-34].

The unit cell parameter, *a*, was calculated through equation 2:

$$a = \frac{2}{\sqrt{3}} d_{100} \qquad \text{equation 2}$$

From equation 2 and considering the values of interplanar distance (d_{100}) of each carbon, the calculated unit cell parameter was 10.7 nm for MA, and 10.8 nm for PA; they match with the value for the SBA-15 used as template. Therefore, both carbons were properly replicated and retained the ordered structure of the parent silica template.

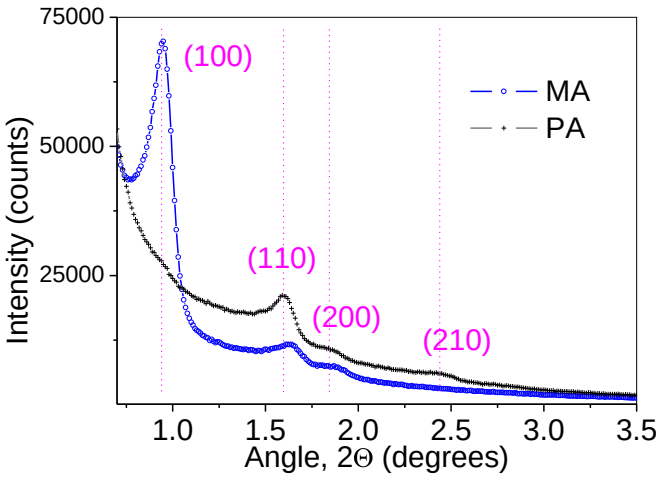

Figure 1. Low-angle XRD patterns of the carbons.

The nitrogen adsorption isotherms and pore size distributions (PSDs) of the carbons before and after ibuprofen loading are recorded in Figure 2. Both carbon materials (before ibuprofen loading) exhibit type IV isotherms with capillary condensation

above the relative pressure of 0.4 (Figure 4A and B), pointing to the presence of mesoporosity. Sample MA presents a sharp adsorption around 0.5 P/P_0, which is a characteristic of materials having narrow and uniform PSDs in the mesopore range. The isotherm for PA carbon has a large N_2 uptake over the entire pressure range, which indicates the presence of mesopores with different sizes. The corresponding PSDs (Figure 4C and D) confirm these statements. Thus, both carbons show bimodal PSDs constituted by two peaks in the micro and mesopore ranges. The first, broad peak consists of micropores with diameters between 0.6 and 2 nm and maxima at 0.78 and 1.05 nm for MA and PA, respectively. The second peak has a higher intensity (confirming that these carbons are mainly mesoporous) and is narrower than the first one; the maximum is at 3.37 nm for both carbons. Comparing the PSDs for MA and PA carbons, one can see that the second peak (mesopore range) is narrower for MA than for PA sample, as expected from the shape of their isotherms. This is consistent with the different structural arrangement observed by XRD, being CMK-3 type in MA and CMK-5 type in PA. Thus, the structure of PA carbon could consist of hollow tubes with an inner diameter similar to that of the mesopores existing between the carbon tubes, around 2.5-5 nm, while MA carbon could be composed of solid bars exhibiting mainly micropores of around 0.78 nm. Such assumptions will be latter confirmed by TEM.

The textural parameters obtained from the nitrogen isotherms, as well as the carbon content and carbonization yield, are presented in Table 1. These data indicate that the PA carbon possesses a more developed porosity. This carbon has a higher surface area and micropore volume and much higher total pore volume and mesopore volume than MA sample. Thus, these differences between both carbons are due to the very large V_{mp} of PA sample, as it could be expected from the difference structure of PA and MA. If MA is a CMK-3 carbon and PA is a CMK-5 one, the latter will be formed by rods and the former by a tubular structure, which provides a double surface (outside and inside the tubes).

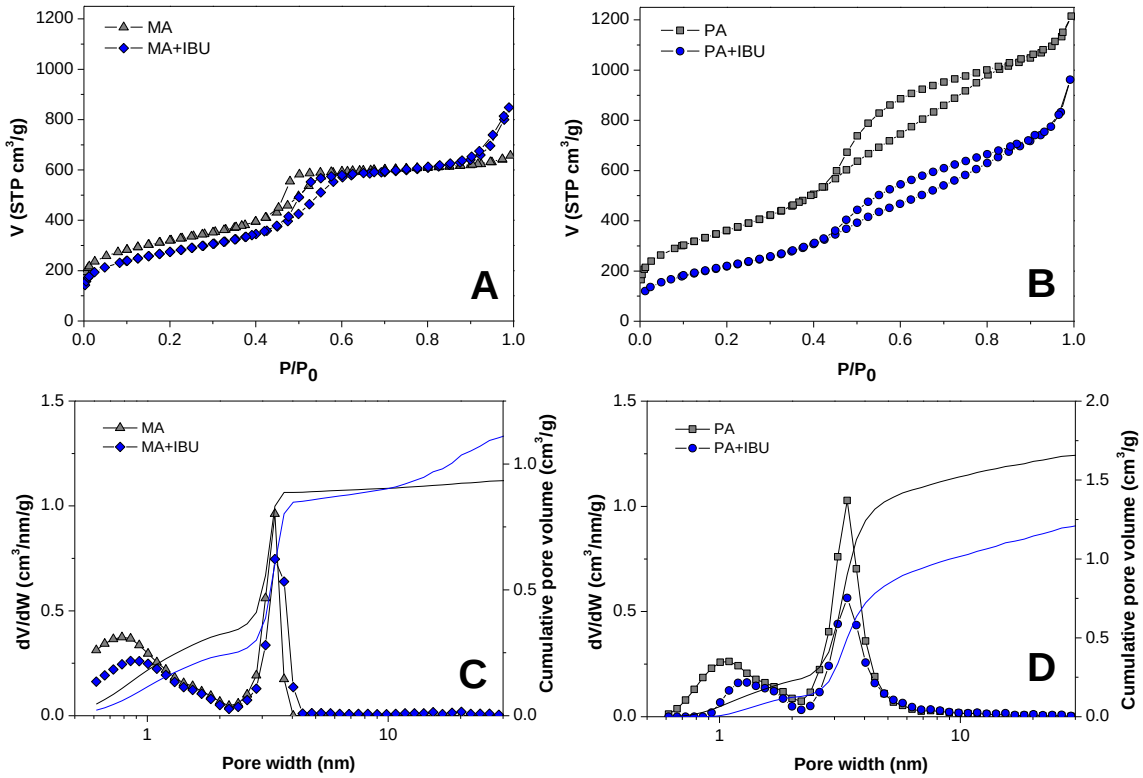

Figure 2. Nitrogen adsorption/desorption isotherms measured at -196 ºC for: (A) MA and MA+IBU (after ibuprofen loading) and (B) PA and PA+IBU (after ibuprofen loading) carbons and their corresponding pore size distributions and cumulative pore volume for MA (C) and PA (D), respectively.

Table 1. Several textural parameters deduced from the N_2 adsorption isotherms at –196 ºC data of the carbons, carbon content (η_{carbon}) in the carbon/silica composite, carbonization yield ($\eta_{carbonization}$), pH of the zero charge point and ibuprofen loading.

SAMPLE	S_{BET} (m^2/g)	V_T (cm^3/g)	$V_{\mu p}$ (cm^3/g)	V_{mp} (cm^3/g)	η_{carbon} (wt.%)	$\eta_{carbonization}$ (wt.%)	pH_{ZCP}	IBU loading (wt.%)
MA	1058	1.02	0.45	0.61	39.0	58.2	6.6	-
PA	1322	1.88	0.49	1.44	20.8	54.6	7.1	-
MA-IBU	940	1.24	0.37	0.89	-	-	-	21.2
PA-IBU	807	1.29	0.29	1.11	-	-	-	22.2

The structural features of the carbons were examined by TEM. Figure 3 shows TEM

micrographs displaying longitudinal and cross-sectional images of the carbon arrangements. As shown in Figure 3A and C, longitudinal sections for both carbons exhibit pore channels arranged in a bidimensional ordered array. One main pore system is evidenced in Figure 3A (MA carbon), while two pore systems can be distinguished in Figure 3C (PA carbon). This can be clearly observed by examining cross-sectional views for both carbons in Figure 4B and D. The cross-section image of MA carbon (Figure 3B) displays a well-defined mesopore network between the carbon rods, which comes from the silica template walls and has a pore size around 3.4 nm. On the other hand, the cross-sectional view of Figure 3D exhibits carbon tubes with two types of mesopores, either between the carbon tubes (those from the template walls with a size around 3.4 nm) or inside them. As shown in Figure 3D, the diameter of the inner mesopores varies in the range between 2.5 and 5 nm, which explains the wider mesopore size distribution exhibited by PA carbon in Figure 2D obtained from the N_2 adsorption data. Thus, TEM images confirm XRD and N_2 adsorption findings, which pointed to a CMK-3 type structure of MA carbon and a CMK-5 one of PA.

The different carbon structure (CMK-3 or CMK-5) obtained from either precursor (MABA or PABA) can be explained taking into account the different carbonization yields ($\eta_{carbonization}$) and therefore the different carbon contents (η_{carbon}) in the composites, which are reported in Table 1. As we indicated in the Experimental Section, the same amount of monomer (MABA or PAMA) was used for infiltrating the porosity of the template, therefore differences in the carbon content in the composites are due to the different mechanism of carbonization for both polymers. The higher carbonization yield of MABA precursor agrees with results from previous studies of carbon materials obtained from meta-substituted polyaramide precursors [35]. It was proved that meta-substituted polymers, such as PMIA, exhibit higher carbonization yields than para-substituted polymers, such asPPTA because of different thermal degradation mechanisms. In addition to this, we have found that the structure of the carbons prepared from these two monomers varies depending on the amount of precursor used to infiltrate the template. So, we prepared carbons by infiltrating SBA-15 silica with different amounts of monomer, and CMK-3

or CMK-5 type carbons were obtained depending on the final amount of carbon in the composite. Thus, η_{carbon} above 37% are needed for obtaining CMK-3 carbons [29].

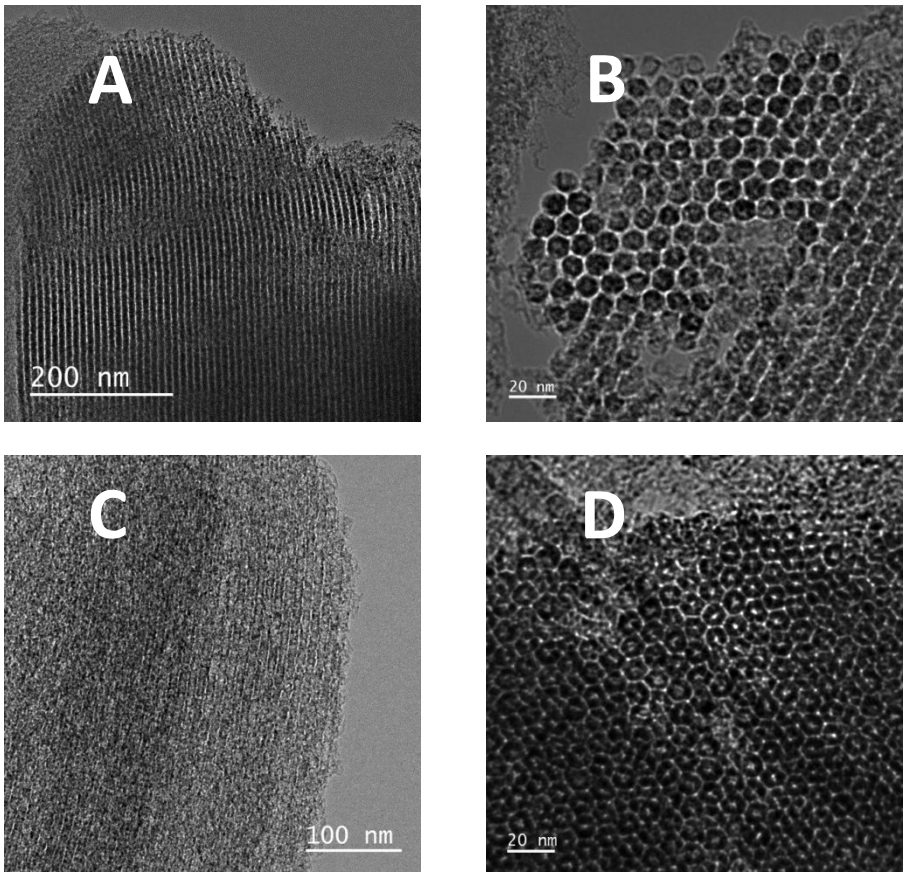

Figure 3. TEM micrographs of MA carbon in the cross-sectional (A) and longitudinal (B) views and of PA carbon in the cross-sectional (C) and longitudinal (D) views.

Table 2. Chemical composition data for carbons deduced from elemental analysis (left) and XPS (right). Concentrations of elements are expressed as weight percentages (wt.%).

SAMPLE	**Elemental analysis**			**XPS**		
	C	**N**	**O**	**C**	**N**	**O**
MA	79.8	8.3	6.2	88.3	6.7	5.0
PA	83.2	7.8	5.7	85.9	7.6	6.5

Chemical composition data for the carbons as deduced from elemental analysis and

XPS are shown in Table 2. It is well known that elemental analysis provides information about heteroatoms contained in the material bulk, while XPS gives information of its surface. Data contained in Table 2 show that high nitrogen amounts are present in both the bulk and the surface of the carbons. Heteroatoms (N and O) are slightly more concentrated in the bulk of MA carbon, while PA exhibits a homogeneous composition in terms of heteroatoms in its bulk and surface. Hence, bulk and surface distribution of heteroatoms in both carbon materials is different. A possible explanation could lie in different pyrolysis mechanism of meta- and para-substituted precursors (MABA and PABA), by which different low molecular weight compounds are eliminated during carbonization. The nitrogen chemical state was investigated through N1s core level of X-ray photoelectron spectra. The fitting of the N1s envelopes of the MA and PA materials gave rise to four and five contributions, respectively, whose binding energies (BE) and relative areas (A) are collected in Table 3.

Table 3. XPS data resulting from the deconvoluted N1s and O1s profiles of the carbons. BE= binding energy, A= relative area.

SAMPLE	**N1s**			**O1s**		
	Peak	**BE (eV)**	**A (%)**	**Peak**	**BE (eV)**	**A (%)**
MA	N1sA	398.5	37.6	O1sA	530.9	9.8
	N1sB	399.6	8.4	O1sB	532.3	61.2
	N1sC	400.8	50.2	O1sC	533.7	29.0
	N1sD	402.8	3.9			
PA	N1sA	398.6	42.81	O1sA	530.2	2.2
	N1sB	399.8	1.91	O1sB	531.6	34.5
	N1sC	400.7	46.50	O1sC	533.0	63.4
	N1sD	402.4	8.01			
	N1sE	404.2	0.78			

The aforementioned contributions were assigned to pyridinic (N1sA), pyrrolic (N1sB), quaternary nitrogen (N1sC) and oxidized nitrogen (N1sD and N1sE) [29, 36, 37]. As shown in Table 3, most of nitrogen in the surface of the carbons is in the

form of quaternary nitrogen, followed by pyridinic groups. Hence, the original amine functionalities of MABA and PABA precursors have been mainly transformed into these two nitrogen groups. Comparing both carbons, MA carbon has a higher amount of quaternary and pyrrolic groups than PA carbon, while the opposite occurs for pyridinic and oxidized nitrogen groups.

The O1s high resolution spectra of both carbons were fitted by means of three peaks assigned to the presence of C=O bonds in carbonyl and carboxylic acids (O1sA); C=O bonds in ester and anhydride groups, –OH bonds in alcohols and C–O bonds in ethers (O1sB); and non-carbonylic C–O bonds in ester and anhydride functional groups (O1sC) [36, 37]. Taking into account the relative areas of the different peaks, the most abundant oxygen groups of MA carbon are anhydrides, alcohols and ethers; in the case of PA carbon, oxygen is mainly in form of ester and anhydride groups. This could be a further evidence of the different pyrolysis mechanism followed by the meta- and para-substituted precursors that were used (MABA and PABA, respectively).

3.2. Ibuprofen release

The nitrogen adsorption isotherms and PSDs of the carbons loaded with ibuprofen, MA-IBU and PA-IBU, are shown in Figure 2. Textural data of the carbons loaded with ibuprofen as well as the amount of adsorbed ibuprofen are collected in Table 1. Comparing the N_2 adsorption-desorption isotherms for carbons before and after ibuprofen loading in Figure 2, we can observe that the N_2 isotherms of both carbons present similar shapes before and after ibuprofen loading, but the pre-adsorption of ibuprofen causes a decrease in the amount of N_2 adsorbed, indicating that ibuprofen molecules are occupying a fraction of the porosity of the carbons. This decrease in more pronounced for carbon PA, despite the fact that both carbons adsorb similar amount of ibuporofen (21.2 and 22.2 wt.% for MA and PA, respectively, see Table 1). Thus, for PA carbon pre-adsorption of ibuprofen results in a decrease of all textural parameters (see Table 1). This drop in the amount of adsorbed N_2 is also reflected in the PSDs (Figure 2D) for PA and PA-IBU. Comparing both PSDs, ibuprofen is adsorbed in all pore sizes, but especially in the mesopores

as shown by the decrease in the intensity of the peak centered at 3.37 nm. Additionally, ibuprofen adsorption produces the blockage of the micropores < 1nm, in agreement with previous studies, which observed that the adsorption of ibuprofen is hindered in marrow micorpores [38]. Thus, micropores with diameters below the size of ibuprofen (~ 1 nm) could not accommodate the ibuprofen molecules or suffer from blockage.

In the case of MA carbon the decrease in nitrogen uptake at relative pressures < 0.6 after being loaded with ibuprofen is smaller, as shown by the slight difference between the isotherms and PSDs for MA and MA-IBU samples (Figure 2A and C, respectively). The most appreciable difference between both isotherms is in an increase in the amount of nitrogen adsorbed at relative pressures higher than 0.75 in MA-IBU sample. This increase is the reason for the higher mesopore volume, V_{mp}, reported in Table 1 for MA-IBU comparing with the same sample before ibuprofen loading (MA sample). Taking into account that MA and PA carbons adsorb similar amounts of ibuprofen (21.17 and 22.22 wt.%, respectively), the above commented increase in N_2 adsorption at high relative pressures and the fact that the textural parameters for MA hardly decrease, it seems that a part of the ibuprofen is deposited outside the MA particles. These differences in the adsorption of ibuprofen shown by MA and PA carbons could be due to the different structures of both carbons. Thus, it seems that CMK-5 type structure favors the diffusion of the ibuprofen molecules to the porous network of the sample. On the other hand, ibuprofen diffusion on CMK-3 type carbons seem to be hindered and thus drug molecules are deposited in the external surface.

The experiments of ibuprofen release were accomplished at pH=2 and 7.4, simulating the pH of the stomach and small intestine, respectively. Taking into account that the pK_a of ibuprofen is 4.91 [39], the ibuprofen molecules will be in different states, either protonated at pH = 2 or deprotonated (i.e., in anionic form) at pH = 7.4. The pH_{ZPC} is considered to be an indicator of the chemical and electronic properties of the surface functionalities in carbon materials. Its value is an important parameter in the adsorption/desorption process because it quantifies

the global charge of the carbon surface as a function of the pH of the medium and determines the interaction with the charged species of the adsorbate [31, 40]. As displayed in Table 1, MA carbon exhibits a lower pH_{ZCP} value (pH_{ZCP} = 6.3) as compared to PA carbon (pH_{ZCP} = 7.2), possibly due to the presence of a lower surface concentration of nitrogen functionalities (Table 2) and a higher amount of carboxylic functional groups (Table 3). Thus, at pH=2 ibuprofen is in the protonated form and both carbons exhibit surfaces with positive charge. At pH=7.4 the deprotonated form of ibuprofen is predominant and the surfaces of the carbons present a different charge: the surface of MA is negatively charged and that of PA is practically neutral. The electrostatic interactions between adsorbate molecules and carbon surface functionalities may greatly influence the release of ibuprofen.

The kinetics of ibuprofen release at pH=2 and 7.4 are shown in Figure 4A and B, respectively. As shown in this figure, the amount of ibuprofen released after the first 15 min (the first point measured) is almost equal to the maximum ibuprofen release at each pH and remains constant until 24 hours (1440 min) in all cases. Previous studies have demonstrated that incorporation of amine groups onto the surface of MCM-41 mesoporous silica or CMK-5 type carbons decreases the rate of ibuprofen delivery, regardless of the size or shape of the particles [41]. In our case, both carbons exhibit very fast kinetics, which are of great importance in pharmaceutical applications seeking a quick release of poorly water-soluble drugs, and a sustained delivery of the drug.

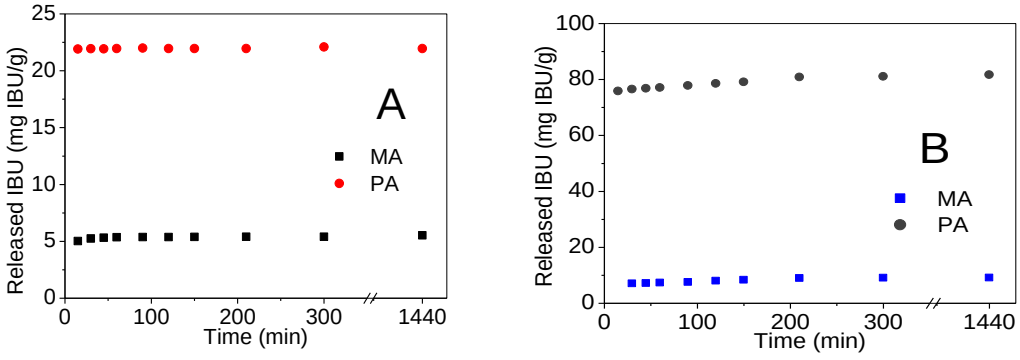

Figure 4. Ibuprofen release profiles of MA-IBU and PA-IBU samples at 37 °C and: A) pH=2 and B) pH=7.4.

At pH=2 (Figure 4A), the release profiles reach a plateau in the first 15-30 minutes. The equilibrium concentration of ibuprofen released from MA carbon is 5.5 mg IBU / g, while PA carbon releases 22 mg IBU / g at equilibrium. These concentrations are 2 and 8 wt.%, respectively, of the amount of ibuprofen adsorbed in these carbons. At pH=7.4, the ibuprofen concentration increases progressively until reach a plateau at 9.1 mg IBU / g for the MA carbon and 81.6 mg IBU / g for the PA carbon, corresponding respectively to 3.4 and 30 wt.% of the initial ibuprofen loading. Thus, it is clear that the ibuprofen release is highly dependent on the pH, especially for PA carbon. However, the ibuprofen release from MA at pH=7.4 is not much higher than at pH=2. This may be related to the existence of specific interactions with the surface functional groups and not by the global charge of the carbon surface. Thus, as said before, at pH=7.4 the surface of PA is almost neutral, while MA exhibits a more negatively charged surface. Therefore, a higher ibuprofen release would be expected in the case MA carbon. The existence of specific interactions attracting ibuprofen to the MA surface could explain the lower release of ibuprofen than for PA carbon. The main presence in the MA surface of anhydrides, ethers and esters (which can interact with the aromatic ring of ibuprofen [25, 42]) and the different proportion of N-containing functional groups (see Table 3) could explain its lower ibuprofen release efficiency as compared with PA carbon. It is noteworthy that the tubular structure of PA does not produce a restriction of the ibuprofen diffusion to the medium, but the amount of drugs released is sustained up to 24 h although very fast initial kinetics of release. Hence, this pH-dependent mode of ibuprofen release is associated with specific interaction between this drug and the carbon surface functionalities. Hence, ibuprofene is adsorbed at specific surface sites. As the pH change, the interactions between a specific group and ibuprofen molecules are modified and the latter is released. At another pH, the interaction between ibuprofen and other groups will be changed, and more ibuprofen is released. This explains that ibuprofen release is practically instantaneous as the pH changes and also why no more ibuprofen is released as time progress. Thus, one can conclude that carbon surface chemistry is the main factor controlling ibuprofen release.

4. CONCLUSIONS

Nitrogen-doped OMCs exhibiting high pore volumes and surface nitrogen contents around 7 wt.% can be successfully synthesized using MABA or PABA precursors through nanocasting techniques. For the same initial amount of precursor (1.2 g MABA, PABA/ g SBA-15), MABA gives rise to CMK-3 type carbons and PABA originates CMK-5 type ones. The CMK-3 type structure of MA consists of carbon rods separated by carbon connectors; micropores are located in the carbon bars, while mesopores are located between the bars. The tubular structure of PA is composed of mesopores, both inside the tubes and between the carbon tubes, as well as abundant micropores in the tube walls. The studied carbon materials act as good adsorbents towards ibuprofen, but PA carbon exhibits a higher efficiency as carrier for ibuprofen delivery. The delivery kinetics of the drug from both carbons is very fast and assures a sustained drug level in solution from the first 15 min to 24 h. Moreover, the surface chemistry of the carbons induces a specific response to pH, since a pH increase from 2 to 7.4 produces an enhanced delivery. The most noticeable pH-responsive delivery is found for PA carbon, since at pH=2 the equilibrium drug concentration is sustained at 8 wt.% and increases to 30 wt.% at pH=7.4. The short time to reach equilibrium concentrations, the sustained delivery of drug and the pH-induced response make the OMCs obtained from polyaramide precursors promising materials for the carriage and delivery of poorly soluble drugs.

Acknowledgments

The authors gratefully acknowledge the Spanish MINECO and FEDER (project MAT2012-34011) for financial support.

5. REFERENCES

[1] Vallet-Regi M, Balas F, Arcos D. Mesoporous materials for drug delivery. Angew Chem Int Ed 2007;46(40):7548-58.

[2] Wang S. Ordered mesoporous materials for drug delivery. Microporous Mesoporous Mat 2009;117(1–2):1-9.

[3] Zhu Y-F, Shi J-L, Li Y-S, Chen H-R, Shen W-H, Dong X-P. Storage and release of ibuprofen drug molecules in hollow mesoporous silica spheres with modified pore surface.

Microporous Mesoporous Mat 2005;85(1–2):75-81.

[4] Flanagan RJ. Guidelines for the interpretation of analytical toxicology results and unit of measurement conversion factors. Ann Clin Biochem 1998;35:261-7.

[5] Bajpai AK, Shukla SK, Bhanu S, Kankane S. Responsive polymers in controlled drug delivery. Prog Polym Sci 2008;33(11):1088-118.

[6] Peppas NA, Bures P, Leobandung W, Ichikawa H. Hydrogels in pharmaceutical formulations. Eur J Pharm Biopharm 2000;50(1):27-46.

[7] Liu J, Huang Y, Kumar A, Tan A, Jin S, Mozhi A, et al. pH-Sensitive nano-systems for drug delivery in cancer therapy. Biotechnol Adv 2014;32(4):693-710.

[8] Huxford RC, Della Rocca J, Lin W. Metal-organic frameworks as potential drug carriers. Curr Opin Chem Biol 2010;14(2):262-8.

[9] Meek ST, Greathouse JA, Allendorf MD. Metal-organic Frameworks: A rapidly growing class of versatile nanoporous materials. Adv Mater 2011;23(2):249-67.

[10] Sharpe LA, Daily AM, Horava SD, Peppas NA. Therapeutic applications of hydrogels in oral drug delivery. Expert Opin Drug Deliv 2014;11(6):901-15.

[11] Kataoka K, Harada A, Nagasaki Y. Block copolymer micelles for drug delivery: design, characterization and biological significance. Adv Drug Deliv Rev 2001;47(1):113-31.

[12] Jeong B, Bae YH, Lee DS, Kim SW. Biodegradable block copolymers as injectable drug-delivery systems. Nature 1997;388(6645):860-2.

[13] Gupta P, Vermani K, Garg S. Hydrogels: from controlled release to pH-responsive drug delivery. Drug Discov Today 2002;7(10):569-79.

[14] Chen D, Wang H. Novel pH-Sensitive Biodegradable Polymeric Drug Delivery Systems Based on Ketal Polymers. J Nanosci Nanotechnol 2014;14(1):983-9.

[15] Vallet-Regi M, Rámila A, del Real RP, Pérez-Pariente J. A New Property of MCM-41: Drug Delivery System. Chem Mater 2001;13(2):308-11.

[16] Yang P, Gai S, Lin J. Functionalized mesoporous silica materials for controlled drug delivery. Chem Soc Rev 2012;41(9):3679-98.

[17] Horcajada P, Ramila A, Perez-Pariente J, Vallet-Regi M. Influence of pore size of MCM-41 matrices on drug delivery rate. Microporous Mesoporous Mat 2004;68(1-3):105-9.

[18] Huang S, Fan Y, Cheng Z, Kong D, Yang P, Quan Z, et al. Magnetic Mesoporous Silica Spheres for Drug Targeting and Controlled Release. J Phys Chem C 2009;113(5):1775-84.

[19] Slowing II, Vivero-Escoto JL, Wu C-W, Lin VSY. Mesoporous silica nanoparticles as controlled release drug delivery and gene transfection carriers. Adv Drug Deliv Rev 2008;60(11):1278-88.

[20] Kortesuo P, Ahola M, Karlsson S, Kangasniemi I, Yli-Urpo A, Kiesvaara J. Silica xerogel as an implantable carrier for controlled drug delivery—evaluation of drug distribution and tissue effects after implantation. Biomaterials 2000;21(2):193-8.

[21] Saha D, Warren KE, Naskar AK. Soft-templated mesoporous carbons as potential materials for oral drug delivery. Carbon 2014;71(0):47-57.

[22] Niu X, Wan L, Hou Z, Wang T, Sun C, Sun J, et al. Mesoporous carbon as a novel drug carrier of fenofibrate for enhancement of the dissolution and oral bioavailability. Int J Pharm 2013;452(1-2):382-9.

[23] Karavasili C, Amanatiadou EP, Sygellou L, Giasafaki DK, Steriotis TA, Charalambopoulou GC, et al. Development of new drug delivery system based on ordered mesoporous carbons: characterisation and cytocompatibility studies. J Mat Chem B 2013;1(25):3167-74.

[24] Haydar S, Ferro-García MA, Rivera-Utrilla J, Joly JP. Adsorption of p-nitrophenol on an activated carbon with different oxidations. Carbon 2003;41(3):387-95.

[25] Franz M, Arafat HA, Pinto NG. Effect of chemical surface heterogeneity on the adsorption mechanism of dissolved aromatics on activated carbon. Carbon 2000;38(13):1807-19.

[26] Mestre AS, Pires J, Nogueira JMF, Carvalho AP. Activated carbons for the adsorption of ibuprofen. Carbon 2007;45(10):1979-88.

[27] Zhu S, Chen C, Chen Z, Liu X, Li Y, Shi Y, et al. Thermo-responsive polymer-functionalized mesoporous carbon for controlled drug release. Mater Chem Phys 2011;126(1–2):357-63.

[28] Zhao DY, Feng JL, Huo QS, Melosh N, Fredrickson GH, Chmelka BF, et al. Triblock copolymer syntheses of mesoporous silica with periodic 50 to 300 angstrom pores. Science 1998;279(5350):548-52.

[29] Sánchez-Sánchez A, Suárez-García F, Martínez-Alonso A, Tascón JMD. Aromatic polyamides as new precursors of nitrogen and oxygen-doped ordered mesoporous carbons. Carbon 2014;70(0):119-29.

[30] Neimark AV, Lin Y, Ravikovitch PI, Thommes M. Quenched solid density functional theory and pore size analysis of micro-mesoporous carbons. Carbon 2009;47(7):1617-28.

[31] Rivera-Utrilla J, Bautista-Toledo I, Ferro-García MA, Moreno-Castilla C. Activated carbon surface modifications by adsorption of bacteria and their effect on aqueous lead adsorption. J Chem Technol Biotechnol 2001;76(12):1209-15.

[32] Lu AH, Li WC, Schmidt W, Kiefer W, Schüth F. Easy synthesis of an ordered mesoporous carbon with a hexagonally packed tubular structure. Carbon 2004;42(14):2939-48.

[33] Kruk M, Jaroniec M, Kim T-W, Ryoo R. Synthesis and Characterization of Hexagonally Ordered Carbon Nanopipes. Chem Mater 2003;15(14):2815-23.

[34] Darmstadt H, Roy C, Kaliaguine S, Kim T-W, Ryoo R. Surface and Pore Structures of CMK-5 Ordered Mesoporous Carbons by Adsorption and Surface Spectroscopy. Chem Mater 2003;15(17):3300-7.

[35] Villar-Rodil S, Suárez-García F, Paredes JI, Martínez-Alonso A, Tascón JMD. Activated carbon materials of uniform porosity from polyaramid fibers. Chem Mater 2005;17(24):5893-908.

[36] Briggs D. Surface analysis of polymers by XPS and static SIMS. Cambridge: Cambridge University Press; 1998.

[37] Briggs D, Grant JT. Surface analysis by Auger and x-ray photoelectron spectroscopy. Chichester: IM Publications; 2003.

[38] Mestre AS, Pires J, Nogueira JMF, Parra JB, Carvalho AP, Ania CO. Waste-derived activated carbons for removal of ibuprofen from solution: Role of surface chemistry and pore structure. Bioresource Technol 2009;100(5):1720-6.

[39] Lindqvist N, Tuhkanen T, Kronberg L. Occurrence of acidic pharmaceuticals in raw and treated sewages and in receiving waters. Water Res 2005;39(11):2219-28.

[40] Radovic LR, Moreno-Castilla C, Rivera-Utrilla J. Carbon materials as adsorbents in aqueous solutions. In: Radovic LR, ed. Chemistry and Physics of Carbon; 2001 p. 227-405.

[41] Manzano M, Aina V, Arean CO, Balas F, Cauda V, Colilla M, et al. Studies on MCM-41 mesoporous silica for drug delivery: Effect of particle morphology and amine functionalization. Chem Eng J 2008;137(1):30-7.

[42] Mattson JA, Mark Jr HB, Malbin MD, Weber Jr WJ, Crittenden JC. Surface chemistry of

active carbon: Specific adsorption of phenols. J Colloid Interface Sci 1969;31(1):116-30.

PUBLICACIÓN 5:

'Evolution of the complex surface chemistry in mesoporous carbons obtained from polyaramide precursors'. *Appl Surf Sci 2014;299:19-28.*

Con el fin de profundizar en el conocimiento de la naturaleza química de los materiales de carbono, en este trabajo se estudia la química superficial de CMOs dopados con nitrógeno, oxígeno y fósforo usando la técnica de XPS. Se sintetizaron diferentes carbones mediante *hard-templating* utilizando una sílice mesoporosa tipo SBA-15 como plantilla, y ácido 3-aminobenzoico (MABA) como fuente simultánea de carbono, nitrógeno y oxígeno. Tras la polimerización térmica a 160 °C, el material compuesto polímero/SBA-15 se carbonizó en presencia de diferentes concentraciones de ácido fosfórico (0; 5; 50 y 150% en peso) a temperaturas entre 700 y 900 °C, tal y como se indica en el **Apartado 3.1.2.2**.

Los datos de composición superficial obtenidos por XPS indican que los CMOs sintetizados en ausencia de H_3PO_4 presentan químicas superficiales ricas en nitrógeno y oxígeno. Las concentraciones máximas de ambos heteroátomos se obtienen para las muestras carbonizadas a 700 °C, siendo del 7.1% en peso para el nitrógeno y del 5.8% en peso para el oxígeno. Además, en ausencia de ácido fosfórico, al aumentar la temperatura de carbonización disminuye el contenido de nitrógeno y no se producen variaciones significativas en el de oxígeno. El nitrógeno se encuentra mayormente en forma de nitrógeno cuaternario, y en menor proporción como nitrógeno piridínico y pirrólico. El oxígeno superficial se encuentra formando parte de una gran variedad de grupos funcionales: a 700 °C forma parte principalmente de grupos funcionales éster y anhídrido, aumentando la proporción de grupos hidroxilo a temperaturas superiores.

Cuando se carboniza el monómero MABA en presencia de H_3PO_4, la composición superficial de heteroátomos varía en función de la concentración de H_3PO_4 y de la temperatura de carbonización: cuanto mayor es la concentración de H_3PO_4 y más alta la temperatura, se obtienen mayores proporciones de nitrógeno cuaternario. Añadiendo un 5% en peso de H_3PO_4 y carbonizando a 700 °C se alcanzan

concentraciones superficiales de nitrógeno del 9.6% en peso, principalmente en forma de nitrógeno cuaternario (60%) y nitrógeno piridínico (30%). Los heteroátomos oxígeno y fósforo están relacionados estrechamente entre sí y su evolución es más compleja: una baja concentración de H_3PO_4 a 700 °C genera preferentemente ésteres, anhídridos, éteres y grupos hidroxilo, sin presencia detectable de compuestos de fósforo. Sin embargo, al añadir mayores concentraciones de H_3PO_4 aumenta la concentración de carbonilos, ácidos carboxílicos, ésteres y anhídridos, y se obtienen altas concentraciones de fósforo pentavalente tetracoordinado en forma de estructuras fosfato y polifosfato. Cuando la carbonización se lleva a cabo a 800 °C, el fósforo se reduce con el carbono de la estructura; esto hace que se generen materiales de carbono más oxidados y que disminuya la concentración superficial de fósforo. En este caso, la química superficial se compone de ésteres, anhídridos, alcoholes y éteres, así como estructuras tipo fosfato y polifosfato para concentraciones de H_3PO_4 superiores al 50% en peso. Cuando se añade H_3PO_4 en una concentración del 150% en peso, se produce un aumento de la concentración de ácidos carboxílicos y se favorece la formación de compuestos de fósforo oxidados (grupos funcionales tipo C-O-PO_3). Finalmente, las condiciones más severas que utilizan altas concentraciones de H_3PO_4 y temperaturas de carbonización de 900 °C, dan lugar a los contenidos superficiales más altos de oxígeno (10.2% en peso) y fósforo (5.4% en peso). El oxígeno se encuentra formando parte de ésteres, anhídridos, hidroxilos y éteres, mientras que el fósforo (junto con el oxígeno) se encuentra en forma de funcionalidades fosfato y polifosfato.

Applied Surface Science 299 (2014) 19–28

Contents lists available at ScienceDirect

Applied Surface Science

journal homepage: www.elsevier.com/locate/apsusc

Evolution of the complex surface chemistry in mesoporous carbons obtained from polyaramide precursors

A. Sánchez-Sánchez, F. Suárez-García *, A. Martínez-Alonso, J.M.D. Tascón

Instituto Nacional del Carbón, INCAR-CSIC, Apartado 73, 33080 Oviedo, Spain

ARTICLE INFO

Article history:
Received 5 December 2013
Received in revised form 24 January 2014
Accepted 27 January 2014
Available online 5 February 2014

Keywords:
X-ray photoelectron spectroscopy
Surface chemistry
Ordered mesoporous carbons
Phosphoric acid activation

ABSTRACT

Chemical evolution of micro/mesoporous ordered carbons containing nitrogen, oxygen and phosphorus surface functionalities was investigated by XPS. Nanocasting was selected as synthetic route: SBA-15 mesoporous silica was the solid template, 3-aminobenzoic acid was used as carbon, nitrogen and oxygen precursor, and phosphoric acid was selected to achieve doping with phosphorus. The evolution of the surface chemistry as a function of phosphoric acid concentration and carbonization temperature was studied, and carbons with a wide range of type and number of surface functional groups were identified. Thus, we show an easy way to successfully design ordered carbons exhibiting a specific surface composition by selecting certain experimental conditions.

1. Introduction

Ordered mesoporous carbons (OMCs) are considered as promising materials for many electrochemical, molecule separation, catalytic, adsorption or sensor applications [1–6]. They possess interesting properties such as uniform and tunable porous structures, large specific surface areas and pore volumes, good thermal stability and chemical inertness [2,6–10]. Their highly developed porous structure plays a key role in physical adsorption processes, but these materials normally present a poorly functionalized and hydrophobic surface which hinders all those applications requiring the interaction of specific functional groups. The surface chemical nature of OMCs can be modified by the introduction of heteroatoms like oxygen, nitrogen, phosphorus, sulfur, boron, etc. using heteroatom-containing precursors or applying post-treatments [11]. The improvement in properties of doped carbons is well known: oxygen functional groups enhance the hydrophilic character of the carbon surface, act as active sites in catalytic reactions or in selective adsorption of cationic species, provide specific sites for anchoring other functionalities and facilitate metal dispersion on the carbon surface [11–13]; nitrogen functional groups give basic character to the surface, increase the adsorption of acidic molecules, improve the catalytic activity and pseudocapacitance by means of redox reactions and enhance the anion exchange properties of carbon [14,15]; phosphorus-containing surface groups increment the resistance of the carbon material to oxidation, provide strong acidic character to the carbon surface, improve the cation exchange properties and enhance the supercapacitor energy density [16–18].

The doping process requires not only to introduce large amounts of heteroatom-containing groups on the carbon surface, but also to characterize as accurately as possible the type and density of the surface functionalities in order to adapt their chemical nature to a specific application. Significant work has been devoted to the identification of surface functional groups containing a single heteroatom like oxygen or nitrogen, and many of these studies used X ray photoelectron spectroscopy (XPS), alone or in combination with other techniques (temperature-programmed desorption, chemical titration methods, infra-red spectroscopy, etc.) [19–22]. The issue is complex and becomes quite a challenge when several heteroatoms are present on the same carbon surface. Moreover, most of the studied carbon materials are activated carbons, high surface area graphite (HSAG), carbon fibers, etc. and most of the functionalization processes are focused on oxidation or activation treatments [15,21,23,24].

In an attempt to shed light on the surface chemical characteristics of doped carbons, we report in this work the evolution of the complex surface chemistry in ordered mesoporous carbons (OMCs) by means of XPS. Thus, different OMCs were synthesized through nanocasting method, where SBA-15 was used as mesoporous silica template and 3-aminobenzoic acid (MABA) as the nitrogen, oxygen and carbon precursor. The MABA monomer was introduced inside the SBA-15 porosity, polymerized and submitted to pyrolysis in the presence of different amounts of phosphoric acid at temperatures

* Corresponding author. Tel.: +34 985 11 90 90; fax: +34 985 29 76 62.
E-mail addresses: fabian@incar.csic.es, fabian.suarez@csic.es (F. Suárez-García).

0169-4332/$ – see front matter © 2014 Elsevier B.V. All rights reserved.
http://dx.doi.org/10.1016/j.apsusc.2014.01.171

between 700 and 900 °C. Phosphoric acid was used as phosphorus source because it leads to the inclusion of phosphorus functional groups into the carbon network under certain conditions [25–28]. Identification of the nitrogen, oxygen and phosphorus surface functionalities depending on the phosphoric acid concentration and carbonization temperature was carried out in order to provide useful information for designing OMCs with specific surface chemistry.

2. Experimental

2.1. Synthesis of the silica template and the ordered mesoporous carbons

The mesoporous template (SBA-15 silica) was prepared according to the method described by Zhao et al. [29], and the OMC synthesis was performed following a solid-state thermal polymerization method. SBA-15 mesoporous silica (1 g) was placed in a rotatory evaporator and degassed under vacuum (150 °C, 2 h). After being cooled down to room temperature, a solution containing MABA (1.40 g; *Across*) and acetone (50 mL; *Sigma-Aldrich*) was added to the SBA-15 template at incipient wetness. The solvent was removed under vacuum and the resulting composite was heated in a nitrogen flow (150 mL/min; 160 °C, 1 h) in order to promote the polymerization of the MABA monomer. Then, aqueous solutions with different concentrations (5, 50 or 150 wt%, regarding the MABA content) of 85% H_3PO_4 (ACS reagent, *Sigma-Aldrich*) were added to the composite, and the final mixture was carbonized under a nitrogen flow (150 mL/min) to the target temperature (700, 800 or 900 °C). OMCs without phosphoric acid were also synthesized applying the same experimental conditions for comparison. The acid-containing carbonized composites were washed in a Soxhlet apparatus with distilled water until reaching a conductivity value <3 μS/cm, with the aim of removing the excess of phosphoric acid and the products generated by its thermal decomposition or reaction with the precursor. All the carbonized composites were finally treated with hydrofluoric acid (48%, *Fluka*) at room temperature to remove the silica template, filtered and dried in an oven (80 °C, 12 h). The resulting OMCs were named as *PACx/T*, where *x* indicates the concentration of the phosphoric acid solution used in the synthesis (not present in samples obtained without adding H_3PO_4) and *T* the carbonization temperature.

2.2. Characterization

X-ray photoelectron spectroscopy (XPS) was performed on a SPECS system, using a monochromatic Al *Kα* excitation source (1486.3 eV, 150 W) and working at a pressure of 10^{-9} mbar. The photo-excited electrons were analyzed in constant pass energy mode (pass energy of 30 eV for the survey spectra and 10 eV for the high-resolution core level spectra). Details on the determination of the resolution of the system and on the calibration of the energy scale can be found at Supporting Information.

The data processing was carried out with CasaXPS software, the background was subtracted by a Shirley line and the core level spectra envelopes were peak-fitted to a mixed Gaussian–Lorentzian convoluted function (80/20). The compositions (expressed as wt%) were determined from the survey spectra by considering the integrated areas of the main XPS peaks assigned to the different elements (C1s, N1s, O1s and P2p) and their respective sensitivity factors. Compositional calibration was carried out via the transmission function of the PHOIBOS analyzer according to the method proposed by Hemminger et al. [30] (see details at Supporting information).

Table 1
Element content of the carbon materials, expressed as weight percentage (wt%).

Sample	XPS (wt%)			
	C	N	O	P
PAC700	87.11	7.13	5.76	–
PAC5/700	82.24	9.62	8.14	–
PAC50/700	85.25	7.66	5.86	1.23
PAC150/700	86.39	5.95	6.29	1.37
PAC800	87.21	6.24	6.55	–
PAC5/800	82.04	7.38	9.95	0.63
PAC50/800	86.50	5.08	7.94	0.48
PAC150/800	85.36	5.20	8.75	0.68
PAC900	89.19	5.20	5.61	–
PAC5/900	86.12	3.78	6.86	3.24
PAC50/900	82.03	4.75	8.62	4.60
PAC150/900	80.87	3.49	10.20	5.43

3. Results and discussion

3.1. Evolution of elemental concentrations

The composition of the carbon materials expressed as weight percentage of the different elements is recorded in Table 1. As evidenced by the survey spectra, no elements other than carbon, nitrogen, oxygen and phosphorus were found (see the survey spectrum of a P-containing sample displayed in Fig. S1 at Supporting information). High nitrogen and oxygen amounts were retained in the carbon framework after carbonization of the precursor and removal of the silica template. We can also see that the heteroatom content changes depending on carbonization temperature and, in the case of samples synthesized in acidic medium, on the H_3PO_4 concentration.

As indicated by the composition data collected in Table 1 for the carbons prepared in the absence of phosphoric acid (PAC series), increasing carbonization temperatures yield materials gradually richer in carbon and poorer in nitrogen. This is consistent with the denitrogenation process of carbon material surfaces submitted to high temperatures [31]. Furthermore, in the absence of phosphoric acid, the surface oxygen remains at around 6 wt% and a remarkable oxygen release with increasing temperature is not observed; for this reason, we assume that oxygen is provided by the polyaramide precursor (MABA) and after carbonization it is attached to the surface forming thermally stable groups.

On the other hand, phosphoric acid exerts a significant influence on the surface composition since the elemental content changes considerably, as shown in Table 1 for the PAC5, PAC50 and PAC150 series at each temperature. The data for samples treated with the lowest phosphoric acid concentration in the entire temperature range (PAC5 series) show a decrease of the carbon content along with an increase in the heteroatom concentration. Thus, comparing the nitrogen percentages at each temperature for the samples synthesized in the absence of H_3PO_4 and those obtained with 5 wt% of H_3PO_4, a nitrogen increment is produced in the last case; note the significant nitrogen content of 9.62 wt% obtained for sample PAC5/700 and 7.38 wt% for PAC5/800, which are, respectively, ~2.5 and 1.1% higher than for the corresponding samples PAC700 and PAC800. Larger H_3PO_4 concentrations of 50 and 150 wt% lead to the progressive loss of nitrogen atoms, as we can see in Table 1; the carbonization temperature enhances this effect, since 1.7% nitrogen is lost at both the highest carbonization temperature and phosphoric acid concentration (sample PAC150/900) regarding the non-acidic conditions. This indicates that low phosphoric acid concentrations and a maximum temperature of 800 °C favor nitrogen retention from the MABA precursor during the carbonization process; this is mainly due to the occurrence of a different pyrolysis mechanism of the precursor and the retention of nitrogen localized in

aromatic rings of polymer fragments by the formation of phosphate/polyphosphate bridges. Under harsher conditions, the strong activating effect of the H_3PO_4 media could explain the different nitrogen concentration [32].

Nevertheless, the oxygen evolution is far more complex. Previous works of Puziy et al. [33] and Suárez-García et al. [34] studied the chemical transformations of carbons obtained from fruit stones and poly(*m*-phenylene isophthalamide) (PMIA) fibers activated with phosphoric acid, respectively. They observed that oxygen retention was greatly influenced by phosphoric acid transformations as a function of pyrolysis temperature. Thus, the evolution of both heteroatoms should be examined at once, although some differences exist among the results from these authors [33,34] and those presented here for temperatures above 800 °C, due probably to the different nature of the carbon material and the spatial restriction inside the template porosity. Sample PAC5/700 displays 8.14 wt% oxygen, i.e. 2.4% higher than for the corresponding sample synthesized without H_3PO_4 (PAC700), despite no phosphorus was detected in its surface. The samples synthesized with 50 and 150 wt% of H_3PO_4 at the same temperature (PAC50/700 and PAC150/700, respectively), exhibit oxygen and phosphorus contents that increase simultaneously with increasing phosphoric acid concentration; it is noteworthy that the surface oxygen concentrations decrease regarding PAC5/700 and have the same order of magnitude as the starting sample, PAC700. It seems that 5 wt% H_3PO_4 not only increments the retention of nitrogen but also that of oxygen, but is not high enough to incorporate any detectable phosphorus compounds to the carbon surface.

At 800 °C, 5 wt% of H_3PO_4 produces an increase in the concentrations of nitrogen and oxygen at the expense of decreasing the carbon content with respect to PAC800, and the retention of a small phosphorus concentration is produced. The evolution of the surface chemistry at this temperature can be explained taking into account some reactions of phosphorus compounds above 750–800 °C: (i) phosphates, P_2O_5 and polyphosphate compounds are formed to some extent by phosphoric acid dehydration, and P_4 (elemental phosphorus) is generated by reduction of phosphates with carbon [32,33]; (ii) the volatilization of P_4 and the removal of soluble phosphates and polyphosphates during the washing step decrease the phosphorus content at 800 °C regarding 700 °C; (iii) during the reduction reaction of phosphorus compounds into P_4, carbon is simultaneously oxidized and, therefore, the concentration of oxygen increases (according to the increase in oxygen content commented above).

Finally, the carbons prepared at 900 °C present the same trend as those obtained at 800 °C but more pronounced. The phosphates reduction becomes more significant at this temperature, and this induces the retention of higher oxygen and phosphorus concentrations in the carbon surface when increasing temperatures and H_3PO_4 concentrations are used: phosphorus functionalities with different reduction degrees are bonded to the carbon network and, additionally, the amount of surface oxygen increases due to carbon oxidation. Thus, both heteroatoms reach the largest concentration values (10.20 wt% oxygen and 5.43 wt% phosphorus) for the sample synthesized under the most severe conditions of acidic medium and carbonization temperature (PAC150/900) [33].

3.2. Evolution of surface functionalities

Deconvolution of the high-resolution core level spectra was carried out to gain information on the nature of surface functionalities present in the studied carbons.

C1s high-resolution spectra of the samples carbonized at 700, 800 and 900 °C are shown in columns A–C, respectively, of Fig. 1, and the corresponding binding energies (BE) and relative area percentages (A%) are listed in Tables S1–S3 (at Supporting Information). The complex profiles indicate the occurrence of several different carbon species. The C1s spectra were satisfactory fitted by means of six peaks, whose binding energies (BE) ranged from 284.6 to 290.9 eV. As shown in Fig. 1, the major peak was C1, assigned to C=C linkages ($\pi \rightarrow \pi^*$ transitions of delocalized bondings). C2 and C3 peaks appeared around 285.2 and 286 eV, respectively; C2 was ascribed to C=C localized bonds, and C3 to $C_{sp}{}^3$, C≡N groups, C–O bonds in ether, phenol and anhydride functional groups and C–N bonds in aromatic rings. C4 peak (~287.1 eV) was attributed to C=O and C=N bonds and the $\pi \rightarrow \pi^*$ transitions of C2 shake-up satellite. Due to the similar electronegativities of nitrogen and phosphorus attached to carbon, C=N (aromatic rings), C–NR_2/C–P and C=N bonds cannot be distinguished from each other; thus, in the case of phosphorus-containing samples, the former bonds should be considered as part of C3 and the latest ones as a contribution to C4. Moreover, the signals of the C–O–P, –C–OH and C–P=O linkages in phosphate-like structures are detected at around 286 eV, and could appear in the C3 peak. Peaks C5 and C6 were found between ~288.3 and 291.5 eV; they were assigned, respectively, to C–O bondings (in carboxylic acids) and nitrogen component (CO–N–CO like groups); and C=C linkages ($\pi \rightarrow \pi^*$ transitions in highly ordered and graphitic structures) [21,35,36].

When carbonization is carried out in the absence of H_3PO_4, the relative area of C1 increases with the rise of temperature while the relative area of C2 peak decreases, indicating that the graphitic character of the carbons has been enhanced and surface defects have been eliminated. At 900 °C, a sharp decline in C3 area is produced along with increments in C4 and C5 areas, suggesting that part of single-bonded carbon to oxygen and nitrogen is transformed into C=O, C=N and carboxylic C–O linkages.

For a given temperature, the C1s envelopes change considerably when phosphoric acid is added to the synthesis medium. Comparing with the carbons obtained without H_3PO_4 at 700 and 800 °C, addition of 5 and 50 wt% of H_3PO_4 produces almost the same effect: on the one hand, the peaks are shifted to lower BE values; on the other hand, the relative areas of C1 and C2 peaks decrease while the relative areas of the other peaks increase. This suggests that the chemical environment of carbon has changed, possibly due to the introduction of oxygen and phosphorus-containing functionalities that attract electronic density from carbon [37]. The amounts of all the heteroatoms (N, P and O) in samples prepared in the presence of H_3PO_4 increase with respect to the carbons prepared in its absence (see Table 1). At 900 °C, the trend of both the relative areas and the BE of the peaks is slightly different as compared to those for PAC900 carbon: C1 and C4 present lower relative areas while the rest of the peaks increase; the BE of C1, C2 and C3 remains unaltered but changes in the case of C4 and C5. Thus, the surface graphitic carbon and C=O/C=N groups are present in a lesser extent and, probably, the amount of phosphate-type groups has increased in the carbon surface (the maximum amount of P in the carbons is retained at this carbonization temperature, see Table 1). This will be confirmed later. It is important to note that samples synthesized with 150 wt% of H_3PO_4 do not follow the trend observed for lower concentrations at any temperature. This is because phosphoric acid induces differences in the pyrolysis mechanism of the precursor and a different type of carbon is finally obtained [38].

The N1s core level spectra of the OMCs carbonized at 700, 800 and 900 °C are collected, respectively, in column A of Figs. 2–4. The BE values and the amounts of the different nitrogen components, expressed as relative area percentage, at each temperature are given in Tables 2–4. The N1s profiles of Figs. 2–4 exhibit complex shapes, indicating that the amine and amide functional groups of the precursor have given rise to different nitrogen functionalities in the carbon material surface. Both phosphoric acid concentration and carbonization temperature induce changes in the spectral profiles, but the temperature effect is more pronounced. A satisfactory

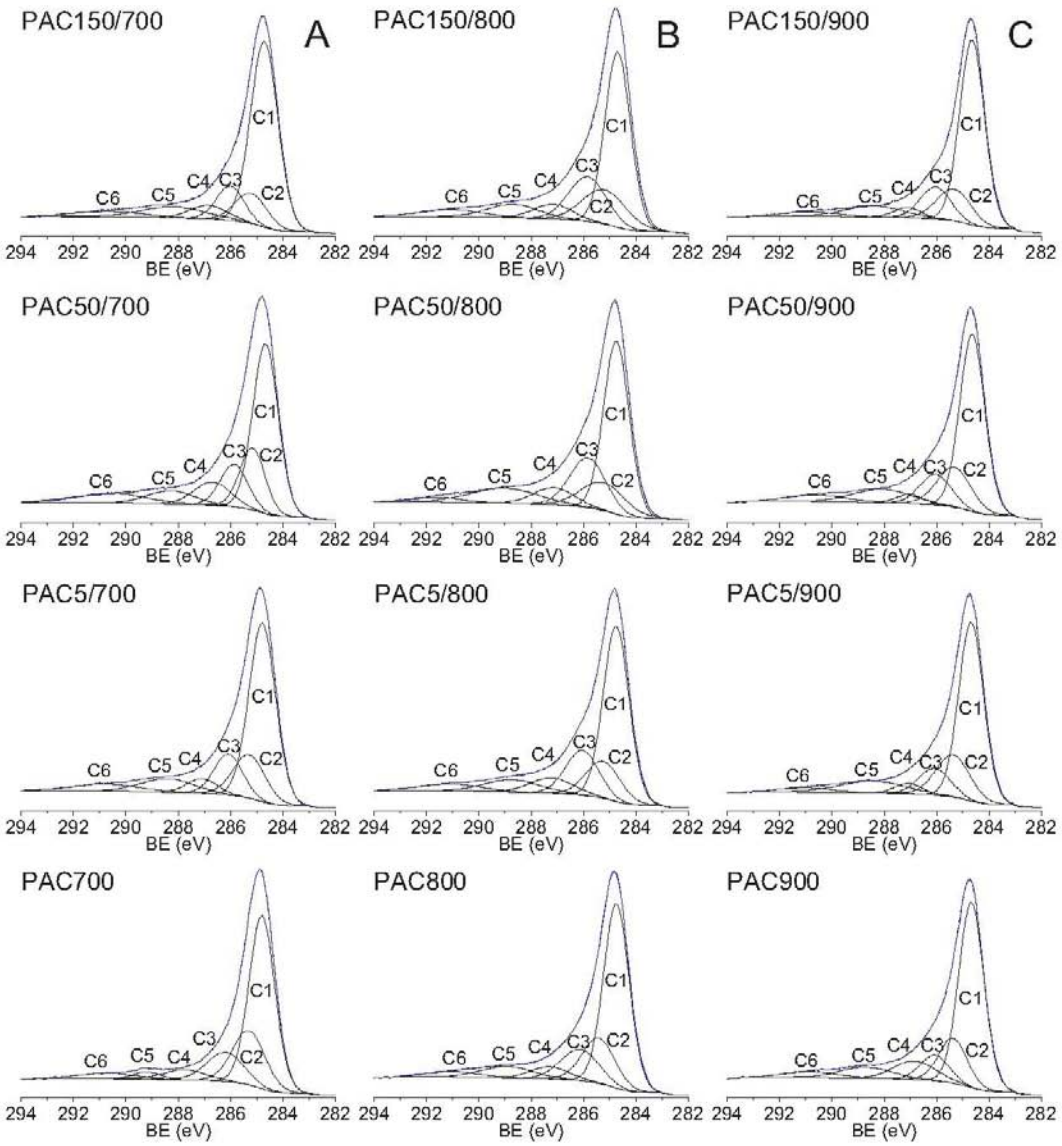

Fig. 1. C1s high-resolution spectra of the OMCs carbonized at 700 °C (column A), 800 °C (column B) and 900 °C (column C) in the presence of different phosphoric acid concentrations.

fit was obtained using five components, whose binding energies ranged from 398.3 to 404.2 eV, approximately. The most prominent peak was N3, localized at around 400.9 eV and assigned to quaternary nitrogen; peaks with lower binding energies were found at ~398.2 and 399.1 eV, named as N1 and N2 in the spectra of Figs. 2–4, respectively. The presence of N1 revealed the existence of pyridinic nitrogen and C≡N linkages, and N2 indicated that nitrogen is also in form of pyrrolic and arylnitrile functional groups. The peaks found at the higher binding energies of ~402.3 and 404.1 eV, were designated as N4 and N5, respectively, and indicated the presence of different nitrogen oxides [31]. The samples synthesized in the presence of phosphoric acid could present a contribution of N=P and N–P bonds in the N1 and N3 peaks, respectively, but the relatively small amount of phosphorus that is retained in the carbon surface makes such contribution unimportant [15].

Comparing the N1s high-resolution spectra of all samples (column A of Figs. 2–4) and the relative area percentages of each type of nitrogen (Tables 2–4), the increase of H_3PO_4 concentration has the same effect on the nitrogen functionalities as the increase in carbonization temperature, that is to say, the relative amount of quaternary nitrogen increases at the expense of decreasing the relative amounts of pyridinic and pyrrolic functionalities, as well as nitrogen oxides. In fact, the sample for which the N3 peak has the largest area is PAC150/900 (66.7%), which is around 10% higher than in the corresponding carbon PAC900 and 8% higher than in PAC150/700. This may be due to the catalytic effect of phosphoric acid, promoting dehydration, cyclization and condensation of the carbon structure by means of bond-cleavage and crosslinking reactions [16], and the preferential elimination of pyridinic and pyrrolic nitrogen at increasing temperatures. Moreover, the N1, N2 and N3

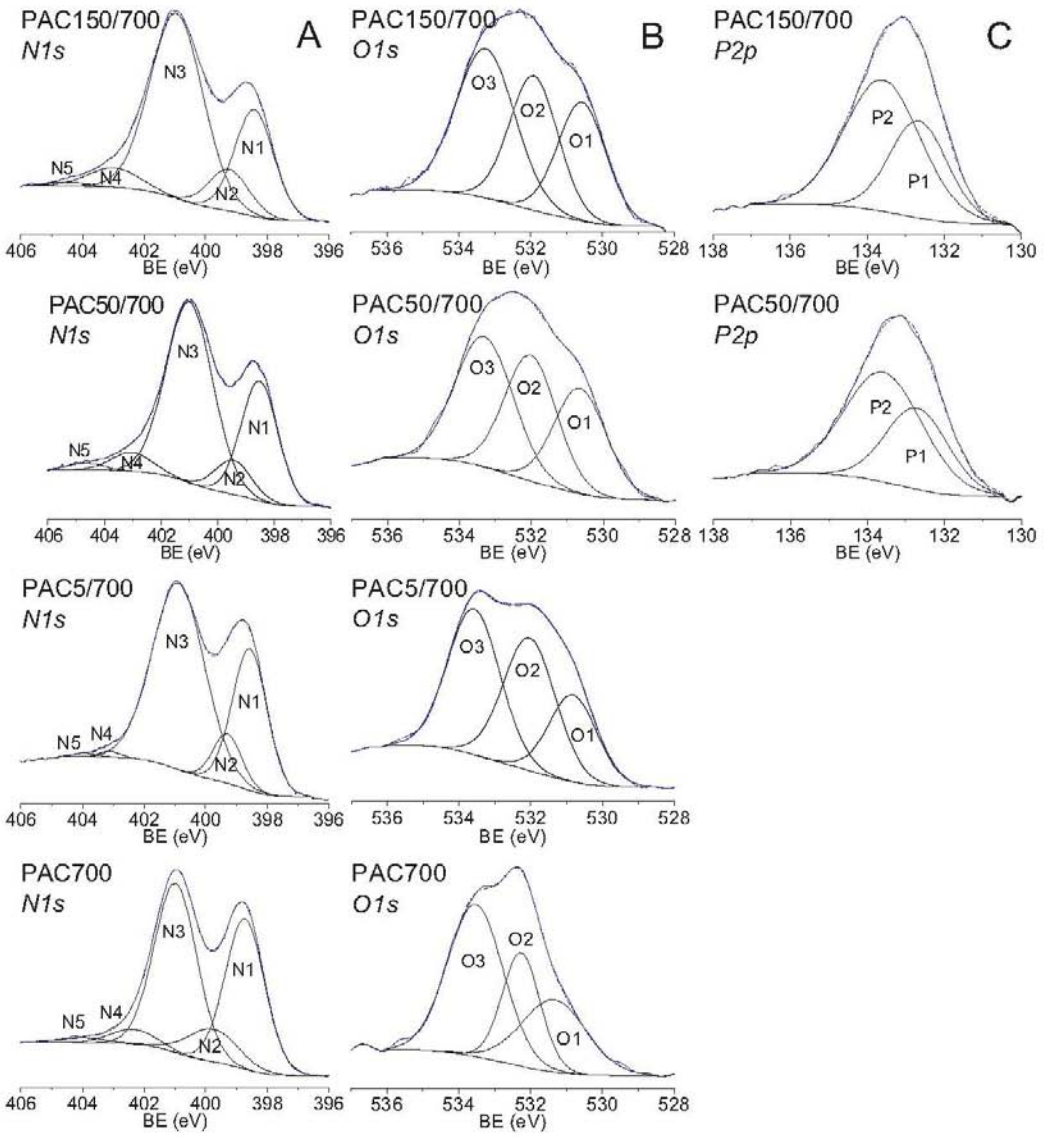

Fig. 2. Deconvoluted high-resolution spectra of the OMCs carbonized at 700 °C in the presence of different H_3PO_4 concentrations: (column A) N1s, (column B) O1s and (column C) P2p. The sample PAC5/700 (and obviously PAC700 as well) does not present phosphorus in its surface.

peaks of the samples synthesized in the presence of H_3PO_4 at 800 and 900 °C shifted to higher BEs (column A of Figs. 3 and 4 and Tables 3 and 4); the pyridinic, pyrrolic and quaternary nitrogen atoms are more electropositive in a more electronegative chemical environment that removes electron density from them and, therefore, this may indicate that a larger oxygen content is incorporated in the carbon structure as a result of increasing the H_3PO_4 concentration. This is in agreement with the elemental analysis results (Table 1) and also with the evolution of the C 1s spectra commented before. Thus, the relative areas for C3, C4, C5 and C6 increase with increasing the carbonization temperature for samples prepared in the presence of H_3PO_4, indicating the introduction of oxygen and phosphorus-containing functionalities, as was explained previously.

The O1s high-resolution spectra of the samples carbonized at 700, 800 and 900 °C are displayed in column B of Figs. 2–4, respectively, and the corresponding binding energies and relative amounts of the different oxygen components are shown in Tables 2–4. A satisfactory fit was achieved by means of three components: C=O bonds in carbonyl and carboxylic acids (peak O1, 530.5 eV); C=O bonds in ester and anhydride groups, –OH bonds in alcohols and C–O bonds in ethers (peak O2, 532.0 eV); and non-carbonylic C–O bonds in ester and anhydride functional groups (peak O3, 533.3 eV). Regarding the carbons containing phosphorus, we must take into account the contributions from non-bridging oxygen in phosphates/polyphosphates (C–O–PO_3 groups) and C–O–P species to the O1 peak, located at ~531 eV, and the bridging oxygen of phosphates/polyphosphates (C–O–PO_3 groups)

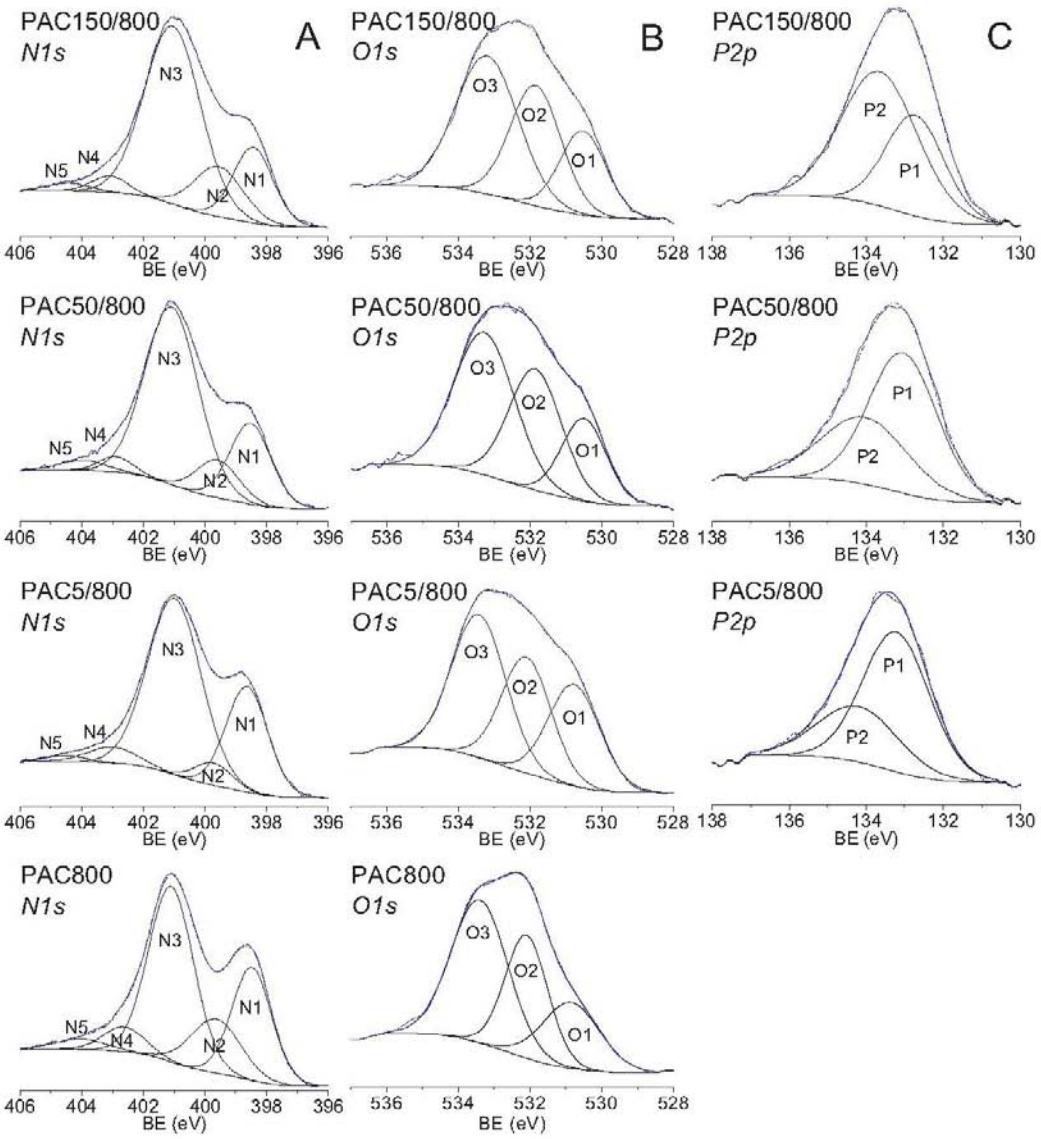

Fig. 3. Deconvoluted high-resolution spectra of the OMCs carbonized at 800 °C in the presence of different H_3PO_4 concentrations: (column A) N1s, (column B) O1s and (column C) P2p.

to the O2 peak at 532.0 eV [36]. Comparing the evolution of the O 1s profiles, we observe in Tables 2 and 4 that the O2/O1 relative area ratio increases with increasing H_3PO_4 concentration when the carbonization is carried out at 700 and 900 °C; this is related to the increase in amount of C–PO_3 and C–O–P bonds, indicating the formation of phosphates/polyphosphates in the carbon surface. On the contrary, the samples carbonized at 800 °C (Table 3) undergo the preferential formation of C–O–P linkages as well as oxidized species like ester and anhydride groups.

As expected, the results presented so far agree with those obtained from the P2p high-resolution spectra. The OMCs synthesized in the presence of H_3PO_4 present P2p high-resolution profiles that could be deconvoluted into two peaks. The deconvolution of the P2p high-resolution spectra was also done taking into account that both phosphorous signals (P1 and P2) are constituted by two doublet peaks, separated from each other by 0.84 eV and with a $P2p_{1/2}/P2p_{3/2}$ area ratio of 0.5; no additional information was found, so only two singlet peaks (P1 and P2) were taken into account to make the discussion simpler.

In the case of the samples PAC50/700 and PAC150/700, with phosphorus contents of 1.23 and 1.37 wt%, respectively, the spectra consist of a minor component at ~132.7 eV, assigned to reduced phosphorus compounds such as C_3–PO groups, and a main component at ~133.6 eV attributed to pentavalent tetracoordinated phosphorus (PO_4) in phosphate-like structures (C–PO_3, C_2–PO_2 and C–O–PO_3 groups). Thus, the preferential formation at 700 °C of polyphosphate-type groups is confirmed [16].

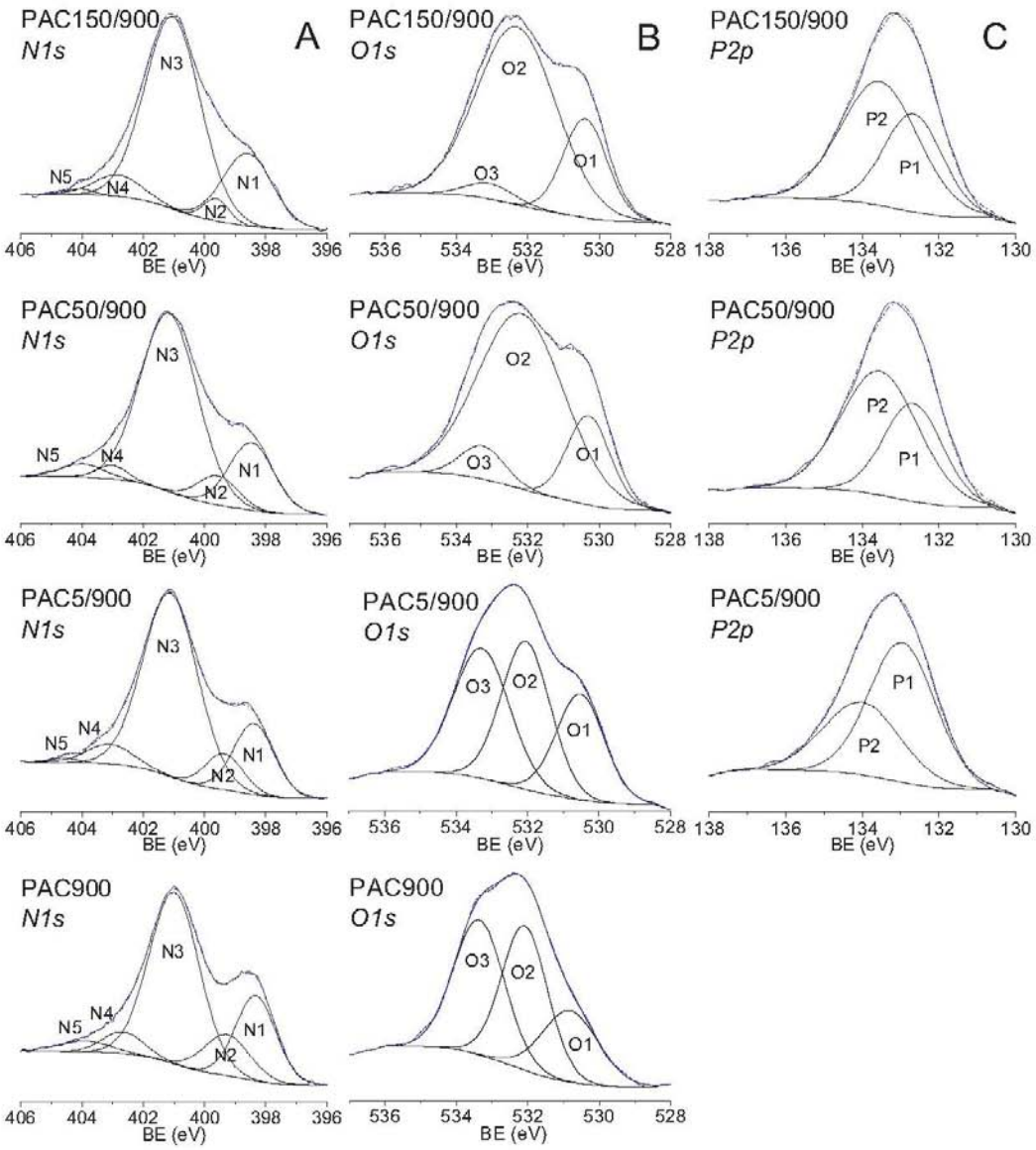

Fig. 4. Deconvoluted high-resolution spectra of the OMCs carbonized at 900 °C in the presence of different H_3PO_4 concentrations: (column A) N1s, (column B) O1s and (column C) P2p.

As previously mentioned, the total surface phosphorus content in the samples carbonized at 800 °C (~0.6 wt%) is the lowest one; moreover, the P1 and P2 peaks of the corresponding P2p deconvoluted spectra (column C of Figs. 2–4 and Table 3) are shifted to higher BE values, indicating the permanence of phosphorus species bound to a more oxidized carbon surface. Thus, H_3PO_4 concentrations up to 50 wt% (PAC5/800 and PAC50/800 samples) yield a major component at ~133.4 eV (P1) of phosphate-like structures and a minor component at ~134 eV (P2) assigned to C–O–PO_3 groups, including $(CO)_3PO$, $(CO)_2PO_2$ and $(CO)PO_3$ species. When 150 wt% H_3PO_4 is added into the synthesis medium, the surface primarily contains more oxidized C–O–PO_3 compounds (main component P2) as the redox reactions and phosphorus incorporation take place to a greater extent.

Finally, the samples containing the highest amounts of phosphorus are obtained at 900 °C; the BE values of the P1 and P2 peaks for the samples obtained at 700 and 900 °C are very similar to each other (see column C of Figs. 2 and 4, and Tables 2 and 4, respectively): in both cases, P1 appears at ~132.7 eV and P2 at ~133.7 eV. A decrease of BE for P1 and P2 at 900 °C regarding 800 °C indicates that phosphoric acid undergoes dehydration and condensation into polyphosphates, and phosphorus interacts to a greater extent with the aromatic carbon surface [36]. As we can see in Table 4, the amount of different phosphorus functionalities is strongly dependent on H_3PO_4 concentration: a low concentration (5 wt%) mainly yields more reduced phosphorus compounds (C_3–PO type), whereas higher concentrations primarily generate phosphate and polyphosphate groups (C–PO_3, C_2–PO_2 and C–O–PO_3).

Table 2
Binding energies (eV) and relative area percentages of the N1s, O1s and P2p components in OMCs carbonized at 700 °C with different concentrations of H_3PO_4.

Sample		N1	N2	N3	N4	N5	O1	O2	O3	P1	P2
PAC700	BE	398.73 ± 0.15	399.76 ± 0.16	400.98 ± 0.15	402.35 ± 0.61	403.99 ± 0.95	531.34 ± 0.66	532.26 ± 0.21	533.53 ± 0.31	–	–
	A%	37.87 ± 0.22	10.47 ± 0.24	45.98 ± 0.27	4.23 ± 0.28	1.45 ± 0.16	26.88 ± 1.76	24.14 ± 1.24	48.38 ± 1.34	–	–
PAC5/700	BE	398.57 ± 0.23	399.30 ± 0.31	400.88 ± 0.11	403.13 ± 0.44	403.92 ± 0.35	530.82 ± 0.39	532.03 ± 0.33	533.58 ± 0.26	–	–
	A%	30.23 ± 0.26	8.68 ± 0.26	59.82 ± 0.13	0.72 ± 0.06	0.55 ± 0.09	22.29 ± 0.77	37.02 ± 0.91	40.68 ± 0.60	–	–
PAC50/700	BE	398.53 ± 0.25	399.45 ± 0.49	401.00 ± 0.18	403.04 ± 0.44	404.64 ± 0.99	530.64 ± 0.38	532.02 ± 0.35	533.31 ± 0.43	132.71 ± 0.31	133.59 ± 0.39
	A%	29.30 ± 0.26	8.32 ± 0.26	55.77 ± 0.26	5.04 ± 0.20	1.57 ± 0.11	28.06 ± 0.84	33.43 ± 1.24	38.51 ± 1.05	37.19 ± 1.78	62.81 ± 1.78
PAC150/700	BE	398.42 ± 0.19	399.25 ± 0.35	400.95 ± 0.25	402.99 ± 0.68	404.48 ± 0.99	530.57 ± 0.31	531.91 ± 0.31	533.25 ± 0.39	132.65 ± 0.25	133.58 ± 0.33
	A%	24.86 ± 0.21	9.90 ± 0.27	58.61 ± 0.27	5.86 ± 0.28	0.78 ± 0.24	27.28 ± 0.64	31.02 ± 0.99	41.70 ± 0.85	35.91 ± 1.39	64.09 ± 1.40

Table 3
Binding energies (eV) and relative area percentages of the N1s, O1s and P2p components in OMCs carbonized at 800 °C with different concentrations of H_3PO_4.

Sample		N1	N2	N3	N4	N5	O1	O2	O3	P1	P2
PAC800	BE	398.48 ± 0.27	399.64 ± 0.58	401.10 ± 0.24	402.63 ± 0.98	404.04 ± 0.68	530.85 ± 0.52	532.10 ± 0.28	533.40 ± 0.37	–	–
	A%	27.04 ± 0.40	16.06 ± 0.41	47.60 ± 0.45	6.19 ± 0.30	3.10 ± 0.29	22.05 ± 1.19	30.76 ± 1.54	47.19 ± 1.23	–	–
PAC5/800	BE	398.64 ± 0.22	399.74 ± 0.44	400.98 ± 0.23	403.01 ± 0.48	404.52 ± 1.31	530.77 ± 0.30	532.10 ± 0.34	533.42 ± 0.30	133.22 ± 0.33	134.21 ± 0.61
	A%	28.02 ± 0.21	5.30 ± 0.26	60.32 ± 0.28	4.92 ± 0.21	1.45 ± 0.15	28.06 ± 0.54	30.75 ± 0.76	41.19 ± 0.63	67.41 ± 2.77	32.59 ± 2.75
PAC50/800	BE	398.52 ± 0.26	399.59 ± 0.37	401.08 ± 0.18	402.89 ± 0.68	403.96 ± 0.68	530.50 ± 0.29	531.86 ± 0.32	533.28 ± 0.36	133.04 ± 0.26	134.04 ± 0.46
	A%	21.63 ± 0.24	10.37 ± 0.30	61.67 ± 0.28	3.33 ± 0.21	2.99 ± 0.21	19.83 ± 0.54	34.14 ± 0.88	46.03 ± 0.76	62.33 ± 1.71	37.68 ± 1.69
PAC150/800	BE	398.43 ± 0.22	399.56 ± 0.41	401.05 ± 0.24	403.10 ± 0.40	404.44 ± 0.89	530.52 ± 0.30	531.84 ± 0.25	533.19 ± 0.34	132.72 ± 0.27	133.65 ± 0.37
	A%	18.45 ± 0.22	15.01 ± 0.31	61.09 ± 0.32	3.54 ± 0.20	1.91 ± 0.12	20.81 ± 0.46	32.97 ± 0.72	46.23 ± 0.63	36.35 ± 1.65	63.65 ± 1.67

Table 4
Binding energies (eV) and relative area percentages of the N1s, O1s and P2p components in OMCs carbonized at 900 °C with different concentrations of H_3PO_4.

Sample		N1	N2	N3	N4	N5	O1	O2	O3	P1	P2
PAC900	BE	398.32 ± 0.26	399.27 ± 0.40	400.98 ± 0.15	402.66 ± 0.39	403.90 ± 1.03	530.82 ± 0.46	532.09 ± 0.24	533.37 ± 0.32	–	–
	A%	22.29 ± 0.22	12.15 ± 0.21	56.41 ± 0.21	5.62 ± 0.20	3.33 ± 0.15	22.87 ± 0.66	37.91 ± 0.88	39.22 ± 0.68	–	–
PAC5/900	BE	398.38 ± 0.35	399.35 ± 0.43	401.11 ± 0.16	403.08 ± 0.45	404.59 ± 1.79	530.53 ± 0.26	532.05 ± 0.30	533.29 ± 0.41	132.96 ± 0.22	134.01 ± 0.31
	A%	18.84 ± 0.34	8.75 ± 0.36	65.81 ± 0.30	5.86 ± 0.27	0.74 ± 0.19	25.94 ± 0.47	36.82 ± 0.90	37.24 ± 0.82	62.32 ± 0.87	37.68 ± 0.87
PAC50/900	BE	398.47 ± 0.35	399.58 ± 0.65	401.16 ± 0.21	403.02 ± 0.93	403.99 ± 1.22	530.30 ± 0.15	532.18 ± 0.33	533.27 ± 0.28	132.69 ± 0.17	133.65 ± 0.22
	A%	19.61 ± 0.36	7.56 ± 0.42	66.25 ± 0.42	3.81 ± 0.30	2.76 ± 0.30	18.69 ± 0.35	74.24 ± 0.69	7.07 ± 0.63	38.42 ± 0.58	61.58 ± 0.59
PAC150/900	BE	398.59 ± 0.34	399.62 ± 0.31	401.04 ± 0.19	402.82 ± 0.71	404.06 ± 1.76	530.39 ± 0.14	532.32 ± 0.29	533.07 ± 0.42	132.67 ± 0.19	133.55 ± 0.23
	A%	22.56 ± 0.35	3.43 ± 0.42	66.72 ± 0.47	6.35 ± 0.38	0.94 ± 0.32	22.56 ± 0.29	73.51 ± 0.55	3.93 ± 0.51	37.51 ± 0.58	62.49 ± 0.57

4. Conclusions

MABA can be used as feedstock to successfully obtain OMCs enriched in nitrogen and oxygen (7.1 wt% N and 5.8 wt% O at 700 °C). In the absence of phosphoric acid, an increase in carbonization temperature leads to a decrease in nitrogen content while the surface oxygen content remains unmodified. Nitrogen is mainly in the quaternary form, and as pyridinic and pyrrolic nitrogen to a lesser extent. Oxygen forms part of a wide variety of surface functional groups: at 700 °C a majority of esters and anhydrides is obtained, and an increment in the content of hydroxyl groups is observed at higher temperatures.

When MABA is carbonized in the presence of phosphoric acid, the surface heteroatom composition can be sharply changed by varying the H_3PO_4 concentration and the carbonization temperature: the higher the phosphoric acid concentration and carbonization temperature, the higher the proportions of quaternary nitrogen that are obtained; high surface nitrogen concentrations of 9.6 wt% are reached using 5 wt% H_3PO_4 at 700 °C, being primarily in form of quaternary (60%) and pyridinic (30%) nitrogen; oxygen and phosphorus are closely correlated with each other, and their evolution is more complex: a low H_3PO_4 concentration at 700 °C produces a high number of ester, anhydride, ether and hydroxyl groups whereas no phosphorus compounds are detected; higher H_3PO_4 concentrations rise the amount of carbonyls, carboxylic acids, esters and anhydrides, as well as the amount of pentavalent tetracoordinated phosphorus in phosphate and polyphosphate structures. At 800 °C, phosphorus reduction with carbon leads to more oxidized carbon networks and lower phosphorus concentrations; in this case, the surface chemistry consists of esters, anhydrides, alcohols and ethers, as well as phosphate/polyphosphate like structures (PO_4 groups) for H_3PO_4 concentrations up to 50 wt%; the use of 150 wt% H_3PO_4 increases the amount of carboxylic acids and favors the preferential formation of oxidized phosphorus compounds (C–O–PO_3 type groups). Finally, the most severe conditions of both high phosphoric acid concentrations and carbonization temperatures give rise to the largest surface contents of oxygen (10.2 wt%) and phosphorus (5.4 wt%); oxygen is in form of ester, anhydride, hydroxyl and ether functional groups, while phosphorus (together with oxygen) is in form of phosphate and polyphosphate functionalities.

Acknowledgment

The authors gratefully acknowledge the Spanish Ministerio de Economía y Competitividad and FEDER (project MAT2012-34011) for financial support.

Appendix A. Supplementary data

Supplementary data associated with this article can be found, in the online version, at http://dx.doi.org/10.1016/j.apsusc.2014.01.171.

References

[1] B. Yuan, X. Wu, Y. Chen, J. Huang, H. Luo, S. Deng, Adsorption of CO(2), CH(4), and N(2) on ordered mesoporous carbon: approach for greenhouse gases capture and biogas upgrading, Environ. Sci. Technol. 47 (2013) 5474–5480.
[2] A. Walcarius, Mesoporous materials and electrochemistry, Chem. Soc. Rev. 42 (2013) 4098–4140.
[3] D. Saha, S. Deng, Hydrogen adsorption on ordered mesoporous carbons doped with Pd, Pt, Ni, and Ru, Langmuir 25 (2009) 12550–12560.
[4] M. Park, S.S. Park, M. Selvaraj, D. Zhao, C.-S. Ha, Hydrophobic mesoporous materials for immobilization of enzymes, Microporous Mesoporous Mater. 124 (2009) 76–83.

[5] M. Sevilla, P. Valle-Vigón, P. Tartaj, A.B. Fuertes, Magnetically separable bimodal mesoporous carbons with a large capacity for the immobilization of biomolecules, Carbon 47 (2009) 2519–2527.
[6] H. Nishihara, T. Kyotani, Templated nanocarbons for energy storage, Adv. Mater. 24 (2012) 4473–4498.
[7] H.F. Yang, D.Y. Zhao, Synthesis of replica mesostructures by the nanocasting strategy, J. Mater. Chem. 15 (2005) 1217–1231.
[8] A.H. Lu, F. Schüth, Nanocasting: a versatile strategy for creating nanostructured porous materials, Adv. Mater. 18 (2006) 1793–1805.
[9] C.D. Liang, Z.J. Li, S. Dai, Mesoporous carbon materials: synthesis and modification, Angew. Chem. Int. Ed. 47 (2008) 3696–3717.
[10] R. Ryoo, S.H. Joo, M. Kruk, M. Jaroniec, Ordered mesoporous carbons, Adv. Mater. 13 (2001) 677–681.
[11] A. Stein, Z.Y. Wang, M.A. Fierke, Functionalization of porous carbon materials with designed pore architecture, Adv. Mater. 21 (2009) 265–293.
[12] T.J. Bandosz, J. Jagiełło, J.A. Schwarz, A. Krzyzanowski, Effect of surface chemistry on sorption of water and methanol on activated carbons, Langmuir 12 (1996) 6480–6486.
[13] J.-w. Lang, X.-b. Yan, W.-w. Liu, R.-t. Wang, Q.-j. Xue, Influence of nitric acid modification of ordered mesoporous carbon materials on their capacitive performances in different aqueous electrolytes, J. Power Sources 204 (2012) 220–229.
[14] S. Matzner, H.P. Boehm, Influence of nitrogen doping on the adsorption and reduction of nitric oxide by activated carbons, Carbon 36 (1998) 1697–1703.
[15] D. Hulicova-Jurcakova, M. Seredych, G.Q. Lu, N.K.A.C. Kodiweera, P.E. Stallworth, S. Greenbaum, T.J. Bandosz, Effect of surface phosphorus functionalities of activated carbons containing oxygen and nitrogen on electrochemical capacitance, Carbon 47 (2009) 1576–1584.
[16] J.M. Rosas, R. Ruiz-Rosas, J. Rodríguez-Mirasol, T. Cordero, Kinetic study of the oxidation resistance of phosphorus-containing activated carbons, Carbon 50 (2012) 1523–1537.
[17] A.M. Puziy, O.I. Poddubnaya, A. Martínez-Alonso, F. Suárez-García, J.M.D. Tascón, Synthetic carbons activated with phosphoric acid III. Carbons prepared in air, Carbon 41 (2003) 1181–1191.
[18] D. Hulicova-Jurcakova, A.M. Puziy, O.I. Poddubnaya, F. Suárez-García, J.M.D. Tascón, G.Q. Lu, Highly stable performance of supercapacitors from phosphorus-enriched carbons, J. Am. Chem. Soc. 131 (2009) 5026–5027.
[19] J. Wang, I. Senkovska, M. Oschatz, M.R. Lohe, L. Borchardt, A. Heerwig, Q. Liu, S. Kaskel, Imine-linked polymer-derived nitrogen-doped microporous carbons with excellent CO_2 capture properties, ACS Appl. Mater. Interfaces 5 (2013) 3160–3167.
[20] H.F. Gorgulho, F. Goncalves, M.F.R. Pereira, J.L. Figueiredo, Synthesis and characterization of nitrogen-doped carbon xerogels, Carbon 47 (2009) 2032–2039.
[21] A.B. Dongil, B. Bachiller-Baeza, A. Guerrero-Ruiz, I. Rodriguez-Ramos, A. Martinez-Alonso, J.M. Tascon, Surface chemical modifications induced on high surface area graphite and carbon nanofibers using different oxidation and functionalization treatments, J. Colloid Interface Sci. 355 (2011) 179–189.
[22] A.M. Puziy, O.I. Poddubnaya, A.M. Ziatdinov, On the chemical structure of phosphorus compounds in phosphoric acid-activated carbon, Appl. Surf. Sci. 252 (2006) 8036–8038.
[23] K. Xia, Q. Gao, C. Wu, S. Song, M. Ruan, Activation, characterization and hydrogen storage properties of the mesoporous carbon CMK-3, Carbon 45 (2007) 1989–1996.
[24] B. Xiao, J.P. Boudou, K.M. Thomas, Reactions of nitrogen and oxygen surface groups in nanoporous carbons under inert and reducing atmospheres, Langmuir 21 (2005) 3400–3409.
[25] H. Benaddi, T.J. Bandosz, J. Jagiello, J.A. Schwarz, J.N. Rouzaud, D. Legras, F. Béguin, Surface functionality and porosity of activated carbons obtained from chemical activation of wood, Carbon 38 (2000) 669–674.
[26] F. Suárez-García, A. Martínez-Alonso, J.M.D. Tascón, Nomex polyaramid as a precursor for activated carbon fibres by phosphoric acid activation. Temperature and time effects, Microporous Mesoporous Mater. 75 (2004) 73–80.
[27] R. Fu, L. Liu, W. Huang, P. Sun, Studies on the structure of activated carbon fibers activated by phosphoric acid, J. Appl. Polym. Sci. 87 (2003) 2253–2261.
[28] A.M. Puziy, O.I. Poddubnaya, A. Martínez-Alonso, F. Suárez-García, J.M.D. Tascón, Synthetic carbons activated with phosphoric acid: I. Surface chemistry and ion binding properties, Carbon 40 (2002) 1493–1505.
[29] D.Y. Zhao, J.L. Feng, Q.S. Huo, N. Melosh, G.H. Fredrickson, B.F. Chmelka, G.D. Stucky, Triblock copolymer syntheses of mesoporous silica with periodic 50 to 300 angstrom pores, Science 279 (1998) 548–552.
[30] C.S. Hemminger, T.A. Land, A. Christie, J.C. Hemminger, An empirical electron spectrometer transmission function for applications in quantitative XPS, Surf. Interface Anal. 15 (1990) 323–327.
[31] W. Kim, M.Y. Kang, J.B. Joo, N.D. Kim, I.K. Song, P. Kim, J.R. Yoon, J. Yi, Preparation of ordered mesoporous carbon nanopipes with controlled nitrogen species for application in electrical double-layer capacitors, J. Power Sources 195 (2010) 2125–2129.
[32] S. Villar-Rodil, F. Suárez-García, J.I. Paredes, A. Martínez-Alonso, J.M.D. Tascón, Activated carbon materials of uniform porosity from polyaramid fibers, Chem. Mater. 17 (2005) 5893–5908.
[33] A.M. Puziy, O.I. Poddubnaya, A. Martínez-Alonso, F. Suárez-García, J.M.D. Tascón, Surface chemistry of phosphorus-containing carbons of lignocellulosic origin, Carbon 43 (2005) 2857–2868.
[34] F. Suárez-García, S. Villar-Rodil, C.G. Blanco, A. Martínez-Alonso, J.M.D. Tascón, Effect of phosphoric acid on chemical transformations during Nomex pyrolysis, Chem. Mater. 16 (2004) 2639–2647.
[35] A. Sánchez-Sánchez, F. Suárez-García, A. Martínez-Alonso, J.M.D. Tascón, Surface modification of nanocast ordered mesoporous carbons through a wet oxidation method, Carbon 62 (2013) 193–203.
[36] A.M. Puziy, O.I. Poddubnaya, R.P. Socha, J. Gurgul, M. Wisniewski, XPS and NMR studies of phosphoric acid activated carbons, Carbon 46 (2008) 2113–2123.
[37] D. Briggs, Surface Analysis of Polymers by XPS and Static SIMS, Cambridge University Press, Cambridge, 1998.
[38] F. Suárez-García, A. Martínez-Alonso, J.M.D. Tascón, Activated carbon fibers from Nomex by chemical activation with phosphoric acid, Carbon 42 (2004) 1419–1426.

Evolution of the complex surface chemistry in mesoporous carbons obtained from polyaramide precursors

A. Sánchez-Sánchez, F. Suárez-García, A. Martínez-Alonso and J. M. D. Tascón.

Instituto Nacional del Carbón, INCAR-CSIC, Apartado 73, 33080 Oviedo, Spain

Supporting information

1. Experimental details of the XPS analysis.

1.1. Calibration of the BE scales

Metallic samples of pure copper, silver and gold were used in order to calibrate the BE scales; the photoelectron lines were measured near the extremes of the working BE scale: Au 4f7/2 (83.98 ±0.02 eV), Cu 2p3/2 (932.67±0.02) and Ag 3d5/2 (368.26±0.02), being the BE difference between Au 4f7/2 and Cu 2p3/2 peaks of 848.66 ±0.03 eV [1]. The linearity of BE scale was checked by measuring the Ag reference lines, following the procedures of the instrument manufacturer.

1.2. Determination of the resolution of the system

The resolution was determined by using the full width at half-maximum intensity (FWHM) of the Ag 3d5/2 peak from sputter cleaned silver. The independence of the peak position on pass energy was checked by running the spectra of sputter-cleaned silver at different pass energies; the peak positions of the resulting spectra differ for each other by less than 100 meV.

1.3. Measurement of XPS spectra

First, we obtained a general spectrum over the entire BE range between 0-1350 eV, by using a constant analyzer transmission energy of 50 eV and an energy step of 0.5 eV. Since no peaks were detected at binding energies greater than 600 eV and in order to achieve better resolution, general spectra for all samples were obtained up to 600 eV using pass energy of 30 eV, 0.5 eV per step and 20 scans. Finally, the high-resolution spectra were measured in our case by using 10 eV of pass energy, with energy per step of 0.1 eV.

1.4. Composition calibration

The compositional calibration was carried out via the transmission function of the PHOIBOS analyzer according to the method proposed by Hemminger et al. [2]. Thus, the intensity of the Ag 3d5/2 peak was measured for pass energy values between 3 and 80 eV; the resulting data were plotted for different lens modes of the PHOIBOS 100 MCD-5 analyzer, and the experimental data were finally fitted according to this plot. The exact set of parameters and function form was determined from the entry in the CasaXPS.trf file. The transmission curve was exported in the VAMAS block as a second variable according to Speclab software.

2. Figures

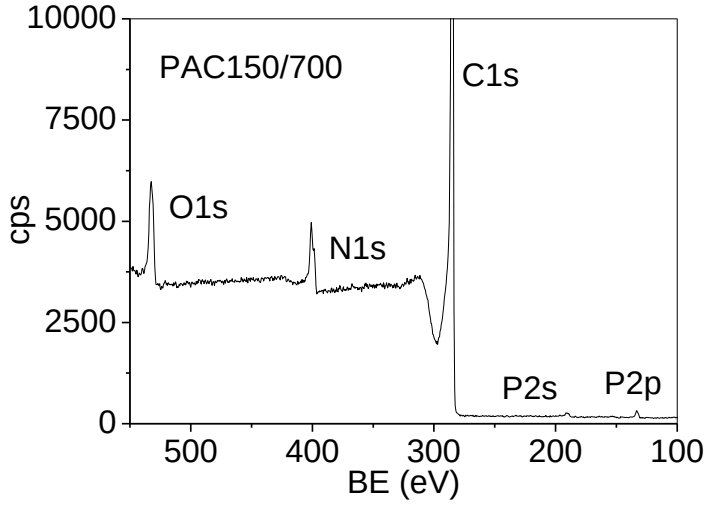

Figure S1. Survey spectrum of a P-containing representative sample (PAC150/700).

3. Tables

Table S1. Binding energies (eV) and relative area percentages of the C1s high-resolution spectra components corresponding to the OMCs carbonized at 700 ºC.

SAMPLE		**C1**	**C2**	**C3**	**C4**	**C5**	**C6**
PAC700	BE	284.80 ± 0.13	285.30 ± 0.13	286.20 ± 0.13	287.76 ± 0.48	289.20 ± 0.25	290.71 ± 0.34
	A%	54.56 ± 0.18	21.35 ± 0.17	12.95 ± 0.20	4.98 ± 0.18	2.35 ± 0.12	3.80 ± 0.09
PAC5/700	BE	284.79 ± 0.17	285.29 ± 0.17	286.09 ± 0.17	287.09 ± 0.40	288.43 ± 0.39	290.82 ± 0.39
	A%	53.88 ± 0.18	15.37 ± 0.17	12.89 ± 0.17	4.75 ± 0.15	7.96 ± 0.13	5.14 ± 0.09
PAC50/700	BE	284.66 ± 0.16	285.16 ± 0.16	285.86 ± 0.16	286.69 ± 0.36	288.29 ± 0.43	290.54 ± 0.41
	A%	47.33 ± 0.18	17.01 ± 0.15	12.72 ± 0.16	9.19 ± 0.14	6.69 ± 0.11	7.05 ± 0.10
PAC150/700	BE	284.71 ± 0.11	285.21 ± 0.11	286.01 ± 0.11	286.85 ± 0.32	288.21 ± 0.11	290.66 ± 0.31
	A%	59.55 ± 0.11	11.05 ± 0.09	10.89 ± 0.13	5.82 ± 0.09	8.28 ± 0.09	4.41 ± 0.07

Table S2. Binding energies (eV) and relative area percentages of the C1s high-resolution spectra components corresponding to the OMCs carbonized at 800 ºC.

SAMPLE		**C1**	**C2**	**C3**	**C4**	**C5**	**C6**
PAC800	BE	284.74 ± 0.13	285.43 ± 0.34	286.14 ± 0.13	287.29 ± 0.39	288.94 ± 0.42	290.98 ± 0.38
	A%	54.52 ± 0.25	16.93 ± 0.24	13.51 ± 0.20	5.27 ± 0.18	6.59 ± 0.18	3.19 ± 0.10
PAC5/800	BE	284.75 ± 0.10	285.25 ± 0.10	286.05 ± 0.10	287.21 ± 0.39	288.75 ± 0.43	291.10 ± 0.42
	A%	50.21 ± 0.13	13.90 ± 0.17	16.16 ± 0.17	7.30 ± 0.17	7.58 ± 0.16	4.84 ± 0.10
PAC50/800	BE	284.74 ± 0.11	285.24 ± 0.11	285.84 ± 0.26	287.14 ± 0.40	289.03 ± 0.38	291.57 ± 0.42
	A%	47.57 ± 0.19	13.19 ± 0.24	18.99 ± 0.17	7.32 ± 0.19	10.67 ± 0.15	2.27 ± 0.11
PAC150/800	BE	284.69 ± 0.10	285.19 ± 0.10	285.85 ± 0.21	287.17 ± 0.33	288.70 ± 0.36	291.02 ± 0.35
	A%	47.73 ±0.18	16.08 ± 0.22	17.56 ± 0.14	6.09 ± 0.15	7.51 ± 0.10	4.83 ± 0.08

Table S3. Binding energies (eV) and relative area percentages of the C1s high-resolution spectra components corresponding to the OMCs carbonized at 900 ºC.

SAMPLE		C1	C2	C3	C4	C5	C6
PAC900	BE	284.67 ± 0.06	285.37 ± 0.06	286.07 ± 0.06	286.84 ± 0.38	288.68 ± 0.33	290.81 ± 0.38
	A%	56.48 ± 0.08	15.16 ± 0.10	8.68 ± 0.13	9.37 ± 0.12	6.82 ± 0.12	3.50 ± 0.07
PAC5/900	BE	284.67 ± 0.08	285.37 ± 0.08	286.07 ± 0.08	287.06 ± 0.37	288.46 ± 0.33	290.99 ± 0.37
	A%	56.14 ± 0.11	17.79 ± 0.15	10.39 ± 0.17	3.49 ± 0.15	9.47 ± 0.11	2.72 ± 0.08
PAC50/900	BE	284.63 ± 0.08	285.33 ± 0.08	286.03 ± 0.08	287.02 ± 0.39	288.09 ± 0.38	290.56 ± 0.37
	A%	54.89 ± 0.13	16.61 ± 0.18	11.64 ± 0.20	2.79 ± 0.17	9.46 ± 0.15	4.61 ± 0.10
PAC150/900	BE	284.64 ± 0.08	285.34 ± 0.08	286.04 ± 0.08	287.10 ± 0.39	288.39 ± 0.36	290.82 ± 0.34
	A%	59.19 ± 0.12	13.82 ± 0.16	12.38 ± 0.19	3.50 ± 0.16	8.12 ± 0.13	2.99 ± 0.09

4. References

[1] M.P. Seah, I.S. Gilmore, G. Beamson, XPS: binding energy calibration of electron spectrometers 5—re-evaluation of the reference energies, Surf. Interface Anal., 26 (1998) 642-649.

[2] C.S. Hemminger, T.A. Land, A. Christie, J.C. Hemminger, An empirical electron spectrometer transmission function for applications in quantitative XPS, Surf. Interface Anal., 15 (1990) 323-327.

PUBLICACIÓN 6:

'Influence of porous texture and surface chemistry on the CO_2 adsorption capacity of porous carbons: acidic and basic site interactions'. *ACS Appl Mater Interfaces. DOI: 10.1021/am506176e*

Numerosos estudios han demostrado el efecto beneficioso que ejercen los grupos funcionales nitrogenados sobre la adsorción de CO_2. Sin embargo, tan sólo en un número reducido de casos se han identificado las funcionalidades de nitrógeno involucradas. En general, el aumento de la adsorción de CO_2 se asocia a la presencia del grupo nitrogenado más abundante, determinado por XPS. Por tanto, no se dispone de correlaciones que asocien grupos nitrogenados específicos con valores de CO_2 adsorbido. La mayor parte de los estudios que han sido realizados concluyen que la cantidad total de CO_2 adsorbido depende en gran parte de la porosidad del carbón, principalmente del volumen de microporos estrechos, mientras que la presencia de grupos superficiales nitrogenados sería responsable del aumento en los valores del calor isostérico de adsorción (Q_{st}) a bajo recubrimiento.

En este trabajo analizamos la influencia de la textura porosa y la química superficial sobre las interacciones entre la superficie del carbón (sitios ácidos y básicos) y las moléculas de CO_2. Con este fin, se prepararon materiales de carbono dopados mediante polimerización térmica en estado sólido de un precursor de poliamidas aromáticas (ácido 3-aminobenzoico, MABA) dentro de la porosidad de la plantilla SBA-15. La síntesis fue llevada a cabo en ausencia y en presencia de H_3PO_4. El procedimiento experimental se explica con detalle en el **Apartado 3.1.2.2**.

Como resultado de la síntesis realizada en ausencia de H_3PO_4, se obtuvieron materiales de carbono funcionalizados con nitrógeno y oxígeno, mientras que en presencia de H_3PO_4 se obtuvieron materiales dopados con nitrógeno, oxígeno y fósforo. De este modo, se obtuvieron carbones con una gran variedad de grupos superficiales, tanto ácidos como básicos. Variando las condiciones de preparación (temperatura de carbonización y concentración de H_3PO_4) se puede modificar tanto la textura porosa de los materiales como sus propiedades químicas superficiales. Se

observa que el mecanismo de carbonización es modificado por el ácido fosfórico. Éste produce una degradación progresiva del orden estructural y de los canales mesoporosos cuando se añade en concentraciones superiores al 50% en peso. Por el contrario, bajas concentraciones de H_3PO_4 dan lugar a materiales de carbono mesoporosos con PSDs muy estrechas. Las características de la química superficial de estos materiales fueron discutidas detalladamente en la **publicación 5**.

Los datos de adsorción de CO_2, medidos a 0 °C y 1 bar, muestran que ésta depende principalmente del volumen de microporos estrechos y prácticamente no se ve afectada por la química superficial de los materiales de carbono estudiados. De hecho, la máxima cantidad de CO_2 adsorbida (5.04 mmol/g) se alcanzó para el carbón con la estructura de ultramicroporos más desarrollada. Por otro lado, teniendo en cuenta los datos de adsorción de CO_2, medidos a 25 o 50 °C y 1 bar, se observa una dependencia con el tipo y concentración de los heteroátomos presentes en la superficie.

A través de la cantidad normalizada de CO_2 adsorbido, obtenida dividiendo la cantidad de CO_2 adsorbida a 1 bar por el volumen de ultramicroporos, demostramos que a 25 y 50 °C los grupos funcionales de nitrógeno ejercen una influencia positiva sobre la captura de CO_2, mientras que los grupos funcionales de oxígeno y fósforo ejercen una influencia negativa. También probamos que, entre los grupos nitrogenados, las funcionalidades pirrólicas producen el mayor incremento en la adsorción de CO_2, siendo más débil el efecto favorable de los grupos piridínicos y de nitrógeno cuaternario.

Por último, los carbones que poseen mayores concentraciones superficiales de nitrógeno (sintetizados en presencia de bajas concentraciones de H_3PO_4) son los que presentan los valores más altos de calor isostérico de adsorción de CO_2 a recubrimiento cero. Este hecho es consistente con el efecto positivo de los grupos funcionales de nitrógeno. Por tanto, dichos materiales podrían ser utilizados como adsorbentes selectivos, apropiados para la captura de CO_2 en condiciones de postcombustión.

ACS APPLIED MATERIALS & INTERFACES

Research Article

www.acsami.org

Influence of Porous Texture and Surface Chemistry on the CO_2 Adsorption Capacity of Porous Carbons: Acidic and Basic Site Interactions

Ángela Sánchez-Sánchez, Fabián Suárez-García,* Amelia Martínez-Alonso, and Juan M. D. Tascón

Instituto Nacional del Carbón, INCAR-CSIC, Apartado 73, 33080 Oviedo, Spain

Supporting Information

ABSTRACT: Doped porous carbons exhibiting highly developed porosity and rich surface chemistry have been prepared and subsequently applied to clarify the influence of both factors on carbon dioxide capture. Nanocasting was selected as synthetic route, in which a polyaramide precursor (3-aminobenzoic acid) was thermally polymerized inside the porosity of an SBA-15 template in the presence of different H_3PO_4 concentrations. The surface chemistry and the porous texture of the carbons could be easily modulated by varying the H_3PO_4 concentration and carbonization temperature. Porous texture was found to be the determinant factor on carbon dioxide adsorption at 0 °C, while surface chemistry played an important role at higher adsorption temperatures. We proved that nitrogen functionalities acted as basic sites and oxygen and phosphorus groups as acidic ones toward adsorption of CO_2 molecules. Among the nitrogen functional groups, pyrrolic groups exhibited the highest influence, while the positive effect of pyridinic and quaternary functionalities was smaller. Finally, some of these N-doped carbons exhibit CO_2 heats of adsorption higher than 42 kJ/mol, which make them excellent candidates for CO_2 capture.

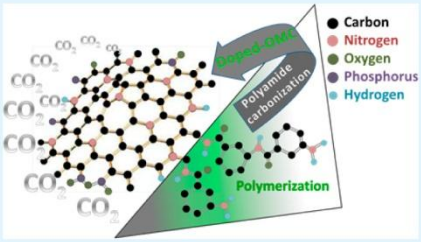

KEYWORDS: *CO_2 capture, heat of adsorption, nitrogen surface functionalities, oxygen surface functionalities, phosphorus surface functionalities*

INTRODUCTION

In recent years, serious environmental problems related to global warming have focused great attention in the reduction of greenhouse gas emissions. Carbon dioxide is considered to be one of the major contributors, being mainly released to the atmosphere from anthropogenic sources such as fossil fuel combustion in power plants and other industrial facilities. The development of new materials and technologies that capture selectively and efficiently large CO_2 uptakes from these sources deserves increasing interest.[1−4]

Adsorption of CO_2 by porous materials is one of the most promising technologies because of the possibility of developing materials with high specific surface areas and well-defined porous structures.[1,5−10] Many types of porous solids such as metal−organic frameworks,[8,11−16] zeolites,[4,17,18] amine-functionalized silicas,[19−21] or porous organic polymers[22,23] have been tested for this purpose. Among them, porous carbon materials are advantageous candidates because of their low cost, tunable porosity and morphology, fast kinetics of adsorption, high thermal and chemical stability, and controllable surface functionalization.[1,9,10,24−34] In this regard, it has been proved that incorporation of basic functionalities, especially nitrogen functional groups, into the carbon network can improve the CO_2 adsorption capacity at low pressures and high temperatures, as interactions between Lewis basic nitrogen atoms and CO_2 molecules (presenting a soft acidic character) are established.[35,36] But, to date, nitrogen doping is a complex issue and the synthesis of carbon materials having highly developed pore structures with large nitrogen densities still constitutes a great challenge. Methods for nitrogen functionalization include, for example, post-treatments in ammonia atmosphere at high temperature,[26,37,38] grafting of amine functional groups on previously oxygen-functionalized carbons[39,40] or in situ doping.[27,29,30,32,35,36,41−47] However, such methods present some disadvantages: the first two ones are expensive and time-consuming, and the last one does not allow a tight control on the specific nitrogen group which is introduced.

Although numerous works have proved that incorporation of nitrogen atoms in porous carbons exerts a beneficial effect on CO_2 adsorption,[26,27,30,35−46] only few of them have identified the different nitrogen functionalities (e.g., by X-ray photoelectron spectroscopy (XPS)).[38,42,43,46,47] In general, these works simply associated the CO_2 adsorption improvement to the presence of the most abundant nitrogen group determined by XPS;[42,43,46,47] therefore, no general correlations between the type of nitrogen containing-group and the CO_2 uptakes are available. In point of fact, most of the studies concluded that

Received: September 12, 2014
Accepted: October 27, 2014

   dx.doi.org/10.1021/am506176e | ACS Appl. Mater. Interfaces XXXX, XXX, XXX−XXX

the total amount of adsorbed CO_2 depends largely on the porosity of the carbon (mainly on the volume of narrow micropores),[29,44,48] while the presence of nitrogen surface groups is responsible for the increase of the isosteric heat of adsorption at low surface coverage; actually, heats of adsorption higher than 40 kJ/mol have been reported for N-doped carbons.[35,43,45]

In addition to nitrogen-containing groups, carbon materials present other surface functional groups like oxygenated ones and, in the case of carbons activated with H_3PO_4, phosphorus functionalities. The last ones are acidic groups and, in principle, they could be unfavorable to the CO_2 adsorption. However, oxygenated functionalities can be either acidic or basic, adding some complexity to the interaction of these groups with CO_2. Thereby, studying the influence of the different nitrogen, oxygen and phosphorus functionalities on the CO_2 adsorption becomes an interesting subject.

In the present work, we have not only faced the challenge of synthesizing porous carbons that present high contents of nitrogen, oxygen and phosphorus, but we have also deepened in the study of the interaction between basic and acidic sites in carbons and CO_2 molecules. To this end, ordered mesoporous carbons (OMCs) with high surface areas and pore volumes have been synthesized through polymerization of a polyamide precursor (3-aminobenzoic acid, MABA) inside the SBA-15 template porosity; the synthesis was accomplished in phosphoric acid medium in order to achieve an additional porosity development while keeping the ordered arrangement as unchanged as possible. Finally, we provide a systematic analysis of the influence of porous texture and heteroatoms on interactions between carbon surface and CO_2 molecules.

EXPERIMENTAL SECTION

Synthesis of the SBA-15 Silica Template. The mesoporous silica SBA-15 used as template was prepared using the method described by Zhao et al.[49] In the present work, Pluronic P123 (MW = 5800, Aldrich) was dissolved in an aqueous solution of HCl (Merck). After that, tetraetoxysilane (TEOS, Aldrich) was added dropwise and the mixture was kept under stirring (40 °C, 4 h). The molar composition of the starting reaction mixture was 0.017 P123/1 TEOS/145.8 H_2O/6.04 HCl. The resulting product was aged (125 °C, 72 h), filtered and calcined in air (550 °C, 6 h). The results from porous texture characterization of the SBA-15 used as template can be found in Supporting Information.

Synthesis of the Ordered Mesoporous Carbons. The OMC synthesis was performed by solid-state thermal polymerization of 3-aminobenzoic acid inside the porosity of the SBA-15 template. Details about this process can be found in our previous work.[50] Briefly, 1 g of SBA-15 was degassed under vacuum in a rotatory evaporator. Then, a solution containing 1.40 g of MABA (Across) and 50 mL of acetone (Sigma-Aldrich) was added to the silica template, stirring the mixture until complete SBA-15 infiltration. The solvent was removed under vacuum and the resulting MABA/silica composite was heated in a nitrogen flow (150 mL/min) at 160 °C for 1 h to thermally polymerize the MABA monomer. Afterward, the composite was impregnated with different amounts of H_3PO_4 (ACS reagent, Sigma-Aldrich). The impregnated composites were carbonized under a nitrogen flow (150 mL/min) at different temperatures (700, 800, or 900 °C). MABA/silica composites without H_3PO_4 were also carbonized under the same experimental conditions. The carbonized composites synthesized with H_3PO_4 were washed with water in a Soxhlet apparatus until the washing liquids reached conductivity values lower than 3 μS/cm. Finally, the OMCs were obtained by etching the silica template with HF. The resulting carbons were named as PACx/T, where x (not present in the samples obtained without H_3PO_4) indicates the impregnation ratio (5, 50, and 150 wt %) (i.e., H_3PO_4 weight (g)/MABA weight (g)) and T the carbonization temperature in °C.

Characterization. Thermal degradation of the MABA/silica composites in the presence of different amounts of H_3PO_4 was evaluated by thermogravimetric analysis under an argon flow (50 mL/min) up to 900 °C (heating rate of 2 °C/min), using a CI Electronics microbalance.

Structural and morphological characterizations were carried out by X-ray diffraction (XRD), scanning electron microscopy (SEM) and transmission electron microscopy (TEM), using a Siemens D5000 diffractometer (Cu Kα radiation; scanning range 2θ = 0.5–5°; step width = 0.01°; time per step = 1 s), a Carl Zeiss DMS-942 microscope and a JEOL 2000 EX/II microscope (operating potential of 160 kV), respectively.

Porous texture of the samples was characterized by N_2 adsorption/desorption isotherms at −196 °C using a volumetric adsorption apparatus ASAP 2010 (Micromeritics). From these isotherms, we obtained porous texture parameters such as the apparent BET surface area, S_{BET}, calculated by means of the BET method; the total pore volume, V_T, calculated from the amount of nitrogen adsorbed in liquid form at the relative pressure of 0.97; the total micropore volume, $V_{\mu p}$ (N_2) calculated by applying the Dubinin–Radushkevich equation; and the mesopore volume, Vmeso, which was calculated as the difference between V_T and $V_{\mu p}$ (N_2). Pore size distributions (PSDs) were obtained by applying the NLDFT method to the nitrogen adsorption branch of the isotherms. CO_2 adsorption isotherms at 0 °C were measured in a NOVA 4200e apparatus (Quantachrome Instruments). From them, the ultramicropore volume (i.e., volume of pores < 0.7 nm),[51] $V_{\mu p}$ (CO_2), was determined by applying the Dubinin–Radushkevich equation. The samples were degassed at 150 °C during 16 h prior to N_2 or CO_2 adsorption measurements.

Chemical characterization was performed by elemental analysis and XPS. Elemental analysis was carried out using a TruSpec Micro analyzer provided with a TruSpec O accessory for oxygen. XPS analysis was carried out in a SPECS system, using a monochromatic Al Kα excitation source (1486.3 eV, 150 W) and working at a pressure of 10^{-9} mbar. The photoexcited electrons were analyzed in constant pass energy mode (pass energy of 30 eV for the survey spectra and 10 eV for the high-resolution core level spectra). The data processing was carried out with CasaXPS software, the background was subtracted by a Shirley line and the core level spectra envelopes were peak-fitted to a mixed Gaussian–Lorentzian convoluted function (80/20).

Carbon Dioxide Capture. Carbon dioxide capture was accomplished by measuring the adsorption isotherms on the carbons at 0, 25, and 50 °C, measured in a NOVA 4200e apparatus (Quantachrome Instruments). The samples were degassed at 150 °C during 16 h before each analysis. The isosteric heat of adsorption was calculated by applying the Clausius–Clapeyron equation to the adsorption isotherms measured at the aforementioned three temperatures.

RESULTS AND DISCUSSION

Characterization of Carbon Materials. The TG curves in argon between 125 and 900 °C of the MABA/silica composites (partially polymerized at 160 °C for 1 h), both in the absence and in the presence of H_3PO_4 (5, 50, or 150 wt %), are displayed in Figure 1. The composites impregnated with H_3PO_4 present a very large weight loss at temperatures below 125 °C because of the evaporation of water from the acidic solution, so data obtained at temperatures below 125 °C are not shown in Figure 1.

Clear differences between the TG curves of the MABA/silica composites carbonized in the absence or presence of H_3PO_4 can be found throughout the studied temperature range, indicating a strong effect of the latter on their thermal behavior that could be explained by a different degradation mechanism. Taking into account the DTG curve (not shown) of the MABA/silica composite carbonized without H_3PO_4, four weight losses with well-defined temperature intervals can be

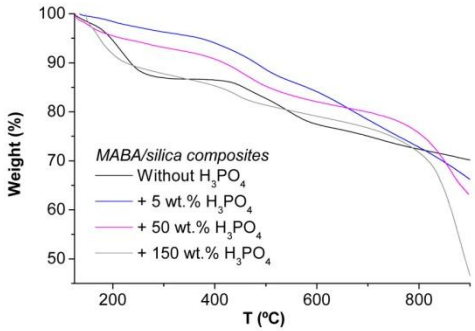

Figure 1. TG curves in argon for the MABA/silica composites polymerized at 160 °C for 1 h in the absence or presence of three different amounts of H_3PO_4.

distinguished. The first one, between 150 and 300 °C (weight loss of 11.7%) is mainly due to partial MABA evaporation,[52] which is produced above 179 °C (melting point of the monomer[53]); the polymerization stage at 160 °C for 1 h yields a mixture of polymeric chains and monomer units, sufficient to prevent a sharp evaporation of the monomer molecules above 180 °C. The second and the third steps, from 405 to 506 °C and from 506 to 620 °C, with mass losses of 4.1% and 5.4%, respectively, correspond to the effective degradation of the polymer. Comparing with the well-studied thermal degradation of other meta-polyaramides such as poly(*m*-phenylene isophthalamide) (PMIA),[54,55] these two steps can be explained by heterolythic and homolythic ruptures of the amide linkages, respectively. Finally, the mass loss above 620 °C is related to polycondensation and aromatization reactions that lead to the final carbon material.

As one can see in the TG curves of Figure 1, the addition of H_3PO_4 has a great effect on the MABA thermal degradation, even for amounts of H_3PO_4 as small as 5 wt %. In fact, the TG curves of the MABA/silica composites carbonized in the presence of different H_3PO_4 amounts present a continuous mass loss through the whole studied temperature range. It is noteworthy that the magnitude of the first step (below 350 °C) is drastically reduced by the presence of small amounts of H_3PO_4, but it increases when higher amounts of this agent are added. As we indicated above, this weight loss step corresponds to MABA evaporation; therefore, its reduction could be due to the formation of phosphate bridges between H_3PO_4 and the polymer.[56] On the other hand, the loss of water from condensed forms of H_3PO_4 (i.e., di-, tri-, polyphosphoric acid, etc.) is also produced in this temperature range;[53,57] this could explain the rise in weight loss with increasing H_3PO_4 amounts. It is known that H_3PO_4 has a great effect on the degradation steps of polyamides:[54] it decreases the extent of the reaction, the temperature and the number of degradation steps by changing the pyrolysis mechanism (heterolytic rupture reaction is favored over homolytic linkage cleavage). These changes are clearly observed between 400 and 600 °C in the TG curves of Figure 1. Finally, a new mass loss step is found above 800 °C; this mass loss increases when using higher H_3PO_4 concentrations, and can be assigned to the volatilization of phosphorus compounds.[54,58]

The effects of the carbonization temperature and H_3PO_4 addition over the carbon structure and morphology were studied by XRD, SEM, and TEM. Small-angle XRD patterns (Figure 2) show a clear evolution of the degree of structural order. The PAC samples obtained at 700, 800, and 900 °C in

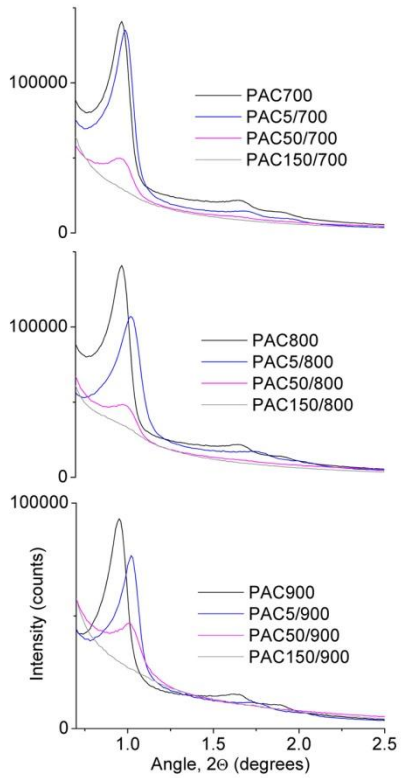

Figure 2. X-ray diffraction patterns of the carbon materials obtained at 700, 800, or 900 °C in the presence of 0, 5, 50, and 150 wt % H_3PO_4.

the absence of H_3PO_4 (PAC700, PAC800, and PAC900, respectively) exhibit three well-defined peaks which can be indexed as the (100), (110), and (200) reflections, indicative of a two-dimensional hexagonal pore structure with *P6mm* symmetry. The unit cell parameter (a) has been calculated from eq 1, applied to a *P6mm* symmetry group. In this equation, $d(100)$ is the interlayer spacing along the (100) series of planes. The a values of the mentioned samples range from 10.5 to 10.8 nm.

$$a = (2/\sqrt{3})d(100) \quad (1)$$

As Figure 2 shows, when the synthesis was accomplished in 5 wt % H_3PO_4 and regardless of the carbonization temperature, the diffraction peaks became slightly broader and their intensity decreased and shifted to higher angles, which was reflected in a lower unit cell parameter (a values between 10 and 10.3 nm). These changes are consistent with a partial loss of ordering of the mesoporous arrangement. The addition of 50 wt % H_3PO_4 to the carbon precursor led to the disappearance of the (110) and (200) reflections in the XRD patterns, suggesting that a reduction of the hexagonal order degree was produced as the structure was partially destroyed. No peaks are observed in Figure 2 when using 150 wt % H_3PO_4, thus indicating that the mesoporous arrangement has been definitively lost.

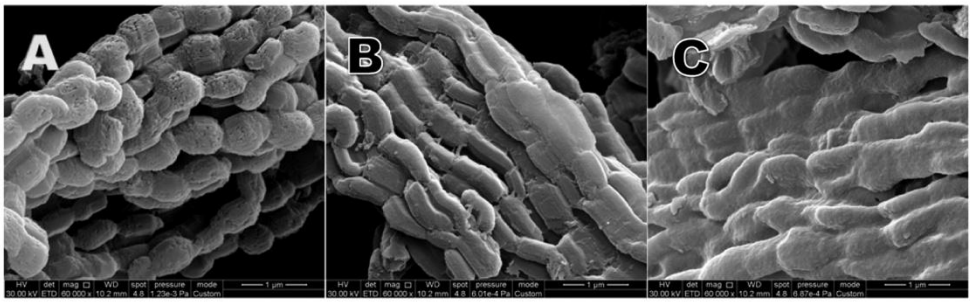

Figure 3. SEM micrographs of carbon materials obtained at 800 °C in the presence of 5 (A), 50 (B), and 150 wt % H_3PO_4 (C). Scale bar: 1 μm.

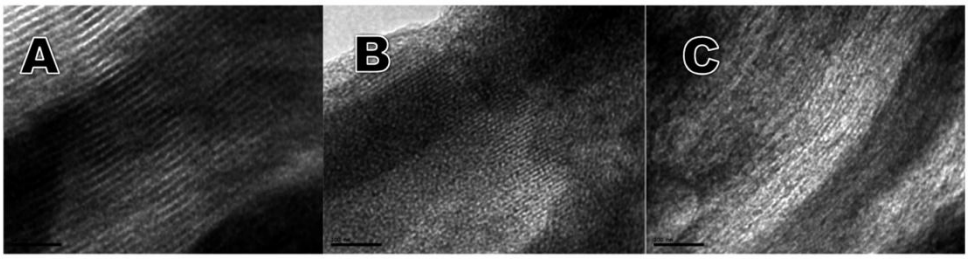

Figure 4. TEM micrographs of carbon materials obtained at 800 °C in the presence of 5 (A), 50 (B) and 150 wt % H_3PO_4 (C). Scale bar: (A) 50 nm; (B, C) 100 nm.

The progressive degradation of the structural order as larger concentrations of H_3PO_4 are added to the carbon precursor is also proved by SEM and TEM micrographs, displayed in Figure 3 and 4, respectively. As one can see in Figure 3A, a concentration of 5 wt % H_3PO_4 does not alter the particle morphology, which is essentially the same as that of the carbons synthesized in the absence of H_3PO_4 (not shown here). The TEM micrograph from Figure 4A confirms that the aforementioned carbon possesses a highly ordered periodic structure, consisting of mesoporous channels around 4.5 nm wide (white lines) and black zones between them that correspond to the carbon rods. As can be seen in Figure 3B and 4B, the particle morphology and the long-term order, respectively, are partially preserved when 50 wt % H_3PO_4 is added, while the micrographs collected in Figure 3C and 4C show that they are finally lost at the highest H_3PO_4 concentration.

The above results can be explained by a combination of several factors: (i) The effect of the carbonization temperature, which alters the SBA-15 structure;[59] (ii) The degradation of the silica template, which is attacked by H_3PO_4.[60] El Mourabit et al.[60] demonstrated that H_3PO_4 has a great effect on both SBA-15 structure and porosity. SBA-15 silica is especially sensitive to this acid since it is partially solved, resulting in a gel; in a first stage, the microporosity of the SBA-15 template is blocked by the gel, leading to a decrease in the micropore volume; finally, the mesopore walls are also affected by the same process. As a result, the morphology as well as the template porosity and structure are lost. Therefore, the carbon materials synthesized in the presence of large amounts of H_3PO_4 are obtained from a "low-quality" template; (iii) Additionally, H_3PO_4 molecules could be introduced into the SBA-15 micropores and prevent the proper formation of the connectors linking the carbon rods. (iv) Finally, the volatilization of different molecules that takes place above 750 °C (see Figure 1), especially phosphorus compounds, could also contribute to the loss of structural order of the resulting carbons.

The variations of the porous texture with the carbonization temperature and the concentration of H_3PO_4 were studied by N_2 and CO_2 adsorption. Different textural parameters for the porous carbons are recorded in Table 1, while nitrogen adsorption isotherms and pore size distributions (PSDs) are plotted in Figure 5.

As shown in Figure 5, all samples yield type-IV isotherms, typical of mesoporous materials. However, the shape of the

Table 1. Porous Texture Parameters Deduced from the N_2 and CO_2 Isotherms at −196 and 0 °C, Respectively, for Carbons Prepared at 700, 800, or 900 °C in the Presence of 0, 5, 50, or 150 wt.% H_3PO_4

sample	S_{BET} (m^2/g)	V_T (cm^3/g)	$V_{\mu p}$ (N_2) (cm^3/g)	V_{meso}(N_2) (cm^3/g)	$V_{\mu p}$(CO_2) (cm^3/g)
PAC700	1230	1.25	0.44	0.81	0.25
PAC5/700	968	1.29	0.38	0.91	0.24
PAC50/700	789	1.30	0.32	0.98	0.21
PAC150/700	818	1.08	0.32	0.76	0.22
PAC800	1178	1.19	0.43	0.76	0.22
PAC5/800	1106	1.36	0.45	0.91	0.32
PAC50/800	1298	1.85	0.52	1.33	0.34
PAC150/800	1137	1.28	0.45	0.83	0.39
PAC900	1084	1.09	0.43	0.66	0.22
PAC5/900	1031	1.43	0.43	1.00	0.31
PAC50/900	1883	3.01	0.77	2.24	0.30
PAC150/900	1244	1.49	0.47	1.02	0.28

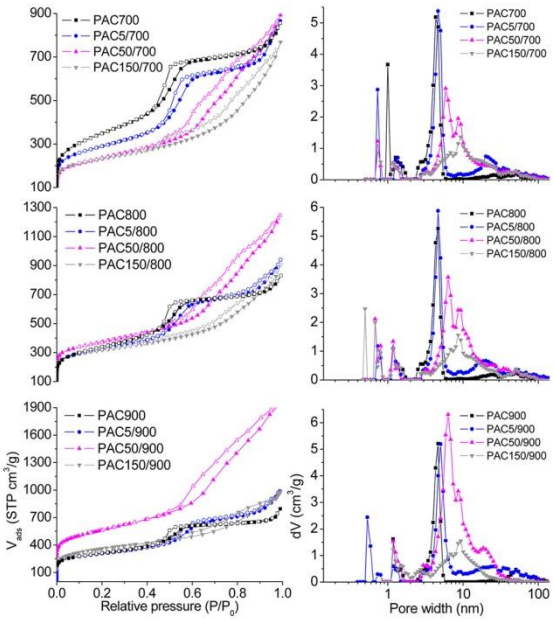

Figure 5. N_2 adsorption−desorption isotherms at −196 °C for carbon materials prepared at 700, 800, or 900 °C in the presence of 0, 5, 50, or 150 wt % H_3PO_4 (left) and the corresponding pore size distributions (right).

isotherms differs depending on the amount of H_3PO_4 used. Thus, the carbons prepared with 0 or 5 wt % H_3PO_4 (PAC and PAC5 series) exhibit a sharp jump in the isotherm around the relative pressure of 0.5, which is typical of mesoporous materials with very narrow PSDs; this is clearly reflected in their corresponding PSDs of Figure 5.

These carbons possess uniform mesopores with diameters around 4.3 nm that correspond to the space between the hexagonally arranged carbon bars (this being consistent with the TEM findings), and micropores with different size depending on the carbonization temperature. On the other hand, higher amounts of H_3PO_4 produce a widening of the PSDs (see Figure 5), which is related to a partial loss of the degree of structural order (as was demonstrated previously).

Generally speaking, it is expected to obtain more developed porosities with increasing H_3PO_4 concentrations, because of the activating effect of the latter.[56,61,62] However, this does not occur with the studied ordered mesoporous carbons. In general, higher S_{BET} values were obtained for the carbons prepared in the absence of H_3PO_4, with the exception of the samples synthesized with 50 wt % H_3PO_4 and carbonized at 800 and 900 °C, as well as PAC150/900 sample. This trend can be explained by the combination of two opposite effects induced by H_3PO_4: (i) Development of porosity due to chemical activation and (ii) Progressive loss of structural order. Thus, at the temperature of 700 °C the porosity development by activation is less import than the loss of mesostructural order. At higher temperatures, the porosity development by activation (which creates mainly micropores) is more important than the loss of structural order for the PAC50 series and, thereby, S_{BET} surface areas of 1298 and 1883 m^2/g are achieved at 800 and 900 °C, respectively. The opposite situation occurs in the case of the PAC150 series, for which, despite the micropore volume is enlarged, the loss of structural order stands as the dominant factor.

The evolution of the heteroatom (nitrogen, oxygen and phosphorus) concentrations as a function of H_3PO_4 concentration and carbonization temperature was studied in both the bulk and the surface of the carbons by means of elemental analysis and XPS, respectively. A detailed study of the surface chemistry evolution of these carbons by XPS can be found in our previous work.[63] The chemical composition values obtained by elemental analysis and XPS are collected in Table S1 in Supporting Information.

XPS data do not show the presence of any elements other than carbon, nitrogen, oxygen or phosphorus.[63] Therefore, no silicon or fluorine from the SBA-15 silica or the HF solution (used to remove the template) was retained in the material surface. It is noteworthy the retention of large amounts of nitrogen and oxygen from the carbonization of MABA, either alone or in the presence of H_3PO_4. This is clearly shown by the high bulk and surface weigh ratios, N/C and O/C, in Figures 6

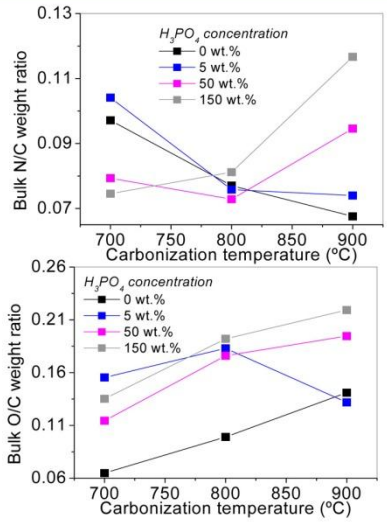

Figure 6. Temperature dependence of the bulk nitrogen to carbon (N/C) and oxygen to carbon (O/C) weight ratios from elemental analysis for materials synthesized in the presence of different H_3PO_4 concentrations.

and 7. The P/C weight ratios of Figure 7 also indicate that different amounts of phosphorus can be successfully incorporated into the carbon surface by varying the temperature of carbonization and the H_3PO_4 concentration.

Moreover, carbonization temperature and H_3PO_4 concentration exert different effects on the evolution of nitrogen, oxygen and phosphorus in the surface and the bulk of the carbons. When no H_3PO_4 is used, increasing carbonization temperatures reduce the bulk and surface nitrogen content as indicated by the decreasing N/C weight ratios (black line corresponding to 0 wt % H_3PO_4) in Figures 6 and 7. This can be explained by the loss of thermally unstable nitrogen groups.[64] As one can see in Figure 6, the bulk N/C weight ratios at 900 °C are generally higher for the samples synthesized in the presence of H_3PO_4 than for those synthesized in its absence, indicating that H_3PO_4 favors nitrogen retention in the bulk of the carbons at high

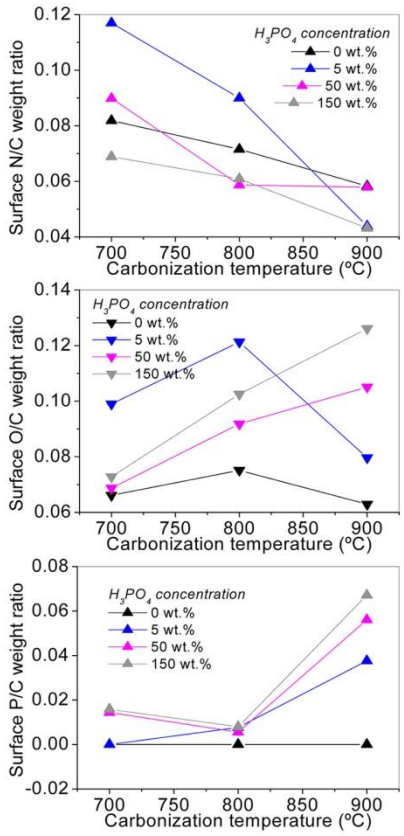

Figure 7. Temperature dependence of the surface nitrogen to carbon (N/C), oxygen to carbon (O/C), and phosphorus to carbon (P/C) weight ratios from XPS analysis for materials synthesized in the presence of different H_3PO_4 concentrations.

temperature. The highest bulk N/C weight ratio is found for sample PAC150/900, in which the nitrogen content reaches 8.9 wt % (see Supporting Information Table S1).

On the other hand, the nitrogen evolution in the surface of the carbons is rather different: the N/C weight ratios of all the studied carbons decrease with increasing carbonization temperature; as previously commented, this can be due to a thermally induced denitrogenation process of the carbon surface.[64] It should be noted that only the samples PAC5/700, PAC50/700, and PAC5/800 display N/C weight ratios higher than for the corresponding carbons synthesized without H_3PO_4 at each temperature (PAC700 for the first two samples and PAC800 for the last one). Moreover, they exhibit the highest surface nitrogen concentrations of, respectively, 9.6, 7.7, and 7.4 wt % (see Supporting Information Table S1).

As concerns oxygen evolution, the O/C bulk and surface ratios increase with increasing carbonization temperatures (Figure 6 and 7). Moreover, comparing the surface O/C and P/C weight ratios of Figure 7, it can be observed that the trends for surface oxygen and phosphorus run in parallel with each other. It has been previously proved that H_3PO_4 transformations with carbonization temperature exert a significant influence on oxygen retention.[54,65] Therefore, changes of both heteroatoms in the carbon surface will be examined together.

Among the samples carbonized at 700 °C, PAC5/700 exhibits the highest surface oxygen concentration and no detectable amount of surface phosphorus. With increasing H_3PO_4 concentration, the O/C weight ratios remain very similar to that of the PAC700 sample while the P/O weight ratios increase slightly. On the other hand, the samples carbonized at 800 °C contain the lowest P/C weight ratios and the highest O/C weight ratios. These findings can be explained by phosphorus reactions occurring above 750−800 °C: (i) Phosphates, polyphosphates and phosphorus pentoxide are generated from H_3PO_4 and reduced in some extension with carbon to elemental P_4; P_4 is removed by volatilization and phosphates and polyphosphates are solubilized and withdrawn in the washing step, so the surface phosphorus content of the carbons decreases; (ii) Surface carbon is simultaneously oxidized and the oxygen concentration (and surface O/C weight ratio) increases.[54]

As concerns the samples carbonized at 900 °C, both the O/C and P/C weight ratios increase with increasing H_3PO_4 concentration and generally reach higher values than for the samples obtained at 800 °C. This indicates that the reduction reaction of phosphates, polyphosphates and P_2O_5 is more pronounced and larger amounts of oxygen and phosphorus are introduced in the carbon surface (stable compounds of oxygen and phosphorus are formed and remain in the carbon surface after the washing step).

Carbon Dioxide Capture. The CO_2 adsorption isotherms on the studied OMCs were measured at 0, 25, and 50 °C and pressures up to 1 bar and are given in Figure S2 in Supporting Information. The CO_2 uptakes at each adsorption temperature and 1 bar are plotted in Figure 8A−C as a function of the H_3PO_4 concentration used in the OMC synthesis.

The ultramicropore volumes, $V_{\mu p}(CO_2)$, calculated from the CO_2 adsorption isotherms at 0 °C, are also included in Figure 8. Two clear conclusions can be drawn from this figure: (i) The CO_2 uptakes decrease with increasing adsorption temperature, which is expected for a physisorption process (exothermal process); (ii) the CO_2 uptakes, in general, are connected with the narrow microporosity of the carbons, following the same trend as the $V_{\mu p}(CO_2)$ values. Thus, the highest CO_2 uptake (5.04 mmol/g) is obtained at 0 °C for the PAC150/800 sample, which possesses the most developed ultramicroporous structure ($V_{\mu p}(CO_2)$ of 0.39 cm^3/g). The second statement is true for CO_2 adsorption at the three adsorption temperatures for the samples prepared at 700 °C. For those prepared at 800 and, especially, 900 °C, adsorption of CO_2 at 25 and 50 °C no longer follows the same trend as $V_{\mu p}(CO_2)$. Such discrepancy could be explained making provision for the additional effects of the micropore size distribution and the relative pressure achieved by CO_2 as a function of the adsorption temperature and the effect of the surface functional groups. At 0 °C and 1 bar, the saturation pressure of CO_2 is 34.85 bar and, therefore, P/P^0 is about 0.03. The saturation pressure increases with increasing temperature, so at 25 °C and 1 bar it becomes 64.34 bar and P/P^0 reaches a value of 0.016. At low pressure and 0 or 25 °C, adsorption is expected to take place mainly in the narrowest micropores. However, 50 °C is above the critical temperature of CO_2; because of this, a saturation pressure does not exist anymore and adsorption is believed to occur in pores even narrower than at lower temperatures. The difference between $V_{\mu p}(N_2)$ and $V_{\mu p}(CO_2)$ increases with increasing carbonization temperature for the samples prepared in the presence of 50 or 150 wt % H_3PO_4 (see Table 1). This

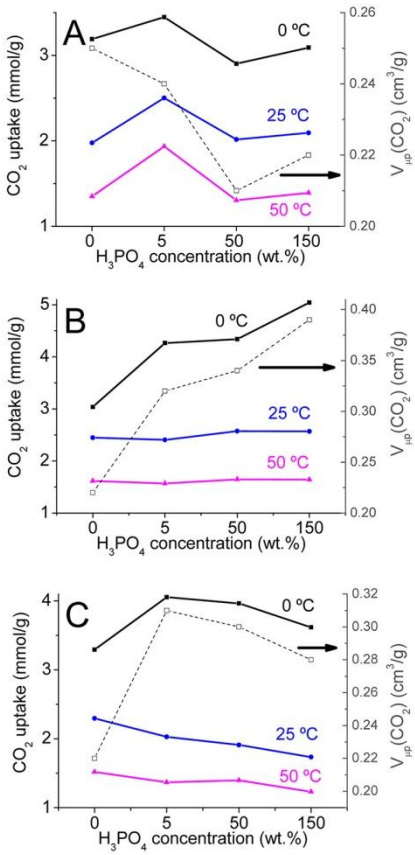

Figure 8. CO_2 uptakes at 1 bar (solid lines and left axis) and different temperatures (0, 25, or 50 °C) on the OMCs prepared at (A) 700, (B) 800, and (C) 900 °C, as a function of the H_3PO_4 concentration used in the synthesis. The ultramicropore volume, $V_{\mu p}$ (CO_2) of the samples is represented as dashed lines (right axis).

indicates a wider micropore size distribution,[51] which could explain the lower CO_2 adsorption capacity of the samples prepared under the hardest activation conditions (highest H_3PO_4 concentration and carbonization temperature).

Additionally, increasing H_3PO_4 concentration and carbonization temperature yield increasing amounts of oxygen- and phosphorus-containing groups and decreasing contents of nitrogen functionalities. Nitrogen functional groups act as basic sites and, generally speaking, they would be beneficial to CO_2 adsorption; however, oxygen and phosphorus functionalities are expected to act as acidic sites and, therefore, would lead to a decrease in the CO_2 adsorption capacity (see below). This is clearly observed for sample PAC5/700, which is the carbon exhibiting one of the highest CO_2 uptakes at 25 °C (2.50 mmol/g) and the highest one at 50 °C (1.9 mmol/g). This carbon has a relative low micropore volume, $V_{\mu p}(CO_2)$, (0.24 cm^3/g, see Table 1) but possesses the highest surface nitrogen content (9.6 wt %, see Supporting Information Table S1).

To investigate the influence of the surface functional groups on the CO_2 adsorption capacity, one should ideally consider the uptake values excluding the contribution from the porous texture. For this purpose, the CO_2 uptake at 1 bar was normalized dividing it by the ultramicropore volume, $V_{\mu p}$ (CO_2), of the carbons and plotted versus the surface heteroatom content (Figure 9). Data were fitted to linear regressions for a better remark of the trends.

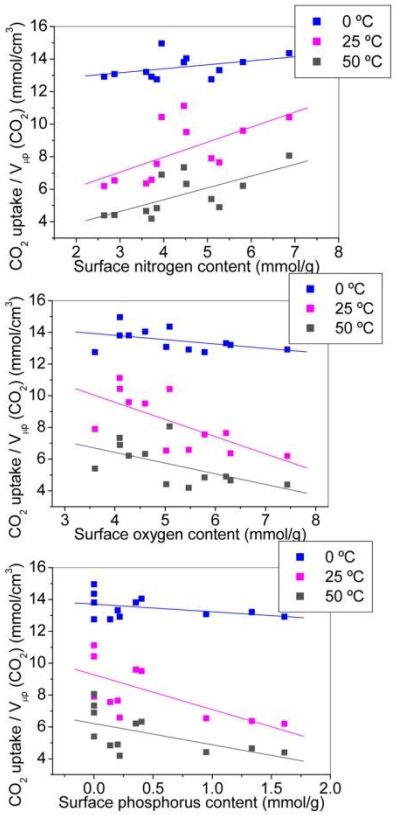

Figure 9. Influence of N, O, and P concentrations on the normalized CO_2 adsorption capacity.

There is a certain agreement in the literature about the beneficial effect of the nitrogen content for CO_2 adsorption.[27,35,42,43,45−47,66] However, a number of works suggest that the sample porosity (in particular, the micropore volume) is the key parameter that controls the CO_2 uptake.[9,10,29,48,67] As shown in Figure 9, each heteroatom has a different influence on CO_2 adsorption by the studied carbons. In addition, this effect is different for different adsorption temperatures. Thus, the CO_2 adsorption capacities at 0 °C and 1 bar are almost independent of heteroatom concentration. At this temperature and 1 bar pressure, all the carbons exhibit practically the same value of the normalized CO_2 adsorption (around 14 mmol/cm^3) (see Figure 9).

Unlike this, the CO_2 uptakes at 25 or 50 °C and 1 bar are influenced by the heteroatom content: the normalized CO_2 uptakes increase with increasing nitrogen content, but decrease with increasing oxygen and phosphorus contents. Oxygen is often present in porous carbon materials, and phosphorus is present in activated carbons prepared by chemical activation with H_3PO_4, but their effect on the CO_2 uptake has not been systematically studied before. Our results clearly demonstrate

dx.doi.org/10.1021/am506176e | ACS Appl. Mater. Interfaces XXXX, XXX, XXX−XXX

that both heteroatoms (oxygen and phosphorus) are detrimental for the CO_2 adsorption at 25 and 50 °C.

Also, the effect of the different N-containing functional groups on the CO_2 uptake has not been clarified in previous works. In general, the enhancement of CO_2 adsorption has been correlated with the total amount of nitrogen,[26,27,30,35−46] or attributed to the presence of the most abundant nitrogen group in those studies identifying the different N-containing functionalities by XPS.[42,43,46,47] For this reason, it is very interesting to gain further information on the role of the different nitrogen functional groups in improving the CO_2 capture at each adsorption temperature. To this end, the normalized CO_2 uptakes (CO_2 adsorbed at 1 bar/$V_{\mu p}$ (CO_2)) were plotted as a function of the surface pyridinic, pyrrolic, and quaternary nitrogen concentrations (expressed in mmol/g), as shown in Figure 10. The surface concentration of the different

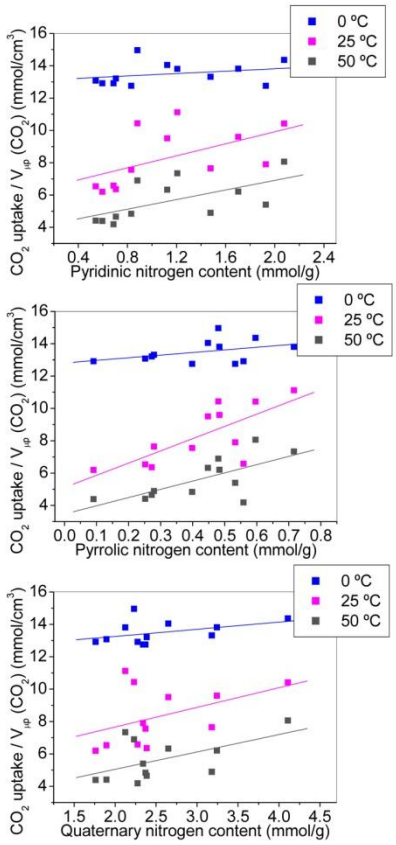

Figure 10. Influence of the surface pyridinic, pyrrolic, and quaternary nitrogen functionalities on the normalized carbon dioxide adsorption capacity.

nitrogen functionalities was determined by XPS from the deconvoluted N 1s high-resolution spectra of each sample, which have been reported elsewhere.[63]

We can observe in Figure 10 that the pyridinic, pyrrolic and quaternary nitrogen groups favor CO_2 adsorption since enhanced adsorbate uptakes are obtained, especially at 25 and 50 °C, as the surface concentration of these groups increases. Therefore, the studied surface nitrogen groups exert a beneficial influence on CO_2 capture at 25 and 50 °C (and to a minor extent at 0 °C), as expected from the existence of specific interactions; but the different values of the slopes reveal that the behavior of the three nitrogen groups is not the same. In this regard, the nitrogen groups exhibiting the greatest slope are the pyrrolic ones, followed by the pyridinic and quaternary functionalities (see Figure 10). This suggests that stronger interactions occur between pyrrolic groups and CO_2 molecules.

The results discussed so far prove the complex and determinant influence of the surface chemistry on CO_2 adsorption in the studied temperature range. A suitable way to estimate the adsorbent−adsorbate interactions is through calculation of the isosteric heat of adsorption (Q_{st}). This parameter was obtained by applying the Clausius−Clapeyron eq 2 at various adsorbate coverages (n) to the set of CO_2 adsorption isotherms measured at 0, 25, and 50 °C. The heat of adsorption vs coverage curves for the OMC−CO_2 systems are displayed in Figure 11A−C.

$$\left[\frac{\delta(\ln P)}{\delta\left(\frac{1}{T}\right)}\right]_n = \frac{Q_{st}}{R} \quad (2)$$

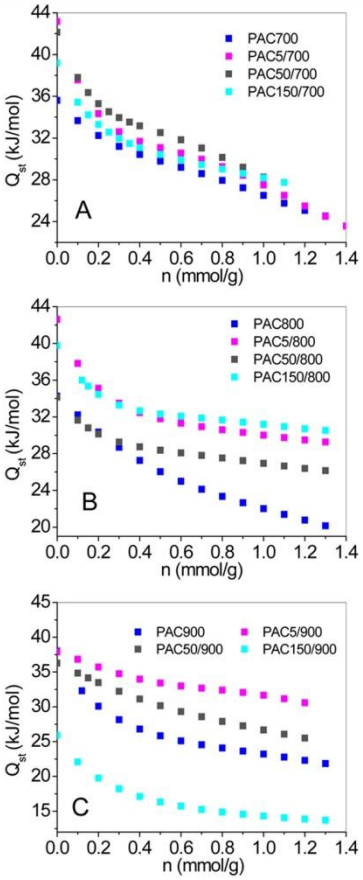

Figure 11. Isosteric heat of adsorption (Q_{st}) for OMCs synthesized at 700 (A), 800 (B), and 900 °C (C) as a function of CO_2 uptake.

Carbon dioxide adsorption is an exothermic process, so the parameter Q_{st} of eq 2 is equivalent to the adsorption enthalpy $(-\Delta H_{ads})$ at a given surface coverage (n); P is the equilibrium pressure, T is the absolute temperature; and R is the universal gas constant.

According to the shape of the curves shown in Figure 11A–C, Q_{st} values decrease with increasing CO_2 coverage. This agrees with the existence of a variety of surface sites: in the first interaction of CO_2 with the carbon surface, the covering of the sites that are thermodynamically more favorable is produced, and then, interactions with progressively less energetic sites occur. The Q_{st} values at zero coverage (extrapolated to $n = 0$) are, in general, higher than 34 kJ/mol, indicating that the surface chemistry of the carbons has a beneficial effect on the initial gas adsorption. Note that the samples exhibiting the highest surface concentrations of nitrogen are those with the highest values of Q_{st} at $n = 0$, despite containing acidic sites (oxygen and phosphorus functionalities) in their surface; such samples are PAC5/700, PAC50/700, and PAC5/800, and their Q_{st} are, respectively, 43.2, 42.1, and 42.6 kJ/mol. These values are higher than those obtained for the corresponding samples synthesized in the absence of H_3PO_4 at the same temperature (PAC700 and PAC800), which confirm the positive effect of the N-containing functional groups on the CO_2 adsorption.

Comparing with previously reported isosteric heats of adsorption, the values achieved in the present work can be considered among the highest ones obtained for porous carbons, zeolites, and metal–organic frameworks.[16,42,43,45] For zeolites, the isosteric heat of adsorption largely depends on the structure and composition of the zeolite. Specifically, the type of exposed cations will determine to a large extent the isosteric heat at low coverage, which typically ranges between 30 and 42 kJ/mol.[16,18] In the case of MOFs, their typical heats of adsorption are lower than 30 kJ/mol,[16] but larger values (between 40 and 60 kJ/mol and even higher) were reported for MOFs with exposed cations or having amine functional groups.[16] In the case of carbon materials, nondoped carbons typically exhibit isosteric heats of adsorption around 20–25 kJ/mol.[42,68] The presence of N-containing functional groups enhances Q_{st} to the range of 25 to 35 kJ/mol,[27,29,35,42,46] although some authors have reported even higher values (from 35 to 48 kJ/mol) for some nitrogen-doped carbon materials,[35,43,45] and Wang et al.[45] have reported Q_{st} values as high as 57 kJ/mol for a polyimide-based carbon prepared at 600 °C. The fact that a carbon has a higher isosteric heat that another one does not necessarily imply that the former has a higher CO_2 adsorption capacity, but it may be associated with a greater selectivity for the CO_2 adsorption as that carbon has a stronger interaction with the adsorbate. Therefore, the enhanced interaction between the CO_2 molecules and the adsorbent is expected to be positive for the CO_2 separation from other combustion flue gases.[16] As seen in Figure 11, the isosteric heat of adsorption is at a maximum for low adsorptions (i.e., when the surface coverage tends to zero); therefore, it is expected that N-doped carbons prepared in this work have an improved behavior for the CO_2 separation from dilute streams.

In the context of fossil fuel-based power plants, there are three approaches for the reduction of CO_2 emissions: precombustion, postcombustion, and oxy-combustion.[2,3,5,16,34,67]

Precombustion implies gasification of fossil fuel, producing a high-pressure flue gas containing H_2 and CO_2; CO_2 is separated before H_2 combustion. Typical characteristics of this flue gas stream are CO_2 concentrations (after the water-shift reaction) up to 35–40 vol % and pressures around 30–50 bar.[2,3] In the case of postcombustion, CO_2 is separated after fossil fuel combustion from a low-pressure (around atmospheric pressure) flue gas, which contains CO_2 at a concentration that typically is <15 vol % in mainly N_2.[2,3,5] Finally, oxy-combustion consists on the use of pure O_2 for the combustion of fossil fuel. Thus, only CO_2 and water are obtained after combustion, which can be efficiently separated from each other using existing technologies. This last option does not involve CO_2 sequestration but O_2/N_2 separation from air, which is out of the scope of this work. The CO_2 separation from flue gas stream in the two other options is more difficult in the case of postcombustion process because of the low pressure of the stream and, mainly, because of the very low CO_2 concentration (i.e., low partial pressure). Under postcombustion conditions (1 bar and a CO_2 concentration of 15 vol %), the partial pressure of CO_2 is 0.15 bar. This is the beginning of CO_2 adsorption (pressures lower than 0.15 bar). Looking to the CO_2 isotherms (not shown here) for the carbon materials prepared in this work, the highest amounts of adsorbed CO_2 for the sample PAC5/700 at 0.15 bar were 0.77 and 0.43 mmol/g at 25 and 50 °C, respectively. This implies low surface coverages, for which the isosteric heat of adsorption is high (see Figure 11). Therefore, it could be expected that the N-doped carbons prepared in this work can be suitable and selective adsorbents for CO_2 capture in postcombustion conditions.

CONCLUSIONS

Nanocasting of 3-aminobenzoic acid inside the porosity of an SBA-15 template in the presence of different H_3PO_4 concentrations gave rise to porous carbons exhibiting large pore volumes and a great variety of functional groups. Both the textural and surface chemical properties of the carbons could be easily controlled by varying the H_3PO_4 concentration and carbonization temperature. H_3PO_4 was found to change the pyrolysis mechanism of the thermally polymerized precursor and to produce the progressive degradation of both the structural order and mesopore arrangement when concentrations higher than 50 wt % were used. On the contrary, low H_3PO_4 concentrations led to mesoporous carbon materials with very narrow PSDs and favored nitrogen retention at the carbon surface.

We also proved that the CO_2 adsorption measured at 0 °C and 1 bar mainly depends on the narrow micropore volume of the carbons and is almost unaffected by the surface chemistry; the largest CO_2 uptake of 5.04 mmol/g was obtained for the carbon with the most developed ultramicroporous structure. On the other hand, CO_2 adsorption at 25 or 50 °C and 1 bar is influenced by the type and concentration of heteroatoms on the carbon surface. Through the normalized CO_2 uptakes, obtained by dividing the CO_2 adsorption at 1 bar by the ultramicropore volume, we demonstrated that at these two adsorption temperatures the nitrogen functional groups exert a beneficial influence on CO_2 capture, while oxygen and phosphorus functionalities exert a negative influence. Moreover, among the N-containing groups, the pyrrolic functionalities provoked the largest improvements in CO_2 adsorption; the effects of pyridinic and quaternary groups were weaker. The high Q_{st} values at zero coverage obtained for the samples with the highest surface concentrations of nitrogen (synthesized in the presence of low H_3PO_4 concentrations) is also consistent with the positive effect of the nitrogen functional groups. Such N-

doped carbons can constitute suitable selective adsorbents for CO_2 capture in postcombustion conditions.

■ ASSOCIATED CONTENT

Supporting Information

Porous textural characterization of the SBA-15 template, chemical composition of the carbon materials obtained from elemental analysis and XPS, and CO_2 adsorption isotherms at 0, 25, and 50 °C on the carbon materials. This material is available free of charge via the Internet at http://pubs.acs.org.

■ AUTHOR INFORMATION

Corresponding Author

*E-mail: fabian@incar.csic.es.

Notes

The authors declare no competing financial interest.

■ ACKNOWLEDGMENTS

The authors gratefully acknowledge the Spanish Ministerio de Economía y Competitividad and FEDER (project MAT2012-34011) for financial support.

■ REFERENCES

(1) Metz, B. *IPCC Special Report on Carbon Dioxide Capture and Storage*; Cambridge University Press for the Intergovernmental Panel on Climate Change: Cambridge, U.K., 2005.

(2) Olajire, A. A. CO_2 Capture and Separation Technologies for End-of-Pipe Applications—A Review. *Energy* **2010**, *35*, 2610−2628.

(3) D'Alessandro, D. M.; Smit, B.; Long, J. R. Carbon Dioxide Capture: Prospects for New Materials. *Angew. Chem., Int. Ed.* **2010**, *49*, 6058−6082.

(4) Choi, S.; Drese, J. H.; Jones, C. W. Adsorbent Materials for Carbon Dioxide Capture from Large Anthropogenic Point Sources. *ChemSusChem* **2009**, *2*, 796−854.

(5) Samanta, A.; Zhao, A.; Shimizu, G. K. H.; Sarkar, P.; Gupta, R. Post-Combustion CO_2 Capture Using Solid Sorbents: A Review. *Ind. Eng. Chem. Res.* **2012**, *51*, 1438−1463.

(6) Wang, Q.; A.; Luo, J. Z.; Zhong, Z. Y.; Borgna, A. CO_2 Capture by Solid Adsorbents and Their Applications: Current Status and New Trends. *Energy Environ. Sci.* **2011**, *4*, 42−55.

(7) Hornbostel, M. D.; Petruska, M. A.; Dubois, L.; Bao, J.; Krishnan, G.; Nagar, A.; Jayaweera, I.; Kobayashi, T.; Sanjurjo, A.; Sweeney, J.; Carruthers, D. Characteristics of an Advanced Carbon Sorbent for CO_2 Capture. *Carbon* **2013**, *56*, 77−85.

(8) Meek, S. T.; Greathouse, J. A.; Allendorf, M. D. Metal−Organic Frameworks: A Rapidly Growing Class of Versatile Nanoporous Materials. *Adv. Mater.* **2011**, *23*, 249−267.

(9) Marco-Lozar, J. P.; Kunowsky, M.; Suárez-García, F.; Carruthers, J. D.; Linares-Solano, A. Activated Carbon Monoliths for Gas Storage at Room Temperature. *Energy Environ. Sci.* **2012**, *5*, 9833−9842.

(10) Marco-Lozar, J. P.; Juan-Juan, J.; Suárez-García, F.; Cazorla-Amorós, D.; Linares-Solano, A. MOF-5 and Activated Carbons as Adsorbents for Gas Storage. *Int. J. Hydrogen Energy* **2012**, *37*, 2370−2381.

(11) Ma, S.; Zhou, H.-C. Gas Storage in Porous Metal−Organic Frameworks for Clean Energy Applications. *Chem. Commun.* **2010**, *46*, 44−53.

(12) Khan, N. A.; Hasan, Z.; Jhung, S. H. Adsorptive Removal of Hazardous Materials Using Metal−Organic Frameworks (MOFs): A Review. *J. Hazard. Mater.* **2013**, *244*−*245*, 444−456.

(13) Debatin, F.; Thomas, A.; Kelling, A.; Hedin, N.; Bacsik, Z.; Senkovska, I.; Kaskel, S.; Junginger, M.; Müller, H.; Schilde, U.; Jäger, C.; Friedrich, A.; Holdt, H.-J. In Situ Synthesis of an Imidazolate-4-Amide-5-Imidate Ligand and Formation of a Microporous Zinc−Organic Framework with H_2-and CO_2-Storage Ability. *Angew. Chem., Int. Ed.* **2010**, *49*, 1258−1262.

(14) Wu, D.; Yang, Q.; Zhong, C.; Liu, D.; Huang, H.; Zhang, W.; Maurin, G. Revealing the Structure−Property Relationships of Metal−Organic Frameworks for CO_2 Capture from Flue Gas. *Langmuir* **2012**, *28*, 12094−12099.

(15) Yu, J.; Ma, Y.; Balbuena, P. B. Evaluation of the Impact of H_2O, O_2, and SO_2 on Postcombustion CO_2 Capture in Metal−Organic Frameworks. *Langmuir* **2012**, *28*, 8064−8071.

(16) Sumida, K.; Rogow, D. L.; Mason, J. A.; McDonald, T. M.; Bloch, E. D.; Herm, Z. R.; Bae, T.-H.; Long, J. R. Carbon Dioxide Capture in Metal−Organic Frameworks. *Chem. Rev.* **2012**, *112*, 724−781.

(17) Chatti, R.; Bansiwal, A. K.; Thote, J. A.; Kumar, V.; Jadhav, P.; Lokhande, S. K.; Biniwale, R. B.; Labhsetwar, N. K.; Rayalu, S. S. Amine Loaded Zeolites for Carbon Dioxide Capture: Amine Loading and Adsorption Studies. *Microporous Mesoporous Mater.* **2009**, *121*, 84−89.

(18) Grajciar, L.; Čejka, J.; Zukal, A.; Otero Areán, C.; Turnes Palomino, G.; Nachtigall, P. Controlling the Adsorption Enthalpy of CO_2 in Zeolites by Framework Topology and Composition. *ChemSusChem* **2012**, *5*, 2011−2022.

(19) Cui, S.; Cheng, W.; Shen, X.; Fan, M.; Russell, A.; Wu, Z.; Yi, X. Mesoporous Amine-Modified SiO_2 Aerogel: A Potential CO_2 Sorbent. *Energy Environ. Sci.* **2011**, *4*, 2070−2074.

(20) Xu, X.; Song, C.; Andresen, J. M.; Miller, B. G.; Scaroni, A. W. Novel Polyethylenimine-Modified Mesoporous Molecular Sieve of Mcm-41 Type as High-Capacity Adsorbent for CO_2 Capture. *Energy Fuels* **2002**, *16*, 1463−1469.

(21) Heydari-Gorji, A.; Belmabkhout, Y.; Sayari, A. Polyethylenimine-Impregnated Mesoporous Silica: Effect of Amine Loading and Surface Alkyl Chains on CO_2 Adsorption. *Langmuir* **2011**, *27*, 12411−12416.

(22) Furusho, Y.; Endo, T. Capture and Release of CO_2 by Polyamidine. *J. Polym. Sci., Polym. Chem.* **2013**, *51*, 3404−3411.

(23) Lu, W.; Sculley, J. P.; Yuan, D.; Krishna, R.; Zhou, H.-C. Carbon Dioxide Capture from Air Using Amine-Grafted Porous Polymer Networks. *J. Phys. Chem. C* **2013**, *117*, 4057−4061.

(24) Plaza, M. G.; García, S.; Rubiera, F.; Pis, J. J.; Pevida, C. Post-Combustion CO_2 Capture with a Commercial Activated Carbon: Comparison of Different Regeneration Strategies. *Chem. Eng. J.* **2010**, *163*, 41−47.

(25) Plaza, M. G.; González, A. S.; Pevida, C.; Pis, J. J.; Rubiera, F. Valorisation of Spent Coffee Grounds as CO_2 Adsorbents for Postcombustion Capture Applications. *Appl. Energy* **2012**, *99*, 272−279.

(26) Plaza, M. G.; Rubiera, F.; Pis, J. J.; Pevida, C. Ammoxidation of Carbon Materials for CO_2 Capture. *Appl. Surf. Sci.* **2010**, *256*, 6843−6849.

(27) Xia, Y.; Mokaya, R.; Walker, G. S.; Zhu, Y. Superior CO_2 Adsorption Capacity on N-Doped, High-Surface-Area, Microporous Carbons Templated from Zeolite. *Adv. Energy Mater.* **2011**, *1*, 678−683.

(28) Chandra, V.; Yu, S. U.; Kim, S. H.; Yoon, Y. S.; Kim, D. Y.; Kwon, A. H.; Meyyappan, M.; Kim, K. S. Highly Selective CO_2 Capture on N-Doped Carbon Produced by Chemical Activation of Polypyrrole Functionalized Graphene Sheets. *Chem. Commun.* **2012**, *48*, 735−737.

(29) Sevilla, M.; Falco, C.; Titirici, M. M.; Fuertes, A. B. High-Performance CO_2 Sorbents from Algae. *RSC Adv.* **2012**, *2*, 12792−12797.

(30) Zhao, Y.; Zhao, L.; Yao, K. X.; Yang, Y.; Zhang, Q.; Han, Y. Novel Porous Carbon Materials with Ultrahigh Nitrogen Contents for Selective CO_2 Capture. *J. Mater. Chem.* **2012**, *22*, 19726−19731.

(31) Wei, H.; Deng, S.; Hu, B.; Chen, Z.; Wang, B.; Huang, J.; Yu, G. Granular Bamboo-Derived Activated Carbon for High CO_2 Adsorption: The Dominant Role of Narrow Micropores. *ChemSusChem* **2012**, *5*, 2354−2360.

(32) Presser, V.; McDonough, J.; Yeon, S. H.; Gogotsi, Y. Effect of Pore Size on Carbon Dioxide Sorption by Carbide Derived Carbon. *Energy Environ. Sci.* **2011**, *4*, 3059−3066.

(33) Liang, C. D.; Li, Z. J.; Dai, S. Mesoporous Carbon Materials: Synthesis and Modification. *Angew. Chem., Int. Ed.* **2008**, *47*, 3696–3717.
(34) García, S.; Pis, J. J.; Rubiera, F.; Pevida, C. Predicting Mixed-Gas Adsorption Equilibria on Activated Carbon for Precombustion CO_2 Capture. *Langmuir* **2013**, *29*, 6042–6052.
(35) Zhou, J.; Li, W.; Zhang, Z. S.; Xing, W.; Zhuo, S. P. Carbon Dioxide Adsorption Performance of N-Doped Zeolite Y Templated Carbons. *RSC Adv.* **2012**, *2*, 161–167.
(36) Xing, W.; Qiao, S. Z.; Liu, C.; Zhou, Z. Y.; Zhang, L.; Zhou, J.; Zhuo, S. P.; Yan, Z. F.; Gao, H.; Wang, G. Q. Superior CO_2 Uptake of N-Doped Activated Carbon through Hydrogen-Bonding Interaction. *Energy Environ. Sci.* **2012**, *5*, 7323–7327.
(37) Plaza, M. G.; García, S.; Rubiera, F.; Pis, J. J.; Pevida, C. Evaluation of Ammonia Modified and Conventionally Activated Biomass Based Carbons as CO_2 Adsorbents in Postcombustion Conditions. *Sep. Purif. Technol.* **2011**, *80*, 96.
(38) Pevida, C.; Plaza, M. G.; Arias, B.; Fermoso, J.; Rubiera, F.; Pis, J. J. Surface Modification of Activated Carbons for CO_2 Capture. *Appl. Surf. Sci.* **2008**, *254*, 7165–7172.
(39) Houshmand, A.; Daud, W. M. A. W.; Lee, M.-G.; Shafeeyan, M. S. Carbon Dioxide Capture with Amine-Grafted Activated Carbon. *Water Air Soil Pollut.* **2012**, *223*, 827–835.
(40) Zhao, L.; Bacsik, Z.; Hedin, N.; Wei, W.; Sun, Y. H.; Antonietti, M.; Titirici, M. M. Carbon Dioxide Capture on Amine-Rich Carbonaceous Materials Derived from Glucose. *ChemSusChem* **2010**, *3*, 840–845.
(41) Zhu, X.; Hillesheim, P. C.; Mahurin, S. M.; Wang, C.; Tian, C.; Brown, S.; Luo, H.; Veith, G. M.; Han, K. S.; Hagaman, E. W.; Liu, H.; Dai, S. Efficient CO_2 Capture by Porous, Nitrogen-Doped Carbonaceous Adsorbents Derived from Task-Specific Ionic Liquids. *ChemSusChem* **2012**, *5*, 1912–1917.
(42) Fan, X.; Zhang, L.; Zhang, G.; Shu, Z.; Shi, J. Chitosan Derived Nitrogen-Doped Microporous Carbons for High Performance CO_2 Capture. *Carbon* **2013**, *61*, 423–430.
(43) Gu, J.-M.; Kim, W.-S.; Hwang, Y.-K.; Huh, S. Template-Free Synthesis of N-Doped Porous Carbons and Their Gas Sorption Properties. *Carbon* **2013**, *56*, 208–217.
(44) Liu, Z.; Du, Z.; Song, H.; Wang, C.; Subhan, F.; Xing, W.; Yan, Z. The Fabrication of Porous N-Doped Carbon from Widely Available Urea Formaldehyde Resin for Carbon Dioxide Adsorption. *J. Colloid Interface Sci.* **2014**, *416*, 124–132.
(45) Wang, J.; Senkovska, I.; Oschatz, M.; Lohe, M. R.; Borchardt, L.; Heerwig, A.; Liu, Q.; Kaskel, S. Highly Porous Nitrogen-Doped Polyimine-Based Carbons with Adjustable Microstructures for CO_2 Capture. *J. Mater. Chem. A* **2013**, *1*, 10951–10961.
(46) Sevilla, M.; Valle-Vigón, P.; Fuertes, A. B. N-Doped Polypyrrole-Based Porous Carbons for CO_2 Capture. *Adv. Funct. Mater.* **2011**, *21*, 2781–2787.
(47) Hao, G.-P.; Li, W.-C.; Qian, D.; Lu, A.-H. Rapid Synthesis of Nitrogen-Doped Porous Carbon Monolith for CO_2 Capture. *Adv. Mater.* **2010**, *22*, 853–857.
(48) Sevilla, M.; Parra, J. B.; Fuertes, A. B. Assessment of the Role of Micropore Size and N-Doping in CO_2 Capture by Porous Carbons. *ACS Appl. Mater. Interfaces* **2013**, *5*, 6360–6368.
(49) Zhao, D. Y.; Feng, J. L.; Huo, Q. S.; Melosh, N.; Fredrickson, G. H.; Chmelka, B. F.; Stucky, G. D. Triblock Copolymer Syntheses of Mesoporous Silica with Periodic 50 to 300 Angstrom Pores. *Science* **1998**, *279*, 548–552.
(50) Sánchez-Sánchez, A.; Suárez-García, F.; Martínez-Alonso, A.; Tascón, J. M. D. Aromatic Polyamides as New Precursors of Nitrogen and Oxygen-Doped Ordered Mesoporous Carbons. *Carbon* **2014**, *70*, 119–129.
(51) Lozano-Castelló, D.; Cazorla-Amorós, D.; Linares-Solano, A. Usefulness of CO_2 Adsorption at 273 K for the Characterization of Porous Carbons. *Carbon* **2004**, *42*, 1233–1242.
(52) Yoon, S. M.; Hwang, L-C.; Shin, N.; Ahn, D.; Lee, S. J.; Lee, J. Y.; Choi, H. C. Vaporization–Condensation–Recrystallization Process-Mediated Synthesis of Helical M-Aminobenzoic Acid Nanobelts. *Langmuir* **2007**, *23*, 11875–11882.
(53) Lide, D. R. *CRC Handbook of Chemistry and Physics*, Internet Version 2005, 85th ed.; CRC Press: Boca Raton, FL, 2005.
(54) Suárez-García, F.; Villar-Rodil, S.; Blanco, C. G.; Martínez-Alonso, A.; Tascón, J. M. D. Effect of Phosphoric Acid on Chemical Transformations During Nomex Pyrolysis. *Chem. Mater.* **2004**, *16*, 2639–2647.
(55) Villar-Rodil, S.; Martínez-Alonso, A.; Tascón, J. M. D. Studies on Pyrolysis of Nomex Polyaramid Fibers. *J. Anal. Appl. Pyrolysis* **2001**, *58*, 105–115.
(56) Suárez-García, F.; Martínez-Alonso, A.; Tascón, J. M. D. Activated Carbon Fibers from Nomex by Chemical Activation with Phosphoric Acid. *Carbon* **2004**, *42*, 1419–1426.
(57) Cotton, F. A.; Wilkinson, G. *Advanced Inorganic Chemistry*; John Wiley and Sons: New York, 1988.
(58) Puziy, A. M.; Poddubnaya, O. I.; Martínez-Alonso, A.; Suárez-García, F.; Tascón, J. M. D. Synthetic Carbons Activated with Phosphoric Acid—I. Surface Chemistry and Ion Binding Properties. *Carbon* **2002**, *40*, 1493–1505.
(59) Cassiers, K.; Linssen, T.; Mathieu, M.; Benjelloun, M.; Schrijnemakers, K.; Van Der Voort, P.; Cool, P.; Vansant, E. F. A Detailed Study of Thermal, Hydrothermal, and Mechanical Stabilities of a Wide Range of Surfactant Assembled Mesoporous Silicas. *Chem. Mater.* **2002**, *14*, 2317–2324.
(60) El Mourabit, S.; Guillot, M.; Toquer, G.; Cambedouzou, J.; Goettmann, F.; Grandjean, A. Stability of Mesoporous Silica under Acidic Conditions. *RSC Adv.* **2012**, *2*, 10916–10924.
(61) Suárez-García, F.; Martínez-Alonso, A.; Tascón, J. M. D. Nomex Polyaramid as a Precursor for Activated Carbon Fibres by Phosphoric Acid Activation. Temperature and Time Effects. *Microporous Mesoporous Mater.* **2004**, *75*, 73–80.
(62) Puziy, A. M.; Tascón, J. M. D., Adsorption by Phosphorous-Containing Carbons. In *Novel Carbon Adsorbents*, Tascon, J. M. D., Ed. Elsevier: Amsterdam, The Netherlands, 2012; Chapter 8, pp 245–267.
(63) Sánchez-Sánchez, A.; Suárez-García, F.; Martínez-Alonso, A.; Tascón, J. M. D. Evolution of the Complex Surface Chemistry in Mesoporous Carbons Obtained from Polyaramide Precursors. *Appl. Surf. Sci.* **2014**, *299*, 19–28.
(64) Kim, W.; Kang, M. Y.; Joo, J. B.; Kim, N. D.; Song, I. K.; Kim, P.; Yoon, J. R.; Yi, J. Preparation of Ordered Mesoporous Carbon Nanopipes with Controlled Nitrogen Species for Application in Electrical Double-Layer Capacitors. *J. Power Sources* **2010**, *195*, 2125–2129.
(65) Puziy, A. M.; Poddubnaya, O. I.; Martínez-Alonso, A.; Suárez-García, F.; Tascón, J. M. D. Surface Chemistry of Phosphorus-Containing Carbons of Lignocellulosic Origin. *Carbon* **2005**, *43*, 2857–2868.
(66) Babarao, R.; Dai, S.; Jiang, D.-e. Nitrogen-Doped Mesoporous Carbon for Carbon Capture—A Molecular Simulation Study. *J. Phys. Chem. C* **2012**, *116*, 7106–7110.
(67) Marco-Lozar, J. P.; Kunowsky, M.; Suárez-García, F.; Linares-Solano, A. Sorbent Design for CO_2 Capture under Different Flue Gas Conditions. *Carbon* **2014**, *72*, 125–134.
(68) Saha, B. B.; Jribi, S.; Koyama, S.; E-Sharkawy, I. I. Carbon Dioxide Adsorption Isotherms on Activated Carbons. *J. Chem. Eng. Data* **2011**, *56*, 1974–1981.

Influence of Porous Texture and Surface Chemistry on the CO_2 Adsorption Capacity of Porous Carbons: Acidic and Basic Site Interactions

Ángela Sánchez-Sánchez, Fabián Suárez-García, Amelia Martínez-Alonso and Juan M. D. Tascón

Instituto Nacional del Carbón, INCAR-CSIC, Apartado 73, 33080 Oviedo, Spain.

Supporting Information

1. SBA-15 porous texture characterization.

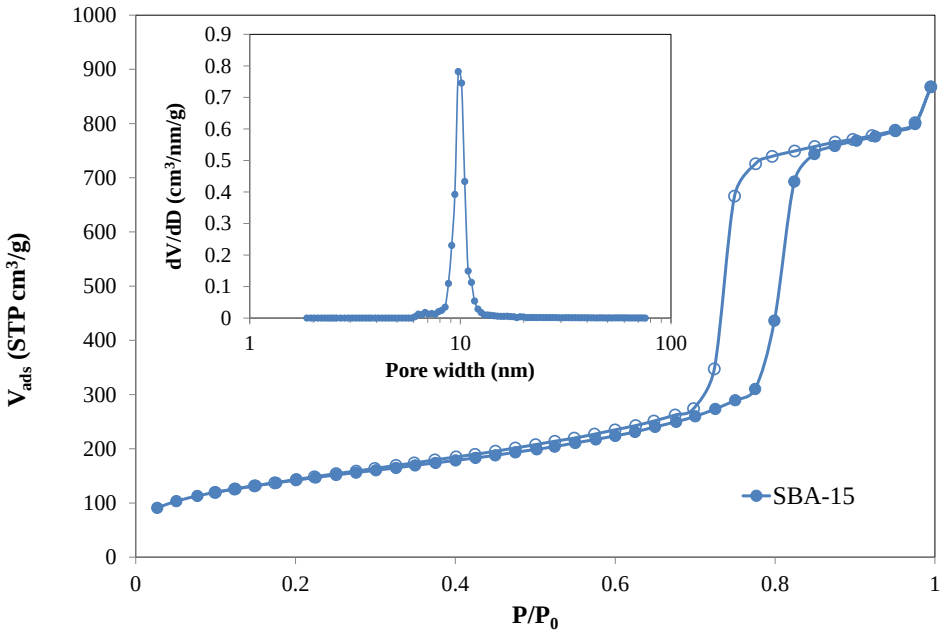

Figure S1. N_2 adsorption-desorption isotherm at – 196 ºC for the SBA-15 silica used as template and the corresponding pore size distribution (inset plot).

SBA-15 yields a type IV isotherm with a type H1 hysteresis loop, which are characteristics of mesoporous materials with a very narrow pore size distribution (PSD) of uniform pore size (main mesopore size of 9.7 nm). This silica has a BET surface area, S_{BET}, of 513 m^2/g and micropore, $V_{\mu p}$, mesopore, V_{meso}, and total pore volumes, V_T, of 0.22, 0.93 and 1.15 cm^3/g, respectively.

2. Chemical composition obtained from elemental analysis and XPS.

Table S1. Chemical composition for carbon materials prepared at 700, 800 or 900 ºC in the presence of 0, 5, 50 or 150 wt.% H_3PO_4 obtained from elemental analysis and XPS.

Sample	Elemental Analysis (wt.%)			XPS (wt.%)			
	C	N	O	C	N	O	P
PAC700	80.2	7.8	5.2	87.1	7.1	5.8	-
PAC5/700	76.8	8.0	11.9	82.2	9.6	8.1	-
PAC50/700	79.2	6.3	9.1	85.3	7.7	5.9	1.2
PAC150/700	79.3	5.9	10.7	86.4	5.9	6.3	1.4
PAC800	78.9	6.1	7.8	87.2	6.2	6.6	-
PAC5/800	79.8	6.1	14.6	82.0	7.4	9.9	0.6
PAC50/800	76.6	5.6	13.5	86.5	5.1	7.9	0.5
PAC150/800	77.5	6.3	14.9	85.4	5.2	8.8	0.7
PAC900	81.7	5.5	11.5	89.2	5.2	5.6	-
PAC5/900	77.3	5.7	10.2	86.1	3.8	6.9	3.2
PAC50/900	73.8	7.0	14.4	82.0	4.8	8.6	4.6
PAC150/900	76.0	8.9	16.7	80.9	3.5	10.2	5.4

3. CO_2 adsorption isotherms

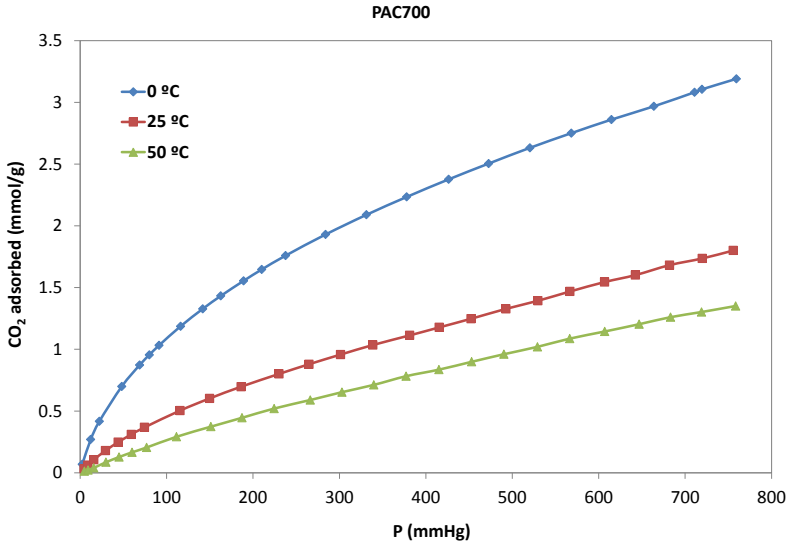

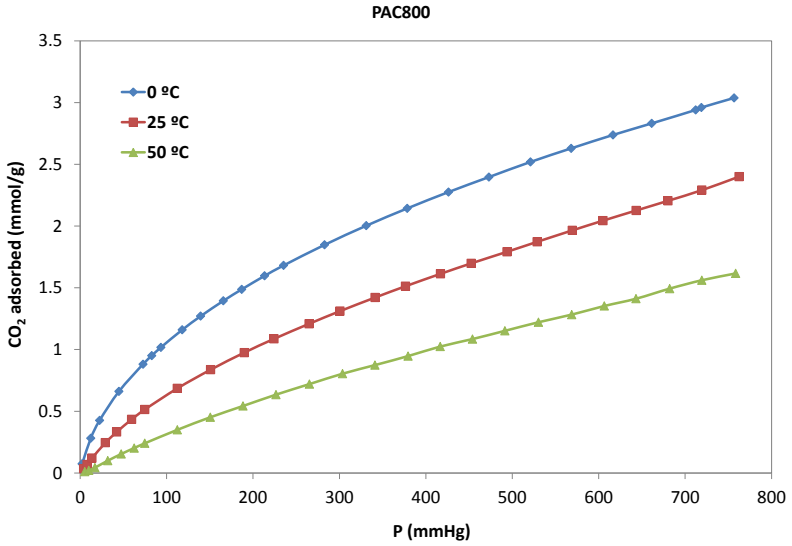

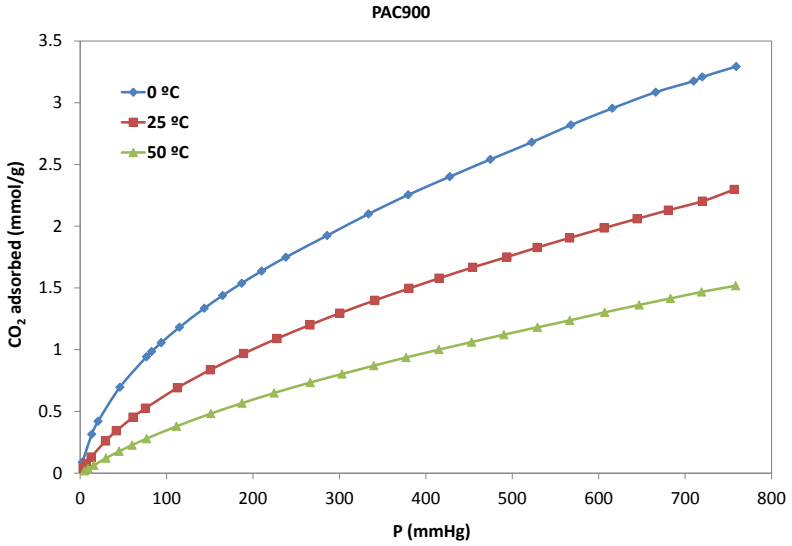

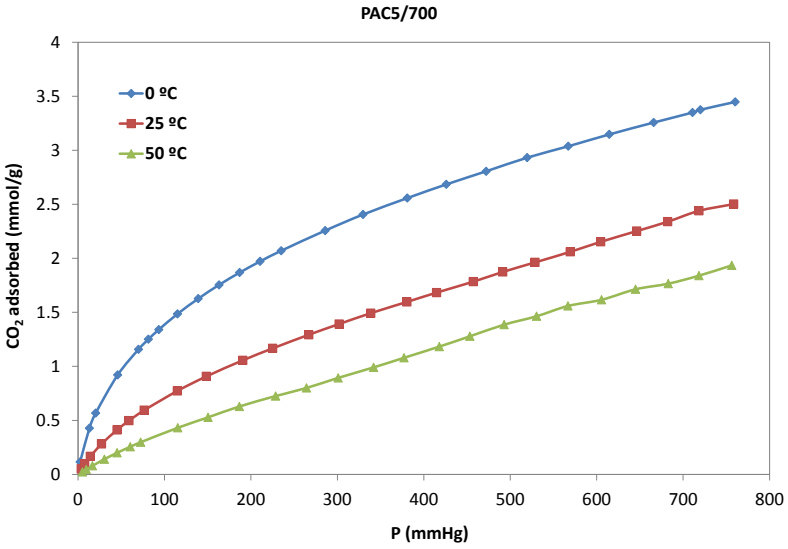
PAC5/700
0 ºC
25 ºC
50 ºC
CO2 adsorbed (mmol/g)
P (mmHg)
0
0.5
1
1.5
2
2.5
3
3.5
4
0
100
200
300
400
500
600
700
800

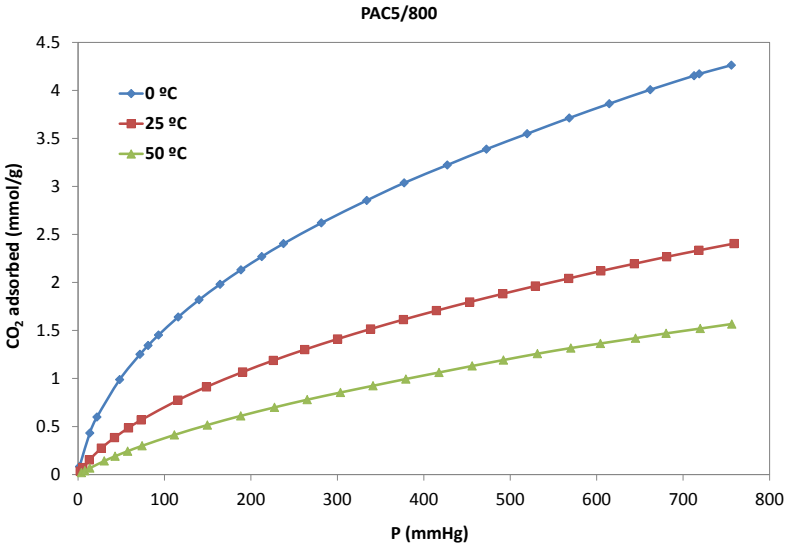
PAC5/800
0 ºC
25 ºC
50 ºC
CO2 adsorbed (mmol/g)
P (mmHg)
0
0.5
1
1.5
2
2.5
3
3.5
4
4.5
0
100
200
300
400
500
600
700
800

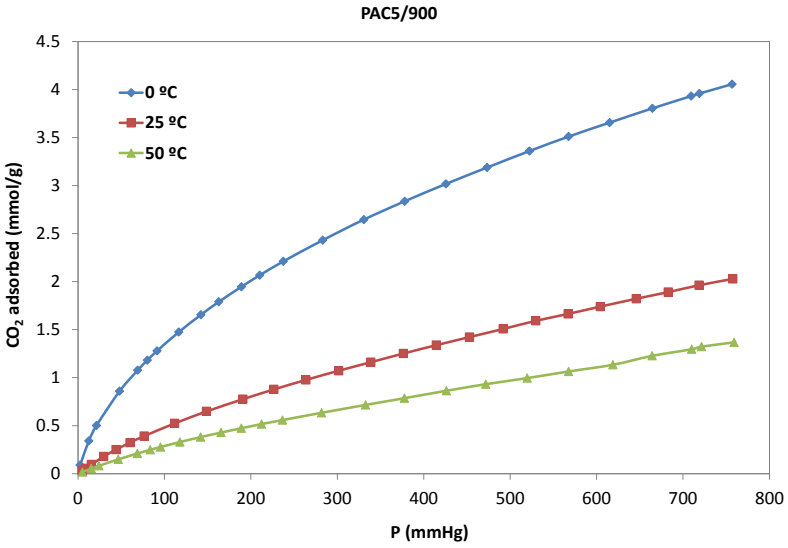
PAC5/900
0 ºC
25 ºC
50 ºC
CO2 adsorbed (mmol/g)
P (mmHg)
0
0.5
1
1.5
2
2.5
3
3.5
4
4.5
0
100
200
300
400
500
600
700
800

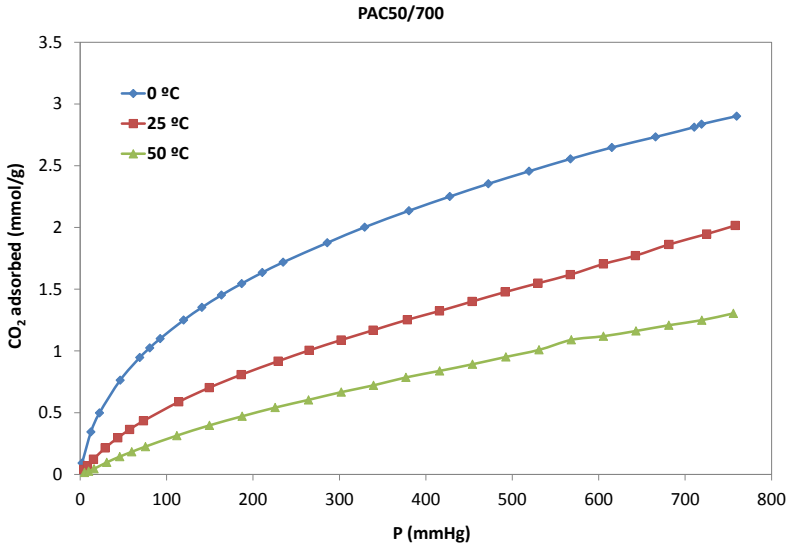
PAC50/700
0 ºC
25 ºC
50 ºC
CO2 adsorbed (mmol/g)
P (mmHg)
0
0.5
1
1.5
2
2.5
3
3.5
0
100
200
300
400
500
600
700
800

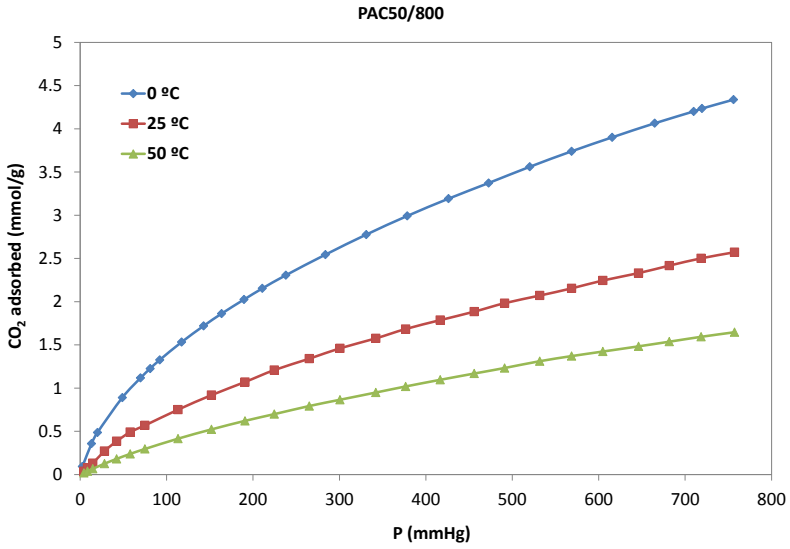
PAC50/800
0 ºC
25 ºC
50 ºC
CO2 adsorbed (mmol/g)
P (mmHg)
0
0.5
1
1.5
2
2.5
3
3.5
4
4.5
5
0
100
200
300
400
500
600
700
800

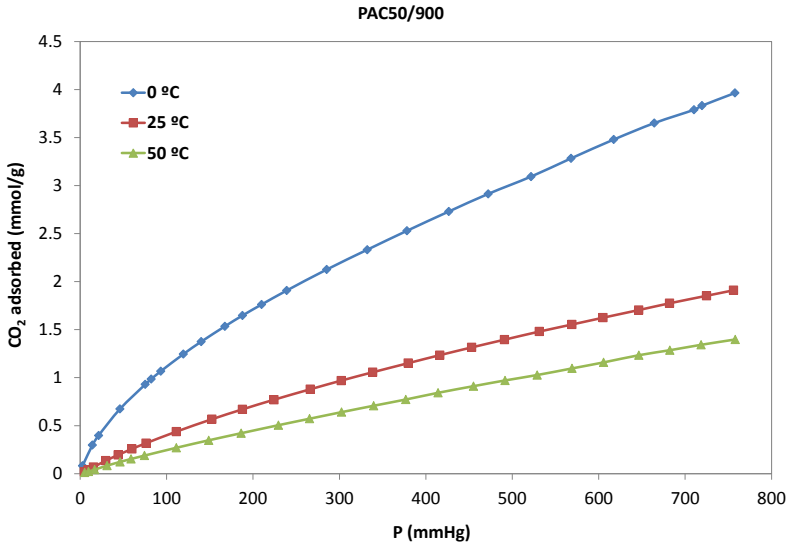
PAC50/900
0 ºC
25 ºC
50 ºC
CO2 adsorbed (mmol/g)
P (mmHg)
0
0.5
1
1.5
2
2.5
3
3.5
4
4.5
0
100
200
300
400
500
600
700
800

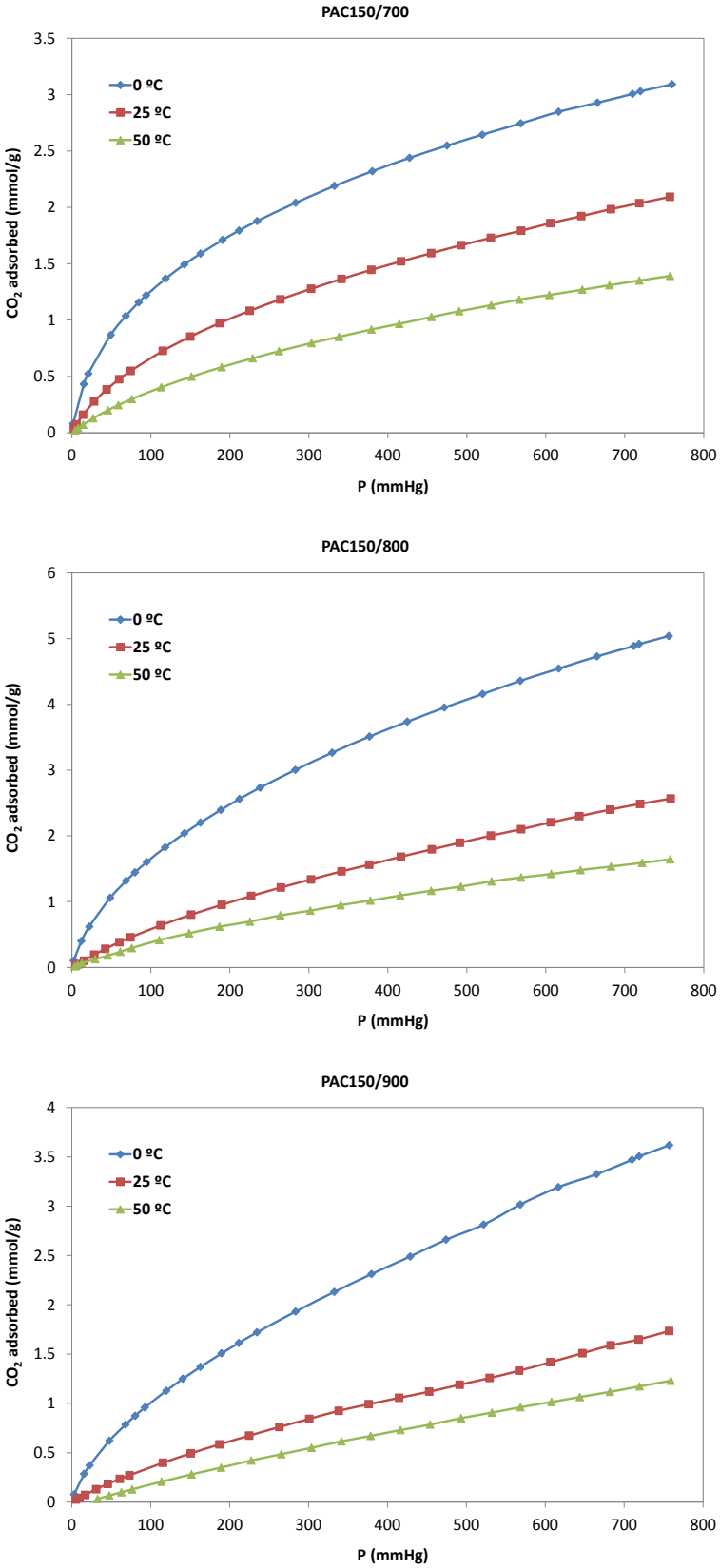

Figure S2. CO_2 adsorption isotherms at 0, 25 and 50 ºC on carbon materials prepared at 700, 800 or 900 ºC in the presence of 0, 5, 50 or 150 wt.% H_3PO_4

Capítulo 6:

Conclusiones

CONCLUSIONES

En base a los resultados expuestos en la presente tesis doctoral, se puede concluir que el ***objetivo general*** planteado al inicio de la misma ha sido alcanzado, puesto que se ha logrado sintetizar ***materiales de carbono mesoporosos dopados con heteroátomos (nitrógeno, oxígeno y fósforo) utilizando técnicas de nanomoldeo*** como herramienta de preparación.

Asimismo, los resultados obtenidos permiten extraer las siguientes conclusiones generales:

- Mediante tratamientos de oxidación con HNO_3 y H_2O_2 es posible introducir una gran variedad de funcionalidades oxigenadas en CMOs obtenidos por CVD de propileno, sin alterar ni su textura porosa ni su orden estructural. La cantidad y naturaleza de los grupos funcionales introducidos pueden ser moduladas variando la naturaleza del agente oxidante, su concentración y el tiempo de tratamiento.

- Mediante los tratamientos de oxidación más severos con HNO_3 se introduce hasta un 9% en peso de oxígeno en la superficie del material. Éste se encuentra principalmente formando parte de ácidos carboxílicos, fenoles e hidroquinonas. El H_2O_2 tiene un efecto oxidante más débil, permitiendo la introducción de hasta un 3% en peso de oxígeno, mayormente en forma de grupos fenólicos e hidroquinonas.

- Se han obtenido CMOs dopados con nitrógeno y oxígeno mediante CVD de acetonitrilo a 850 °C. La concentración superficial de nitrógeno alcanza el 9.4% en peso, encontrándose principalmente en forma de nitrógeno cuaternario. El contenido superficial de oxígeno varía inversamente con el de nitrógeno; su concentración oscila entre el 3 y el 5% en peso, y forma parte principalmente de ésteres, anhídridos y alcoholes, así como carbonilos y ácidos carboxílicos en menor proporción.

- La presencia de funcionalidades nitrogenadas en la superficie de los CMOs dificulta la adsorción de colorantes catiónicos como el azul de metileno, pero no afecta a la adsorción de colorantes aniónicos, como el naranja de metilo o la fucsina ácida, que depende esencialmente de la porosidad de los carbones. Sin embargo,

las cinéticas de adsorción de ambos tipos de colorantes se ven mejoradas por la presencia de grupos funcionales, alcanzándose virtualmente el 100% de las capacidades máximas de adsorción en menos de 15 minutos.

- En esta tesis se han utilizado por primera vez con éxito poliamidas aromáticas como precursores para la síntesis de CMOs dopados con nitrógeno y oxígeno. Se desarrollaron dos métodos de síntesis: síntesis en fase orgánica y polimerización térmica en estado sólido.

- El método de ***síntesis en fase orgánica*** se basa en la síntesis de poliamidas mediante la reacción de Yamazaki. Los grados de polimerización de los precursores polimerizados son mayores que en el método de polimerización térmica en estado sólido, y por ello se obtienen rendimientos de carbonización y contenidos de carbono más altos, pero también porosidades menos desarrolladas. El principal inconveniente de este método es que la infiltración del precursor en la plantilla de sílice es heterogénea y, a pesar de que la plantilla es replicada correctamente, el ordenamiento estructural del material de carbono es menor.

- El método de ***polimerización térmica en estado sólido*** presenta una serie de ventajas con respecto al anterior: el procedimiento experimental es más sencillo y menos contaminante, los CMOs poseen porosidades más desarrolladas y mayor ordenamiento estructural de largo alcance, ya que la infiltración de la plantilla es homogénea.

- En los dos casos anteriores, se alcanzan concentraciones superficiales de nitrógeno y oxígeno del 6 y 6.4% en peso, respectivamente. El nitrógeno se encuentra principalmente en forma de nitrógeno cuaternario, piridínico y pirrólico, mientras que el oxígeno forma parte esencialmente de grupos funcionales éster y anhídrido.

- Variando el tipo de precursor (ácido 3-aminobenzoico o ácido 4-aminobenzoico) se obtienen CMOs con diferentes estructuras y químicas superficiales debido al diferente mecanismo de pirólisis de ambos precursores. El ácido 3-aminobenzoico da lugar a CMOs con estructura tipo CMK-3, mientras que el ácido 4-aminobenzoico genera CMOs con estructura tipo CMK-5. Ambos

precursores dan lugar a CMOs con concentraciones superficiales de nitrógeno del 6.7 y 7.6% en peso, respectivamente, que se encuentra principalmente en forma de nitrógeno piridínico y cuaternario. La concentración de oxígeno es del 5% en peso en el carbón tipo CMK-3 y del 6.5% en peso en el de tipo CMK-5; en el primero, se encuentra mayormente en forma de anhídridos, alcoholes y éteres, y, en el segundo, en forma de ésteres y anhídridos.

- Los dos tipos de CMOs anteriores son materiales prometedores para su uso como portadores para la liberación controlada de medicamentos poco solubles. Estos carbones muestran una respuesta específica al pH del medio, puesto que el aumento del pH de 2 a 7.4 produce un incremento de la cantidad de ibuprofeno liberada, especialmente en el caso del carbón tipo CMK-5. Además, dicha liberación de ibuprofeno se produce de manera inmediata en respuesta al cambio de pH.

- Se han obtenido materiales de carbono dopados con nitrógeno, oxígeno y fósforo mediante la carbonización de composites poliamida/SBA-15 en presencia de H_3PO_4. Variando la concentración de H_3PO_4 y la temperatura de carbonización se puede modificar tanto la textura porosa de los materiales como su química superficial. Para concentraciones de H_3PO_4 superiores al 50% en peso se produce la pérdida del orden estructural de los CMOs. Por otro lado, la adición de bajas concentraciones de H_3PO_4 favorece la retención de nitrógeno en la superficie del material, mientras que altas concentraciones de H_3PO_4 favorecen la fijación de oxígeno y fósforo.

- En función de la cantidad de H_3PO_4 y de la temperatura de carbonización, la concentración superficial (medida por XPS) de nitrógeno varía entre el 3.8 y el 9.6% en peso, la de oxígeno entre el 5.6 y el 10.2% en peso y la de fósforo entre 0 y el 5.4% en peso. El nitrógeno se encuentra en forma de nitrógeno cuaternario, piridínico y pirrólico. El oxígeno forma parte de ácidos carboxílicos, carbonilos, anhídridos, ésteres, éteres e hidroxilos; también se encuentra unido al fósforo, en forma de fosfatos y polifosfatos. La proporción relativa de cada grupo funcional depende de las condiciones de preparación.

- La adsorción de CO_2, medida a 0 °C y 1 bar, depende principalmente del

volumen de microporos estrechos y prácticamente no se ve afectada por la química superficial de los materiales de carbono obtenidos. Por otro lado, la cantidad de CO_2 adsorbido a 25 ó 50 °C y 1 bar depende del tipo y concentración de heteroátomos presentes en la superficie. Los grupos funcionales de nitrógeno ejercen una influencia positiva, mientras que los grupos funcionales de oxígeno y fósforo ejercen una influencia negativa. Entre los grupos nitrogenados, las funcionalidades pirrólicas producen el mayor incremento en la adsorción de CO_2, siendo más débil el efecto favorable de los grupos piridínicos y de nitrógeno cuaternario.

- Los carbones que poseen mayores concentraciones superficiales de nitrógeno presentan los valores más altos de calor isostérico de adsorción de CO_2 a recubrimiento cero, debido al efecto favorable de los grupos funcionales de nitrógeno. Dichos materiales podrían ser utilizados como adsorbentes selectivos, apropiados para la captura de CO_2 en condiciones de postcombustión.

Anexo:

Asistencia a congresos

ANEXO

Asistencia a congresos

El trabajo desarrollado en esta tesis ha permitido presentar las siguientes comunicaciones en congresos y la publicación de los siguientes capítulos de libros, recogidos en la **Tabla A.1**:

Tabla A.1 Comunicaciones en congresos y capítulos de libros a los que ha dado lugar el trabajo recogido en la presente memoria.

	Publicación	
Conferencias	*Preparación de carbones a partir de poliamidas mediante nanomoldeo.* A. Sánchez-Sánchez, F. Suárez-García, A. Martínez-Alonso, J.M.D. Tascón.	XII Congreso Nacional de Materiales y XII Congreso Iberoamericano de Materiales, Alicante, España. 2012
	Modificación de la química superficial en carbones mesoporosos ordenados. A. Sánchez-Sánchez, F. Suárez-García, A. Martínez-Alonso, J.M.D. Tascón.	XI Reunión del Grupo Español del Carbón (GEC), Badajoz, España. 2011.
Pósters	*Influence of the acidic and basic sites on the CO_2 adsorption capacity of doped ordered mesoporous carbons.* A. Sánchez-Sánchez, F. Suárez-García, A. Martínez-Alonso, J.M.D. Tascón.	Carbon, Corea. 2014.
	Polyamides as new precursors of nitrogen and oxygen-doped ordered mesoporous carbons. A. Sánchez-Sánchez, F. Suárez-García, A. Martínez-Alonso, J.M.D. Tascón.	Carbon, Corea. 2014.
	Carbones micro-mesoporosos ordenados mediante carbonización de composites de poliaramida/SBA-15 en presencia de ácido fosfórico A. Sánchez-Sánchez, F. Suárez-García, A. Martínez-Alonso, J.M.D. Tascón.	XII Reunión del Grupo Español del CArbón (GEC), Madrid, España. 2013.
	Preparación de carbones mesoporosos ordenados dopados con nitrógeno mediante CVD. A. Sánchez-Sánchez, F. Suárez-García, A. Martínez-Alonso, J.M.D. Tascón.	XII Reunión del Grupo Español del Carbón (GEC), Madrid, España. 2013.

	Aromatic polyamides as precursors of nitrogen-doped ordered mesoporous carbons. A. Sánchez-Sánchez, F. Suárez-García, A. Martínez-Alonso, J.M.D. Tascón.	XII Pre-Carbon, Budapest, Hungría. 2012.
Capítulos de libros	*Carbones micro-mesoporosos ordenados mediante carbonización de composites de poliaramida/SBA-15 en presencia de ácido fosfórico.* A. Sánchez-Sánchez, F. Suárez-García, A. Martínez-Alonso, J.M.D. Tascón.	Grupo Español del Carbón, 2013. ISBN 978-84-695-8694-5. Pág. 78.
	Preparación de carbones mesoporosos ordenados dopados con nitrógeno mediante CVD. A. Sánchez-Sánchez, F. Suárez-García, A. Martínez-Alonso, J.M.D. Tascón.	Grupo Español del Carbón, 2013. ISBN 978-84-695-8694-5. Pág. 79.
	Modificación de la química superficial en carbones mesoporosos ordenados. A. Sánchez-Sánchez, F. Suárez-García, A. Martínez-Alonso, J.M.D. Tascón.	Grupo Español del Carbón. Ed. Abecedario, 2011. ISBN 978-84-9978-020-7. Pág. 51-52.